ARISTOTLE UNIVERSITY OF THESSALONIKI
Interinstitutional Program of Postgraduate Studies in
PALAEONTOLOGY – GEOBIOLOGY

NIKOLAOS PAPARIZOS
Geologist

LATE MIOCENE CARNIVORES FROM THE CLASSICAL LOCALITY OF PIKERMI (ATTICA, GREECE)

MASTER THESIS

DIRECTION: Macropalaeontology
Directed by: Aristotle University of Thessaloniki

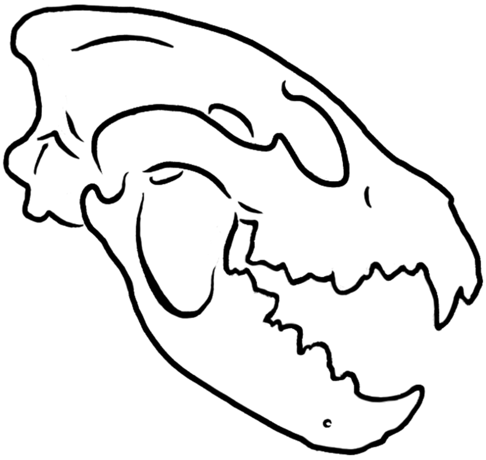

ATHENS
2023

Interinstitutional
Program of
Postgraduate
Studies in
PALAEONTOLOGY – GEOBIOLOGY

supported by:

Τμήμα Γεωλογίας ΑΠΘ
School of Geology AUTh

Τμήμα Βιολογίας ΑΠΘ
School of Biology AUTh

Τμήμα Γεωλογίας & Γεωπεριβάλλοντος
ΕΚΠΑ
Faculty of Geology & Geoenvironment
NKUA

Τμήμα Γεωλογίας Παν/μίου Πατρών
Department of Geology, Patras Univ.

Τμήμα Γεωγραφίας Παν/μίου Αιγαίου
Department of Geography, Aegean Univ.

NIKOLAOS PAPARIZOS
ΝΙΚΟΛΑΟΣ ΠΑΠΑΡΙΖΟΣ
Πτυχιούχος τμήματος Γεωλογίας και Γεωπεριβάλλοντος
του Εθνικού και Καποδιστριακού Πανεπιστημίου Αθηνών

LATE MIOCENE CARNIVORES FROM THE CLASSICAL LOCALITY OF PIKERMI (ATTICA, GREECE)

ΣΑΡΚΟΦΑΓΑ ΤΟΥ ΑΝΩΤΕΡΟΥ ΜΕΙΟΚΑΙΝΟΥ ΑΠΟ ΤΗΝ ΚΛΑΣΙΚΗ ΘΕΣΗ ΤΟΥ ΠΙΚΕΡΜΙΟΥ (ΑΤΤΙΚΗ, ΕΛΛΑΔΑ)

Υποβλήθηκε στο ΔΠΜΣ Παλαιοντολογία-Γεωβιολογία

Ημερομηνία Προφορικής Εξέτασης: 20/01/2023
Oral Examination Date: 20/01/2023

Three-member Examining Board

Assistant Professor Socrates Roussiakis, Supervisor
Associate Professor George Lyras, Member
Professor Evangelia Tsoukala, Member

Τριμελής Εξεταστική Επιτροπή

Επίκουρος Καθηγητής Σωκράτης Ρουσιάκης, Επιβλέπων
Αναπληρωτής Καθηγητής Γεώργιος Λύρας, Μέλος Τριμελούς Εξεταστικής Επιτροπής
Καθηγήτρια Ευαγγελία Τσουκαλά, Μέλος Τριμελούς Εξεταστικής Επιτροπής

External Assistant/Εξωτερικός Συνεργάτης (σύμφωνα με ΕΔΕ5/15-7-2019)

LATE MIOCENE CARNIVORES FROM THE CLASSICAL LOCALITY OF PIKERMI (ATTICA, GREECE) – *Master Thesis*

ΣΑΡΚΟΦΑΓΑ ΤΟΥ ΑΝΩΤΕΡΟΥ ΜΕΙΟΚΑΙΝΟΥ ΑΠΟ ΤΗΝ ΚΛΑΣΙΚΗ ΘΕΣΗ ΤΟΥ ΠΙΚΕΡΜΙΟΥ (ΑΤΤΙΚΗ, ΕΛΛΑΔΑ) – *Μεταπτυχιακή Διπλωματική Εργασία*

Citation:
Paparizos N., 2023. – Late Miocene carnivores from the classical locality of Pikermi (Attica, Greece). Master Thesis, Interinstitutional Program of Postgraduate Studies in Palaeontology-Geobiology. School of Geology, Aristotle University of Thessaloniki, 205 pp.

Cover Figure: Hyaenid skull by Nikolaos Paparizos

Contents

Acknowledgments

This section is dedicated to everyone who helped and supported me during the process of writing this Master's Thesis as well as during the course of the IPSP in Palaeontology–Geobiology. For their valuable help and guidance throughout the course of this master, I would like to thank its director, Professor D. S. Kostopoulos as well as the educational staff. I would like to deeply thank and extend my gratitude towards my supervisor, Assistant Prof. S. Roussiakis for his invaluable help, guidance and permission of this study. For their help, guidance and insight, I would like to thank the committee members, Associate Prof. G. Lyras and Professor E. Tsoukala, without whose assistant, this Thesis would not be achieved. I would also like to extend my thanks and gratitude to the Palaeontology and Geology Museum of the National and Kapodistrian University of Athens, its director Professor E. Koskeridou and again Assistant Prof. S. Roussiakis for trusting me with the material of my thesis as well as the museum collections. I would also like to personally thank Dr. N. Kargopoulos for his help and photographic material from various foreign museums and institutions, Prof. Emeritus G. Theodorou for providing me the opportunity to participate in the new excavations in Pikermi and, of course, the rest of the colleagues from the Palaeontology and Geology Museum. Lastly, I would like to thank my parents for their help and support throughout all these years as well as my friend G. Giannaki for her help and insight.

Abstract

This Master's Thesis focuses on the taxonomy of carnivoran fossils from the Late Miocene (~7.3 Ma) classical locality of Pikermi (Attica, Greece). This work aims to show that the study of old collections can often result in new and interesting information, as well as to hopefully enrich the carnivoran knowledge from the locality of Pikermi. The already celebrated Late Miocene locality's carnivoran diversity also reflects through this work, as it includes representatives from Hyaenidae, which constitute the largest portion of this study, Felidae, Ailuridae, Mustelidae and Ursidae. As part of this work's process both craniodental and postcranial material were studied and the presence of the following taxa was identified: the family of Hyaenidae is represented with the species (1) *Ictitherium viverrinum*, (2) *Plioviverrops orbignyi*, (3) *Adcrocuta eximia*, (4) *Lycyaena chaeretis*, (5) the enigmatic *Hyaenictis graeca*, and, (6) maybe *Hyaenictitherium wongii* were recognized. The family of Felidae is represented with the species (1) *Amphimachairodus giganteus*, (2) *Pontosmilus orientalis*, and possibly (3) *"Metailurus parvulus"*, (4) *Pristifelis attica* and (5) *Paramachaerodus schlosseri*. The family of Ailuridae is represented with the taxon *Simocyon primigenius* through some rare postcranial material. The families of Mustelidae and Ursidae are represented by *Promeles palaeattica* and *Indarctos atticus* respectively.

Περίληψη

Η παρούσα διπλωματική μεταπτυχιακή εργασία αφορά την ταξινομία απολιθωμένων σαρκοφάγων θηλαστικών από το Ανώτερο Μειόκαινο (~7.3 εχπ.) της κλασικής θέσης του Πικερμίου (Αττική, Ελλάδα). Στόχος της εργασίας είναι η ανάδειξη των παλαιών μουσειακών συλλογών και πώς η μελέτη αυτών μπορεί συχνά να οδηγήσει σε νέες και ενδιαφέρουσες πληροφορίες, καθώς επίσης και ο πιθανός παράλληλος εμπλουτισμός των γνώσεων της απολιθωμένης σαρκοφαγικής πανίδας του Πικερμίου. Στο πλαίσιο της παρούσας εργασίας αναδεικνύεται, επίσης, η περίφημη και πλούσια πανίδα σαρκοφάγων θηλαστικών του Πικερμίου καθώς αντιπροσωπεύεται από την πλειονότητα των σαρκοφαγικών οικογενειών που έχουν αναγνωρισθεί στη θέση αυτή. Πιο συγκεκριμένα προσδιορίστηκαν είδη από την οικογένεια των Hyaenidae, που και αποτελούν τον κύριο όγκο του υλικού της μεταπτυχιακής μελέτης, των Felidae, των Ailuridae, των Mustelidae και των Ursidae. Κατά την εκπόνηση της διπλωματικής μελετήθηκε τόσο κρανιοδοντικό όσο και μετακρανιακό υλικό και αναγνωρίσθηκαν τα παρακάτω taxa: από την οικογένεια των Hyaenidae αναγνωρίσθηκαν τα είδη (1) *Ictitherium viverrinum*, (2) *Plioviverrops*, (3) *Adcrocuta eximia*, (4) *Lycyaena chaeretis*, (5) το μέχρι πρότινος αινιγματικό *Hyaenictis graeca* και ενδεχομένως (6) το *Hyanictitherium wongii*. Από την οικογένεια των Felidae αναγνωρίσθηκαν τα είδη (1) *Amphimachairodus giganteus*, (2) *Pontosmilus orientalis* και ίσως των (3) *"Metailurus parvulus"*, (4) *Pristifelis attica* και (5) *Paramachaerodus schlosseri*. Η οικογένεια των Ailuridae εκπροσωπείται από το *Simocyon primigenius* μέσα από ορισμένα δείγματα σπάνιου μετακρανιακού υλικού, ενώ από τις οικογένειες των Mustelidae και Ursidae αναγνωρίσθηκαν τα *Promeles palaeattica* και *Indarctos atticus* αντίστοιχα.

1. Introduction

1.1 Scope of the study

The Late Miocene classical locality of Pikermi (Attica, Greece) has been known and excavated since the mid-19th century and up until 1912 by various scientists (e.g., Gaudry, Woodward and Skouphos, Abel, etc.). The accumulated fossils from these excavations were either sent to various foreign institutions and museums throughout the world or stored in the Palaeontology and Geology Museum, Faculty of Geology and Geoenvironment, National and Kapodistrian University of Athens (see chapter 1.23 for more information). Concerning the latter specimens, many of them still lied in their original blocks of matrixes up until recently where they were prepared primarily by the effort of S. Roussiakis. Despite the numerous studies published regarding the fossils of the classical locality, an important number of fossils – from various taxonomic groups –from the aforementioned museum's collections that are of potential scientific interest still remains unpublished. In light of that, the study of some rare and – for the most part – unpublished craniodental and postcranial material from carnivorans from these old collections was assigned to me as a Master Thesis. As such, this study aims to exemplify the importance and relevance in the study of old museum collections and how it can potentially lead in new and interesting information, as well as, to hopefully increase the knowledge of carnivorans from the classical locality of Pikermi in the process.

1.2 The classical locality of Pikermi

The classical fossiliferous locality of Pikermi (Attica, Greece) constitutes one of the oldest (concerning its discovery) and most celebrated localities across the Late Miocene of Europe. The Turolian locality's rich vertebrate fauna biodiversity, dubbed today as the "Pikermian biome", has a pivotal role as a reference locality (Bernor et al., 1996) for the continental European Late Miocene.

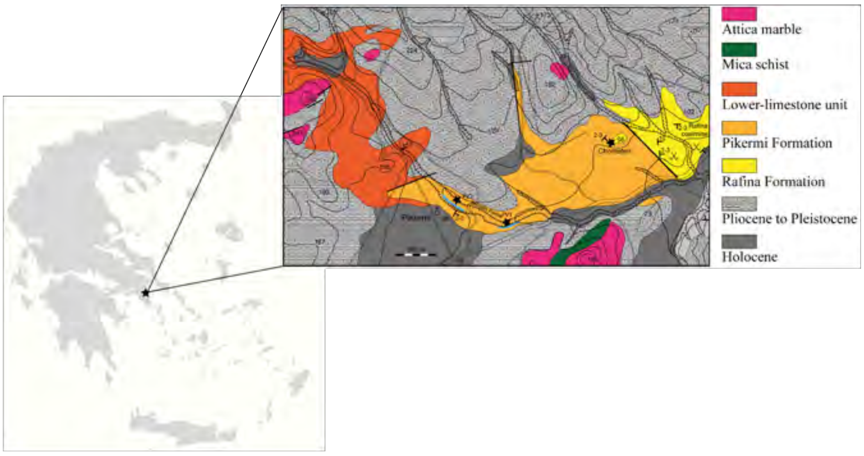

Figure 1. Geological map of Pikermi (right) by Böhme et al. (2017). Black stars indicate fossiliferous sites. From the left: PV3: Pikermi Valley 3 coincides with the classical locality and the historical excavations lead by Gaudry 1855–1860, Woodward and Skoufos 1901 and Abel 1911–1912. PV1: Pikermi Valley 1 marks the new excavational site of Theodorou (2008–Present). Chomateri marks the site of excavations lead by Symeonidis & Bachmayer during 1972–1980.

1.21 Geology

The fossil accumulations of Pikermi are located within the Mesogea Basin of Attica, Greece (Fig. 1). Their development occurred during the Late Miocene due to the activation of a major detachment fault that separates the Internal Hellenides carbonates from the metamorphic rocks of the Mesozoic (Papanikolaou et al., 2007). Böhme et al. (2017) divided the basin's sediments into two formations: the Pikermi Formation and the Rafina Formation. The former refers to a terrestrial/alluvial stratigraphic sequence, rich in terrestrial vertebrate fossil fauna, with a thickness up to 30 meters, while the latter overlays the Pikermi Formation and is of palustrine/lacustrine origin.

Furthermore, the stratigraphic sequence of the Pikermi Formation can be discerned into two members. The lower Red Conglomerate Member alternates red silts with a weak pedogenic overprint and debris flows deposits. Most of the historical and recent excavations refer to the red silts of the lower Red Conglomerate Member (Gaudry, 1862; Böhme et al., 2017, Roussiakis et al., 2019). The Upper Chomateri Member alternates yellowish to reddish silts with fluvial channels and channel–fill trains. The upper Member refers to the Chomateri site, where fossils of mammals may be contained in calcareous palaeosols in silts away from the channels (Symeonidis et al., 1973; Böhme et al., 2017) (Fig. 2).

Overlaying the Chomateri Member of the Pikermi Formation, lie concordantly palustrine clays, coals, lacustrine marls and limestones of the Rafina Formation. Underneath the Red Conglomerate Member of the Pikermi Formation, lie discordantly lacustrine to palustrine grey marls and coals (Böhme et al., 2017).

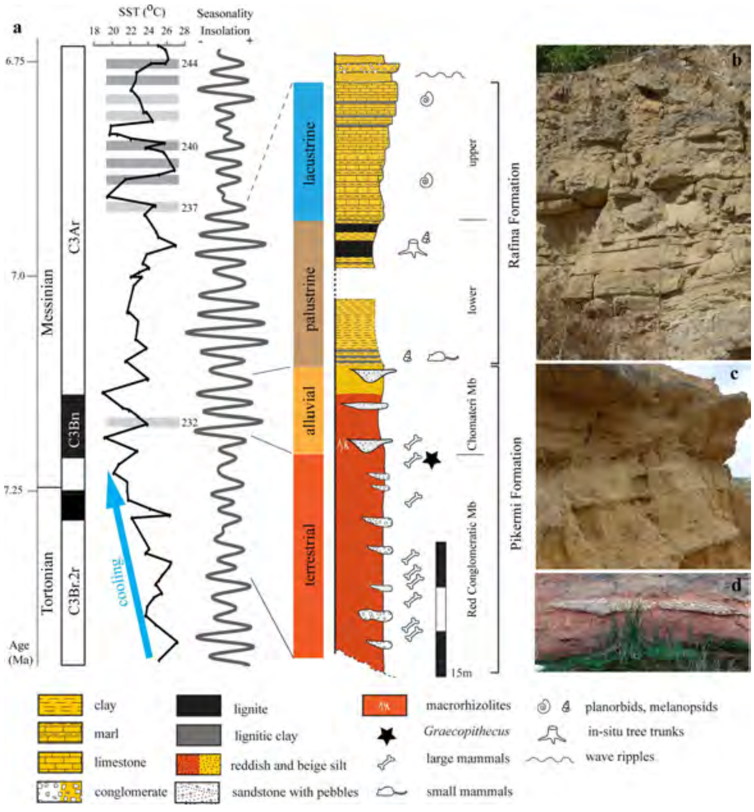

Figure 2. Simplified stratigraphic column of Rafina and Pikermi formation by Böhme et al. (2017). The typical red slits of the classical locality are marked with (d) on the right.

1.22 Age

The first estimations regarding the age of the Pikermian fauna were based on material from the old collections. However, the issue with this was that since some early authors (Gaudry, 1855; 1862–1867; Woodward, 1901; Abel, 1922) noted as well, the fossiliferous sites occur on at least two distinct stratigraphic levels along the Megalo Rema's stream ravine. Thus, it makes dating the Pikermian fauna using the old collections housed in museums unreliable, since the fauna may not be homogeneous and may contain fossils of different horizons and age (Theodorou et al., 2010; 2013, Roussiakis et al, 2014; Koufos, 2021).

Initially, Pikermi was correlated with the upper part of the biozone MN 12 (Mein, 1975; 1990; de Brujin et al., 1992). Later, Bernor et al. (1996) correlated the fauna from Pikermi with the biozone of late MN 11 (circa 8.3–8.2 Ma), identifying it as the same age with the locality of Samos and Maragheh. Contrasting Bernor et al. (1996), biochronological data acquired from the more homogeneous collection of Gaudry from the Muséum national d'Histoire naturelle, Paris, France, suggest a correlation with the uppermost part of the biozone MN 12 (circa 7.1 Ma) (Koufos, 2013 and references therein; Koufos, 2021). The most recent data from the magnetostratigraphic analysis performed by Böhme et al. (2017) suggest a date of 7.37–7.11 Ma for the Pikermi Formation, with the classical locality dating between 7.33–7.29 Ma, essentially placing it approximately in the middle of the Turolian in MN 12.

1.23 Brief history of the excavations at the classical site of Pikermi

The fossil collections from the classical locality of Pikermi are the collective product of several excavations throughout the course of many decades. The initial discovery of fossils took place in the mid-19th century (1836) and is attributed to the Scottish historian G. Finlay. Finlay's initial discovery led to a number of other major and minor expeditions both by palaeontologists and naturalists alike as follows: in 1843 by A. Lindermayer, in 1852 by J. Roth, in 1853 by H. Mitzopoulos, in 1882 by W. Dames, in 1885 by M. Neumayr and L. v. Tausch. The excavations, however, that yielded the most material were those conducted by A. Gaudry during 1855–56 and 1860, A. S. Woodward and Th. Skouphos in 1901 and O. Abel in 1912 (Roth & Wagner, 1854; Gaudry, 1862–1867; Dames, 1883a; Weithofer, 1888; Woodward, 1901; Abel, 1922). Abel's excavation was the last in the classical site. It was followed by a period of excavational hiatus before resuming in 1972–1980 by N. Symeonidis, F. Bachmayer and H. Zapfe in the nearby locality of Chomateri or Kisdari (Symeonidis et al., 1973; Bachmayer & Symeonidis, 1982).

Today, these fossils from the aforementioned excavations adorn almost all major natural history museum collections of Europe (London, Berlin, Athens, Vienna, Munich, Paris, etc.). In addition to that, these collections have been used extensively as a reference for comparative studies in many publications concerning the early development the palaeontology of mammals (e.g., Wagner, 1839; 1840; Roth & Wagner, 1854; Gaudry, 1862–1867).

After a second period of hiatus, excavations in Pikermi finally resumed in 2008 under the direction of, the now emeritus, Professor G. Theodorou (Theodorou et al., 2010; 2013). Further prospecting of the area led to the discovery of the new and promising sites of Pikermi

Valley (PV1–PV3) which have yielded a lot of material (Filis et al., 2019; Roussiakis et al., 2019). Since 2008, excavations are performed on an almost yearly basis.

1.24 Pikermian fauna and palaeoenvironment

The Pikermian fauna is characterized by its rich macromammalian diversity, having representatives from most mammalian taxa that inhabited Greece during the Turolian (Bernor et al., 1996; Theodorou et al., 2010; and references therein). Despite the fact that the vast majority of the fauna comprises of mammals, a small number of reptilian and avian representatives have also been recorded.

Herbivores constitute the majority of the mammalian taxa excavated in the locality. Amongst the most common representatives are the three-toed hipparionin horses, many species of bovids, giraffids and rhinocerotids. Other less common taxa include proboscideans, hyracoids, cervids, hyracoids, chalicotheriids, murids, hystricids and insectivores. Carnivorans exhibit an exceptional diversity of at least eighteen different species. Their taxa include six representatives from the family Hyaenidae Gray, 1869, with the species *Adcrocuta eximia* (Roth and Wagner, 1854), *Hyaenictis graeca* Gaudry, 1861, *Ictitherium viverrinum* Roth and Wagner, 1854, *Lycyaena chaeretis* (Gaudry, 1861), *Hyaenictitherium wongii* (Zdansky, 1924) and *Plioviverrops orbignyi* (Gaudry and Lartet, 1856), five representatives from the family Felidae (Fischer von Walheim, 1817) with the species *"Metailurus parvulus"* (Hensel, 1862), *Paramachaerodus schlosseri* (Weithofer, 1888), *Pristifelis attica* (Wagner, 1857), *Amphimachairodus giganteus* (Wagner, 1848) and *Pontosmilus orientalis* (Kittl, 1887), one representative from the family Ailuridae Gray, 1843 with the species *Simocyon primigenius* (Roth & Wagner, 1854), four representatives from the family Mustelidae G. Fischer de Waldheim, 1817 with the species *Promeles palaeattica* (Weithofer, 1888), *Martes woodwardi* Pilgrim, 1931, *?Enhydriodon latipes* Pilgrim, 1931, *?Sinictis pentelici* (Gaudry, 1861), one representative from the family Mephitidae Bonaparte, 1845 with the species *Promephitis lartetii* Gaudry, 1861 and one representative from the family Ursidae Linnaeus, 1758 with the species *Indarctos atticus* (Weithofer, 1888) ex Dames 1883 (see Appendix). The frequency of those carnivorans varies greatly depending on the species. The humeral remains described by Symeonidis (1974) as *Plesiogulo* sp. Zdansky, 1924 are not taken into consideration in this study, as they may very well belong to another taxon.

Presently, the prevailing theory concerning the palaeoenvironment of the Pikermian fauna is that of Böhme et al. (2017), a multidimensional approach that includes isotope analysis, sediment analysis, palynology, magnetostratigraphy up to the potential dietary habits of fossilized taxa. This work suggests that the Late Miocene environment of the Pikermian Formation was a wooded grassland to woodland within a C4 grasses savannah biome, essentially verifying the initial hypotheses proposed by Gaudry (1862).

1.3 Carnivora

The mammalian order Carnivora was erected by Bowdich in 1821. Currently, about 286 extant carnivoran species exist (Van Valkenburgh & Wayne, 2010). Members of this order have often been the subject of interest in the lives of humans (e.g., competition with the early humans, household pets, etc.) that eventually led to the conduct of many scientific studies. Representatives of the order exhibit great diversity both in body mass and dietary and morphofunctional adaptations. (Eizirik et al., 2010; Werdelin & Wesley-Hunt, 2010).

Although the name of the order might imply a carnivorous diet for its members, that is not entirely accurate. The dietary preferences range from strictly flesh eaters (obligatory carnivores) like cats, pescatarians like seals, non-exclusive meat-eaters (mesocarnivory) like dogs and foxes, to a strictly herbivorous or insectivorous diet like the giant panda and the aardwolf respectively (Werdelin & Wesley-Hunt, 2010).

Morphofunctionally, carnivorans have developed various locomotor adaptations that range from cursorial (cheetah), arboreal (kinkajou), ambulatory (giant panda) to semi-aquatic (seal) (Werdelin & Wesley-Hunt, 2010). Anatomically, members of the order share some common, although not evident in every family, traits. A prime example of that are the carnassial teeth (fourth upper premolar and first lower molar) which are used to shear the flesh during the mastication process. In some families however these teeth have been secondarily modified, thus, losing this trait (e.g., aardwolf, seals) (Stains, 1984; Vaughan, et al., 2000).

Carnivorans have a worldwide distribution, covering almost all major land masses and oceans, occupying almost every type of terrestrial and aquatic habitats. They can be found in forests, mountains, the desert and even the frozen poles. Similarly, they can also be found in aquatic environments, from rivers and lakes to the open sea (Eizirik et al., 2010).

The mass size within the order is quite remarkable, as it varies greatly from small animals like the least weasel that weighs <0.05 kg to animals that weigh more than 1500 kg like the southern sea elephant (Eizirik et al., 2010; Werdelin & Wesley-Hunt, 2010).

The phylogeny of the carnivorans has often times been complicated. The first carnivorans appeared around 63 Ma but their main radiation occurred around some 20 million years later (Van Valkenburgh & Wayne, 2010). Two evolutionary lineages have been recognized: those of the Caniformia Kretzoi, 1943, and Feliformia Kretzoi, 1945, suborders. In turn, each suborder consists of various families (Fig. 3). This initial taxonomic arrangement was proposed on the basis of the form and structure of the auditory bullae by Flower (1869) and continues its advancement to this day as new information (e.g., molecular, anatomical) become available (Eizirik et al., 2010).

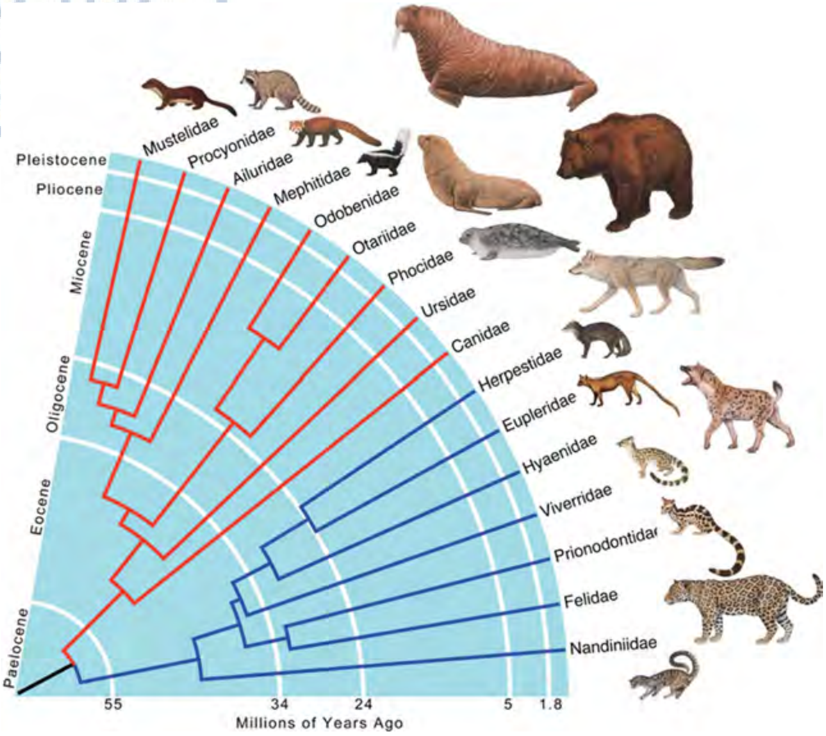

Figure 3. Time-calibrated phylogeny of the order Carnivora at the family level based on multiple nuclear gene sequences, with millions of years on the horizontal axis and Cenozoic epochs on the near vertical axis. Caniformia shown in red, Feliformia shown in blue. Figure from Van Valkenburgh et al. (2014).

2. Material & Methods

The material studied in this Thesis includes elements of both craniodental and postcranial nature of various carnivorans from the classical locality of Pikermi (Attica, Greece). All the specimens are from the old collections (historical excavations) that were initially excavated during the 19th century and are presently stored in the Palaeontology and Geology Museum, Faculty of Geology and Geoenvironment, National and Kapodistrian University of Athens, Greece.

The material herein is described, compared both morphologically and metrically to similar taxa from Pikermi and other localities, and is systematically attributed as closely as possible to the species-level. Specifically for the dental material, Simpson's (1941) log-ratio diagrams were also used. This method is a non-statistical technique, which graphically illustrates the dental proportions of a taxon relative to another, which is considered the standard. In addition, aside from biometric measurements, some indexes were also used, which are provided below. The measurements were obtained using digital callipers and were rounded on the second decimal and were organized in tables. Measurements in parentheses (…) indicate an approximate value which is close to the original (e.g., slightly chipped tooth). Brackets […] indicate only an approximate value, which for the most part is ignored in further comparisons and analysis's and are provided only as a rough estimate for the reader (e.g., measurement of the alveolus).

The greatest challenge encountered is probably the almost complete absence of taphonomic data. This poses an issue in the association of some of the specimens thus limiting the available information gained. These associations could refer either to erroneous ones made in the past (e.g., some questionable restorations) but also to some probably associated material. This shall be examined further in each specimens dedicated section.

The stratigraphy follows the geochronological scale of Berggren et al. (1995) and Cohen et al. (2013) and Steininger et al. (1996) for the European mammal zones.

Abbreviations

Institutional

AMNH: American Museum of Natural History, New York, USA. AMPG: Museum of Palaeontology and Geology, National and Kapodistrian University of Athens, Greece. (F)CPT: Fundación Conjunto Paleontológico de Teruel-Dinópolis, Gobierno de Aragón, Spain. EUNHM: Ege Universitesi Natural History Museum, Bornova, Izmir, Turkey. ICP: Institut Català de Paleontologia Miquel Crusafont, Universitat Autònoma de Barcelona, Spain. IPUW: Institute of Palaeontology, University of Vienna, Austria. IVPP: Institute of Vertebrate Palaeontology and Paleoanthropology, Chinese Academy of Sciences, Beijing, China. LGPUT: Laboratory of Geology and Palaeontology, Aristotle University of Thessaloniki, Greece. MNCN-CSIC: Museo Nacional de Ciencias Naturales-CSIS, Madrid, Spain. MNHN: Museum Nationale d'Histoire Naturelle, Paris, France. NHMA: Natural History Museum of the Aegean, Samos, Greece. NHMUK: National History Museum, London, United Kingdom. NHMW: Naturhistorisches Museum, Wien, Austria. NMNH-A: Paleontological Museum-

Assenovgrad, branch of the National Museum of Natural History–Sofia, Bulgaria. NMNHS: National Museum of Natural History, Bulgarian Academy of Sciences, Sofia, Bulgaria. PMU: Palaeontological Museum, department of Palaeontology, University of Uppsala, Uppsala, Sweden. SAM: Iziko South African Museum, Cape Town, South Africa. SNSB-BSPG: Staatliche Naturwissenschaftliche Sammlungen Bayerns-Bayerische Staatssammlung für Paläontologie und Geologie, Munich, Germany.

Anatomical

Dental: L: length W: width. The abbreviations for the craniodental terminology follow Werdelin (1988a; b) and Werdelin & Solounias (1990; 1991). The only addition would be HP4 and Hm1: maximum height of the upper and lower carnassial's crown respectively, measured from the base. L(P2–P4): length from the mesial margin of P2 to the distal margin of P4. L(p2–m1): length from the mesial margin of p2 to the distal margin of m1.

Dental indexes: Robusticity index (R.I.): the ratio of the width to the length of a respective tooth multiplied by a hundred. L(P3/P4) × 100: the ratio of the length of P3 to the length of P4. W(P3/P4) × 100: the ratio of the width of P3 to the width of P4. L(mP4/P4) × 100: the ratio of the length of P4's metastyle blade to the total length of P4. LP4/(LP2+LP3) × 100: the ratio of the length of P4 to the lengths of P2 and P3. L(p4/m1) × 100: the ratio of the length of p4 to the length of m1. L(pp4/p4) × 100: the ratio of p4's main cuspid to the total length of p4. L(tm1/m1) × 100: the ratio of the m1's trigonid to the total length of m1.

Axis: Lmax: maximum preserved length of the axis. Hmax: maximum preserved height of the axis. Wmax: maximum preserved width of the axis. Hce: height of the centrum. Wce: width of the centrum. HSAF: height of the superior articular facets for the atlas. WSAF: width of the superior articular facets for the atlas.

Humerus: L: maximum length of the humerus, measured from the tubercle. H.f: maximum functional length of the humerus, measured from the head. DAPpr.: maximum antero-posterior length at the proximal end. DTpr.: maximum medio-lateral length at the proximal end. DAPdia.: antero-posterior length at the middle of the shaft. DTdia.: medio-lateral length at the middle of the shaft. DAPdist.epic.: antero-posterior length measured from the medial epicondyle. DTdist.: maximum medio-lateral length at the distal end. DTdist.art.: medio-lateral length of the distal articular surface.

Ulna: L: maximum length of the ulna. OH: olecranon height measured from the anconeal process to the anterior olecranon tuberosities. Ht.n: height of the trochlear notch. DAPpr.: maximum antero-posterior length of the olecranon at its proximal end. DAPanc.: maximum antero-posterior length at the anconeal process. DAPr.n: maximum antero-posterior length at the radial notch. DAPt.n: minimum antero-posterior length at the trochlear notch. DTpr.: maximum medio-lateral length at the proximal end of the olecranon. DTr.n.: maximum medio-lateral length at the radial notch. DAPdia.: antero-posterior length at the middle of the shaft. DTdia.: medio-lateral length at the middle of the shaft. DTdist.: medio-lateral length at the styloid process.

Radius: L: maximum length of the radius. DAPpr.: maximum antero-posterior length in the proximal end. DTpr.: maximum medio-lateral length in the proximal end. DAPdia.: antero-posterior length at the middle of the shaft. DTdia.: medio-lateral length at the middle of the shaft. DAPdist.: maximum antero-posterior length in the distal end. DTdist.: maximum medio-lateral length in the distal end.

Femur and tibia: L: maximum length of the femur/tibia. DAPpr.: maximum antero-posterior length of the femur/tibia at the proximal end. DTpr.: maximum medio-lateral length of the femur/tibia at the proximal end. DAPdia.: antero-posterior length of the femur/tibia at the middle of the shaft. DTdia.: medio-lateral length of the femur/tibia at the middle of the shaft. DAPdist: maximum antero-posterior length of the femur/tibia at the distal end. DTdist: maximum medio-lateral length of the femur/tibia at the distal end.

Carpal and navicular: Hmax: maximum height of the carpal/tarsal. DAPmax.: maximum dorso-plantar length of the carpal/tarsal. DTmax.: maximum medio-lateral length of the carpal/tarsal. Additionally for cuboid: DAPpr.art.: dorso-palmar length at the proximal articular surface. DTpr.art.: medio-lateral length at the proximal articular surface.

Calcaneum: L: maximum length of the calcaneum. DAPpr.: dorso-plantar length at the proximal end of the calcaneum. DTpr.: medio-lateral length at the proximal end of the calcaneum. DAPcol.: dorso-plantar length at the middle of the calcaneum’s neck. DTcol.: medio-lateral length at the middle of the calcaneum’s neck. DAPmax.: maximum dorso-plantar length. DTmax.: maximum medio-lateral length. DAPdist.: dorso-plantar length at the distal end of the calcaneum. DTdist.: medio-lateral length at the distal end of the calcaneum.

Metapodial: L: maximum length of the metapodial. DAPpr.: maximum dorso-plantar length of the metapodial at the proximal end. DTpr.: maximum medio-lateral length of the metapodial at the proximal end. DAPdia.: dorso-plantar length of the metapodial at the middle of the shaft. DTdia.: medio-lateral length of the metapodial at the middle of the shaft. DAPdist.: maximum dorso-plantar length of the metapodial at the distal end. DTdist.: maximum medio-lateral length of the metapodial at the distal end.

Phalange: L: maximum length of the phalange. DAPpr.: maximum dorso-plantar length of the phalange at the proximal end. DTpr. maximum medio-lateral length of the phalange at the proximal end. DAPdia.: dorso-plantar length of the phalange at the middle of the shaft. DTdia.: medio-lateral length of the phalange at the middle of the shaft. DAPdist.: maximum dorso-plantar length of the phalange at the distal end. DTdist.: maximum medio-lateral length of the phalange at the distal end.

Statistics

n: population size, S.D: standard deviation, V: coefficient of variation.

3. Systematics

Order Carnivora Bowdich, 1821
Suborder Caniformia Kretzoi, 1931

Family Ailuridae Gray, 1843

The family of Ailuridae is represented today by only one extant species, *Ailurus fulgens* F. Cuvier, 1825 or, as it is most commonly known, the red panda or lesser panda. Along with the families of Mustelidae, Mephitidae and Procyonidae Gray, 1825, they comprise the clade of Musteloidea Fischer, 1817 (Flynn et al., 2000; Koufos, 2022a and references therein).

The ancestry of the family originates from the non-specialized carnivore of the genus *Amphictis* Pomel, 1853, from the Amphictinae Winge, 1896, sub-family. *Amphictis* is considered a basal musteloid from Europe that appeared during the Late Oligocene–Early Miocene of Europe, approximately 25–18 Ma. Along with Amphictinae, Ailuridae is further sub-dived into the subfamilies Simocyoninae Dawkins, 1868, and Ailurinae Gray, 1843 (Morlo & Peigné, 2010; Salesa et al., 2022; Koufos, 2022a and references therein).

It is interesting that unlike the strictly herbivorous red panda and its more recent ancestors, some of its extinct Simocyoninae relatives had carnivorous adaptations in their dentition (e.g., *Alopecocyon* Camp & Vanderhoof, 1940 and *Simocyon* Wagner, 1858). (Salesa et al., 2022). Another quite unique morphological trait about Ailuridae is the possession of a “false thumb”, which is basically a hypertrophied sesamoid bone acting like an opposable thumb. While this character is indeed quite unique among the carnivorans, it also shared with the giant panda, *Ailuropoda melanoleuca* David, 1869. However, since molecular studies has shown, the two extant pandas actually belong to different families, and this trait has evolved convergently. Thus, while on both extant pandas the “false thumb” is used as a feeding aid, studies have demonstrated that on the extinct carnivoran *Simocyon batalleri* (Viret, 1929) it was probably used as a means of fast escape from larger predators through climbing (Salesa et al., 2022 and references therein).

As is the case with all ailurid fossils, the Greek record is also rather poor, both in material and localities. The Greek record is represented only by a single species, *Simocyon primigenius* (Roth and Wagner, 1854), originally described from Pikermi and later Halmyropotamos (Melentis, 1967).

Subfamily Simocyoninae Dawkins, 1868
Genus *Simocyon* Wagner, 1858
Simocyon primigenius (Roth & Wagner, 1854)
(Figs. 4–7, Tables 1–2)

1854 *Gulo primigenius* Roth & Wagner, p. 389, Pl viii (ii), Figs. 1, 2
1854 *Canis lupus primigenius* Roth & Wagner, p. 398, Pl. viii, Fig. 7
1857 *Pseudocyon robustus* Wagner, p. 123, Pl. vi, Fig. 13
1858 *Simocyon robustus* Wagner, p. 367
1861 *Metarctos diaphorus* Gaudry, p. 527, Pl. x, Fig. I

Type species: *Gulo primigenius* Roth and Wagner, 1854.

Type locality: Pikermi, Attica, Greece.

Type material: SNSB-BSPG-PIK-AS II.53 (holotype); right mandibular ramus with c–m1 described and figured by Roth and Wagner (1854: Table. 8, Figs. 1, 2). Stored in the Bayrische Staatssamlung für Paläontologie und historische Geologie, Munich, Germany.

Age: MN 9–13; For the classical locality of Pikermi: Middle Turolian, MN 12, 7.33–7.29 Ma (Böhme et al., 2017).

Localities: Greece: Pikermi in Attica (Roth & Wagner, 1854), Halmyropotamos in Evia Island (Melentis, 1967). Spain: Cerro de la Garita (Alcalá 1994). North Macedonia: Karaslari (Spassov & Geraads, 2011). Bulgaria: Kalimanitsi (Bakalov & Nikolov, 1962). Moldova: Chobruchi (Pavlow, 1914). China: Baode, Fugu, Yushe (Zdansky, 1924; Wang, 1997). USA: Rattlesnake Fauna (John Day Basin) in Nevada, eastern Oregon and south-eastern Idaho (Baskin 1998; Tedrow et al. 1999). ?Ukraine: Novoukrainka, Krivoi Rog (Semenov, 2001). ?Kenya: Lemudong'o (Howell & Garcia, 2007; Werdelin & Simpson, 2009).

Material: AMPG-PA 1017/91: left Mc I, AMPG-PA 1018/91: left unciform, AMPG-PA 1019/91: left trapezium, AMPG-PA 1020/91: left radial sesamoid, AMPG-PA 4960/91: sesamoid, AMPG-PA 4962/91: left scapholunate. (Fig. 4).

Remarks: Excluding the scapholunate, the rest of material was found in close proximity within the same block of matrix and belonged to the same individual. Whether the similarly left scapholunate belonged to the same individual, purely based on the scarcity of the material, cannot be ascertained.

Description: Scapholunate: It is medio-laterally elongated. Proximally, the articular surface for the radius is large and strongly convex. The palmar tubercle is very strong and expands towards the palmar direction. A small facet situated close to the disto-palmar margin of the tubercle serves as attachment surface for the flexor retinaculum. The small and elongated facet in the medial border of the tubercle articulates with the radial sesamoid. The distal articular surface is concave towards its lateral margin, for the articulation of the magnum and unciform. The articular area for the former is smaller than the latter. The two articular areas are separated by a small edge. The concave surface dorsally to the unciform would probably articulate with the trapezoid, but the facet is not very well-preserved. The trapezium would probably articulate to the scapholunate through the slight concave articular facet located close to the medial margin of the distal articular surface.

Radial sesamoid: It is elongated and sub-triangular to almost round in cross-section. It articulates to the scapholunate through its flattened lateral surface. The attachment facets for ligaments and muscles lie close to its medial margin. Distally, the bone has a rough concavity that inclines and opens up towards the medial side. A distinct articulation surface with Mc I was not identified.

Trapezium: It is relatively small, dorso-palmarly elongated and slightly flattened in the palmar end of the proximo-distal axis. The distal articular surface is slightly concave and articulates to Mc I. Proximally it is convex without a distinct articulation surface. Laterally, it is sub-triangular shaped and the articulation surface would have served for articulation with the trapezoid. It would also articulate to the scapholunate dorsally.

Unciform: It is very large and elongated proximo-distally. The proximal articulation surface is very convex and would have probably articulated to the scapholunate. The distal articulation surface is concave, almost square in shape and would have probably articulated to both Mc Iv and V. In its lateral side, where it would have articulated with the pyramidal bone, the surface is convex and turns slightly concave distally. The medial articulation surface, where it would have probably articulated with the magnum, is large, slightly concave and hourglass-shaped. In the palmar side, a large ridge develops and protrudes along the proximo-distal axis, probably serving as an attachment point for the adductor digiti quinti muscle.

Mc I: It is short and strong, resulting in its robust appearance. The proximal epiphysis is slightly damaged making the articulation surface appear rough. Nevertheless, its sub-elliptical surface and its dorso-palmar elongation where it articulates with the trapezium is still preserved. In the medial side of the proximal epiphysis a strong tuberosity is observed. This serves as attachment point for the abductor pollicis longus muscle and the dorsal basal ligament. The diaphysis is short, slightly flattened dorso-palmarly and progressively narrows down to the distal epiphysis. The distal epiphysis is sub-triangular in shape; however, it is slightly damaged and appears roughened. In side view, the metacarpal appears slightly convex.

Sesamoid: It is small, oval-shaped and has a convex articulation surface where it would have probably articulated to a metacarpal bone.

Discussion: The genus *Simocyon* has been known, established and discussed in regards to its affinity and taxonomy for a long time, although almost exclusively on the basis of craniodental material (e.g., Roussiakis 2002, Peigné et al., 2005; Spassov & Geraads, 2011 and references therein). Its postcranial skeleton however, has been a mystery that has eluded scientists for decades. A possible explanation to that–excluding the rarity of the material itself– might be the absence of an apparent extant ecological homologue. In turn, this could result in possible misidentification or unidentification of its material. Luckily, the recent discovery of the almost complete skeleton of *Simocyon batalleri* from the Vallesian (MN 10) of Batallones-1 in Spain (Salesa et al., 2005; 2008) may finally provide the necessary information to change that.

The type species of the genus, *Simocyon primigenius*, that was initially erected from material found in Pikermi (Roth & Wagner, 1854) has been subsequently recognized across a number of other Eurasian and possibly North America localities on the basis of craniodental remains (Koufos, 2022a and references therein). The only postcranial attributed to it thus far however, is a femur from Pikermi by Gaudry (1862). Furthermore, Pilgrim (1931) commented that although there were no similar bones from Pikermi in the British Museum, he was still hesitant to share Gaudry's claim.

The material studied herein, although known for some time, lacked proper attribution as they did not really fit any of the known postcranial material from Pikermi. For example, the morphology of the first metacarpal exhibits ursid-like traits. However, there are no bears known from Pikermi which fit these dimensions and morphology. In addition to that, the morphology of the particularly large radial sesamoid only caused further confusion. Although a plethora of carnivorans have this bone, only in a few it is found hypertrophied like that. Further comparison with the radial sesamoid from the extant *Ailuropoda melanoleuca* (Salesa et al., 2005) and the extinct *Indarctos atticus* AMPG-PA 2016b/91 (Roussiakis, 2001a) from Pikermi, showed fundamental differences in their morphologies, pushing it further away from the ursids. In contrast to that, the comparison with the postcranial skeleton of the more recently published ailurid *S. batalleri* (Salesa et al. 2008), showed some remarkable similarities (Fig. 5). In light of that, a more in-depth comparison of the studied material against *Simocyon* shall be considered.

The comparison of Mc I AMPG-PA 1017/91 with Mc I MNCN-CSIC-B-3684 of *S. batalleri* exhibits their evident morphological similarities. Some notable differences observed concern the slightly smaller size of MNCN-CSIC-B-3684 and its straight shaft which contrasts the narrowing shaft of AMPG-PA 1017/91. Comparison of the radial sesamoid AMPG-PA 1020/91 with MNCN-CSIC-B-5441 of *S. batalleri* shows similar striking similarities in both morphology and size. There are, however, a few noticeable differences between these two as well. The concavity of the distal tip in AMPG-PA 1020/91 is not as flat as in MNCN-CSIC-B-5441. Also, the concavity opens up medially, whereas in MNCN-CSIC-B-5441 it doesn't. Regarding the function of this concavity, Salesa et al. (2008) estimate that it probably attached to a cartilaginous mass, similar to the extant *A. fulgens*. Comparison between the scapholunates revealed mostly morphological similarities, as the couple minor morphological differences noticed might as well be attributed to the preservation status of AMPG-PA 4962/91. In proximal view, the surface area located just proximally of the palmar tubercle's palmar margin is smoothened and only mildly concave, as opposed to the more roughened and concave palmar tubercle of MNCN-CSIC-B-2264. Also, the articular facet for the trapezium in AMPG-PA 4962/91seems to be deeper and more developed than in the MNCN-CSIC-B-2264, resulting in a slightly less proximo-distally compressed scapholunate towards the medial side. The similarities continue still with the comparison of their unciforms. Both AMPG-PA 1018/91 and MNCN-CSIC-B-5449 of *S. batalleri* have relatively similar morphology (e.g., dorsal side) and dimensions. Yet again however, there are some differences, such as their medial side morphology.

Concluding, the comparison exemplified the material's morphological similarities to *S. batalleri* and, by extension, to *Simocyon*. The size difference was something to be expected, as the known craniodental remains of *S. batalleri* are smaller than *S. primigenius* (Peigné et al., 2005). The exception to this would be the radial sesamoids and scapholunates, which appear to be of approximately equal size. It is worth keeping in mind however, that the size comparison was based on the photographic material's scale for *S. batalleri*, as Salesa et al. (2008) do not provide raw postcranial data. In regards to their minor morphological differences, considering the different time period each species lived and the fact that they actually belong to different species (e.g., more derived craniodental features of *S. primigenius*) (Spassov & Geraads, 2011) some differences are of course to be expected. Thus, taking into consideration the above, in addition to the fact that no other species of *Simocyon* or with *Simocyon*-like traits are known from Pikermi, the material is attributed to *S. primigenius* is deemed appropriate.

Similar to *S. batalleri*, the lack of a modern analogue has made difficult to ascertain the palaeoecology of *S. primigenius*. Craniodental studies suggest an omnivorous diet with bone-crunching adaptations as an opportunistic carnivore (Spassov & Geraads, 2011; Kargopoulos, 2019). Unfortunately, the material described here does not suffice to deduce further information about *S. primigenius*'s palaeoecological habits and biomechanics. Simply based on its similarities with *S. batalleri* and the general morphology of its "false thumb" it can probably be inferred that it had a similar role, as opposed to the strictly food manipulation of the red panda. Whether that was a specialization for a fast escape from the larger carnivore guild of Pikermi (e.g., *Amphimachairodus giganteus* or hyenids like *Adcrocuta eximia* and *Hyaenictis graeca*) similar to the hypothesized palaeoecology of *S. batalleri* is yet to be uncovered. Hopefully, as more material gets identified, either from old museum collections or new excavations, more information about the biomechanics and palaeoecology of this enigmatic species will be known.

Table 1. Metacarpal measurements (mm) of *Simocyon primigenius* from Pikermi.

	L	DAPpr.	DTpr.	DAPdia.	DTdia.	DAPdist.	DTdist.
Mc I AMPG-PA 1017/91 (sin)	32.70	8.89	12.83	5.60	8.83	7.82	10.43

Table 2. Carpal measurements (mm) of *Simocyon primigenius* from Pikermi.

	Hmax.	DAPmax.	DTmax.
Scapholunate AMPG-PA 4962/91 (sin)	16.81	14.12	28.75
Radial sesamoid AMPG-PA 1020/91 (sin)	15.22	5.83	6.31
Trapezium AMPG-PA 1019/91 (sin)	5.21	12.75	9.05
Unciform AMPG-PA 1018/91 (sin)	15.79	14.38	13.70
Sesamoid AMPG-PA 4960/91	3.18	6.05	4.07

Figure 4. *Simocyon primigenius* carpals and metacarpal I. A: scapholunate AMPG-PA 4962/91 (sin) in (from the left) palmar (1), dorsal (2), proximal (3) and distal (4) view. B: unciform AMPG-PA 1018/91 (sin) in (from the left) dorsal (1), palmar (2), proximal (3), distal (4), medial (5) and lateral (6) views. C: trapezium AMPG-PA 1019/91 (sin) in (from the left) distal (1), proximal (2), medial (3) and lateral (4) views. D: radial sesamoid AMPG-PA 1020/91 (sin) in (from the left) dorsal (1), lateral (2) and medial (3) views. E: sesamoid AMPG-PA 4960/91. F: Mc I AMPG-AMPG-PA 1017/91 (sin) in (from the left) medial (1), dorsal (2), palmar (3), lateral (4), proximal (5) and distal (6) views. Scale bar is 2 cm.

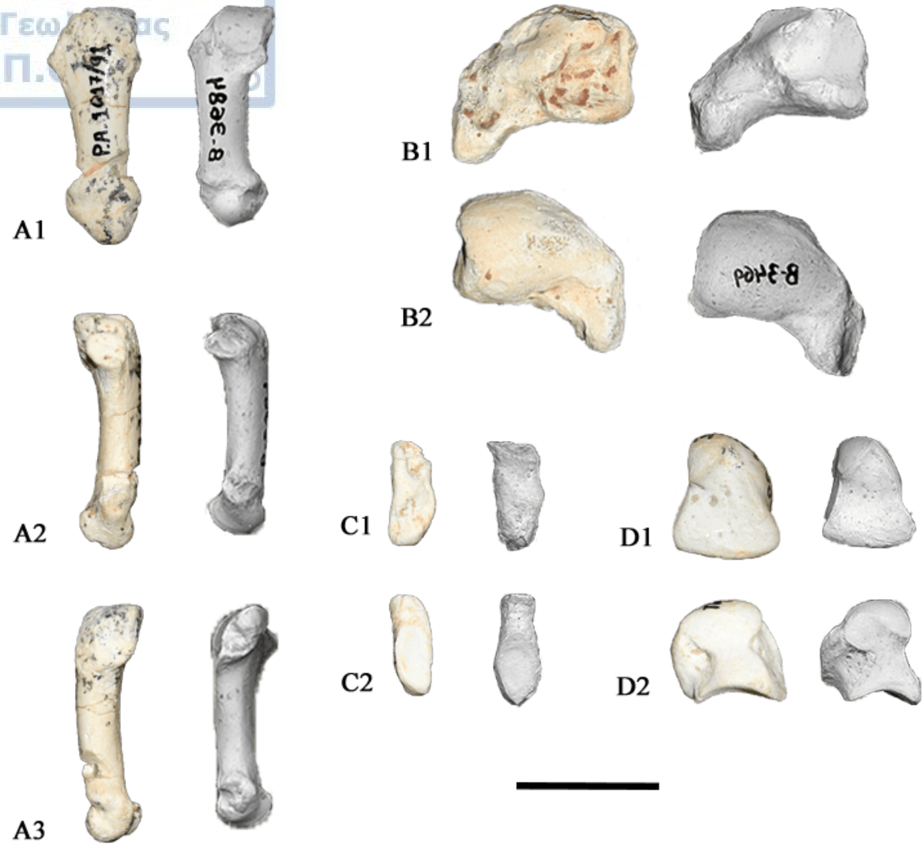

Figure 5. Side by side postcranial comparison between *Simocyon primigenius* (in colour, left) with *Simocyon batalleri* from Spain (in greyscale, right). A: Mc I in lateral (1), dorsal (2) and medial (3) views. B: scapholunates in palmar (1) and dorsal (2) views. C: radial sesamoids in dorsal (1) and lateral (2) views. D: unciforms in dorsal (1) and medial (2) views. Mc I of *S. batalleri* is originally right and was mirrored to match the left *S. primigenius* material. The radial sesamoid and unciform are left. Scale bar is 2 cm.

Figure 6. Attachment points for ligaments and muscles of the radial sesamoid AMPG-PA 1020/91 based on *S. batalleri* by Salesa et al. (2005). 1. Abductor pollicis brevis, 2. Abductor pollicis longus muscle, 3. Opponens pollicis longus. The flattened surface of the lateral side seen in the middle figure articulates to the scapholunate. Not in scale.

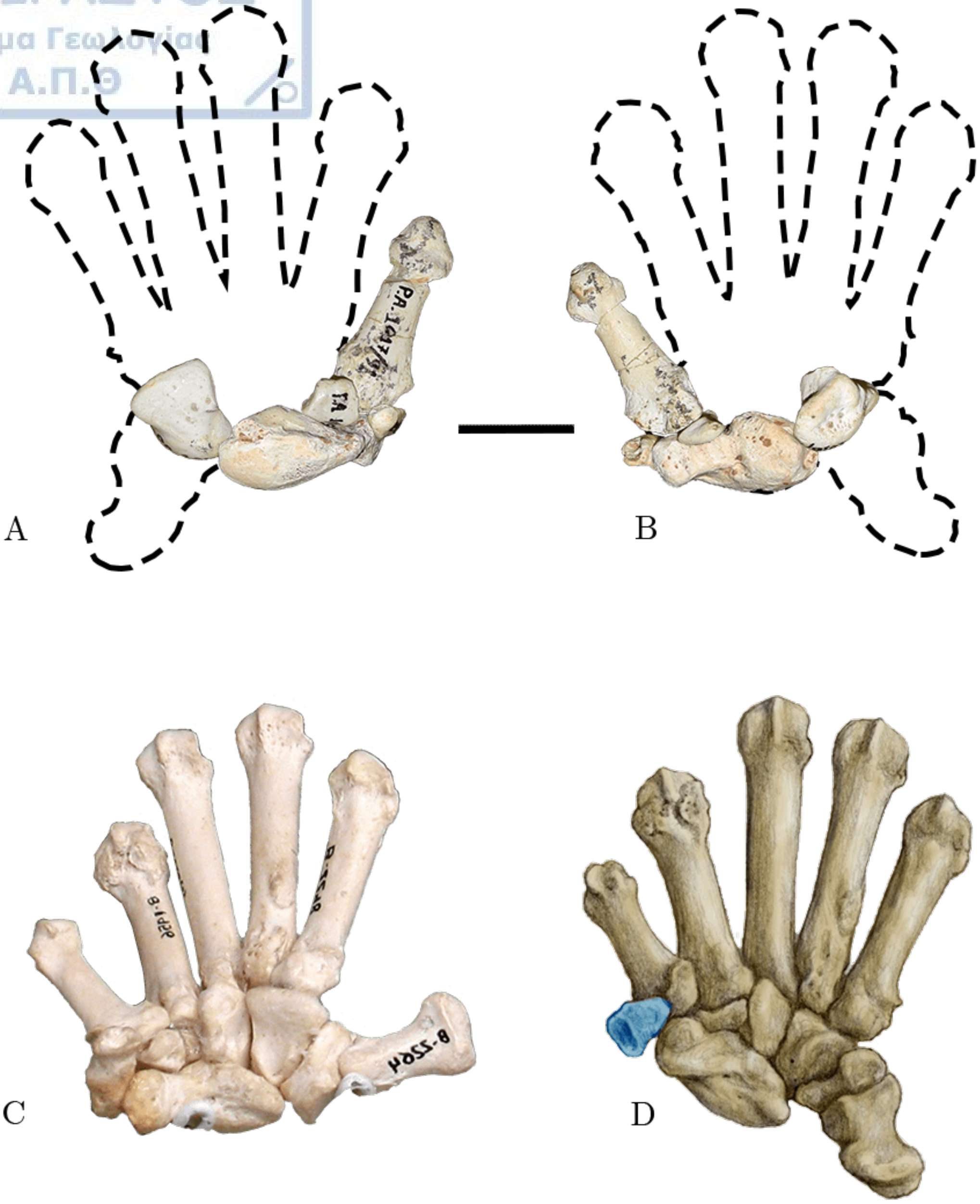

Figure 7. Approximate carpal and metacarpal restoration of the *S. primigenius* material based on *S. batalleri*. A: dorsal view. B: palmar view. C-D: palmar view of the carpals and metacarpals of *S. batalleri*. C and D are originally right, but they are mirrored to match the left *S. primigenius*. Whether the radial sesamoid of *S. primigenius* also articulated directly to either Mc I or the trapezoid cannot be ascertained at present. Although left as well, the scapholunate used for the reconstruction most probably belonged to another individual. Scale bar for A-B is 2 cm. C-D not in scale. Source: C: Wikimedia commons, licence: CC BY-SA 4.0. D: artist Mauricio Antón.

Family Mustelidae Fischer von Waldheim, 1817

The family Mustelidae is part of the superfamily of Musteloidea, along with Mephitidae (skunks), Ailuridae (red pandas) and Procyonidae (racoons) families (Law et al., 2018 and references therein). The former includes representatives such as the weasels, otters, wolverines, minks, badgers, martens and other similar animals and is classified as the most speciose family of the extant Carnivora. The family includes 85 putative extant species from 33 genera while more than 400 extinct species have recorded (Law et al., 2018).

Extant mustelids are morphologically and ecologically diverse (e.g., arboreal, fossorial, aquatic) (Law et al., 2018 and references therein). They also have an almost worldwide distribution, except Antarctica, Australia and some oceanic islands (Wund, 2005 and references therein). Their dietary habits generally depend on the species and its ecological niche. While they do range from carnivorous (e.g., wolverine) to pescatarians (e.g., sea otter), most species fall–within a degree of variation–to the range of opportunistic feeders (Wund, 2005 and references therein). Their size varies similarly, from the small least weasel to the giant river otter and the wolverine. Although there is great diversification amongst family members, some common traits are shared. Those include the elongated body, short muzzle and legs, non-retractile claws and a flattened or inflated auditory bullae (Wund, 2005; Koufos, 2022d).

The earliest Mustelidae is still debated whether it dates to Oligocene or Middle Miocene. The ancestry and evolution of the family is still unclear. Koepfli et al. (2008) suggest two rapid diversification events, during the Miocene and Pliocene, that were driven by climatic changes. The family is considered of Eurasian origin and dispersed to America and Africa at a later time (Koepfli et al., 2008). More recently, an Oligocene (~28.8–23.9 Ma) mustelid described by Paterson et al. (2020) is claimed to be the oldest member of the Mustelidae in North America. Contrasting the rapid diversification to ecological opportunity (Koepfli et al., 2008; Sato et al., 2009; 2012), Law et al. (2018) found no such association. However, their work suggested a link between the body plan elongation in some mustelid clades after the Mid-Miocene climate transition events that eventually allowed them to diversify (Law et al., 2018; 2019).

Mustelids are rare in the Greek fossiliferous record. Even so, 17 certain and 3 possible species from 12 genera have so far been recognized (Koufos, 2022d) from both continental and island localities (Koufos, 2022d). They were first described and recognized in Pikermi and Samos during the 19th century (e.g., Gaudry 1861; Forsyth Major, 1894). The first appearance of the family is marked during the Early/Middle Miocene in Antonios, Chalkidiki (Koufos, 2008). Their presence continues to the present day with extant forms that have appeared since the Late Pleistocene (Koufos, 2022d).

Sub-family Mustelinae Fischer von Waldheim, 1817
Genus *Promeles* Zittel, 1893
Promeles palaeattica (Weithofer, 1888)
(Figs. 8–9, Table 3)

1888 *Mustela palaeattica* sp. nov. in Weithofer, p. 226, Pl. x, Figs. 1–11
1888 *Meles? (Mustela) palaeattica* in Schlosser, p. 128, Pl. vii, Fig. 16
1890 *Meles palaeatticus* in Schlosser, p. 83
1893 *Promeles palaeattica* in Zittel, p. 651
1902 *Mustela palaeattica* in Major, p. 109, Pl. viii
2002 *Promeles palaeatticus* in Roussiakis, pp. 703–707, Fig. 3

Type species: *Mustela palaeattica* Weithofer, 1888.

Type locality: Pikermi, Attica, Greece.

Type material: IPUW-PIK (unnumbered) (holotype); cranium with associated mandible described and figured by Weithofer (1888: p. 226; Table 1, Figs. 1–11) stored in the Institut für Paläontologie, University of Wien, Austria.

Age: MN 11–12; For the classical locality of Pikermi: Middle Turolian, MN 12, 7.33–7.29 Ma (Böhme et al., 2017).

Localities: Greece: Perivolaki in Thessaly (Koufos, 2006a); ?Q1 and ?A in Samos Island (without description) (Solounias, 1981), Italy (Koufos, 2022d), ?Germany: Dorn-Dürkheim 1 (Franzen & Strorch, 1975; Morlo, 1997), Iran: Upper Maragheh (Bernor et al., 1996), Bulgaria: Kalimanitsi (Geraads & Spassov, 2016).

Material: AMPG-PA 4958/91: partially preserved skull without the neurocranium with P2-P3-P4-M1 (sin). (Fig. 9).

Description: Cranium: The preserved rostral area indicates a rather short and relatively wide snout. In left side lateral view, a maxillary depression is observed above the P3. The infraorbital foramen is large (3.75 mm) and opens approximately in-between the anterior margin of the orbit and the middle of the upper carnassial. The preserved left orbit is large and oval-shaped. The posterior orbital margin is situated approximately at the distal margin of M1. The preserved zygomatic arch rises up in parallel to the M1. The transition from the snout to the rest of the skull is gradual, without a distinct cranial vault and the preserved frontal is flattened. In ventral view, the broken choanae would have extended for at least 2.5 mm behind M1.

P2: The main cusp is oriented slightly towards the mesial direction. A mesial cusp or cingulum projection is absent. In the distal part of P2, the cingulum slightly projects, forming a low, vestigial distal cusp. A mesial-distal oriented crest passes across the main cusp and the distal cingulum projection. A very slight diastema is formed with P3.

P3: Besides its larger size and a few morphological differences, it is similar to P2. The main cusp is more symmetrical than that of P2. A miniscule mesial cingulum is formed. The distal cingulum projection is slightly more developed than P2. A minor imbrication between P3 and P4 is present.

P4: The morphology of the upper carnassial is similar to that of the extant *Martes*. The protocone is low but well-developed and situated mesially of the paracone, approximately at the mesial margin of the carnassial. It is also well-separated from the rest of P4 by a deep valley. An inflated mesial cingulum is observed in place of the undeveloped parastyle. The paracone is larger and higher than the other cusps. The metacone is low, elongated and curves slightly buccally. A mesial-distal concave crest connects the paracone with the metacone. The buccal cingulum near the metacone is strong, while the lingual cingulum distally of the protocone forms a shelf.

M1: The morphology of M1 is similar to that of the extant *Meles* Brisson, 1762. The lingual cingulum is extremely thick and well-developed, which results in the protocone's elevation. The separation of the lingual cingulum and the protocone is marked by a narrow mesio-distally oriented channel. The elevated protocone is elongated along the mesio-distal axis and crescent-shaped. The metaconule is well-separated from both the protocone and the metacone. The paracone and metacone are low-cusped. The buccal cingulum is strong and well-developed.

Discussion: The sub-family systematic allocation of *Promeles palaeattica* has been debated on numerous occasions, as some authors consider it a member of the Melinae (Pilgrim, 1931; Petter, 1971; Ginsburg, 1999; Koufos, 2006a) while others a member of the Mustelinae Fischer von Waldheim, 1817 (Weithofer, 1888; Major, 1902; Thenius, 1949; Schmidt-Kittler, 1995; Morlo, 1997; Roussiakis, 2002). This debate is founded on the morphology of *P. palaeattica*, which exhibits characteristics from both sub-families (e.g., Pilgrim, 1931). For the purpose of this work, it will be considered a Mustelinae.

P. palaeattica has been recognized from the Turolian of Pikermi (e.g., Weithofer, 1888, Roussiakis, 2002), Samos (e.g., Major, 1902, Solounias, 1981), Perivolaki (Koufos, 2006a) and in "Upper Maragha" in Iran (Bernor et al., 1996). Apart from *P. palaeattica*, some early Turolian material under *Promeles sp.* have been reported from MTL-A site in Samos (Koufos, 2006a and references therein) and Dorn-Dürkheim 1 in Germany (Franzen & Strorch, 1975; Morlo, 1997).

Comparison of the specimen in question (Fig. 2) with the figure of the type specimen of *P. palaeattica* provided by Weithofer (1888) shows similar dental morphology. Roussiakis (2002) noted that the morphology of M1 can vary a little, as its distal side is slightly concave in some specimens, while on others, such as the holotype, it is almost straight. Such a trait was not observed in AMPG-PA 4958/91 and in that aspect, it is similar to the holotype. Concerning the metrical values, the most noticeable difference is the length of AMPG-PA 4958/91's M1, which is almost 2.5 mm longer than the average M1 from Pikermi.

Craniodental material of *P. palaeattica* have also been described by Major (1902), Pilgrim (1931) and more recently by Roussiakis (2002) and from Perivolaki by Koufos (2006a). Further morphological and metrical comparisons with these specimens did not reveal any differences of importance. The slightly greater width of the upper carnassial (Table. 3) is close to the approximate value of (7) mm in NHMUK-M. 9029 provided by Pilgrim (1931) and, again, the length of the M1 of AMPG-PA 4958/91 is close to the value of 9.7mm for

LGPUT-PER-1280 provided by Koufos (2006a) (Fig. 8). The calculated robusticity index of AMPG-PA 4958/91 P4 is within the observed range of variation for the species, which ranges between 57.14–73.17, corresponding to NHMUK-M. 9029. (dext) and LGPUT-PER-1280 (sin) respectively.

Besides *P. palaeattica*, the species *Promeles macedonicus* Schmidt-Kittler, 1995, has been recognized from the Turolian/Ruscinian locality of Maramena (Serres Basin, Grece). *P. palaeattica* however, differs from P. *macedonicus* both metrically and morphologically. The M1 of the former is larger than the latter (Fig. 8). The morphological differences are mainly due to the metaconule of M1. As already mentioned above, the protocone and the metaconule in *P. palaeattica* are clearly separated, whereas in *P. macedonicus* they are not. Also, the metaconule in *P. macedonicus* extends labially, something not observed in *P. palaeattica*. The upper carnassial of *P. macedonicus* is primarily morphologically different (Fig. 8). Additionally, its mesial cingulum is not as developed as *P. palaeattica* and its P4 robusticity (77.65–82.93) far exceeds that both of AMPG-PA 4958/91 and other *P. palaeattica* specimens.

In conclusion, the morphology and metrical values of AMPG-PA 4958/91 are similar with other specimens of *P. palaeattica* described from Greece. In addition, its metrical values and proportions are within the expected level of variation for the species and allows its attribution to *Promeles palaeattica*.

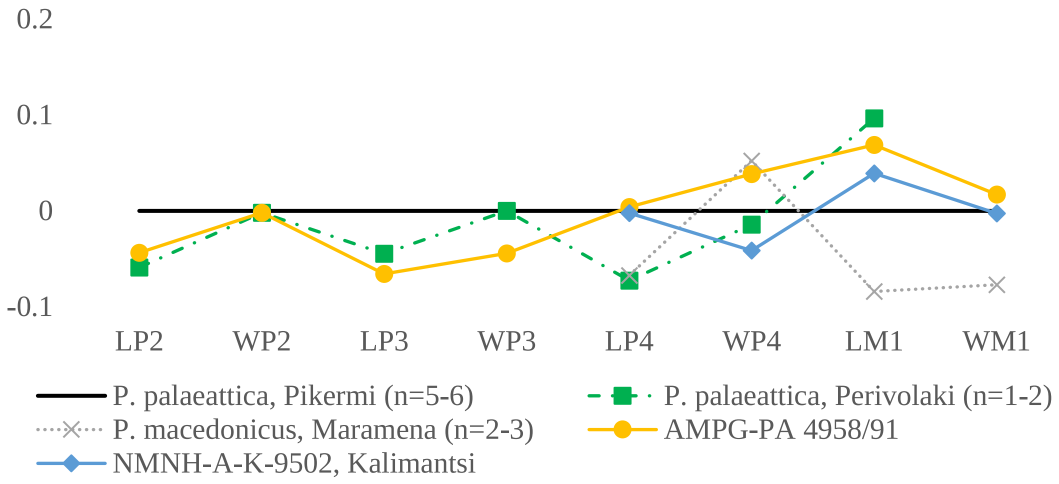

Figure 8. Log-ratio diagram comparing the upper dentition of *Promeles palaeattica*. *P. palaeattica* (n=5–6) from Pikermi was used as standard. Data for *P. palaeattica* were acquired from Roussiakis (2002), Koufos (2006a) and Geraads & Spassov (2016). Data for *P. macedonicus* were acquired from Schmidt-Kittler (1995).

Table 3. Craniodental measurements (mm) of *Promeles palaeattica* from Pikermi and Perivolaki.

	Pikermi							Perivolaki	
	AMPG-PA 4958/91	IPUW-PIK (unnumbered) holotype	NHMUK M. 9028	AMPG-PG 01/105	NHMUK M. 9029 (cast)			LGPUT-PER-1280	
		(Weithofer, 1888)	(Pilgrim, 1931)	(Roussiakis, 2002)			(Major, 1902)	(Koufos, 2006a)	
	sin			dext	dext.	sin		dext	sin
LP2	4.04	4.00	5.00	4.70	4.50	4.30	4.30	3.80	4.00
WP2	2.45	2.50	2.50	2.40	2.50	2.40	—	2.40	2.50
LP3	5.00	6.00	6.50	5.60	5.50	5.30	6.00	5.30	5.20
WP3	3.07	3.30	4.00	3.30	3.20	3.20	—	3.20	3.60
LP4	9.84	9.00	11.00	10.00	9.80	9.50	9.20	8.30	8.20
WaP4	6.49	5.60	(7.00)	(5.90)	5.60	5.60	—	5.50	6.00
HP4	5.10	—	—	—	—	—	—	—	—
LM1	9.10	6.50	9.00	7.90	(7.80)	(7.90)	7.50	—	9.70
WM1	11.51	10.00	13.50	11.30	10.60	10.50	10.50	—	—
L(P2–P4)	19.15	—	—	20.90	19.80	20.30	—	—	—
L(P3/P4)	50.81	66.67	59.09	56.00	56.12	55.79	65.22	63.86	63.41
R.I. P3	61.40	55.00	61.54	58.93	58.18	60.38	—	60.38	69.23
R.I. P4	65.96	62.22	63.64	59.00	57.14	58.95	—	66.27	73.17
Width between postorbital processes (POP)	24.57	—	—	—	—	—	—	—	—

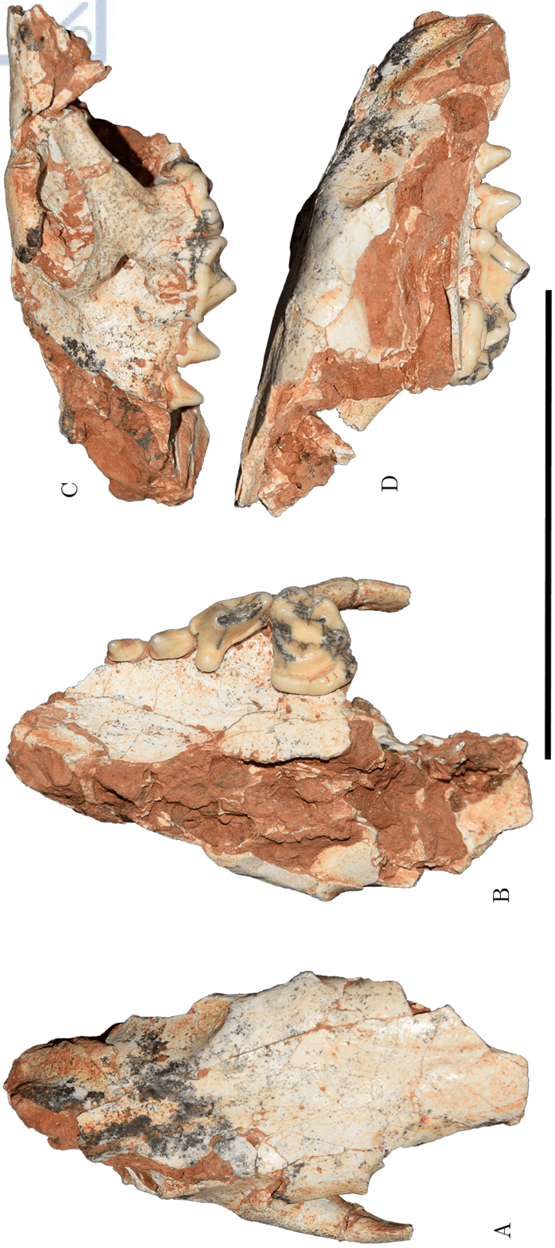

Figure 9. *Promeles palaeattica* AMPG-PA 4958/91 in A: dorsal, B: ventral, C: left and D: right lateral view. Scale bar is 5 cm.

Family Ursidae Fischer de Waldheim, 1817

Extant bears live in almost every continent and are characterized by high intraspecific variability. They are stoutly built, relying more on their brawn rather than agility and speed. Their size varies, from the smaller sun bear to the larger and much heavier polar bear. They are generally plantigrades to semidigitigrades and that is reflected on their postcranial adaptations (Ewer, 1973; Macdonald, 2006). Although most extant bears are omnivorous, the polar bear is carnivorous and the giant panda is herbivorous.

The systematics and phylogeny of Ursidae is in a state of turmoil and has been subjected to many revisions over the years. Morphological and molecular data suggest five extant genera: *Melursus* Meyer, 1793, *Ursus* Linnaeus, 1758, *Helarctos* Horsfield, 1825, *Tremarctos* Gervais, 1855, and *Ailuropoda* Milne-Edwards, 1870. Their fossil record is much richer morphologically and have contributed to the general confusion surrounding their systematics (Erdbrink, 1953; Pacher, 2007). The subfamilies vary from three to five depending on each author's take. More recently, four families have been suggested: Ursinae Fischer de Waldheim, 1817, Ailuropodinae Grevé, 1894, Tremarctinae Merriam & Stock, 1925, and the extinct Agriotheriinae Kretzoi, 1929. (Pappa & Tsoukala, 2022 and references therein).

The evolutionary history of ursids is rather recent compared to other carnivoran families. The first appearance of ursid-like arctoids dates to late Eocene, around 35.7 Ma, where bears diversified from harbor seals. The record of the first true ursid however, dates around 19 Ma with the small-sized *Ursavus* Schlosser, 1899 and *Ballusia* Ginsburg & Morales, 1998. The family eventually diversified and split into two subfamilies, Ursinae and Tremarctinae, around 12.86 Ma. The main radiation of the subfamily Ursinae took place sometime later around 5.39 Ma close to the Miocene/Pliocene boundary and the climate changes that marked that period. The genus *Ursus* first appeared around 5.05 Ma with the small-bodied *Ursus minimus* Devèze and Bouillet, 1827. During the late Pliocene, *Ursus etruscus* Cuvier, 1823 appeared, which gave rise to many other species, often referred to as cave-bears. The climate of the Pleistocene favoured ursids, as many different species have been recognized in their respective deposits (Pappa & Tsoukala, 2022 and references therein).

The Greek fossiliferous record begins in the middle Turolian with only two genera, *Indarctos* Pilgrim, 1913 and *Ursavus*, with scarce remains in a few localities (Samos, Pikermi, Perivolaki, Halmyropotamos) (Pappa & Tsoukala, 2022 and references therein). After a bear gap in the fossiliferous record that lasted from the latest Miocene up until the early Pliocene, bear remains appeared again in various localities (Pappa & Tsoukala, 2022 and references therein). The most notable of them being Loutra Almopias Cave in North Greece and Petralona Cave in Chalkidiki (Pappa & Tsoukala, 2022 and references therein). The presence of bears in Greece continued in palaeolithic sites until the present day with *U. arctos* Linnaeus, 1758 (Pappa & Tsoukala, 2022 and references therein).

Concerning *Ursavus*'s presence in Pikermi specifically, some confusion seems to have been caused in the recent years. Pappa & Tsoukala (2022) mention the presence of a second ursid in Pikermi besides *I. atticus*, *Ursavus* cf. *depereti* Schlosser, 1902, based in reports from Kostopoulos & Vasileiadou (2006) and Koufos et al. (2018a). Indeed, in both of these works, a second ursid from Pikermi, a taxon under *Ursavus* sp. in Kostopoulos & Vasileiadou (2006) and a taxon under *Ursavus* cf. *depereti* in Koufos et al. (2018, Fig. 10), sprung up, probably by mistake. To clarify, such a taxon, or any other ursid besides *I. atticus* for that matter, has not been– as of yet at least – recognized nor has its presence been implied by previous works who discussed Ursidae from Pikermi (e.g., Weithofer, 1888; Roussiakis, 2001a; Koufos, 2011; Roussiakis et al., 2019).

Subfamily Ailuropodinae Grevé, 1894
Tribe Indarctini Abella, Alba et al., 2019
Genus *Indarctos* Pilgrim, 1913
Indarctos atticus (Weithofer, 1888) ex Dames, 1883
(Fig. 10, Table 4)

1883b *Hyaenarctos* sp. Dames, p. 132
1888 *Hyaenarctos atticus* Weithofer, p. 231, Pl. xii, Figs. 1, 2
1926 *Indarctos atticus* Frick, p.88
1931 *Indarctos* (?) cf. *atticus* (Weithofer ex Dames MS), Pilgrim, p.174, Figs. 4, 5
2002 *Indarctos punjabiensis atticus* Weithofer, - Baryshnikov, p. 7, Figs. 1–3

Type species: *Indarctos salmontanus* Pilgrim, 1913, Hasnot, Pakistan, Late Miocene.

Type material: Left mandibular fragment with m1-m2 described and figured by Weithofer (1888: p. 231; pl. 12, figs. 1–2). Stored in the Institute of Palaeontology of the University of Vienna, Austria.

Type locality: Pikermi, Attica, Greece.

Age: Late Miocene, MN 10–13; For the classical locality of Pikermi: Middle Turolian, MN 12, 7.33–7.29 Ma (Böhme et al., 2017).

Localities: Greece: Q1 in Samos Island (Solounias, 1981; Bernor et al., 1996). Ukraine: Ananjev (Baryshnikov, 2002). Spain: Concud, Los Mansuetos, Valdecebro 5, Puente Minero, Terrassa, Crevillente 2, Cerro de la Garrita (Montoya et al., 2001; Pesquero et al., 2013). France: Aubignas. Germany: Dorn Dürkheim 1. Iran: Maraghah. Kazakhstan: Pavlodar, Kalmakpai. China: Lufeng, Songshan, Baode (Baryshnikov & Tleuderdina, 2017 and references therein; Pappa & Tsoukala, 2022 and references therein).

Material: AMPG-PA 4961/91: proximal end of a left radius. (Fig. 10).

Description: The radius is large, robust and preserves the proximal part with its respective epiphysis. The proximal articulation surface is almost entirely flattened and inclines towards the mesial direction. The radial tuberosity is large and well-developed and two muscle attachment areas are evident. The muscles attached there probably refer to the biceps which attaches to the larger area and the supinator longus which attaches to the external tuberosity. A smooth and slightly swollen area separates the two attachment surfaces. The shaft is broken below the radial tuberosity. The visible cross-section of the shaft is crushed and flattened antero-posteriorly.

Discussion: The radius is huge, clearly belonging to a very large individual. Few carnivorans of such size are known from Pikermi. Out of those the Ursidae *Indarctos atticus* seems the most promising. Pilgrim (1931) illustrated and described a left radius under *Indarctos* cf. *atticus*. His description, illustration and measurements fit for the most part the general morphology and measurements of the studied specimen. Some differences, however, do occur. The studied specimen exhibits a much more flattened cross-section due to crushing than the cross-section figured by Pilgrim (1931). Also, Pilgrim (1931) notes a sharp angulation on the dorsal side of the radius. In AMPG-PA 4961/91 such sharp angulation is absent and the dorsal surface is smooth.

More recently, Roussiakis (2001a) published some rare postcranial material from Pikermi belonging to *Indarctos atticus*. Amongst them, there was a right radius. From the description he provided as well as direct comparison with the specimen AMPG-PA 1964/91 it appears that the two radii mirror each other almost perfectly (Fig. 10). Some minor differences noticed concern the slightly less prominent external radial tuberosity of AMPG-PA 4961/91. This is probably due to preservation reasons, as AMPG-PA 1964/91 is far better preserved than AMPG-PA 4961/91. The aforementioned ridge described by Pilgrim (1931) is clearly visible on AMPG-PA 1964/91, however, it is situated in a more distal part of the shaft, which is missing in the studied specimen. Lastly, the crushed and flattened distal shaft of AMPG-PA 4961/91 is made even more evident in the comparison with AMPG-PA 1964/91.

Indarctos consists of moderate to large-sized ursids from the Late Miocene which ranged across North America, Eurasia and northern Africa. The taxonomic state of the genus has been a subject of various revisions (e.g., Petter and Thomas 1986; Kurtén 1976; Ginsburg 1999). *Indarctos atticus* is considered by most authors as the sole representative of the genus that lived during the Turolian in Eurasia (Baryshnikov, 2002 and references therein). It was a relatively large bear, first known from the locality of Pikermi. To this day, material of this taxon–particularly postcranial–from Pikermi remain scarce (e.g., Pilgrim 1931, Roussiakis, 2001a).

The nomenclature and taxonomic history of *I. atticus* is rather complex and has already been covered in greater extent by other authors (Roussiakis, 2001a; Pappa & Tsoukala, 2022). Initially it was described under *Hyaenarctos* sp. Dames, 1883b without being figured. It was Weithofer (1888) who actually described and figured it, placing it under *Hyaenarctos atticus*. Helbing (1932) described the material from Samos and placed it under *Indarctos atticus*. Some years later, the material from Pikermi was transferred by Erdbrink (1953) to *Indarctos atticus*. Baryshnikov, (2002) and Abella et al. (2019) consider *I. atticus* as a subspecies of *I. punjabensis*, while others (Kostopoulos & Vasileiadou, 2006; Koufos et al., 2018a) consider valid its attribution as *I. atticus*. Although the name *I. atticus* is used herein, this issue is considered to be beyond the scope of this study.

Table 4. Radius measurements (mm) of *Indarctos atticus* from Pikermi.

	L	DAPpr.	DTpr.	DAPdia.	DTdia.	DAPdist.	DTdist.
AMPG-PA 4961/91 (sin)	—	41.12	50.35	—	—	—	—
AMPG-PA 1964/91 (dext), (Roussiakis, 2001a)	384.50	38.77	50.70	(26.50)	(37.00)	47.60	70.90
NHMUK-M. 8963 (sin) (Pilgrim, 1931)	381.00	38.50	50.00	—	35.00	—	72.00

Figure 10. *Indarctos atticus* radii from Pikermi. Left: the studied radius AMPG-PA 4961/91 (sin), right: the complete radius AMPG-PA 1964/91 (dext) described by Roussiakis (2001a). A: posterior, B: medial, C: anterior, D: lateral view. E: proximal epiphysis of AMPG-PA 4961/91 (above) and AMPG-PA 1964/91 (below), F: cross-section of the flattened proximal shaft of AMPG-4961/91 (above) compared to Pilgrim's (1931) sub-triangular cross-section of the shaft with the characteristic ridge in its lateral side (below). Scale is 5 cm.

Suborder Feliformia Kretzoi, 1945

Family Hyaenidae Gray, 1869

The family Hyaenidae belongs to the larger Viverroidea Gray, 1821 superfamily along with the extant families of Felidae, Viverridae Gray, 1821 and Herpestidae Bonaparte, 1845 (Werdelin & Solounias 1991). Today, the family of Hyaenidae is rather small with only four living genera that are geographically confined in parts of Asia and Africa (de Bonis et al. 2010). The extant species consist of *Hyaena hyaena* Linnaeus, 1758 (striped hyaena), *Crocuta crocuta* Erxleben, 1777 (spotted hyaena), *Parahyaena brunnea* Thunberg, 1820 (brown hyaena), which are either scavengers and hunters, and the small *Proteles cristata* Sparrman, 1783 (aardwolf), which is an insectivore (de Bonis et al. 2010). Extant hyaenas have longer forelimbs than hindlimbs, are digitigrades with non-retractile claws and with the exception of the simple dentition of *P. cristata*, the rest have bone-crunching adaptations (Myers, 2000). Furthermore, their third incisor is larger and more canine-like (Myers, 2000).

Contrasting today's small family size, Hyaenidae of the past were an abundant and diverse family of both size and morphology that often enough didn't resemble a 'hyaena' in today's sense of the word (Werdelin & Solounias, 1991). They consisted of more than 60 different species that ranged across the Old World and North America and filled many different ecological niches (Werdelin & Solounias, 1991; Werdelin & Solounias, 1996; Tseng et al., 2019). The family's origins are estimated around 17–18 Ma in MN 4, during the Early Miocene of Eurasia (Turner et al., 2008). Their migration to Africa didn't occur until the Middle Miocene (de Bonis et al., 2010) and on North America until ~4.7 Ma (Tseng et al., 2019).

Early hyaenids like *Protictitherium* Kretzoi, 1938 and *Plioviverrops* Kretzoi, 1938, were small civet- and mongoose-like insectivores and omnivores that, in the case of the former, still retained some climbing abilities and had retractable claws (Werdelin & Solounias 1991; Werdelin & Solounias, 1996; Turner et al., 2008). During MN 7–9 the family started to diversify with generalized bone and meat eaters of medium size like *Thalassictis* Nordmann, 1850, *Ictitherium* Wagner, 1848, and *Hyaenictitherium* Kretzoi, 1938 (Werdelin & Solounias, 1991). These forms will continue to diversify and disperse in Eurasia and Africa until their peak in Turolian (Werdelin & Solounias, 1991). During the Middle–Late Miocene, a rapid diversification (Ferretti 2007 and references therein) led to the emergence of larger and more specialized Hyaenidae like the cursorial *Chasmaporthetes* Hay, 1921 and the bone cracking *Adcrocuta* Kretzoi, 1938 (Werdelin & Solounias, 1991; Turner et al., 2008). The turnover of the terrestrial faunas of the Old World during the Miocene/Pliocene boundary eventually led to the decline of the smaller and non-specialized forms (Werdelin & Solounias, 1991; Ferretti, 2007 and references therein; Turner et al. 2008). The sole survivor from that group today is the aardwolf (Werdelin & Solounias, 1991). The surviving hyaenids diversified with a more specialized group of scavengers and bone-crackers, such as *Pliocrocuta perrieri* Kretzoi, 1938 and later the gigantic *Pachycrocuta brevirostris* (Gervais, 1850) (Turner et al., 2008), that lasted well into the Pleistocene (Werdelin & Solounias, 1991). A second and final turnover event that took place in the Middle Pleistocene wiped out the other hyaenas except the extant *Crocuta crocuta* (Turner et al., 2008).

The Greek fossiliferous record is rich in hyaenid remains and they constitute one of the most common carnivoran remains. Several publications from various Greek localities have been made since the 19th century and continues so to the present day (e.g., Gaudry 1862–1867; Melentis, 1967; Koufos, 2011; 2022c). The earliest hyaenid record in Greece is recorded in the Early/Middle Miocene locality of Antonios in Chalkidiki and is attributed to the genus *Protictitherium* (Koufos, 2008). The Late Miocene record of Greek hyaenids is extremely rich and diverse, with many different forms (e.g., *Pliovivverops*, *Ictitherium*, *Adcrocuta*). The Pliocene record is scarce, while the Pleistocene is dominated with large forms like *Pachycrocuta* Kretzoi, 1938, and *Crocuta* Kaup, 1828, that often lived in caves and have been associated with bone accumulations (e.g., Tsoukala, 1989).

Subfamily Ictitheriinae Trouessart, 1897

Genus *Ictitherium* Roth & Wagner, 1854

Ictitherium viverrinum Roth & Wagner, 1854

(Figs. 11–34, Tables 5–7)

1840 *Galeotherium* gen. nov. Wagner, p. 165, Pl. I, Figs. 4–6.
1848 *Ictitherium* gen. nov. Wagner, p. 375.
1854 *Ictitherium viverrinum* sp. nov. Roth & Wagner, p. 392, Pl. 2, Figs. 3–5.
1856 *Thalassictis robusta* von Nordmann - Gaudry & Lartet, p. 271.
1862–67 *Ictitherium robustum* von Nordmann - Gaudry, p. 52, Pls. 7–10.
1862 *Thalassictis gracilis* sp. nov. Hensel, p. 566–567, Fig. 5.
1862 *Thalassictis viverrina* (Roth & Wagner) - Hensel, p. 566, Fig. 4.
1924 *Ictitherium gaudryi* sp. nov. Zdansky, p. 67, Fig. 3, Pl. 12, Figs. 5–6; Pl. 13, Figs. 1–6.
1924 *Ictitherium sinense* sp. nov. Zdansky, p. 72, Pl. 14, Figs. 1–2.
1929 *Ictitherium robustum* Gaudry - Arambourg & Piveteau, p. 65, Pl. 10, Fig. 1.
1938 *Palhyaena? gaudryi* Zdansky - Kretzoi, p. 113.
1938 *Sinictitherium sinense* n. g. Kretzoi, p. 114.
1980 *Ictitherium robustum* Gaudry - Koufos, p. 41, Pl. 4, Figs. 2–3; Pl. 5, Figs. l–4.

Type species: *Ictitherium viverrinum* Roth & Wagner, 1854.

Type locality: Pikermi, Attica, Greece.

Type material: SNSB-BSPG-PIK-AS II.66 (holotype); right mandibular fragment with p2–m1 and left mandibular fragment with c–p4 described and figured by by Roth and Wagner (1854:49; Table 8, figs 3, 5). Stored in the Bayerische Staatssammlung für paläontologie und Geologie, Munich, Germany.

Age: Vallesian–Turolian, MN 9–13 (Turner et al., 2008). For the classical locality of Pikermi: Middle Turolian, MN 12, 7.33–7.29 Ma (Böhme et al., 2017).

Localities: Greece: Ravin des Zouaves 5, Prochoma 1 (Koufos 2000) and Vathylakkos 3 (Arambourg & Piveteau, 1929) in Axios Valley; ?Kryopigi in Chalkidiki (Lazaridis, 2015); Q1 and A in Samos Island (Solounias, 1981). Austria: Vösendorf. France: Montredon. North Macedonia: Titov Veles. Iran: Upper Maragheh. Moldova: Chobruchi. Ukraine: Grebeniki, Belka and Novaya Emetovka. Slovakia: Borský Svätý Jur. China: Chen Chia Mao Kou (Zdansky's Loc. 108), Chen Kou, Huan Lou Kou (Zdansky's Loc. 109), Chin Kou, Loc. 31, Loc. 12, Chou Chia Kou, Liao Wan Kou, Van Mu Kou (Zdansky's Loc. 49), Nan Ho, Ta Tung Kou and Loc. 42 (Werdelin & Solounias, 1991; Sabol & Holec 2002; Anderson & Werdelin, 2005; Turner et al., 2008).

Material: AMPG-PG 01/122: almost complete cranium with P2-P3-P4-M1-M2, AMPG-PG 01/120: almost complete cranium with P3-P4-M2-M1, AMPG-PG 01/119: partially preserved skull with C-P2-P3-P4-M1, AMPG-PA 3716/91: partially preserved skull with P1-P2-P3-P4-M1-M2, AMPG-PA 3710/91: partially preserved skull with C-P3-P4-M2-

M1, AMPG-PA 3715/91: partially preserved skull with C-P1-P2-P3-P4-M1(partially)-M2(partially), AMPG-PA 3717/91: partially preserved skull with P2-P3-P4-M1-M2, AMPG-PA 3719/91: maxillary fragment with P2-P3-P4-M1, AMPG-PA 3720/91: maxillary fragment with P2-P3-P4 (partially)-M1(partially), AMPG-PA 3714/91: maxillary fragment with P2-P3-P4, AMPG-PA 4956/91: maxillary fragment with P2-P3-P4, AMPG-PA 4957/91: isolated M2 (dext), AMPG-PG 01/121: anterior part of a laterally crushed skull with associated mandible in anatomical position with I3/3-C1/1-P1-P2/2-P3/3-P4/4-M1, AMPG-PG 01/115: anterior part of a laterally crushed skull with associated mandible in anatomical position with I1-I2/2-I3/3-C1/1-P1-P2/2-P3/3-P4/4-M1/1-M2/2, AMPG-PA 3713/91: left hemimandible with p2-p3-p4-m1, AMPG-PA 3710/91: right hemimandible with p2-p3-p4-m1, AMPG-PA 3712/91: right hemimandible fragment with p2-p3-p4, AMPG-PG 01/123: almost complete mandible with ramus with c-p2-p3-p4-m1-m2. (Figs. 16–33).

Remarks: Mandible AMPG-PG 01/123 might be associated with the cranium AMPG-PG 01/122, but since they are from the old collections and deformations are in place in both specimens, it is not possible to make more certain assessments (Fig. 34).

Description: Cranium: The cranial morphology is primarily based on the slightly deformed but otherwise preserved AMPG-PG 01/120 and AMPG-PG 01/122. The partially preserved sphenoid-shaped nasal bones end at the anterior orbit margin. The nasal cavity is not preserved in most specimens; however, an elliptical-shaped cavity can be observed in AMPG-PA 3716/91 and AMPG-PA 3715/91 which inclines towards the posterior when viewed from the lateral side. The elliptical infraorbital foramen opens approximately at the distal end of P3. The orbital sockets are elliptical with their anterior border situated above the P4. The postorbital process is strong and approximately situated above the distal margin of M2. The sagittal crest is more prominent in the posterior part of the neurocranium and connects to a well-developed nuchal crest. The zygomatic arch strongly projects laterally and is relatively robust. The concavity that forms posteriorly of the zygomatic arch is relatively deep. The cranial vault is moderate, however, due to deformations its shape is probably not as prominent as it would have originally been. Nevertheless, its cross-section would probably be more rounded than triangular. The palate is moderately elongated and wide, reaching its maximum width at the distal part of the carnassial. The choanae are not clearly discerned, however, they appear deep and large, with their anterior margin located more distally than the distal end of the M2. The auditory bullae are oval-shaped and large and their posterior margins are rather flat. Their anterior border approximates to the posterior border of the postglenoid process. The supraoccipital crest is well defined. The presence or absence of an alisphenoid canal could not be confirmed due to the material's preservation status.

Upper dentition: The premolars are for the most part relatively straight with minor imbrication in some specimens. The angle formed between the upper carnassial and M1 ranges from 51^{o}–67^{o} (Fig. 5).

I: Besides alveoli, incisors are preserved in a few specimens only (AMPG-PG 01/115, AMPG-PG 01/121 and a partially preserved I3 on AMPG-PG 01/122). They are relatively small, single-rooted and rounded. I1 (approximately 3×3mm) is smaller than I2 (approximately 4×3.5mm) which in turn is smaller than the more canine-like I3 (approximately 4.7×3.85mm).

They are labially convex and their cingulum projects strongly in their distal side. A slight crest is formed bucco-lingually.

C: The canine is elliptical in cross-section and relatively long. Close to the root it exhibits a mesial inclination, while the rest of its crown slightly curves distally. A crest forms in the mesio-lingual to distal direction. The more robust base of the crown progressively narrows down a lot towards its tip. The diastema between the canine and I3 is small.

P1: It is a small, single-rooted, and single-cusped tooth. The lingual cingulum projects relatively strongly. A crest passes across the cusp in a mesio-distal direction. Small diastemata form between P1 and the canines and between P1 and P2.

P2: The mesial cusp is absent; some specimens however exhibit a slight swelling of their mesial cingulum. A small and low distal cusp is present. Its development varies from weak (AMPG-PA 3716/91, AMPG-PA 3715/91, AMPG-PA 3714/91) to strong (AMPG-PG01/122) to almost entirely absent (AMPG-PA 3720/91). The cingulum is strong around the tooth and especially so in the lingual side, where it also slightly expands lingually between the main and the distal cusps. AMPG-PA 3716/91 forms a small diastema of approximately 1 mm between P2 and P3.

P3: Morphologically similar with P2, albeit larger and more robust. A rudimentary mesial cusp is present in some specimens (AMPG-PG 01/115, AMPG-PA 3714/91, AMPG-PG 01/120), although most simply exhibit a slight cingulum inflation instead. The cingulum is strong around the tooth, but more so in the lingual side. The distal cusp is better developed than P2. A crest passes across the cusps in a mesio-lingual to distal direction.

P4: The protocone is large, well separated from the smaller parastyle and situated either mesially or at the level of the parastyle. The protocone is connected to the parastyle with a crest in the mesial part of the tooth. In a few specimens (AMPG-PA 3714/91, AMPG-PG 01/122, AMPG-PG 01/120) where the wearing isn’t extensive a crest can be discerned which connects the valley of the protocone to the paracone. A third crest situated in the buccal side of the protocone connects the protocone with the strong cingulum (shelf) of the lingual side. The parastyle connects to the paracone through a crest, which passes across the parastyle’s cusp. The paracone’s cusp is situated higher than the rest. The paracone inclines slightly distally and its mesial half is more elongated than its distal. The metastyle blade is elongated and curves slightly buccally towards the distal part of the tooth. The lingual and buccal margins of P4 are tapered towards the distal end of the tooth. The cingulum is strong all around the tooth, but especially so in the lingual side where it forms a shelf. Specifically, AMPG-PG 01/120 has an exceptionally strong cingulum on the P4 not observed in the rest of the specimens.

M1: The crown is triangular in occlusal view. The protocone is prominent with an especially strong cingulum. A crest connects the protocone, metacone and paracone. A valley is formed in the middle of the tooth. The paracone is situated higher than the rest of the cusps. Towards the distal part, the crest lowers and the valley opens up a little. The cingulum is strong all around the tooth. AMPG-PG 01/122 has an exceptionally large M1.

M2: Approximately 66.29% of M1’s length and has a round to elliptical shaped crown. A valley is formed between the cusps. A crest connects peripherally the protocone, paracone and metacone. The cingulum is strong all around and especially so near the protocone. Towards the distal part of the tooth, to tooth opens up a little. The cusps are approximately the same height.

Mandible: The mandibular corpus is of moderate height. Its mental edge is rounded. The corpus's ventral margin is convex. The maximum height of the corpus is observed close to the distal end of m1 and progressively narrows down towards the symphysis. Two mental foramina are present below p2 and p3 respectively. The ascending ramus is relatively high. The inferior part of the mandible continues almost in a straight line to the angular process, while the upper part ascends after the distal end of m2. The coronoid process and the angular process connect almost in a 90^o angle. The condylar process is wide and well-developed, protruding in the distal part of the ramus. The masseteric fossa is oval-shaped and deep.

i: Only specimen AMPG-PG 01/115 preserves the lower incisors i2-i3. They are single-rooted and monocuspid. The i3 is the largest of the incisor. Also, the cingulum projects slightly in their distal side.

c: The canine is strong, sharp and elliptical shaped in its cross section. A slight cingulum projection is discerned mesio-lingually in the middle of the canine length. It curves distally and bends slightly towards the buccal side.

p1: It is only present on the specimen AMPG-PG 01/115 (dext). It is a small and almost round tooth in cross-section. It is single-rooted and monocuspid. A slight projection of the cingulum is evident on the lingual side of the tooth. A crest passes across the cuspid in an mesio-lingual direction. Although a diastema is evident both from the lower canine to the alveolus of p1 and from it to p2 in AMPG-PG 01/123, in specimen AMPG-PG 01/115 only a diastema from the lower canine to p1 is observed.

p2: It is double-rooted, lacks a mesial cuspid and has a small distal cuspid which is situated atop a slight projection of the cingulum in the distal part of the tooth. A slight crest passes through the main cuspid in a mesio-lingual direction.

p3: Similar in morphology with p2, but overall larger. The mesial cuspid is absent as well, although the cingulum in the mesial part of the tooth is slightly more prominent. The distal cuspid is situated atop a slight projection of the cingulum in the distal part of the tooth.

p4: Similar to p3 but larger and more robust. A small mesial cuspid is observed. The distal cuspid is individualized and high, resembling a talonid.

m1: The lower carnassial is the largest tooth of the lower dentition. The paraconid is low, while the metaconid and the protoconid are almost of the same height in AMPG-PA 3713/91 and AMPG-PA 3710/91. In AMPG-PG 01/123 and AMPG-PG 01/115 (dext) the metaconid is approximately half the protoconid's height. The talonid is long, approximately 36.23% of the carnassial's total length and broad. It has three distinct cuspids, out of which the entoconid is the largest. The talonid's three cuspids, along with the protoconid and metaconid, encircle a gently convex area. The lower carnassial's maximum width is in-between the talonid and trigonid. The buccal and lingual cingulum of the trigonid is strong.

m2: Preserved in specimens AMPG-PG 01/115 (dext) and AMPG-PG 01/123. It is small, approximately 47.28% of m1's length, and elliptical shaped in occlusal view, with a basin in the centre of the crown. Peripherally, four cuspids are discerned, out of which the metaconid end entoconid are the largest. Lingually and in-between the metaconid and the entoconid the basin opens up.

Discussion: The type-species of the genus, *I. viverrinum* Roth & Wagner, 1854, was erected on the basis of material from Pikermi, Greece. This taxon is marked by its long and complex taxonomic and nomenclature history, already discussed in length by other authors (e.g., Werdelin & Solounias, 1991; Koufos, 2021). Therefore, only a brief recap will be given here. Initially, the material from Pikermi was described by Wagner (1840) under the name *Galeotherium* gen. nov. Though, unbeknownst to Wagner, this name had already been claimed by von Jäger (1839). Thus, in turn, Wagner (1848) proposed the name of *Ictitherium* gen. nov., without however, setting a genotype. It wasn't until 1854 that Roth & Wagner proposed the name *Ictitherium viverrinum* for the Pikermi material, which is considered to this day the type species of the genus. Unfortunately, the taxonomic and nomenclature confusion regarding *I. vivverinum*, did not end there. Gaudry & Lartet (1856) synonymized the material from Pikermi with *Thalassictis robusta* Gervais 1850, *ex* Von Nordmann, MS from Kishinev, Moldova, placing both taxa under *"Ictitherium robustum"* (Werdelin & Solounias, 1991; Turner et al., 2008; Koufos, 2021). This association was not met unanimously however, neither by Von Nordmann (Koufos, 2021 and references therein) nor later scientists such as Crusafont Pairó & Petter (1969). As the years went by, more authors started to use the name *"Ictitherium robustum"* as an umbrella term for medium sized hyaenids (Werdelin & Solounias, 1991), perpetuating the confusion. More recent studies (Solounias 1981; Kurtén 1982; Werdelin, 1988a, b; Werdelin & Solounias, 1991; Semenov, 2008) showed that material from Pikermi and the material from Kishinev differ substantially and belong to hyaenids of different morphology and phylogeny. Through some of these works, it occurred that many of the European material described under *"I. robustum"*, actually belonged to neither of those genera, but on a third, far more common in the Turolian localities, *Hyaenictitherium wongii* (Werdelin & Solounias, 1991).

The material in study exhibits similar morphology, and along with its fairly coherent size, its attribution to a single species is considered appropriate. Furthermore, based on its described morphology, size (Table 6) and diagnostic characters provided by Kurtén (1982), Semenov (1989; 2008) and recently summarized by Koufos (2021), the material herein seems to indicate a closer affinity with *I. viverrinum* rather than *Thalassictis* and Hyaenotheriini Semenov, 1989. Therefore, a direct comparison between the material with other *I. viverrinum* specimens from Pikermi as well as from other localities shall be considered first.

The sample size of the material's upper dentition is quite large and although some variation in size is present, overall, it is fairly homogeneous (Fig. 11). Compared to the mean values of *I. viverrinum* from Pikermi provided by Werdelin (1988b) that were used as reference, the bulk of the material belonged to smaller individuals, as evidenced by their premolars (Fig. 11, 12). The molars on the other hand average closer to the reference's mean values (Fig. 12). This may simply be an artifact though, as the sample size of the studied material's molars are smaller (n≈10) than the sample size for the premolars (n≈15–20). An interesting exception to this trend is the markedly large molars on some specimens, namely the length of M1 and width of M2 on AMPG-PG 01/122 and the length of M1 on AMPG-PA 3719/91. It is worth keeping in mind though, that the cranium of AMPG-PG 01/122 is also quite large compared to some specimens of this study and its whole dentition seems to generally average close to or above the mean values of the reference material. Further comparison between their mean values and indexes (Table 6) did not show any particular discrepancies other than exemplifying their similarities. Individually, some outlying metrical and index values were noted, however, they are considered to be within the range of individual variation for the species. Lastly, the angle formed between the upper carnassial and M1 (51°–67°) (Fig. 15) is within the observed range of *I. viverrinum* provided by Semenov (1989) (45°–68°) and Koufos (2021) (52°–65°).

The lower dentition of the material herein is more homogeneous than the upper dentition (Fig. 13). Complementing the upper dentition, it also ranges close to or below the lowest observed values of the *I. viverrinum* from Pikermi by Werdelin (1988b) that was used as a reference. Further comparison between their mean values only made the material's smaller size more evident with the exception of m2 (Fig. 13, Table 7). Nevertheless, comparison of their dental indexes showed remarkable similarities in their proportions, both individually and as a sample.

Besides Pikermi, *I. viverrinum* has been identified in other Greek but also foreign localities:

From the Valley of Axios: Koufos (2021) comments that the Axios material exhibits slightly larger upper dentition in its P1-M1 than the Pikermi material. This also extends to the material in this study, with the exception of M1 which seem to average on approximately similar sizes (Fig. 11–12). The lower dentition of Axios material seems to be only slightly larger than the material of this study, but close to the reference sample (Fig. 13–14).

From the locality of Kryopigi: The material was initially attributed to *Hyaenictitherium wongii* by Lazaridis (2015), but later transferred to *I. viverrinum* (Koufos, 2021; 2022c). The metric values of its upper dentition are slightly larger than the mean values of the studied specimens, but they are similar to the mean values of *I. viverrinum* from Pikermi provided by Werdelin (1988b). In spite of that, a couple of differences were noticed though. The metastyle blade and paracone of the upper carnassial are more elongated and M1 is slightly reduced relatively to both the reference *I. viverrinum* sample and the studied material. Its lower dentition is similarly slightly larger than the mean values of the specimens in study, but the premolars and m1 are within the observed range of variation in Werdelin's (1988b) sample of *I. viverrinum* from Pikermi. The trigonid in the sample of Kryopigi is slightly more elongated and more importantly, its m2 is reduced. Considering that a similar trait is also exhibited by *H. wongii* from Samos (Werdelin, 1988a) (Fig. 12, 14) and strictly based on the metrical values and dental log-ratios, its initial allocation to *H. wongii* might have been more correct.

From Black Sea localities of Grebeniki, Novaya Emetovka and Belka: These are larger than the forms from Pikermi and China, with the ones from Grebeniki being the largest (Fig. 11–14). The latter's larger size has been hypothesized to correlate with the slightly older age of the fauna (Vallesian, MN 10) (Vangengeim & Tesakov, 2013; Koufos, 2021). Interestingly, the larger upper molars mentioned in AMPG-PG 01/122 and AMPG-PA 3719/91 are similar to those from Grebeniki and Novaya Emetovka provided by Semenov (1989). Unlike the overall larger size of the Black Sea's specimens however, the rest of AMPG-PG 01/122 and AMPG-PA 3719/91 dentition are more similar to the samples from China and Pikermi. The lower dentition from the locality of Grebeniki (Fig. 13–14) is also generally larger than from both the material of this study and the reference *I. viverrinum* sample. Even so, the mean values from the Novaya Emetovka material are metrically close to the mean values of the studied material.

From various localities in China: They are generally similar to the forms from Pikermi (Fig. 11–14) and compare with the studied material similarly. They exhibit a greater degree of size variation though, which is probably explained either as an effect of their larger sample size or due to Werdelin's (1988b) merge of specimens from different localities.

Besides the type species, other species of *Ictitherium* have been erected, synonymized or been associated in the past with the genus. Following, dental comparisons will be made between the studied material and some of these taxa.

Ictitherium gaudryi Zdansky, 1924 and *Ictitherium sinense* Zdansky, 1924: Some authors (Kretzoi, 1938; Solounias, 1981; Semenov, 1989) considered *I. sinense* a separate species from *I. viverrinum*, while others (Bakr, 1959; Werdelin, 1988b; Werdelin & Solounias, 1991) consider it simply an aberrant of *Ictitherium gaudryi*, which in turn is considered conspecific with *I. viverrinum* (Werdelin & Solounias, 1991; Semenov, 2008). Concerning this study, the dental comparison for both *I. gaudryi* and *I. sinense* (Fig. 12, 14) showed that they are either well within or close to the maximum values of the reference material from Pikermi, while being slightly larger than the material in study. It is worth noting though, that the P4 of *I. sinense* is approximately more robust (69.04%) than *I. viverrinum* from Pikermi (57.96% for the reference material), and *I. gaudry*'s m2 is reduced in a way similar to *H. wongii* from Samos and the material from Kryopigi.

Ictitherium tauricum Borissiak, 1915: This taxon was erected from material of the Vallesian locality of Sebastopol in Ukraine (Borissiak, 1915; Vangengeim & Tesakov, 2013). It has also been referred to from the Turolian locality of Küçükyozgat in Turkey, initially as *I. robustum anatolicum*, but it was later synonymized with *I. tauricum* by de Bonis (2004). Some authors (e.g., Semenov, 1989; Morlo et al., 2019) synonymized *I. tauricum* with *Protictitherium crassum* Depéret, 1982. Their claim was based on its smaller dental dimensions compared to *I. viverrinum*. Despite that, Werdelin & Solounias (1991) kept *I. tauricum* within the genus of *Ictitherium*, acknowledging however the similarities with *P. crassum* pointed out by the aforementioned authors. Koufos (2021) notes that the limited material does not suffice for a more certain attribution as it could be very well belonged either to a small *I. viverrinum* or a large *P. crassum*. Concerning this study, its upper premolars are smaller than the reference *I. viverrinum* from Pikermi and close only to the lower-most observed values of the studied material (Fig. 12). The only exception would be the length of its upper carnassial that seems to be close to the mean values of the reference material (Fig. 12). The upper M1 is slightly narrower than the *I. viverrinum* from Pikermi but within the range of variation observed for the material herein (Fig. 12). The lower dentition is mostly below the lowest observed values for the Pikermi material and only close to the minimal observed values for the material in question (Fig. 14). The only exception would be its p3 which is metrically close to the mean values of the material in study (Fig. 14).

Ictitherium ibericum Meladze, 1967: This rather poorly known taxon was erected from the late Turolian locality of Bazalethi in Georgia (Koufos, 2021). Werdelin & Solounias (1991) consider it a member of *Ictitherium* based on the larger upper molars and m2. The less mesially projected protocone of *I. ibericum* was regarded by Semenov (1989) a distinguishing character from *I. viverrinum*. On a later publication however, Semenov (2008) associated it with *I. viverrinum*. NOW (2022) database synonymizes it with *I. viverrinum*. Concerning this study, its upper dentition (Fig. 12) is close to the maximal observed values of the reference *I. viverrinum* from Pikermi and larger from the studied specimens. Its lower dentition (Fig. 14) is closer to the mean values of the reference sample and either within or close to the maximal observed range of variation for the studied sample. Contrasting to *I. viverrinum* though, the trigonid of *I. ibericum* is more elongated relative to its m1, taking up approximately 74.70% of its m1's total length, whereas in the former taxon it takes up approximately 66.28–64.25% (reference and studied samples respectively).

Ictitherium pannonicum Kretzoi, 1952: This taxon was initially erected from the late Turolian of Polgárdi in Hungary as *Palhyaena hungarica* Kretzoi, 1938. Later, Semenov (1985; 1989) added more material from the early Turolian site of Novaya Emetovka 2 in Ukraine and from the middle Turolian of Chiobruchi in Moldova. Werdelin & Solounias (1991) note that even though it lacks any distinguishable characters from *I. viverrinum*, its markedly larger size justifies the validity of this taxon (Figs. 12, 14). The dental proportions of *I. pannonicum* are also similar to that of *I. viverrinum* aside from its mildly elongated m1 trigonid.

"Ictitherium" adroveri Crusafont Pairó & Petter, 1969: This taxon was erected from the middle Turolian (MN 12–13) of Arquillo and Los Mansuetos in Spain on the basis of two isolated P4 (Turner et al., 2008). Werdelin & Solounias (1991) considered this taxon a *nomen dubium*. Later, Alcalá (1994), associated this taxon with *Hyaenicitherium wongii*.

Ictitherium kurténi Werdelin, 1988b: initially erected by Werdelin (1988b) based on material from the Turolian (MN 12) locality of Chang Chia Chuang in China. According to Werdelin (1988b) and Werdelin & Solounias (1991) it differs from other *Ictitherium* species and taxa compared here by its greatly enlarged P3 and its broad WblP4 value (Fig. 12).

"Ictitherium" intuberculatum Ozansoy, 1965: erected from the Vallesian (MN 9–10), locality of Yassıören in Turkey. Werdelin & Solounias (1991) note that it could be conspecific with *I. pannonicum* as it is close metrically, although some minor differences with M1 and m2 do exist. Viranta & Werdelin (2003) and Koufos et al. (2018b) have since described some additional material from this species. De Bonis (2004) and Koufos et al. (2018b) attribute this species to *Hyaenictitherium inturbeculatum*, on the basis of its dental metric values and the angle formed between the carnassial and M1, while Semenov (2008) considers it a synonym of *I. viverrinum*. Further comparison with the material in study showed that its upper dentition (Fig. 12) is larger and approximates above the maximum range observed for *I. viverrinum* from other localities. Interestingly, the single available M2 of *"I. intuberculatum"* is greatly reduced in its width. Contrasting its upper dentition's pattern, its lower dentition (Fig. 14) is overall large and approximates that of the large *I. pannonicum* and thus differs with the studied sample in a similar way.

"Thalassictis" sarmatica Pavlow, 1908: initially erected based on material from the Vallesian locality of Kishinev in Moldova. Semenov (1989; 2008) associated the material with *Thalassictis robusta*. Werdelin & Solounias (1991) consider it a separate species on the basis of its narrower premolars placing it under *"Thalassictis" sarmatica* while also noting that it differs from other *Ictitherium* species. Koufos (2021) lists it under *Ictitherium sarmaticum* stating that on NOW database (2020) it has been moved to *I. viverrinum* by Werdelin. However, presently (2022), the database lists it under *Thalassictis sarmatica* with no previous reference history or association with *Ictitherium*. Concerning this study, further comparison (Figs. 12, 14) showed that the metric values of its upper and lower dentition are close both to the studied specimens and the *I. viverrinum* from Pikermi, however the greatly reduced M2 and slightly elongated trigonid on m1 set it apart.

“Thalassictis” spelaea Semenov, 1988: it was initially erected under *Ictitherium spelaeum* on the basis of material from the Vallesian locality (MN 9) of Gritsev in Ukraine. Werdelin & Solounias (1991) argued the initial attribution of this taxon due to the angle formed between its P4 and M1, the metastyle wing reduction on M1 and the reduction of M1-2. According to these authors, those characters indicate a closer affinity to *“Thalassictis”* and *Hyaenictitherium* rather than *Ictitherium*. They also make a note that it may be conspecific with *T. robusta*. Semenov (2008) however, does not agree with this assessment, standing by his initial attribution in *Ictitherium*. As far as this study is concerned, its upper dentition (Fig. 12) indeed indicates a reduction in M2 compared to other *Ictitherium sp.*, which is only observed in *H. wongii* from Samos, *“Th.” sarmatica* and *I. ebu*. Its lower dentition (Fig. 14) differs from *I. viverrinum* and the studied material primarily by the reduced m2, which is, again, only observed in *H. wongii* from Samos and the material from Kryopigi, and its elongated trigonid on the m1 (74.15%) which resembles the proportions of *I. pannonicum*.

Ictitherium ebu Werdelin, 2003: it was erected on the basis of material from the Mio-Pliocene locality of Lothagam in Kenya. According to Werdelin (2003) it is a more cursorially adapted *Ictitherium* with longer and more gracile limbs. The premolars are elongated and slenderer, while the upper and lower molars are slightly reduced. The lower carnassial’s talonid is also reduced. Semenov (2008) argues its attribution in *Ictitherium* on the basis of both craniodental and postcranial material, suggesting a closer affinity with *Hyaenictitherium*. Concerning this study, the upper dentition differs from *I. viverrinum* and studied material by its larger size, especially so at the length of its paracone which is similar to *H. wongii* from Samos and the material from Kryopigi. Likewise, its M2 is also reduced in a similar way with the aforementioned taxa. Likewise, its lower dentition is also large (Fig. 14), although its m1 is within the observed range of variation for *I. viverrinum* from Pikermi. Its elongated trigonid however, resembles that that of *H. wongii* from Samos.

Concluding, the morphology of the craniodental material along with the metrical analysis performed and the indexes calculated (Figs. 11–14, Tables 5–7) lie in accordance with the information for *I. viverrinum* provided in literature. On this basis, the material is thus attributed to that species. As already discussed above, the generally lower values along with a few outliers are within the expected range of intraspecific variation for the species. On the contrary, the relatively low sample size of *I. viverrinum* from Pikermi provided by Werdelin (1988b) might further highlight this difference. This effect actually clarifies when one examines the great range of intraspecific variation exhibited by the larger *I. viverrinum* populations from China (Werdelin, 1988b; Anderson & Werdelin, 2005). To that end, the attribution of the material will hopefully serve to expand the known range of intraspecific variation for the *I. viverrinum* from Pikermi. Whether this variation is caused by sexual dimorphism or due to other reasons however, is yet to be known.

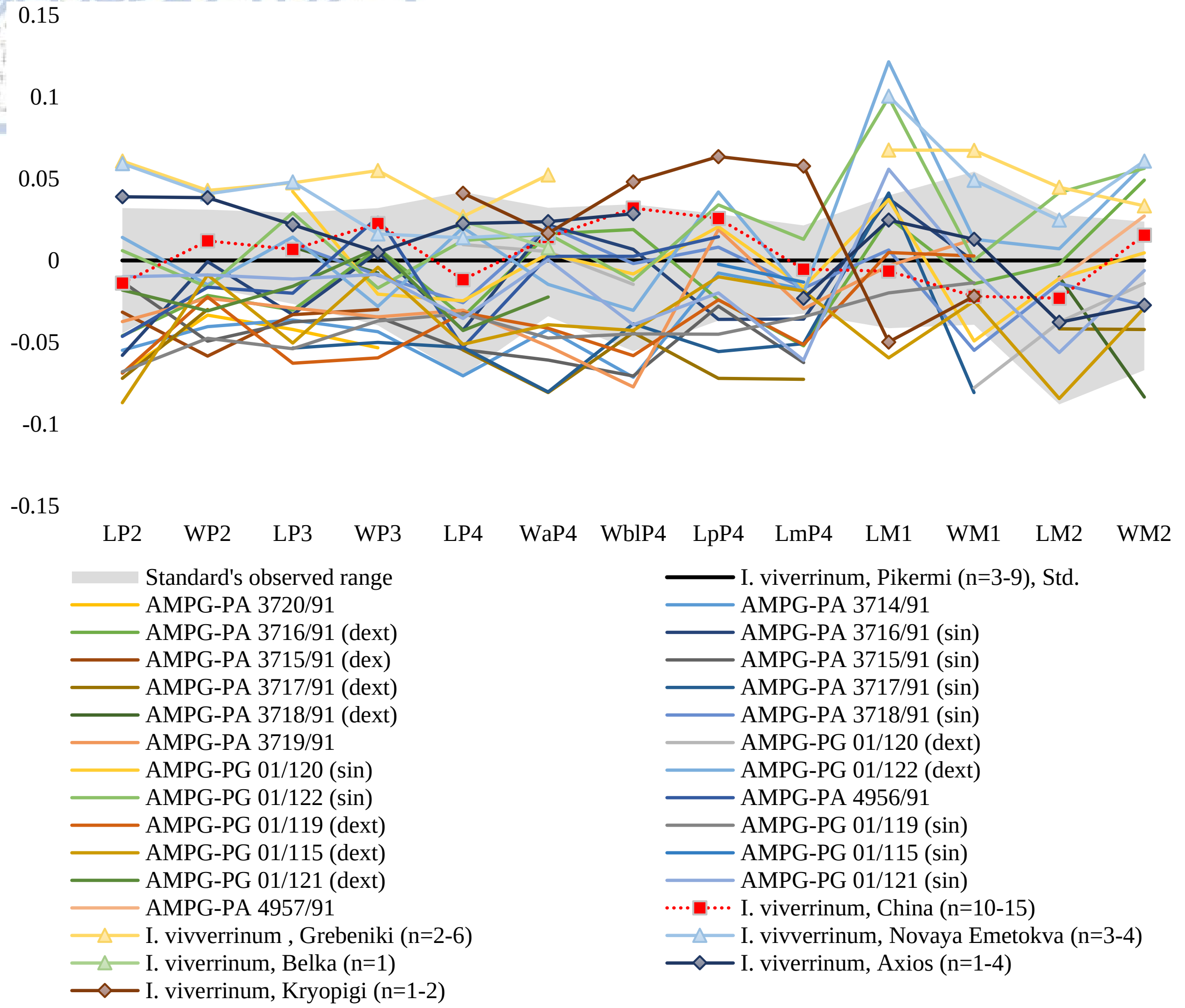

Figure 11. Log-ratio diagram for the upper dentition of *Ictitherium viverrinum* from different localities. The mean values of *Ictitherium viverrinum* from Pikermi (n=3-9) by Werdelin (1988b) were used as a standard. The greyed area indicates the standard's observed range of variation. Data for *I. viverrinum* from China were acquired from Werdelin (1988b). Data for *I. viverrinum* from Grebeniki, Novaya Emetovka and Belka were acquired from Semenov (1989). Data for *I. viverrinum* from Kryopigi were acquired from Lazaridis (2015). Data for *I. viverrinum* from Axios were acquired from Koufos (2021).

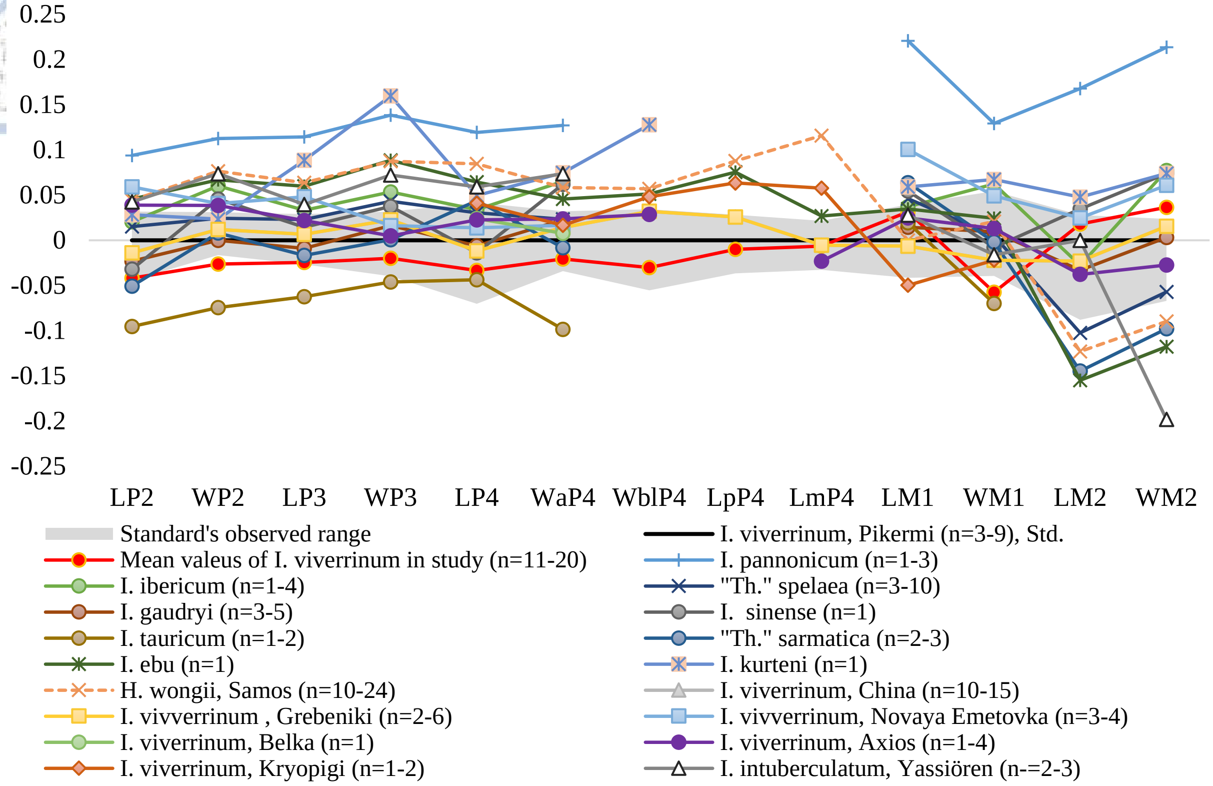

Figure 12. Log-ratio diagram for the upper dentition of various ictitheres. The mean values of *Ictitherium viverrinum* from Pikermi (n=3-9) by Werdelin (1988b) were used as a standard. The greyed area indicates standard's observed range of variation. Data for *Ictitherium viverrinum* from China were acquired from Werdelin (1988b). Data for *Ictitherium viverrinum* from Grebeniki, Novaya Emetovka, Belka, *I. gaudryi*, *I. tauricum*, "*Th*". *Sarmaticum*, *I. sinense*, *I. pannonicum* and *I. ibericum* were acquired from Semenov (1989). Data for *I. viverrinum* from Kryopigi were acquired from Lazaridis (2015). Data for the *I. viverrinum* from Axios were acquired from Koufos (2021). Data for *H. wongii* from Samos were acquired from Werdelin (1988a). Data for *I. ebu* were acquired from Werdelin (2003).

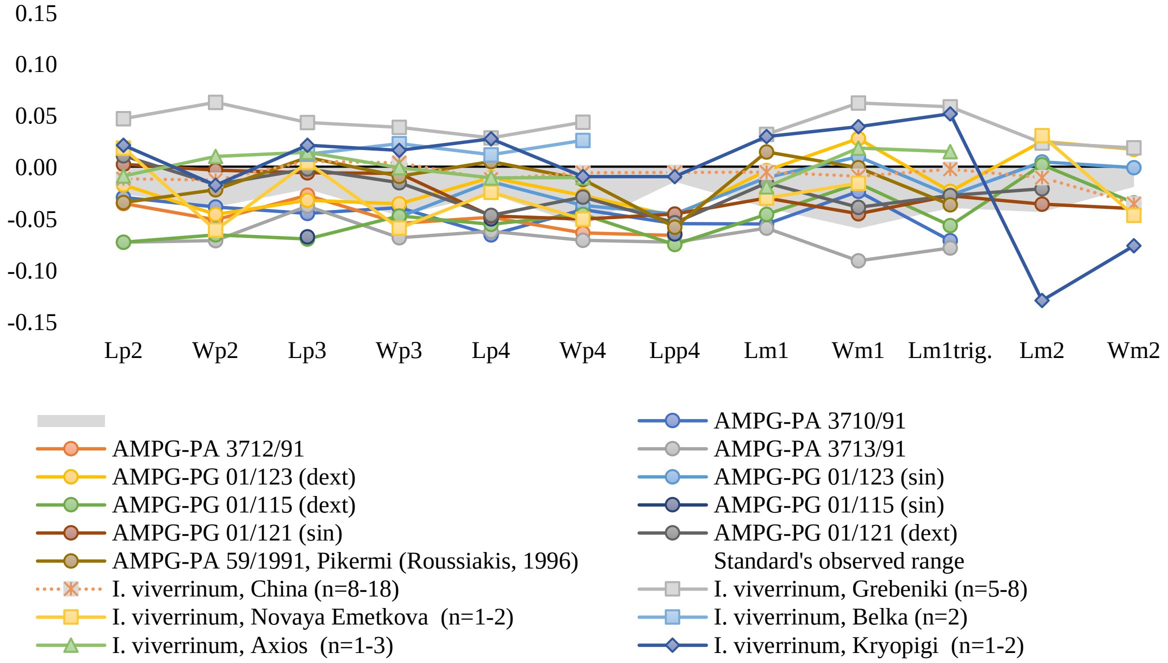

Figure 13. Log-ratio diagram for the lower dentition of *Ictitherium viverrinum*. The mean values of *Ictitherium viverrinum* from Pikermi (n=2-13) by Werdelin (1988b) were used as a standard. The greyed area indicates the standard's observed range of variation. Data for *I. viverrinum* from China were acquired from Werdelin (1988b). Data for *I. viverrinum* from Grebeniki, Novaya Emetovka and Belka were acquired from Semenov (1989). Data for *I. viverrinum* from Kryopigi were acquired from Lazaridis (2015). Data for *I. viverrinum* from Axios were acquired from Koufos (2021).

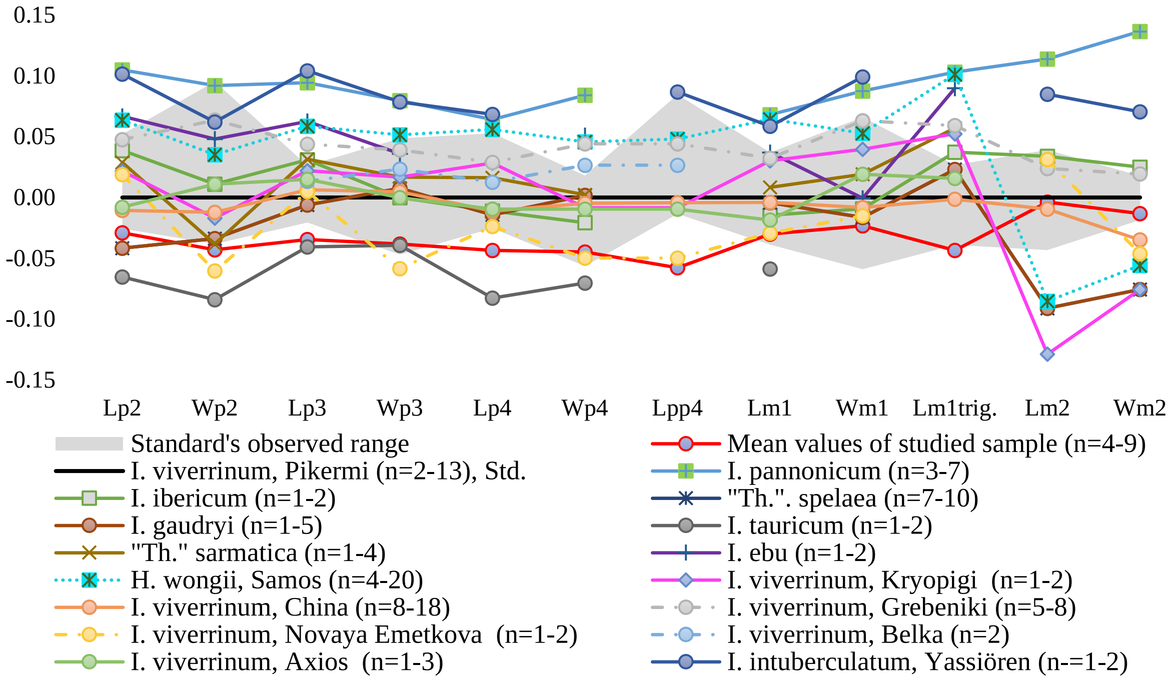

Figure 14. Log-ratio diagram for the lower dentition of various ictitheres. The mean values of *Ictitherium viverrinum* from Pikermi (n=2-13) by Werdelin (1988b) were used as a standard. The greyed area indicates the standard's observed range of variation. The data of *I. viverrinum* from China were acquired from Werdelin (1988b). Data for *I. viverrinum* from Axios were acquired from Koufos (2021). Data for *I. viverrinum* from Kryopigi were acquired from Lazaridis (2015). Data of *I. viverrinum* from Grebeniki, Novaya Emetovka and Belka as well as for *I. ibericum*, *I. gaudryi*, *"Th". sarmaticum*, *I. pannonicum* and *I. spelaeum* were acquired from Semenov (1989). Data for *I. ebu* were acquired from Werdelin (2003). Data for *H. wongii* from Samos were acquired from Werdelin (1988a).

Table 5. Cranial measurements (mm) of *I. viverrinum* from Pikermi.

	AMPG-PA 3716/91	AMPG-PA 3715/91	AMPG-PA 3718/91	AMPG-PG 01/120	AMPG-PG 01/122	AMPG-PG 01/115	AMPG-PG 01/121	AMPG-PG 01/119
Length of the palate (PL)	93.62	—	85.58	—	[91.22]	—	—	—
Width of cranium between the canines (buccal) (C–C)	30.03	29.89	31.3	—	[33.65]	—	—	—
Width of cranium between P4 (buccal) (P–P)	57.44	—	58.5	50.05	53.31	—	—	—
Minimum width between orbits (IOB)	—	—	—	37.68	35.31	—	—	—
Width between postorbital processes (POP)	—	—	—	39.77	38.23	—	—	—
Maximum width at the zygomatic arches (ZB)	—	—	—	—	(96.58)	—	—	—
Maximum width of occipital condyles (CB)	—	—	—	[37.00]	—	—	—	—
Postorbital constriction minimum width (POC)	—	—	—	22.2	21.25	—	—	—
Maximum antero-posterior length of the preserved cranium	—	—	—	—	>126.22	—	—	—
Basion-anterior border of choanae	—	—	—	(64.82)	(64.94)	—	—	—
Basion-anterior border of the orbit	—	—	—	97.00	96.00	—	—	—
Basion-middle of the line connecting the posterior borders of P4	—	—	—	78.20	79.80	—	—	—
Length of bulla	—	—	—	28.00	29.00	—	—	—
Width of bullae	—	—	—	16.50	17.75	—	—	—

Table 6. Upper dentition measurements (mm) and mean values of *Ictitherium viverrinum* from Pikermi and other localities.

	AMPG-PA 3714/91	AMPG-PA 3715/91		AMPG-PA 3716/91		AMPG-PA 3717/91		AMPG-PA 3718/91		AMPG-PA 3719/91	AMPG-PA 3720/91
	sin	dext	sin	dext	sin	dext	sin	dext	sin	dext	dext
LC	—	7.74	[8.08]	—	—	—	—	7.63	(7.67)	—	—
WC	—	5.73	[6.10]	—	—	—	—	5.05	(5.59)	—	—
LP1	[4.80]	3.33	—	4.12	—	—	—	—	—	—	—
WP1	[4.00]	3.27	—	3.14	—	—	—	—	—	—	—
LP2	10.15	10.71	11.18	10.36	10.08	9.76	—	—	—	10.57	9.84
WP2	4.92	4.72	4.82	5.14	5.39	5.04	—	—	—	5.12	5.00
LP3	12.90	13.00	12.87	13.08	13.00	—	12.40	14.30	14.36	13.12	12.73
WP3	6.64	6.85	6.78	7.47	7.43	—	6.54	7.21	7.19	6.78	6.49
LP4	17.29	—	17.94	18.80	18.44	17.93	18.00	[17.63]	19.17	18.96	—
WaP4	10.70	—	10.25	12.24	12.39	9.79	9.80	11.75	12.37	10.45	(10.70)
WblP4	5.88	—	5.89	7.24	7.04	6.26	6.34	—	6.90	5.80	—
LpP4	7.27	—	6.94	7.00	6.81	6.27	6.51	—	7.54	7.73	—
LmP4	7.04	—	6.35	6.50	6.75	6.20	6.52	—	7.05	6.85	—
LM1	—	—	[7.85]	8.53	8.76	—	8.83	[8.14]	8.15	(9.87)	[8.70]
WM1	—	—	[12.01]	14.09	(14.54)	—	12.09	[12.87]	12.83	15.00	[10.37]
LM2	—	—	[5.61]	5.97	—	5.45	—	5.86	5.81	—	—
WM2	—	—	[7.90]	9.54	—	7.73	—	(7.03)	8.00	—	—
R.I. P2	48.47	44.07	43.11	49.61	53.47	51.64	—	—	—	48.44	50.81
R.I. P3	51.47	52.69	52.68	57.11	57.15	—	52.74	50.42	50.07	51.68	50.98
R.I. P4	61.89	—	57.13	65.11	67.19	54.60	54.44	[66.65]	64.53	55.12	—
L(P2–P4)	39.69	—	43.11	43.96	43.02	38.74	—	—	—	38.50	—
W(P3/P4) ×100	62.06	—	66.15	61.03	59.97	—	66.73	61.36	58.12	64.88	(60.65)
L(mP4/P4) ×100	40.72	—	35.40	34.57	36.61	34.58	36.22	—	36.78	36.13	—
LP4/(LP2+LP3) ×100	75.01	—	74.59	80.20	79.90	—	—	—	—	80.03	—

Table 6. (Continued).

	AMPG-PA 4956/91	AMPG-PA 4957/91	AMPG-PG 01/115		AMPG-PG 01/119		AMPG-PG 01/120		AMPG-PG 01/121		AMPG-PG 01/122	
	sin	dext	dext	sin	dext	sin	dext	sin	dext	sin	dext	sin
WI1	—	—		3.14	—	—	—	—	—	—	—	—
LI1	—	—	3.07	—	—	—	—	—	—	—	—	—
LI2	—	—	—	4.00	—	—	—	—	—	—	—	—
WI2	—	—	3.65	3.44	—	—	—	—	—	—	—	—
LI3	—	—	4.99	—	—	—	—	—	—	4.32	—	—
WI3	—	—	3.85	3.94	—	—	—	—	—	3.76	—	—
LC	—	—	6.22	6.78	7.66	7.33	—	—	8.6	8.35	—	—
WC	—	—	4.68	—	5.62	5.59	—	—	6.37	6.03	—	—
LP1	—	—	4.17	—	(3.88)	—	—	—	3.9	4.07	—	—
WP1	—	—	3.60	—	(3.59)	—	—	—	—	3.22	—	—
LP2	(10.35)	—	9.43	9.78	9.83	9.85	—	—	11.05	11.26	11.90	11.68
WP2	(5.20)	—	5.29	—	5.13	4.84	—	—	5.03	5.29	5.22	5.20
LP3	13.40	—	12.49	10.91	12.14	12.39	—	15.46	13.53	13.67	14.50	15.00
WP3	7.80	—	7.27	—	6.40	6.74	—	7.00	7.47	7.20	6.88	7.06
LP4	(18.00)	—	18.08	18.12	18.90	18.87	20.80	19.22	(18.43)	(18.75)	21.30	20.92
WaP4	11.86	—	10.77	—	10.72	10.57	11.94	11.90	11.2	11.80	11.40	12.24
WblP4	6.97	—	6.28	—	6.06	6.25	6.70	6.80	—	6.33	6.46	6.74
LpP4	7.65	—	6.29	6.40	7.00	6.67	—	7.76	7.2	7.07	8.15	8.00
LmP4	—	—	7.54	7.07	6.51	6.77	6.50	7.06	[7.62]	(6.37)	(7.00)	7.55
LM1	—	—	7.00	—	(8.12)	(7.67)	[6.81]	8.75	>8.35	9.13	10.62	10.10
WM1	—	—	13.75	—	(14.65)	(14.11)	(12.17)	13.00	>12.36	14..35	(15.00)	14.57
LM2	—	5.84	4.94	—	—	—	5.50	5.85	—	5.27	6.10	6.60
WM2	—	9.07	7.97	—	—	—	8.25	8.61	—	8.40	9.75	9.70
R.I. P2	(50.24)	—	56.10	—	52.19	49.14	—	—	45.52	46.98	43.87	44.52
R.I. P3	58.21	—	58.21	—	52.72	54.40	—	45.28	55.21	52.67	47.45	47.07
R.I. P4	(65.89)	—	59.57	—	56.72	56.01	57.40	61.91	—	62.93	53.52	58.51
L(P2-P4)	39.2	—	—	—	—	—	—	—	44.00	(43.87)	46.57	44.05
L(P3/P4) ×100	(74.44)	—	69.08	(60.21)	64.23	65.66	—	80.44	73.41	(74.25)	68.08	71.70
W(P3/P4) ×100	65.77	—	67.50	—	59.70	63.77	—	58.82	—	63.44	60.35	57.68
L(mP4/P4) ×100	—	—	41.70	39.02	34.44	35.88	31.25	36.73	(33.26)	(34.60)	(32.86)	36.09
LP4/(LP2+LP3) ×100	(75.79)	—	82.48	(87.58)	86.03	84.85	—	—	(74.98)	(73.85)	80.68	78.41

Table 6. (Continued).

	Studied sample			Pikermi	Axios	Kryopigi	China	Grebeniki	Novaya Emetokva	Belka
	Mean values	S.D	V	n=3-9	n=1-4	n=1-2	n=10-15	n=2-6	n=3-4	n=1
	n=11-20			Werdelin, 1988b	Koufos, 2021	Lazaridis, 2015	Werdelin, 1988b	Semenov, 1989	Semenov, 1989	Semenov, 1989
LP2	10.46	0.73	7.04	11.52	12.60	—	11.16	13.25	13.20	—
WP2	5.08	0.19	3.70	5.40	5.90	—	5.55	5.96	5.93	—
LP3	13.26	1.07	8.03	14.03	14.75	—	14.25	15.65	15.67	—
WP3	7.01	0.38	5.45	7.34	7.43	—	7.73	8.33	7.62	—
LP4	18.84	1.09	5.79	20.34	21.43	22.36	19.80	21.64	21.00	21.50
WaP4	11.24	0.85	7.58	11.79	12.45	12.25	12.18	13.30	12.25	12.00
WblP4	6.47	0.44	6.76	6.93	7.40	7.74	7.46	—	—	—
LpP4	7.23	0.51	7.04	7.40	—	8.57	7.85	—	—	—
LmP4	7.22	0.40	5.51	7.33	6.95	8.37	7.24	—	—	—
LM1	8.64	1.00	11.56	8.03	8.50	7.16	7.91	9.38	10.12	—
WM1	12.75	1.05	8.22	14.56	15.00	13.84	13.84	17.00	16.30	—
LM2	6.25	0.44	7.09	6.00	5.50	—	5.69	6.65	6.35	—
WM2	9.27	0.88	9.50	8.52	8.00	—	8.83	9.20	9.80	—
R.I P2	48.62	—	—	46.88	46.83	—	49.73	44.98	44.92	—
R.I P3	52.86	—	—	52.32	50.34	—	54.25	53.23	48.63	—
R.I P4	59.68	—	—	57.96	58.11	54.79	61.52	61.46	58.33	55.81
L(P3/P4) ×100	70.40	—	—	68.98	68.84	—	71.97	72.32	74.62	—
W(P3/P4) ×100	62.36	—	—	62.26	59.64	—	63.46	62.63	62.20	—
L(mP4/P4) ×100	38.34	—	—	36.04	32.44	37.43	36.57	—	—	—
LP4/(LP2+LP3) ×100	79.42	—	—	79.61	78.34	—	77.92	74.88	72.74	—

Table 7. Mandibular and lower dentition measurements (mm) of *Ictitherium viverrinum* from Pikermi and other localities.

	AMPG-PA 3710/91	AMPG-PA 3712/91	AMPG-PA 3713/91	AMPG-PG 01/115		AMPG-PG 01/121		AMPG-PG 01/123		AMPG-PA 59/1991 (Roussiakis, 1996)[1]
	dext	dext	sin	dext	sin	dext	sin	dext	sin	sin
Wi2	—	—	—	—	3.09	—	—	—	—	3.14
Li3	—	—	—	3.49	—	—	—	—	—	3.78
Wi3	—	—	—	3.14	—	—	—	—	—	4.00
Lc	—	—	—	[7.64]	—	(8.16)	7.82	7.87	7.81	8.37
Wc	—	—	—	[6.19]	—	—	6.37	7.12	6.18	6.31
Lp1	—	—	—	3.05	—	2.74	2.70	—	—	(3.01)
Wp1	—	—	—	2.76	—	2.37	2.60	—	—	(2.91)
Lp2	9.63	9.50	8.71	8.71	—	10.57	10.37	9.90	—	9.52
Wp2	5.00	4.86	4.64	4.70	—	5.26	5.43	4.92	(4.76)	5.20
Lp3	11.65	12.13	11.84	11.00	11.06	12.87	12.76	(12.00)	—	13.20
Wp3	5.81	5.61	5.43	5.70	—	6.14	6.27	5.86	—	6.23
Lp4	12.5	13.00	12.60	12.80	12.95	13.06	13.04	14.21	14.07	14.72
Lpp4	6.10	5.94	5.85	5.82	5.96	6.11	6.23	6.20	6.23	6.05
Wp4	6.64	6.30	6.20	6.57	—	6.83	6.50	6.85	6.70	7.10
Lm1	(15.14)	—	15.00	15.47	—	16.60	16.05	17.06	16.80	17.79
Wm1	7.17	—	6.14	7.30	—	6.92	6.82	8.07	7.75	7.56
Ltm1	9.67	—	9.51	10.00	—	10.70	10.69	10.80	10.70	10.48
Lm2	—	—	—	7.45	—	7.06	6.82	7.85	7.50	[6.49]
Wm2	—	—	—	5.50	—	—	5.43	6.20	5.95	[5.00]
R.I. p2	51.92	51.16	53.27	53.96	—	49.76	52.36	49.70	—	54.62
R.I. p3	49.87	46.25	45.86	51.82	—	47.71	49.14	(48.83)	—	47.20
R.I. p4	53.12	48.46	49.21	51.33	—	52.30	49.85	48.21	47.62	48.23
R.I. m1	(47.36)	—	40.93	47.19	—	41.69	42.49	47.30	46.13	42.50
L(p2─m1)	49.17	—	48.56	46.21	46.21	51.63	51.16	52.45	50.97	51.96
L(pp4/p4)	(48.80)	45.69	46.43	45.47	46.02	46.78	47.78	43.63	44.28	41.10
L(tm1/m1)	63.87	—	63.40	64.64		64.46	66.60	63.31	63.69	58.91
C-cond	—	—	—	—	—	—	—	123.45	119.98	(100.92)
HPC	—	—	—	—	—	—	—	49.22	50.62	(59.66)
Hdia	—	—	—	12.48	—	15.07	16.48	(16.35)	15.57	14.80
Hbehm1	24.86	—	21.30	18.55	—	21.00	(20.71)	23.31	22.47	26.79

[1]: Measurements after the author. Specimen not included in the mean value below.

Table 7. (Continued).

	Studied sample			Pikermi	China	Grebeniki	Novaya Emetkova	Belka	Axios	Kryopigi
	Mean values	S. D	V	(Werdelin, 1988b)	(Werdelin, 1988b)	(Semenov, 1989)	(Semenov, 1989)	(Semenov, 1989)	(Koufos, 2021)	(Lazaridis, 2015)
	n=4-9			n=1-13	n=1-18	n=5-8	n=1-2	n=1	n=1-3	n=1-2
Lp2	9.63	0.73	7.60	10.29	10.04	11.48	10.75	—	10.10	10.82
Wp2	4.95	0.28	5.58	5.46	5.31	6.32	4.75	—	5.60	5.25
Lp3	11.91	0.69	5.78	12.90	13.09	14.27	13.05	13.30	13.35	13.57
Wp3	5.81	0.27	4.75	6.35	6.42	6.95	5.55	6.70	6.35	6.60
Lp4	13.14	0.60	4.58	14.52	14.15	15.52	13.75	14.95	14.20	15.50
Lpp4	6.05	0.16	2.66	6.91	6.84	—	—	—	—	6.78
Wp4	6.57	0.23	3.56	7.29	7.21	8.07	6.50	7.75	7.13	7.15
Lm1	16.02	0.83	5.19	17.17	17.01	18.50	16.05	—	16.45	18.41
Wm1	7.17	0.63	8.84	7.56	7.42	8.74	7.30	—	7.90	8.29
Ltm1	10.30	0.55	5.37	11.38	11.34	13.04		—	11.80	12.84
Lm2	7.34	0.40	5.48	7.40	7.24	7.82	7.95	—	—	5.50
Wm2	5.77	0.37	6.37	5.95	5.49	6.22	5.35	—	—	5.00
R.I. p2	51.38			53.06	52.89	55.05	44.19	—	55.45	48.52
R.I. p3	48.80			49.22	49.05	48.70	42.53	50.38	47.57	48.64
R.I. p4	50.04			50.21	50.95	52.00	47.27	51.84	50.23	46.14
R.I. m1	44.75			44.03	43.62	47.24	45.48	—	48.02	45.00
L(p2–m1)	49.55			51.40	55.70	—	—	—	—	—
L(pp4/p4)	46.05			47.59	48.34	—	—	—	—	43.72
L(tm1/m1)	64.28			66.28	66.67	70.49	—	—	—	69.74
C-cond	118.87			120.70	—	—	—	—	—	—
HPC	49.92			53.00	—	—	—	—	—	—
Hdia	15.19			16.60	15.50	—	—	—	—	—
Hbehm1	21.92			23.40	23.40	—	—	—	—	—

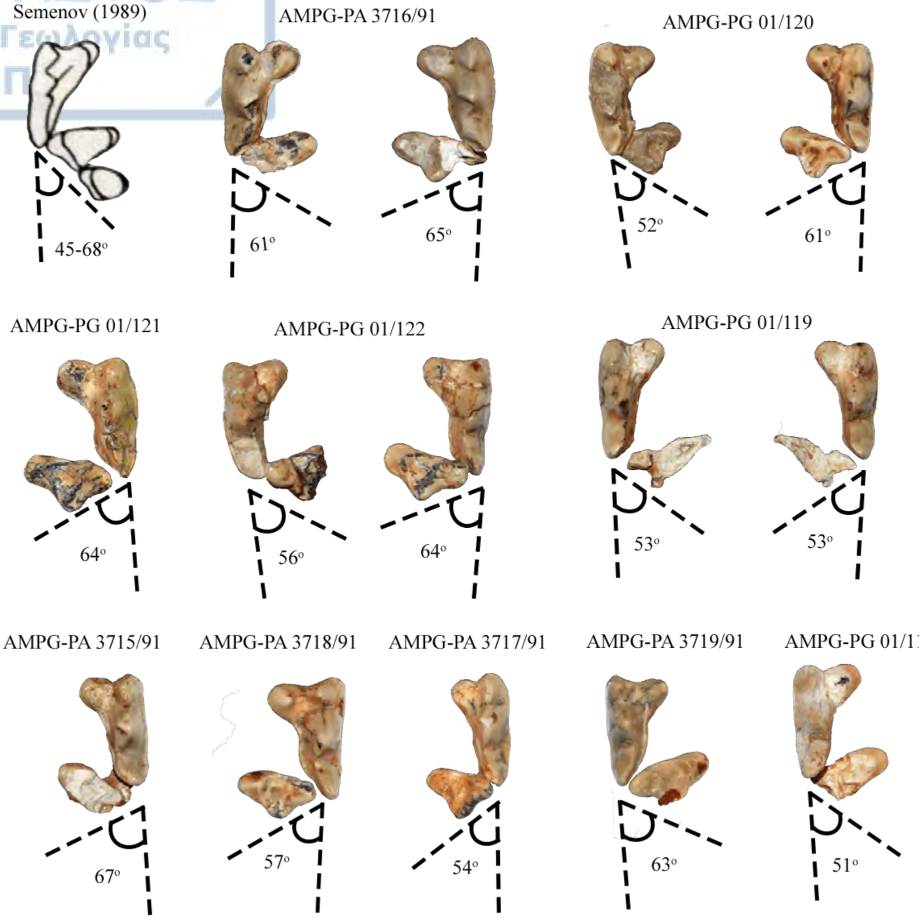

Figure 15. Approximate value of the angles formed between the upper carnassial and M1 for the *I. viverrinum* material. The angles were measured digitally. Not in scale.

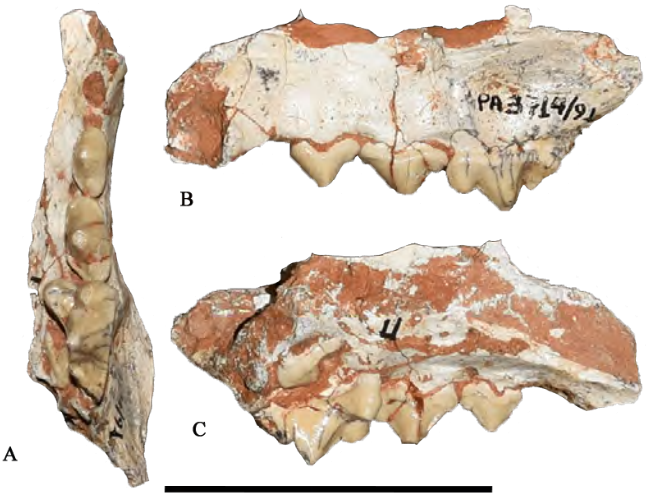

Figure 16. Maxillary fragment of *I. viverrinum* AMPG-PA 3714/91 in A: occlusal, B: lateral and C: medial view. Scale bar is 5 cm.

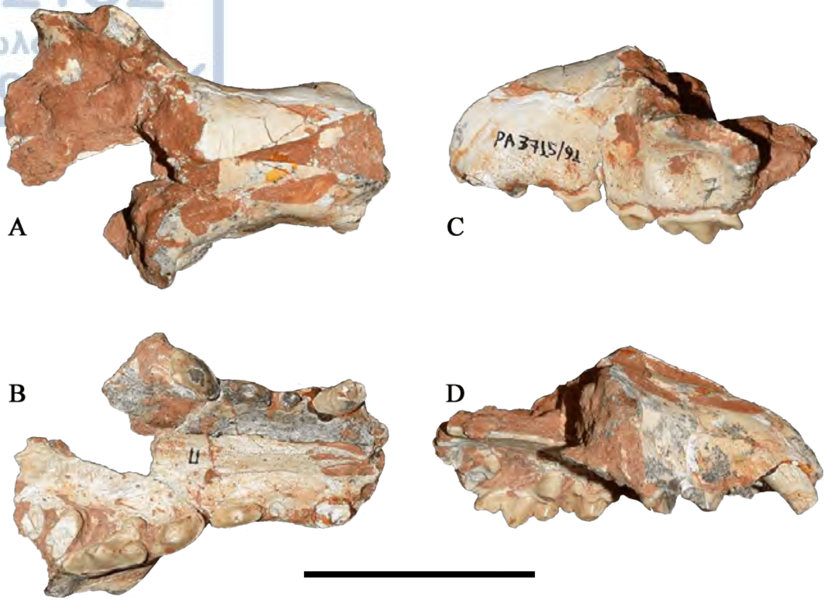

Figure 17. Rostral part of partially preserved cranium of *I. viverrinum* AMPG-PA 3715/91 in A: dorsal, B: ventral and C-D: lateral view. Scale bar is 5 cm.

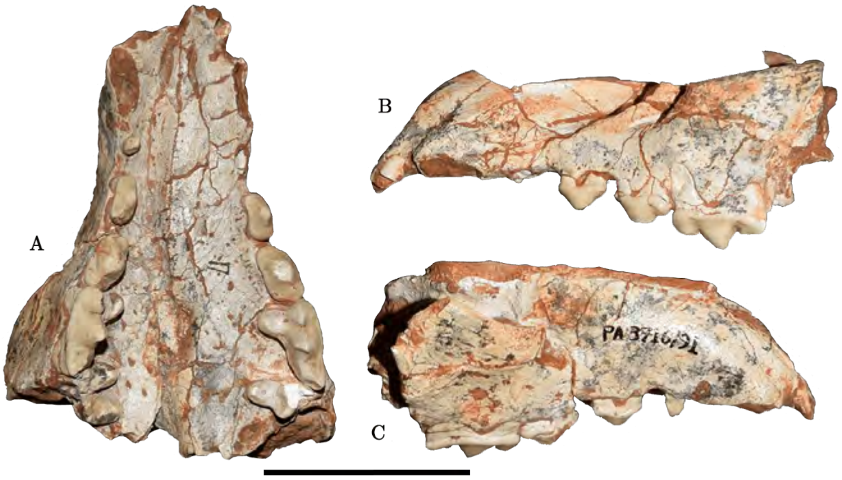

Figure 18. Rostral part of partially preserved cranium of *I. viverrinum* AMPG-PA 3716/91 in A: ventral and B-C: lateral view. Scale bar is 5 cm.

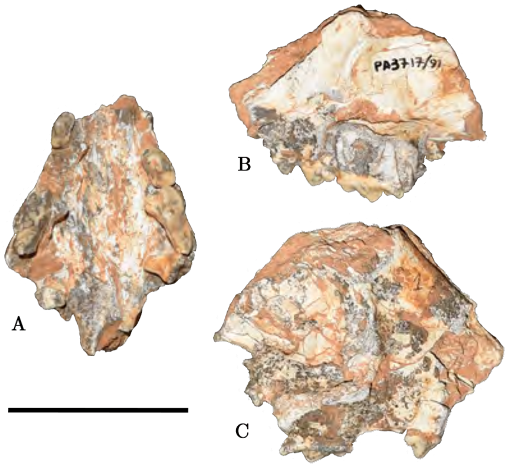

Figure 19. Partially preserved skull of *I. viverrinum* AMPG-PA 3717/91 in A: ventral and B-C: lateral view. Scale bar is 5 cm.

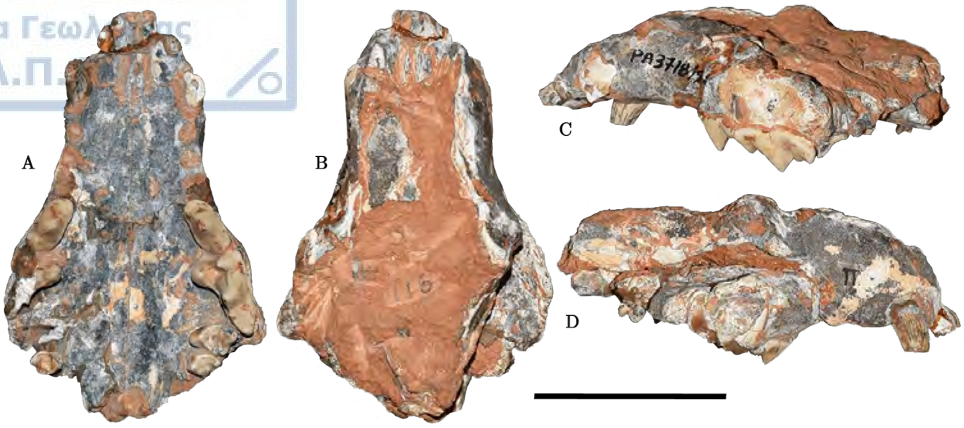

Figure 20. Partially preserved cranium of *I. viverrinum* AMPG-PA 3718/91 in A: ventral, B: dorsal and C-D: lateral view. Scale bar is 5 cm.

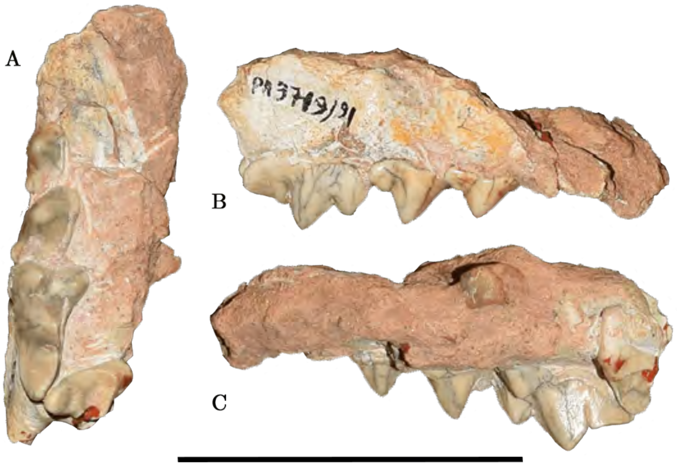

Figure 21. Maxillary fragment of *I. viverrinum* AMPG-PA 3719/91 in A: occlusal, B: lateral and C: medial view. Scale bar is 5 cm.

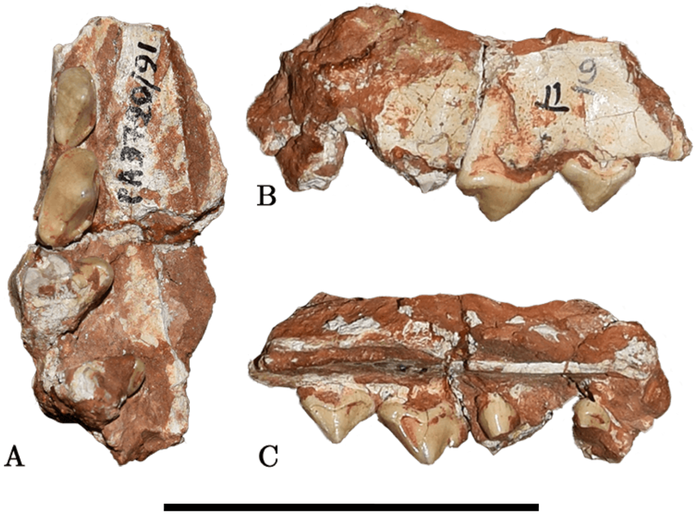

Figure 22. Maxillary fragment of *I. viverrinum* AMPG-PA 3720/91 in A: occlusal, B: lateral and C: medial view. Scale bar is 5 cm.

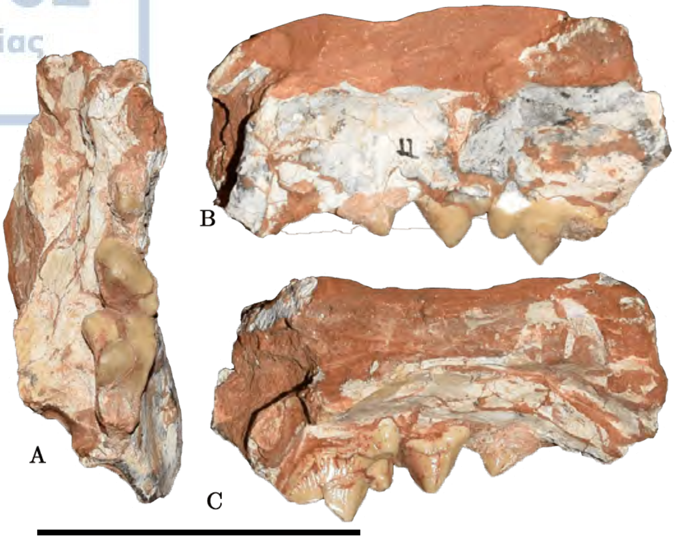

Figure 23. Maxillary fragment of *I. viverrinum* AMPG-PA 4956/91 in A: occlusal, B: lateral and C: medial view. Scale bar is 5 cm.

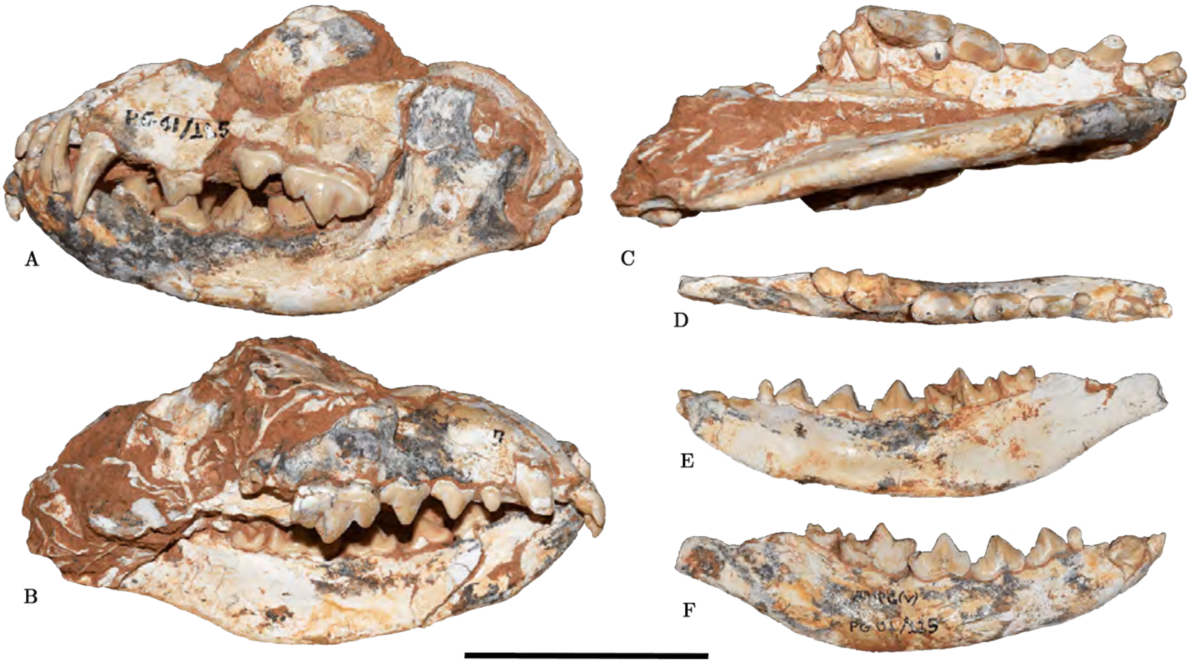

Figure 24. Partially preserved and laterally crushed skull of *I. viverrinum* AMPG-PG 01/115 in A-B: lateral and C: ventral view. Its associated right hemimandible can be observed in D: occlusal, E: medial and F: lateral view. Scale bar is 5 cm.

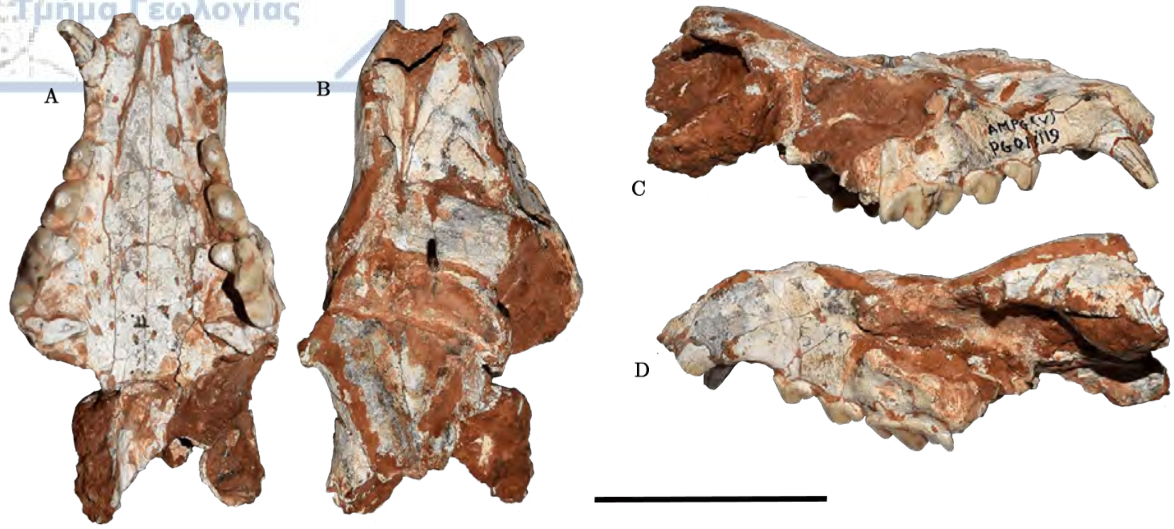

Figure 25. Partially preserved and vertically crushed cranium of *I. viverrinum* AMPG-PG 01/119 in A: ventral, B: dorsal and C-D: lateral view. Scale bar is 5 cm.

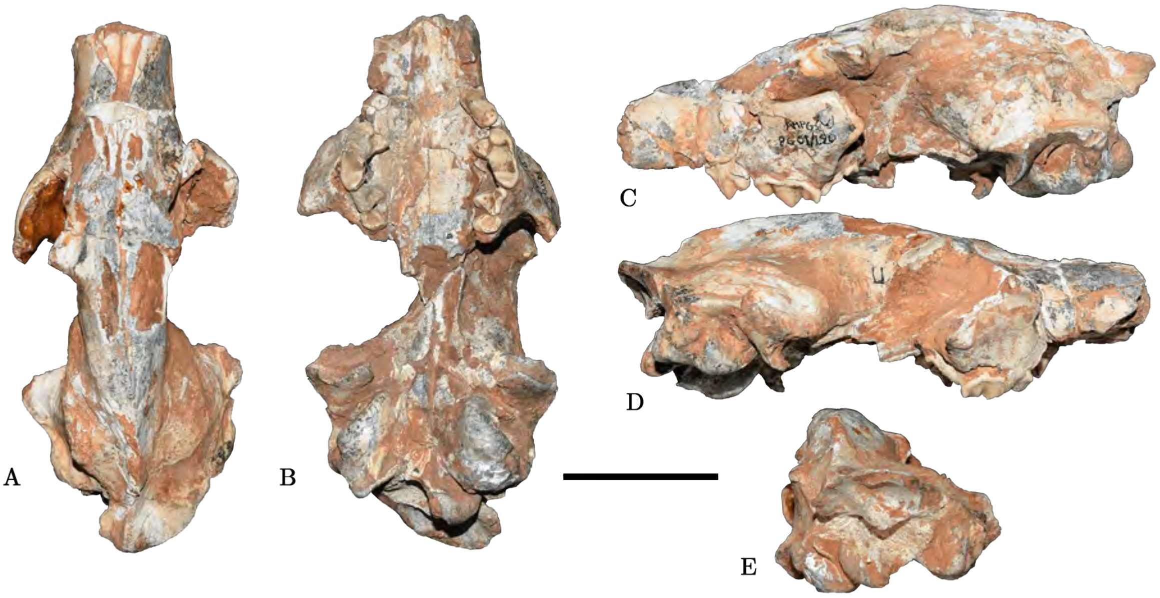

Figure 26. Almost complete cranium of *I. viverrinum* AMPG-PG 01/120 in A: dorsal, B: ventral, C-D: lateral and E: posterior view. Scale bar is 5 cm.

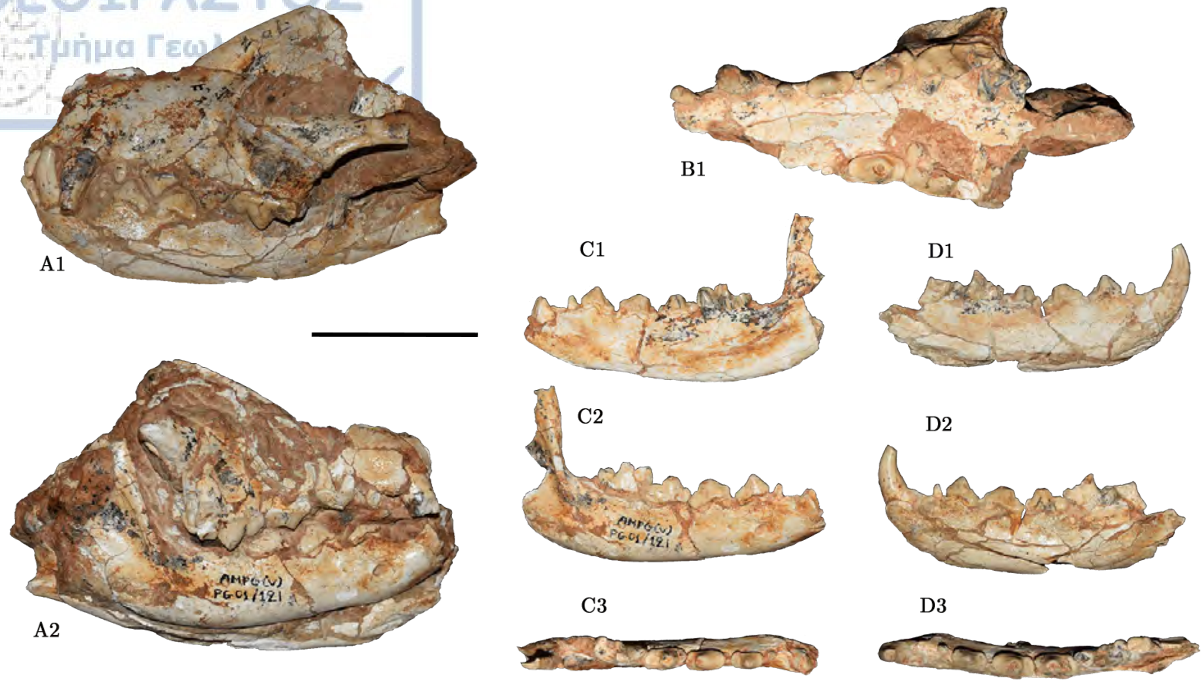

Figure 27. Anterior part of a laterally crushed skull of *I. viverrinum* AMPG-PG 01/121 in lateral view (A1, A2). Further preparation revealed its dentition. B: occlusal view of the cranium after. C: right hemimandible in medial (C1), lateral (C2) and occlusal (C3) view. D: left hemimandible in medial (D1), lateral (D2) and occlusal (D3) view. Scale bar is 5 cm.

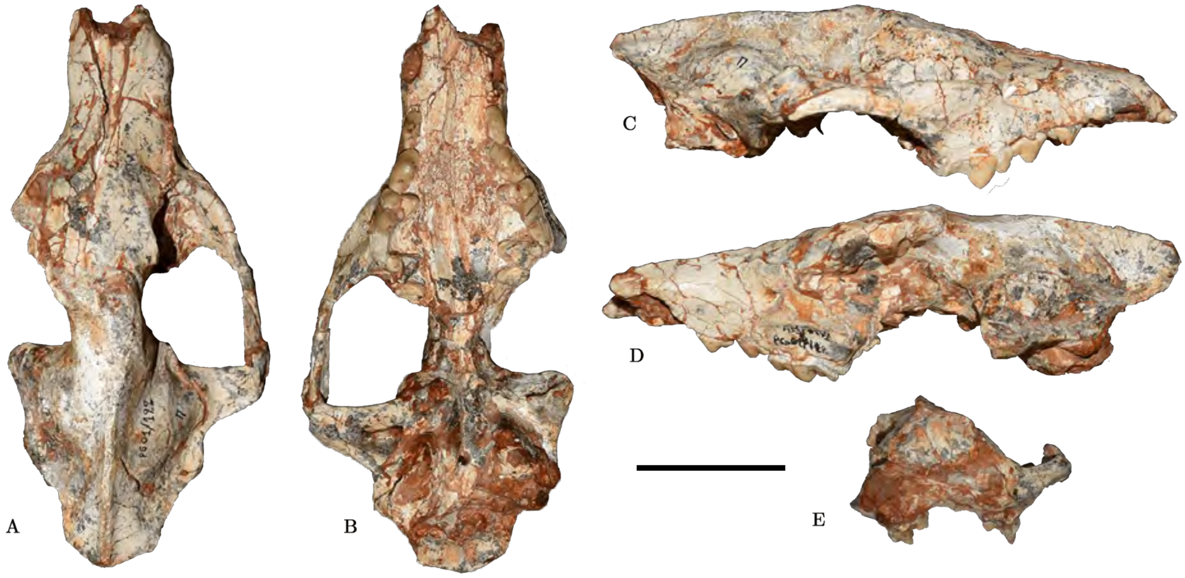

Figure 28. Almost complete and vertically compressed cranium of *I. viverrinum* AMPG-PG 01/122 in A: dorsal, B: ventral, C-D: lateral and E: posterior view. Scale bar is 5 cm.

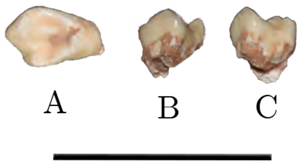

Figure 29. Isolated right M2 of *I. viverrinum* AMPG-PA 4957/91 in A: occlusal, B: lingual and C: buccal view. Scale bar is 2 cm.

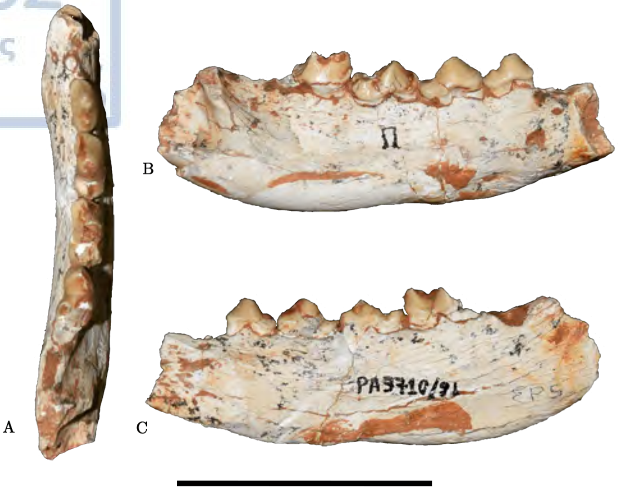

Figure 30. Right hemimandible of *I. viverrinum* AMPG-PA 3710/91 in A: occlusal, B: lateral and C: medial view. Scale bar is 5 cm.

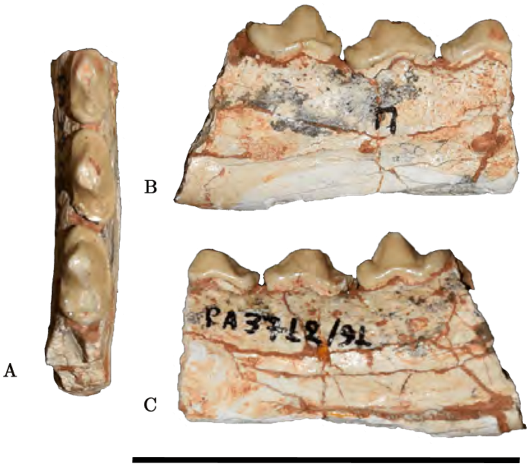

Figure 31. Right hemimandible fragment of *I. viverrinum* AMPG-PA 3712/91 in A: occlusal, B: lateral and C: medial view. Scale bar is 5 cm.

Figure 32. Left hemimandible of *I. viverrinum* AMPG-PA 3713/91 in A: occlusal, B: lateral and C: medial view. Scale bar is 5 cm.

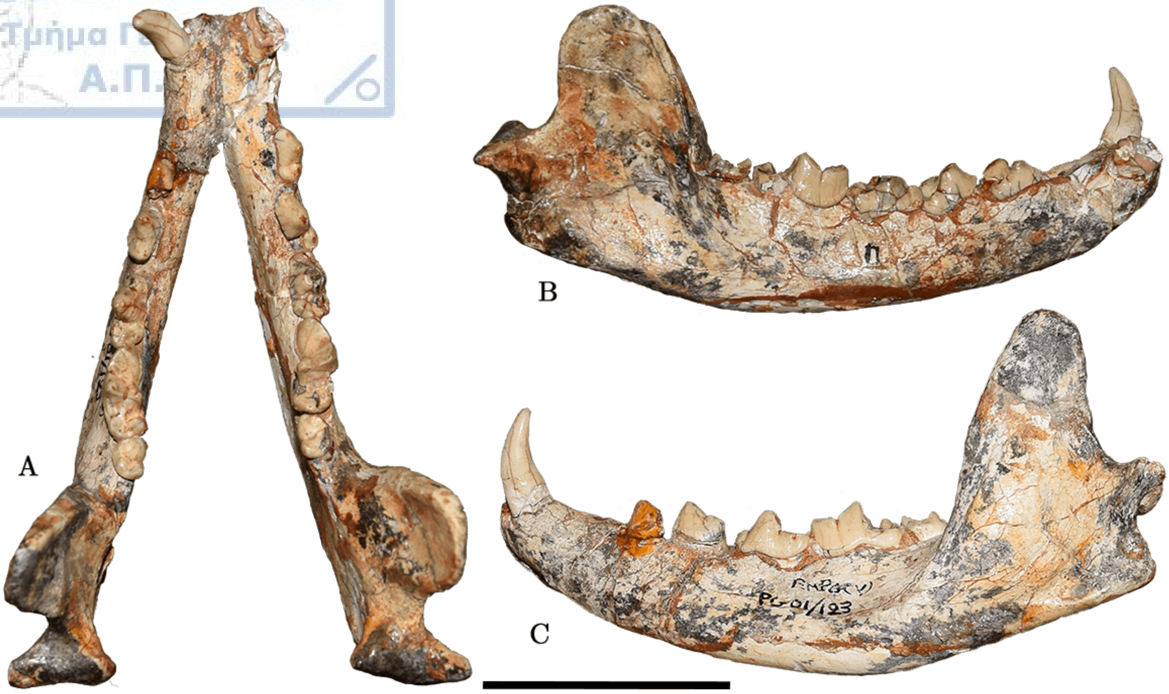

Figure 33. Mandible of *I. viverrinum* AMPG-PG 01/123 in A: occlusal and B-C: lateral view. Scale bar is 5 cm.

Figure 34. *I. viverrinum* cranium AMPG-PG 01/120 with its potentially associated mandible AMPG-PG 01/123 in anatomical position. Absence of taphonomical data along with strong deformations in both specimens prevent further claims. Scale bar is 5 cm.

Genus *Plioviverrops* Kretzoi, 1938

Plioviverrops orbignyi (Gaudry & Lartet, 1856)

(Figs. 35–37, Table 8)

1856 *Viverra orbignyi*, Gaudry & Lartet, p. 273
1861 *Thalassictis orbignyi* (Gaudry & Lartet), Gaudry, p. 533, Pl. 10:3
1862–1867 *Ictitherium orbignyi* (Gaudry & Lartet), Gaudry, p.74, Pl. 11
1938 *Plioviverrops orbignyi* (Gaudry), Kretzoi, p. 114

Type species: *Viverra orbignyi* Gaudry & Lartet, 1856.

Type locality: Pikermi, Attica, Greece.

Type material: MNHN-PIK-3022 (holotype); skull associated with mandible described and figured by Gaudry & Lartet (1856: 273). Stored in the Museum national d'Histoire naturelle of Paris, France.

Age: MN 11–13, ~8.2–6.4 Ma (Koufos, 2022c). For the classical locality of Pikermi: Middle Turolian, MN 12, 7.33–7.29 Ma (Böhme et al., 2017).

Localities: Greece: Ravin des Zouaves 5, Prochoma 1 and Vathylakkos 2, 3 in Axios Valley (Arambourg & Piveteau, 1929; de Bonis et al., 1973; Koufos, 2000; Koufos 2012); Perivolaki in Thessaly (Koufos, 2006a); Mytilinii 1B (Koufos, 2009), Q1 and A (Solounias, 1981) in Samos Island; Kryopigi in Chalkidiki (Lazaridis, 2015). Bulgaria: Kalimanci 2, 4 (Koufos, 2022c); ?Turkey: Çalta-1 (Sen & Saraç, 2018).

Material: AMPG-PG 95/1515: left maxillary fragment with P3-P4-M1-M2 (sin), AMPG-PG 95/1516: right maxillary fragment with P4-M1 and part of M2 alveolus (dext). (Fig. 37).

Remarks: The two dentitions mirror each other almost perfectly and it is possible that they belong to the same individual.

Description: The cusps of teeth are pointed in both toothrows. The external borders of P4-M1 form an angle of approximately 124°–129° (Fig. 36).

P3: It is short and slender. The mesial cusp is absent. A small and low distal cusp is situated in the distal end of the tooth. The mesial cingulum is weak, while the lingual cingulum is strong and forms a shelf. A crest passes across the main cusp in a mesio-lingual to distal direction. The adamantine of the main cusp's lingual surface is slightly broken. A small diastema is formed between P3 and P4.

P4: The upper carnassial is relatively elongated and large. The protocone is large compared to the size of the carnassial and well separated from the others cusps. It is mesio-lingually oriented and extends more mesially than the smaller parastyle. The protocone and the parastyle are connected with a small crest near the mesial margin of P4. The paracone is the highest cusp. It is asymmetrical, with its mesial half being longer than its distal. Also, its tip inclines slightly distally. A crest forms in a mesiodistal direction and passes from the parastyle, paracone and metastyle. A blunter crest passes mesio-lingually into the valley of the protocone, loosely connecting the protocone with the paracone. The metastyle is elongated and slightly curves buccally towards its distal end. The strong lingual cingulum forms a shelf that connects with the protocone. There is a small cingular projection buccally between the parastyle and the paracone. The right carnassial is slightly better preserved and exhibits a slightly stronger buccal cingulum.

M1: It is relatively wide, low, triangular-shaped in occlusal view and three-rooted. The protocone is situated lingually and its cusp is pointed. The paracone is slightly larger than the metacone and extends buccally. The protocone and metacone are approximately equal in height, while paracone's cusp is the highest. A deep valley is formed between the protocone and the metacone. The protocone with connects with the metacone via a crest in the disto-lingual margin of M1. A similar crest connects the protocone connecting with the paracone. The cingulum is strong in the buccal side. As in P4, the right M1 appears to be slightly better preserved.

M2: Morphologically similar with M1, but it is simpler, smaller and more rounded. The central basin is large and open distally near the base of the disto-buccal cingulum. The right M2 preserves only the mesial part of its alveolus.

Discussion: In literature, *P. orbignyi* was initially erected as *Viverra orbignyi* by Gaudry & Lartet (1856). Later, it was transferred to the genera *Thalassictis* (Gaudry, 1861) and *Ictitherium* (Gaudry, 1862–1867) until it was finally placed under *Plioviverrops* (Kretzoi, 1938). Since then (Kretzoi, 1938), it has been referred to as *Plioviverrops orbignyi* (e.g., de Beaumont, 1969; de Beaumont & Mein, 1972; Solounias, 1981; de Bonis & Koufos, 1981; Werdelin & Solounias, 1991; Roussiakis, 1996; Koufos, 2000; 2006a; Lazaridis, 2015). The Greek fossiliferous record of *P. orbignyi* is relatively rich, with specimens recognized from various Miocene localities. It is also the smallest representative of the Hyaenidae recorded in Pikermi.

The dental morphology of AMPG-PG 95/1515 and AMPG-PG 95/1516 examined herein indicates similarities to *Plioviverrops*, such as the presence of the typical for the genus character, mesial extension of the protocone (Werdelin & Solounias, 1991). In the classical locality of Pikermi, only one representative of this species has been recognized, *Plioviverrops orbignyi* (Gaudry & Lartet, 1856). Although other diagnostic characters of *P. orbignyi* could not be identified due to the nature of the material, the descriptions provided by Koufos (2006a; 2009) regarding the type material, seem to match the dental description of the material herein.

Further metrical comparison of AMPG-PG 95/1515 and AMPG-PG 95/1516 against *P. orbignyi* from various Greek localities (Pikermi, Samos, Perivolaki, Axios, Kryopigi) showed only minor metrical differences. More specifically for the locality of Pikermi, the P3 and P4 sizes of AMPG-PG 95/1515 and AMPG-PG 95/1516 are very similar to the mean values of *P. orbignyi* from Pikermi (MNHN-PIK- 3022, MNHN-PIK-3016) (Fig. 35). The most noticeable difference concerns the slightly increased width of the P3 and P4 from Samos both from the studied material, but also from the other *P. orbignyi* (Fig. 35). The specimens from Samos and Kryopigi exhibit a slightly slenderer M1 as opposed to AMPG-PG 95/1515, AMPG-PG 95/1516 and Perivolaki specimens (Fig. 35). The length of M2 for AMPG-PG 95/1515 is also slightly lower than of the other specimens (Fig. 35). The robusticity indexes for P3 and P4 for the material in study (Table 8) generally fall near the lower brackets for the observed values of *P. orbignyi* observed values: (42.86–64.38) for P3 and (58.36–73.86) for P4. Concerning the dental dimensions of *P. orbignyi*, Koufos (2006a) notes that it slightly varies in the Greek fossiliferous record, though its morphology stays rather conservative. This, Koufos (2006a) considers to be either due to sexual dimorphism or due to the geological age difference between the specimens. Lastly, de Beaumont & Mein (1972) exemplified the difference in P4/M1 angles among *P. orbignyi* and other similar taxa such as *P. gaudryi* de Beaumont & Mein, 1972 and *Herpestides antiquus* de Blainville, 1842. Following that, the external margins of P4 and M1 for the material studied form angles of approximately 124°–129°. These angles are close in value with those calculated for some other *P. orbignyi* specimens (~121°–140°) (Fig. 36).

Besides *P. orbignyi*, at least four other representatives have been recognized in the European Miocene. *“P”. collectus* de Bonis, 1973 from Laugnac of France (MN 2) would be the oldest representative both of the genus and the family, if not for its uncertain taxonomic status (Turner et al., 2008). *P. gervaisi* de Beaumont & Mein, 1972 is the oldest recognized true hyaenid found in the Early-Middle Miocene (MN 4–5) of France and possibly Spain (Werdelin & Solounias, 1991; Turner et al., 2008). While the P4 from France (de Beaumont & Mein, 1972) is only slightly slenderer compared to the P4 of *P. orbignyi*, the preserved P3 of *P. gervaisi* from Spain (Petter, 1976) is greatly reduced in width. (Fig. 35). Also, *P. gervaisi* has a higher protocone than parastyle in its P4 (Beumont & Mein, 1972; Petter 1976), whereas in *P. orbignyi* and the studied material they are more or less of the same height. *P. gaudryi* is known from the Middle Miocene locality of La Grive-Saint-Alban L5 in France (MN 7–8) and its P4 is comparable in size with that of *P. orbignyi* and the studied specimens (Fig. 35) (de Beaumont & Mein, 1972; Koufos 2009). Werdelin & Solounias (1991) have commented that *P. gervaisi* and *P. gaudryi* might actually belong to the same species, but the apparent absence of material from both species renders any further claims impossible. The Turolian *P. guerini* Villalta & Crusafont, 1948 found in the Turolian of Spain (MN 11–12) is known only by a few scarce remains, which were described by Montoya (1997). It is larger than both *P. orbignyi* and the material in question (Fig. 1). Its similarly larger P4 has a slightly projecting protocone and its M1 has a strong parastyle of similar size to *P. gaudryi* (Montoya, 1997; Sen & Saraç, 2018). Werdelin & Solounias (1991) mention that it is less derived than *P. orbignyi*, having a higher protoconid and lower metaconid. *P. faventinus* Torre, 1989 is known from the Late Turolian (MN 13) of Brisighella in Italy and Pliocene of Spain (MN 14) (Torre, 1989; Alcalá 1994; Koufos, 2009). It is more evolved and larger in size both from the other *Plioviverrops* and the material in study (Fig. 35), with more molarized premolars amongst other differences.

Concluding, the morphology of the teeth studied, the angle formed between P4–M1 and the subsequent metrical comparisons allow the attribution of the material to *Plioviverrops orbignyi*. The differences observed are minor and not of significant importance, as they fall within the levels of the expected intraspecific variation.

The morphology and evolution of the genus and species has been discussed by de Beaumont (1969) and de Beaumont & Mein (1972) with noteworthy remarks regarding the primitive characters of the genus, such as the auditory bulla and the presence of the alisphenoid canal (Werdelin & Solounias, 1991). Members of the genus have evolved different adaptations from the general trend of hyaenid evolution and adapted towards an insectivore-omnivore niche while also retaining some primitive features such as moderate claw retraction (Werdelin &

Solounias, 1991; Turner et al., 2008). The Late Miocene *P. orbignyi* is considered the culmination of this trend, as it is evidenced by the small premolars, long m1, the low trigonid and high metaconid (Werdelin & Solounias, 1991). It has been noted that within the genus *P. orbignyi* has the most derived dental characters, indicating a hypocarnivorous morphology (Werdelin & Solounias, 1991 and references therein). These dental adaptations probably made Thenius (1966) to suggest that the extant *Proteles cristatus* derived from *P. orbignyi*. This claim has since been disregarded however, as more recent molecular data (Koepfli et al., 2006) suggested that *Proteles* diverged from the other extant hyaenas ~0.6 Ma, while *Plioviverrops* diverged ~18–17 Ma (Turner et al., 2008).

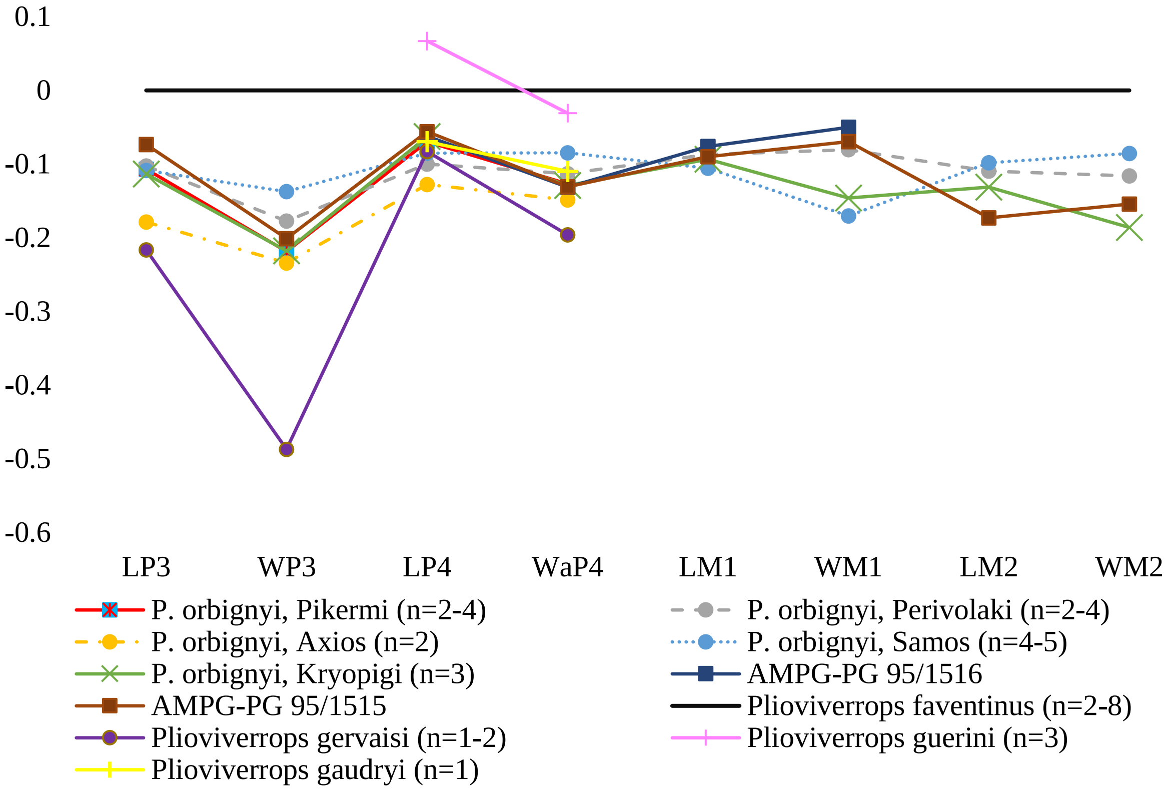

Figure 35. Log-ratio diagram for the upper dentition of *Plioviverrops orbignyi*. *P. faventinus* (n=2-8) mean values from Torre (1989) were used as standard. Data for *P. orbignyi* from Greece were acquired from de Bonis & Koufos (1991), Koufos (2006a; 2009) and Lazaridis (2015). Data for *P. gervaisi* were acquired from de Beaumont & Mein (1972) and Petter (1976). Data for *P. gaudryi* were acquired from de Beaumont & Mein (1972). Data for *P. guerini* were acquired from Montoya (1997).

Table 8. Upper dentition measurements (mm) of *Plioviverrops orbignyi* from Pikermi and other localities.

	Pikermi						Perivolaki	Axios	Samos	Kryopigi
	AMPG-PG 95/1516	AMPG-PG 95/1515	MNHN-PIK- 3022[1]		MNHN-PIK-3016[1]		(Koufos, 2006a)	(de Beaumont, 1969)	[1, 2, 3]	(Lazaridis, 2015)
		(de Bonis & Koufos, 1991)								
	dext	sin	dext	sin	dext	sin	n=2-4	n=2	n=2-5	n=2-3
LP3	—	7.64	7.20	7.10	7.00	7.00	7.15	6.00	7.05	6.97
WP3	—	3.67	4.00	—	3.00	3.10	3.88	3.40	4.25	3.53
LP4	10.17	10.32	10.10	10.30	9.70	10.00	9.33	8.75	9.65	10.16
HP4	5.15	5.08	—	—	—	—	—	—	—	4.90
WaP4	6.09	6.10	6.40	—	5.80	6.00	6.35	5.85	6.78	6.12
WblP4	3.30	3.34	—	—	—	—	—	—	—	4.23
LpP4	4.03	4.04	—	—	—	—	—	—	—	4.05
LmP4	3.29	3.15	—	—	—	—	—	—	—	2.90
LM1	6.15	5.96	—	—	—	—	6.00	—	5.75	5.91
WM1	8.51	8.14	—	—	—	—	7.93	—	8.60	6.82
LM2	—	3.76	—	—	—	—	4.35	—	4.47	4.14
WM2	—	5.61	—	—	—	—	6.13	—	6.57	5.21
R.I. P3	—	48.04	55.56	—	42.86	44.29	54.20	56.67	60.18	50.68
R.I. P4	59.88	59.11	63.37	—	59.79	60.00	68.09	66.86	69.67	60.29

[1]: de Bonis & Koufos (1991), [2]: de Beaumont, (1969), [3]: Koufos (2009).

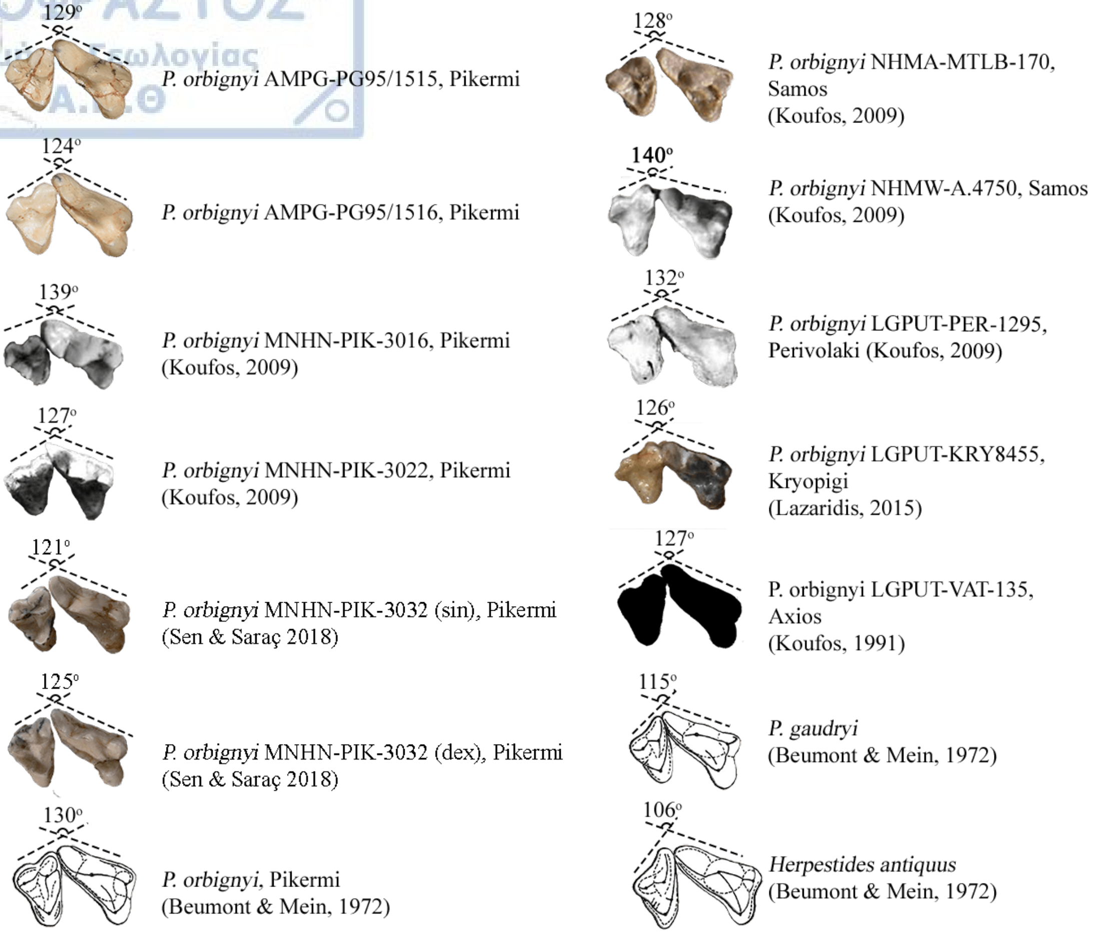

Figure 36. External angles formed between the carnassial and M1 amongst *P. orbignyi* and some other similar forms. The angles were digitally measured from photographs or figures. The angle value for LGPUT-VAT-135 was acquired from de Bonis & Koufos (1991) due to the absence of adequate photographic material. The angles are subject to the shooting angle and therefore some of these figures only represent an approximate value. Source of the photographs is listed next to its related specimen. Not in scale.

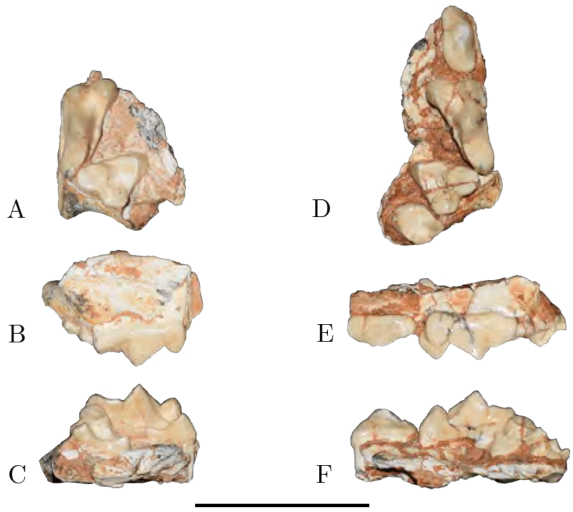

Figure 37. *Plioviverrops orbignyi* AMPG-PG 95/1516 (A-C) and AMPG-PG 95/1515 (D-F) in A, D: occlusal, B, E: buccal and C, F: lingual view. The scale bar is 2 cm.

Ictitheriinae indet.

(Figs. 38–45, Tables 9–23)

The bulk of this section's material refers to *Ictitherium viverrinum* sized taxa, with a few, potentially to *Hyaenictitherium wongii*. According to Pilgrim (1931) *I. viverrinum* is approximately 2/3 the size of *Hyaenictitherium wongii*. However, judging from the craniodental size variance exhibited by *I. viverrinum* (e.g., Gaudry, 1862; Werdelin, 1988b; present work) separation between the two taxa can be daunting. This only gets more challenging considering that, so far, there has only been scarce (e.g., Pilgrim, 1931) or vague (e.g., Semenov, 2008) reports about the possible morphological postcranial differences amongst *I. viverrinum* and *H. wongii*. In light of this, it was considered more appropriate to keep the material of this section under this generic attribution and instead provide some limited remarks regarding their possible allocation, until a more in-depth and larger in scale work between the postcranial material between these two species is undertaken. Granted the abundance of *I. viverrinum* craniodental remains in Pikermi over that of *H. wongii* however, in addition to the generally smaller size of the former, most of the material described herein would potentially fall under *I. viverrinum*.

Material: AMPG-PA 4963/91: proximal right humerus, AMPG-ΠG 88/521: proximal right humerus, AMPG-ΠK 1312: proximal left humerus, AMPG-PA 4964/91: distal epiphysis of right humerus, AMPG-PK 1304: distal epiphysis of right humerus, AMPG-PA 4965/91: distal epiphysis of right humerus, AMPG-PA 4966/91: distal epiphysis of left humerus, AMPG-PA 4985a/91: left humerus, AMPG-PA 4967/91: right proximal end of ulna with olecranon, AMPG-PA 4985b/91: left ulna, AMPG-PG 98/27: distal part of a left radius, AMPG-PA 4968/91: distal end of a left radius, AMPG-PA 4985c/91: left radius, AMPG-PA 4969/91: left scapholunate, AMPG-PA 4970/91: left scapholunate, AMPG-PA 4986/91: left scapholunate, AMPG-PA 4971/91: left magnum, AMPG-PA 4987a/91: left magnum, AMPG-PA 4987b/91: left unciform, AMPG-PA 4972/91: left Mc I, AMPG-PA 4973/91: left Mc I, AMPG-PG 98/24: left MC V, AMPG-PA 4974/91: right proximal epiphysis of Mc V, AMPG-PA 4988a/91: left Mc II, AMPG-PA 4988b/91: left Mc IV, AMPG-PA 4988c/91: left Mc V, AMPG-ΠK 1311: right femur without the distal epiphysis, AMPG-ΠK 1310: left proximal epiphysis, AMPG-PA 4975/91: right proximal epiphysis, AMPG-ΠG 88/523: right distal epiphysis, AMPG-ΠK 1314: left distal epiphysis, AMPG-PG 98/18: right tibia, AMPG-ΠG 88/351: distal half of a left tibia, AMPG-PG88/318: right calcaneum, AMPG-PA 4976/91: right 3rd cuneiform, AMPG-PA 4977/91: right cuboid, AMPG-PA 4978/91: right navicular, AMPG-PA 4979/91: right Mt III, AMPG-PA 4980/91: right Mt IV without the distal epiphysis, AMPG-PA 4981/91: proximal half of right Mt IV, AMPG-PA 4982/91: proximal epiphysis of right Mt V, AMPG-PA 4983/91: proximal half of right Mt V, AMPG-PA 4984a/91: proximal epiphysis of a right Mt II, AMPG-PA 5042/91: proximal half of a right Mt II, AMPG-PA 4984b/91: right Mt III without the distal epiphysis, AMPG-PA 4984c/91: right Mt IV, AMPG-PA 4984d/91: right Mt V without the distal epiphysis. (Figs. 38-45).

Remarks: The humerus AMPG-PA 4985a/91, ulna AMPG-PA 4985b/91, radius AMPG-PA 4985c/91, scapholunate AMPG-PA 4986/91, magnum AMPG-PA 4987a/91, unciform

AMPG-PA 4987b/91, Mc II AMPG-PA 4988a/91, "Mc III" AMPG-PA 4989/91, Mc IV AMPG-PA 4988b/91, Mc V AMPG-PA 4988c/91 were artificially restored and mounted in anatomical position atop a plastered base (Fig. 41). Further preparation revealed that the humerus, radius and ulna are indeed associated with each other as they were still connected by their original matrix. However, the carpals and metacarpals raised some doubts. Although the carpals are of the correct size and morphology to potentially be associated with each other, only the magnum and unciform certainly are, as they were still connected by their original matrix. More precisely, the scapholunate was glued erroneously, with its distal articular surface directed at the distal articular surface of the radius while the magnum and unciform were glued in the proximal surface of the scapholunate. As far as the metacarpals are concerned, the Mc II-IV-V exhibit a typical ictithere morphology and their similar size indicates that they are probably are associated with each other. The "Mc III" however, raises some serious questions, as its proximal half turned out to be a distal metapodial epiphysis from some other, unrelated animal that was glued onto a probably ictithere distal metapodial that could just as likely be any central (III or IV) metapodial. The nature of the erroneous proximal epiphysis (AMPG-PA 4990/91) cannot be further ascertained at the given time, although, it bears some resemblance with the distal epiphysis of Mc I from *A. eximia* described by Roussiakis (1996). It must be noted, that even then, the AMPG-PA 4990/91 is slightly larger than the Mc I and it also has a slight but distinct dorso-plantar edge in its articular surface, which is apparently missing from the smoothened Mc I of *A. eximia*. Considering the size difference between the frontal limb, the carpals and the metacarpals, it is doubted that they were all from one individual and possibly species. To that end, apart from the Mc II-IV-V, the rest are considered associated only if they were still connected by their original matrix.

The right Mt II-V AMPG-PA 4984a-d/91 are probably associated.

Humerus: In the proximal part of the humerus, the greater tuberosity is situated at the antero-lateral side of proximal epiphysis. It is slightly higher than the head of the humerus and has two surfaces, one anterior and one posterior, with the former being convex, which serves as attachment for the supraspinatus, infraspinatus and teres minor muscles. The smaller lesser tuberosity is situated medially in same level as the head and serves for the attachment of the subscapularis. The two tuberosities are separated by the groove for the biceps brachii, the intertubercular sulcus, which is situated slightly towards the medial side. Also, in the lips of intertubercular sulcus, the pectoralis major, teres major and latissimus dorsi insert. The shaft is not preserved in its entirety in any humeri, however, the preserved cross-sections indicate an elliptical shape, with its larger side directed antero-posteriorly. In the distal part of the humerus, the supratrochlear foramen is situated within the coronoid fossa. The supracondyloid foramen is either not preserved or not formed. The bases of the bar however are present in all specimens. On that, Roussiakis (1996) notes that on some specimens (e.g., AMPG-PA 3369/91) the bar is completely ossified. The lateral and medial epicondyles are situated respectively in the lateral and medial side of the distal epiphysis. The medial is the larger of the two and extends more distally. The lateral and medial margins of the distal articular surface in the posterior side are almost vertical. The trochlea, which articulates with the ulna, in the distal articular surface of the humerus extends from the anterior through the posterior side. Posteriorly, the distal articular surface is divided between the capitulum laterally, which articulates with the radius, and the trochlea medially.

The morphology of AMPG-PA 4985a/91 is almost identical as described above. The only noticeable difference, aside from tis larger size, is the enlarged and more prominent greater tuberosity it exhibits. Although, this may be the effect of its transversal compressed. The shaft is elliptical in cross-section. The deltoid tuberosity which serves as attachment point for the deltoid muscle is located in the proximal half of the shaft. Although it does not extend much laterally, it approximately occupies about 1/3 of the shaft.

Discussion: With the exception of AMPG-PA 4985a/91 all the other humeri described are similar both in morphology and size. Thus, they can probably be attributed to the same species. Comparison with the humeri attributed to *I. viverrinum* by Gaudry (1862) and Roussiakis (1996) exemplified their metrical and morphological similarities with that species and therefore probably belong to it as well. Concerning the larger AMPG-PA 4985a/91, as stated above, its morphology is very similar to that of the other humeri described and, by extension, to the humeri of *I. viverrinum* described by the aforementioned authors. Its size however, is about 12% larger than the humeri attributed to *I. viverrinum*. In addition, its greater tuberosity is also more prominent than AMPG-PA 3369/91 that was described by Roussiakis (1996). Still, however, its size is smaller than the referred *H. wongii* size according to Pilgrim (1931) (1/3 larger than *I. viverrinum*). Considering the above, in addition to the absence of any comparative *H. wongii* material, it cannot be currently ascertained further whether this is a large *I. viverrinum* or a probably smaller *H. wongii*.

Ulna: The olecranon is almost flat antero-posteriorly. The anconeal and coronoid process are approximately at the same level. The trochlear notch is not particularly deep. The olecranon is of moderate height. The anconeal process extends only slightly more anteriorly than the most proximal end of the olecranon. The lateral coronoid process preserved in AMPG-PA 4967/91 would have articulated to the radius.

The complete AMPG-PA 4985b/91 exhibits the same general morphology but tis overall larger by approximately 12%. The shaft is triangular in cross-section. The medial olecranon tuberosity is higher than the lateral, yet slenderer at the same time. Distally it is articulated with the radius through a well-developed styloid process. A small articular facet in the distalmost part of the ulna would articulate with the pisiform.

Discussion: The two ulnas are morphologically similar and their only difference is dimensional. The smaller's AMPG-PA 4967/91 morphology and dimensions fit the ulnas described by Gaudry (1862) and Roussiakis (1996) and attributed to *I. viverrinum*. Concerning the larger AMPG-PA 4985b/91, the same arguments mentioned against its associated humerus AMPG-PA 4985a/91 apply here as well. Also, although larger than the ulnas stored at AMPG, it is only slightly so from the ulna MNHN-PIK. 3083 attributed by Gaudry (1862) to *I. viverrinum* according to the dimensions provided by Roussiakis (1996).

Radius: AMPG-PG 98/27 and AMPG-PA 4968/91 preserve only their distal ends. The three grooves observed in posterior view serve–from medial to lateral–as attachment points for the external abductor pollicis longus, the external carpi radialis and the external digitalis communis. The groove for the external abductor pollicis longus is the narrowest. The distal articulation surface articulates with the scapholunate and is slightly concave and medio-laterally elongated. Medially, the shaft articulates with the ulna through a vertically oval articulation surface.

AMPG-PA 4985c/91 is completely preserved and is still articulated with its ulna. The shaft of the radius is convex anteriorly and in cross-section its elliptical. The proximal epiphysis inclines slightly towards the anteromedial direction. Its proximal surface articulates with the humerus. The proximal epiphysis's posterior margin is convex and articulates with the ulna, while its anterior margin is flat. The distal epiphysis is morphologically similar to the radii described above and only differ in their size.

Discussion: The two smaller radii are identical both in size and morphology and can therefore be attributed to the same species. Morphological and metrical comparison with the radii described by Gaudry (1862) and Roussiakis (1996) under *I. viverrinum*, showed that they are similar and probably belong to the same species as well. Concerning the larger AMPG-PA 4985c/91, the same arguments issued against its associated humerus AMPG-PA 4985a/91 apply here as well.

In addition, Roussiakis (1996) and Gaudry (1862) note that the humerus of *Ictitherium viverrinum* is longer than its radius. That is also true for the larger AMPG-PA 4985c/91 radius and its associated humerus AMPG-PA 4985a/91. Unfortunately, these proportions are undocumented in *H. wongii* therefore it is still unknown whether this is a unique trait of *I. viverrinum*.

Scapholunate: It is medio-laterally elongated. Proximally it would articulate with the radius through its dorso-plantarly convex surface. Its dorso-plantar length is almost half its transversal length. The medio-plantar side of the scapholunate is marked by the flexor carpi radialis groove. The plantar tubercle is relatively short but strong. The distal articular surface articulates through some concave facets from medial to lateral with the trapezoid, magnum and unciform. The articular facet for the trapezoid is shallow compared to the others mentioned. These articular surfaces are divided by some small ridges in-between. The articular surface for the unciform is the largest.

Discussion: The AMPG-PA 4969/91 and AMPG-PA 4986/91 scapholunates are morphologically and metrically similar and can therefore be attributed to the same species. Comparison with the scapholunates from Pikermi attributed as *I. viverrinum* by Roussiakis (1996), showed they all probably belong to belong to the same species due to their similar morphology and dimensions.

The larger AMPG-PA 4970/91 scapholunate differs through its larger size and slightly in its morphology. The articular facet for the trapezoid in AMPG-PA 4970/91 is concave and better developed than in the smaller two. Comparing it against *I. viverrinum* material from other authors, not only is it larger in size, but it also cuts really close to the size difference mentioned by Pilgrim (1931) between *I. viverrinum* and *H. wongii*. Additionally, there is the matter of the trapezoid facet to consider. This morphological difference occurs in larger Hyaeninae (Roussiakis, 1996, present work). This could mean that AMPG-PA 4970/91 could either be a *H. wongii* or, potentially, even a *L. chaeretis*. Unfortunately, there are no scapholunates available from either of these taxa for further comparisons.

Magnum: It is elongated in the dorso-palmar direction. The proximal articular surface articulates with the scapholunate through a convex articular surface. A relatively narrow articular facet in its lateral side articulates it with the unciform. It articulates with Mc II medio-plantarly through two elliptical articular facets. Dorsally it articulates with the trapezoid through a small articular surface. The larger plantar articular surface is concave and articulates with Mc III.

Discussion: Both AMPG-PA 4987a/91 and AMPG-PA 4971/91 magnums exhibit the same morphology. They only differ in their size. Further comparison showed that their morphology is the same as the described *I. viverrinum* material from Pikermi by Roussiakis (1996). The size of AMPG-PA 4971/91 is, however, approximately 20% larger than the aforementioned material. Considering the size and morphology of AMPG-PA 4971/91, it could be either a large *I. viverrinum* or a *H. wongii*. The smaller size of AMPG-PA 4987a/91 on the other hand, probably indicates a more clear-cut affinity with the material of *I. viverrinum* described by Roussiakis (1996).

Unciform: It is elongated in the dorso-plantar direction but overall robust. Proximally it’s convex and articulates with the scapholunate. Distally it’s concave and articulates laterally with Mc V and medially with Mc IV. In its lateral side is slightly convex and articulates with the pyramidal and its medial side is concave and articulates with the magnum. The dorsal and plantar sides are relatively flattened, with the latter also being slightly wider.

Discussion: Its morphology is similar to the *I. viverrinum* material described by Roussiakis (1996). Metrically, it is similar aside from its slightly narrower transversal dimensions. Taking into account that it was articulated with the magnum AMPG-PA 4987a/91 whose dimensions and morphology also fit the material of *I. viverrinum* magnums described by Roussiakis (1996), it probably belongs to the same species as well.

Mc I: relatively small. The shaft is oval-shaped in cross-section. The proximal articular surface is concave in the dorso-plantar direction and articulates with the trapezium. The distal articular surface is strongly curved in the dorsal-plantar direction and inclines distally towards its medial side. Mc I AMPG-PA 4972/91 is slightly smaller in size than AMPG-PA 4973/91 but their morphology is similar.

Mc II: straight and has a relatively robust shaft. The proximal articular surface is slightly broken in its plantar edge, but its concave dorso-plantar surface where it would articulate with the trapezoid is still evident. Some small articular facets in the lateral side close to the proximal epiphysis indicate the articulation area with Mc III. The shaft is sub-triangular in cross-section with its more flattened side oriented laterally. The distal epiphysis is slightly rounded.

Mc IV: the longest of the preserved metacarpals. It is also straight but its shaft is less robust than Mc II. The proximal articular surface is elongated in the dorso-plantar direction and it’s slightly convex. There, it would articulate to the unciform and probably with the magnum as well towards its plantar side via a small elevated triangular surface. This surface has also been reported by Pilgrim (1931) for *A. eximia* and *H. wongii*, and more recently by Roussiakis (1996) for *I. viverrinum*. In the proximal epiphysis’s lateral side, a small surface articulates the metacarpal to Mc V. The dorsal side of the shaft is rather flat while its plantar side is marked by a small medially oriented ridge that more prominent close to the proximal epiphysis. The distal epiphysis is more rectangular-shaped than Mc II and Mc V.

Mc V: straight medially but concave laterally. It is slightly shorter than Mc II but has a similarly robust shaft. The proximal articular surface projects laterally, it is convex, sub-triangular and articulates with the unciform. The lateral projection serves as attachment point for the extensor capri ulnaris muscle. The medial proximal articular surface is narrow but elongated and articulates Mc V with Mc IV. The shaft is sub-triangular in cross-section with its flat side oriented medially. The distal epiphysis is sub-triangular in shape.

Discussion: The metacarpals described are morphologically similar to the *I. viverrinum* metacarpals described by Gaudry (1862), Pilgrim (1931) and Roussiakis (1996). Regarding the Mc I AMPG-PA 4973/91, its dimensions are slightly larger than the Mc I material described by Roussiakis (1996) but their morphology is the same. Regarding the metacarpals that were found mounted (Mc II AMPG-PA 4988a/91, Mc IV P AMPG-A 4988b/91, Mc V AMPG-PA 4988c/91), they only differ from the material described by Roussiakis (1996) by their slightly larger dimensions. The "Mc III" AMPG-PA 4989/91 from the mounted frontal limb is not taken into consideration, as it could very well be almost any other metapodial. The isolated Mc V AMPG-PG 98/24 is both morphologically and metrically similar to the *I. viverrinum* material described by Roussiakis (1996).

Considering the above, the isolated larger Mc I AMPG-PA 4973/91 and the aforementioned larger metacarpals of the restored manus could either refer to a larger *I. viverrinum* or a smaller *H. wongii*. Since their size however does not even approximate close to being 1/3 larger than the material attributed to *I. viverrinum* by other authors, it probably simply refers to larger *I. viverrinum* individuals due to intraspecific variation.

Femur: The head of the femur is smooth and rounded with the fovea, where ligamentum teres attaches, situated in the medial and slightly anterior side of it. The anterior margin of the cylindrical neck is horizontal, connecting it laterally with the greater trochanter. The latter serves as attachment point for gluteal muscles, such as gluteus medius, gluteus minimus and piriformis. The anterior margin of the greater trochanter is situated approximately in the same level as the head, except the black, which is slightly lower. In the posterior side, the smaller lesser trochanter is situated distally and in-between the greater trochanter and the neck. The lesser trochanter serves as attachment point for the iliopsoas muscles. The two trochanters are connected in the posterior side with the trochanteric crest. The intertrochanteric line is a ridge that traces in a medial-distal direction of the anterior side of the femur towards the posterior side, passing just below the lesser trochanter. The intertrochanteric line serves as attachment for the iliofemoral ligament. In the posterior side, the two trochanters connect via the almost vertical ridge of the quadrate tubercule. Also, in-between the neck of the head, the intertrochanteric crest and the greater trochanter a reversed triangular in shape groove is formed. The preserved shaft of AMPG-ΠΚ 1311 is relatively slender, almost cylindrical in cross-section and below the second half appears to curve slightly towards the medial side. In the posterior side of the shaft, a weakly linea espera can be observed tracing distally. The medial and lateral condyles at the distal epiphysis articulate with the tibia posteriorly and with the patella anteriorly. The patellar surface in the anterior side extends proximally, just above the epicondyles. The medial and lateral epicondyles are situated in the medial and lateral side respectively and are about the same size. The intercondylar fossa situated in the posterior side of the femur and in-between the two condyles serve as attachment point for ligaments of the knee.

Discussion: The proximal femurs in question are morphologically similar and metrically close, albeit slightly smaller–especially AMPG-ΠΚ 1310 –, to the *I. viverrinum* femur described by Gaudry (1862). The isolated distal ends of the femurs in study are provisionally attributed together with the proximal femurs described based on their size and morphology. The smaller distal femurs (AMPG-ΠΚ 1314 and AMPG-ΠG 88/523) seem to match in size and morphology the femurs preserving their proximal ends. It is acknowledged that AMPG-PA 1304 is way too large compared to the other femurs. Also, the trochanters on its patellar surface are more prominent and better developed than in AMPG-ΠΚ 1314 and AMPG-ΠG 88/523. Considering the metrical data of by Gaudry (1862) however, the larger AMPG-PA 1304's width and morphology is very close to *I. viverrinum*, while AMPG-ΠΚ 1314 and AMPG-ΠG 88/523 would probably be considered small.

Unfortunately, there are no more available specimens for comparison besides that one femur attributed to *I. viverrinum* by Gaudry (1862). Whether the femurs described herein belong to one species that exhibits quite extensive intraspecific variance or to different species is currently unknown until more femurs are studied. Based on their smaller size and Gaudry's (1862) attribution, these femurs are more likely to belong to *I. viverrinum* than *H. wongii*.

Tibia: The tibia is wide proximally, gradually narrows and slightly widens again distally. In the proximal articular surface, the medial and slightly larger lateral condyles of the tibia articulate with the condyles of the femur. In-between the two condyles, there is an area projecting slightly upwards, which refers to the intercondylar eminence in its centre and the lateral and medial intercondylar tubercules in its sides. This area articulates with the intercondylar fossa of the femur and also serves as attachment point for the knee joint ligaments. The popliteal notch, which serves as attachment for the flexor of the joint–the popliteus muscle –, lies in the posterior side, between the two condyles. A prominent and concave tibial tuberosity, where the patellar ligament inserts, projects in the middle of the anterior side's proximal articular surface. The strong tibial tuberosity turns into a prominent tibial crest which continues distally along the shaft's anterior surface, until it gradually fades above the middle of the shaft. The shaft is sub-triangular in cross section and although thick proximally, it narrows down a lot just above its middle. The anterior side of the shaft is almost straight, while the posterior turns slightly convex towards the distal half. In anterior view the distal half of the shaft curves slightly towards the lateral side. In the shaft's posterior surface, two distinct grooves trace towards the distal half in a slight distal-medial direction. The more prominent groove refers to the soleal line, where the soleus muscle originates. The weaker groove probably refers to a nutrient artery. In the distal part of the tibia, the medial malleolus projects distally in the medial side. In the lateral side of the distal end of the tibia, the fibular notch articulates with the fibula. In the posterior side, two grooves serve as attachment points for the tibialis posterior and the flexor longus digitorum (the weaker groove) tendons. The distal articular surface of the tibia articulates with the astragalus and other tarsals to form the pes.

Discussion: The distal half of the left tibia AMPG-ΠG 88/351 has a slightly smaller distal articular surface and a slightly thinner transversally proximal shaft. Their generally close metrical values and identical morphology however, is probably best explained due to intraspecific variation rather than a difference in species.

Although similar in length, the proximal articular surface of AMPG-PG 98/18 is larger than the dimensions provided by Pilgrim (1931) for *I. viverrinum*. Also, Pilgrim (1931) notes that the femur of *I. viverrinum* is slightly longer than its tibia. In regard to that last note, although the femurs described herein and the tibia AMPG-PG 98 are not from the same individuals it seems that the femurs would be much smaller than the tibia. Even taking intraspecific variation into consideration it would probably be a little extreme for both the femurs and the tibia to belong to the same species.

Calcaneum: The proximal surface is flattened, sub-rectangular and the calcaneal tuberosities are low and not very developed. The process of the tuberosity does not extend plantarly but is rather limited close to the proximal level. The body of the calcaneum is elongated relatively to its length. Dorsally, the body narrows down progressively towards the articular facets of the talus. Contrasting this, the plantar side of the body is straight and more robust and exhibits a lateral inclination. The talus articulates with the calcaneum through three distinct articular surfaces in a concave area near the plantar half of the calcaneum. The larger talar articular surface faces almost distally. The medially projecting, sub-triangular sustentaculum tali refers to the second area of articulation. The third articular surface is a small facet below the sustentaculum tali that is facing towards the medial side. On the sustentaculum tali's plantar side, the groove for the flexor hallucis longus tendon can be observed. Laterally, a groove marks the body of the calcaneum in a dorsal-distal direction. The fibular trochlea's projection is subtle on the lateral side of the calcaneum and it's situated approximately at the sustentaculum tali's distal margin level. The distal surface is sub-triangular, almost flat, gently inclines laterally and articulates with the cuboid bone.

Discussion: It is attributed to Ictitheriinae based on its size and morphology. More specifically, based on its similar morphology and size to a partially preserved calcaneum described by Roussiakis (1996), the length of a calcaneum provided by Pilgrim (1931) and a figure by Gaudry (1862; Pl. IX, Fig. 7), this calcaneum might actually belong to *I. viverrinum*.

3rd cuneiform (ectocuneiform): The proximal articular surface is marked by a groove and articulates with the navicular. The distal articular surface is T-shaped and articulates with Mt III. Laterally it articulates with the cuboid through some slight articular facets. Medially it articulates with the Mt II via a projecting articular surface. It articulates with the 2nd cuneiform through some medial and proximal articular surfaces.

Discussion: The morphology is similar to the 3rd cuneiforms described by Roussiakis (1996) and Pilgrim (1931) that are attributed to *I. viverrinum*. The size of AMPG-PA 4976/91 however is larger than the ectocuneiforms described by Roussiakis (1996) and slightly larger than the ectocuneiform described by Pilgrim (1931). Considering their dimensional difference is rather slight however, it is probable that this is the effect of intraspecific variation and AMPG-PA 4976/91 also belongs in the same species.

Cuboid: It is dorso-plantarly elongated. The almost flat, rectangular proximal articular surface is larger than the plantar. Proximally it articulates with the calcaneum. The plantar articular surface separates by a small edge into two facets. The larger, medial facet articulates with Mt IV, while the smaller, lateral facet articulates with Mt V. In the medial side it articulates with the 3rd cuneiform, while in the lateral side it articulates with the navicular. The groove for the peroneus longus is relatively long.

Discussion: Its morphology is that of a hyaenid and except its dorso-palmar elongation, its dimensions are close to the cuboids attributed to *I. viverrinum* by Roussiakis (1996) and Pilgrim (1931). As the enlargement is only in one dimension rather than proportional, a difference in species is more likely. In that case and based on its size, it would probably belong to *H. wongii*. Due to the absence of comparative cuboids from *H. wongii* however, further comparisons are impossible.

Navicular: it is elongated in the dorso-plantar axis and relatively compressed proximo-distally. The proximal articular surface is concave, rectangular-shaped and articulates with the talus. The distal surface articulates with the 3rd cuneiform dorso-laterally, with the 2nd cuneiform dorso-medially and with the 1st cuneiform towards its latero-plantar side. Lastly, it also articulates with the cuboid in its lateral side.

Discussion: Its morphology is similar to that of *I. viverrinum* described by Roussiakis (1996). It is slightly larger however and therefore it could potentially belong to either *H. wongii* or simply a larger *I. viverrinum* individual.

Mt II: only a slightly damaged proximal half is preserved. Its cross-section and proximal articular surface are triangular and elongated in the dorsal-palmar axis. The proximal epiphysis articulates medially with the 1st cuneiform and laterally with Mt III via some not very well-preserved notches. The dorsal side of the preserved shaft is relatively sharp. As Roussiakis (1996), Solounias (1981) Pilgrim (1931) have also noted, Mt II is slightly higher than Mt III when articulated. Solounias (1981) also adds that in more cursorial-adapted taxa Mt II is actually on the same level with Mt III.

Mt III: it is slightly broader than the rest of the metatarsals. Its shaft is slightly concave when viewed from the side. Its cross-section is sub-rectangular. The proximal articular surface is slightly convex and a narrow process projects towards its plantar side. It articulates medially with Mt II via two small articular facets and laterally with Mt IV via a larger articular facet in the concave area created by the aforementioned plantar process.

Mt IV: it is sub-triangular in cross-section with a ridge formed in its plantar side. Similar to Mt III, its shaft is slightly wider than its dorsoplantar length. The proximal articular surface is dorsoplantar elongated and convex. A slight transversal groove marks the proximal epiphysis towards its plantar side. Medially it articulates with Mt III via a medially projecting articular surface. Laterally it articulates with Mt V via two articular surfaces, one close to the proximal epiphysis and one in the slight notch below it. The distal epiphysis is rectangular-shaped.

Mt V: It is triangular in its cross-section and the shaft's lateral side is rather sharp. Additionally, the shaft is slightly concave in dorsal view. The proximal epiphysis is marked by the presence of two tuberosities. The lateral tuberosity is high and situated above the articular surface of the epiphysis while the latero-plantar tuberosity is low and close to the articular surface. Medially it articulates with Mt IV via a slightly projecting articular facet. Concerning the tuberosities, Roussiakis (1996) and Pilgrim (1931) note that they probably serve as insertion areas for the peroneus longus.

Discussion: The metatarsal material described are of similar morphology and size and therefore probably belong to the same species. Comparison with the material attributed to *I. viverrinum* by Roussiakis (1996) further exemplified their similar size and morphology. Based on this, both samples probably belong to the same species. Also, Pilgrim (1931) makes a note about the presence of the tuberosities on Mt V, specifying that they are a unique trait of *I. viverrinum* which sets it apart from *H. wongii*. Taking Pilgrim’s (1931) note into consideration for the material described here, all of these metacarpals can probably be attributed to *I. viverrinum*.

Metapodials: The metapodials attributed to this section lack their proximal epiphysis, but their size and morphology resembles that of Ictitheriinae. A-E in Fig. 45 are probably either II or IV metapodials, while F-I in the same figure are probably central metapodials (III or IV).

Table 9. Humerus measurements (mm) of Ictitheriinae from Pikermi.

	L	H.f	DAPpr.	DTpr.	DAPdia.	DTdia.	DTdist.	DAPdist.	DTdist.art.
AMPG-ΠG 88/521 (dext)	—	—	32.64	21.90	—	—	—	—	—
AMPG-PA 4963/91 (dext)	—	—	33.01	21.64	—	—	—	—	—
AMPG-ΠK 1312 (sin)	—	—	31.00	21.17	—	—	—	—	—
AMPG-PA 4964/91 (dext)	—	—	—	—	—	—	(25.79)	19.98	18.75
AMPG-PK 1304 (dext)	—	—	—	—	—	—	29.28	20.99	18.26
AMPG-PA 4965/91 (dext)	—	—	—	—	—	—	29.05	20.81	18.16
AMPG-PA 4966/91 (sin)	—	—	—	—	—	—	27.76	21.12	19.07
AMPG-PA 4985a/91 (sin)	169.90	162.95	40.32	20.25	19.28	9.24	30.22	21.11	24.25
I. viverrinum AMPG-PA 3369/91 (Roussiakis, 1996)	150.30	145.90	34.30	22.30	13.80	10.80	26.70	18.80	—
I. viverrinum AMPG-PA 3439/91 (Roussiakis, 1996)	—	—	—	—	—	—	28.70	19.50	—
I. viverrinum AMPG-PA 3449/91 (Roussiakis, 1996)	—	—	35.40	21.00	—	—	—	—	—
I. viverrinum MNHN-PIK. 3233 (Roussiakis, 1996)	150.90	142.10	31.00	21.70	11.60	9.10	24.90	18.10	—

Table 10. Ulna measurements (mm) of Ictitheriinae from Pikermi.

	L	DAPanc.	DTpr.	Ht.n	OH	DAPt.n	DAPdia.	DTdia.	DAPdist.	DTdist.
AMPG-PA 4967/91 (dext)	—	19.17	8.43	14.34	16.53	11.43	—	—	—	—
AMPG-PA 4985b/91 (sin)	178.00	24.66	11.47	22.67	16.02	13.40	11.40	(10.00)	(6.58)	8.74
I. viverrinum AMPG-PA 3371/91 (Roussiakis, 1996)	—	—	—	—	—	—	9.50	7.60	9.00	—
I. viverrinum AMPG-PA 3441/91 (Roussiakis, 1996)	—	20.70	12.00	17.80	—	12.20	—	—	—	—
I. viverrinum AMPG-PA 3442/91 (Roussiakis, 1996)	—	20.80	—	—	—	—	—	—	—	—
I. viverrinum AMPG-PA 239/91 (Roussiakis, 1996)	—	21.30	—	—	—	12.00	—	—	—	—
I. viverrinum MNHN-PIK. 3083 (Roussiakis, 1996)	164.00	22.00	—	—	—	12.20	8.50	9.00	8.30	—
I. viverrinum NHMUK-M. 9014 (Pilgrim, 1931)	—	—	—	16.00	—	—	—	—	—	—

Table 11. Radius measurements (mm) of Ictitheriinae from Pikermi.

	L	DAPpr.	DTpr	DTdia.	DAPdia.	DTdist.	DAPdist.
AMPG-PG 98/27 (sin)	—	—	—	9.77	7.56	18.75	12.27
AMPG-PA 4968/91 (sin)	—	—	—	—	—	20.40	13.42
AMPG-PA 4985c/91 (sin)	153.87	10.75	16.11	11.84	(8.05)	20.51	13.91
I. viverrinum AMPG-PA 3370/91 (Roussiakis, 1996)	137.50	10.60	14.70	10.30	6.90	20.00	13.40
I. viverrinum AMPG-PA 3440/91 (Roussiakis, 1996)	—	10.10	14.50	—	—	—	—
I. viverrinum AMPG-PA 1083/91 (Roussiakis, 1996)	—	—	—	—	—	20.20	13.30
I. viverrinum NHMUK-M. 9014 (Pilgrim, 1931)	—	—	15.00	—	—	—	—
I. viverrinum NHMUK-M. 9015 (Pilgrim, 1931)	—	—	—	—	—	20.00	—

Table 12. Scapholunate measurements (mm) of Ictitheriinae from Pikermi.

	Hmax.	DAPmax.	DTmax.
AMPG-PA 4969/91 (sin)	12.01	10.31	17.68
AMPG-PA 4970/91 (sin)	16.23	14.47	24.24
AMPG-PA 4986/91 (sin)	12.66	10.26	17.90
I. viverrinum AMPG-PA 3391/91 (Roussiakis, 1996)	—	11.00	16.20
I. viverrinum MNHN (unnumbered) (Roussiakis, 1996)	—	10.60	16.00

Table 13. Magnum measurements (mm) of Ictitheriinae from Pikermi.

	Hmax.	DAPmax.	DTmax.
AMPG-PA 4971/91 (sin)	9.00	16.48	7.80
AMPG-PA 4987a/91 (sin)	7.11	13.72	7.82
I. viverrinum AMPG-PA 3395/91 (Roussiakis, 1996)	7.20	12.80	6.30
I. viverrinum AMPG-PA 1076/91 (Roussiakis, 1996)	7.30	13.00	6.80

Table 14. Unciform measurements (mm) of Ictitheriinae from Pikermi.

	Hmax.	DAPmax.	DTmax.
AMPG-PA 4987b/91 (sin)	8.46	11.37	7.45
I. viverrinum AMPG-PA 3395/91 (Roussiakis, 1996)	7.60	10.10	9.20
I. viverrinum AMPG-PA 1076/91 (Roussiakis, 1996)	7.70	10.20	8.80

Table 15. Metacarpal measurements (mm) of Ictitheriinae from Pikermi.

	L	DAPpr.	DTpr.	DAPdia.	DTdia.	DAPdist.	DTdist.
Mc I AMPG-PA 4972/91 (sin)	20.43	5.24	5.13	3.85	3.71	3.63	4.07
Mc I AMPG-PA 4973/91 (sin)	24.09	5.98	6.27	3.69	4.01	4.82	5.27
I. viverrinum Mc I AMPG-PA 1087/91 Roussiakis, 1996)	21.00	5.20	5.50	3.90	4.00	5.40	6.00
I. viverrinum Mc I AMPG-PA 3388/91 Roussiakis, 1996)	21.00	5.20	5.80	3.80	4.00	5.30	6.20
Mc II AMPG-PA 4988a/91 (sin)	50.80	—	8.24	5.01	6.69	7.83	8.70
I. viverrinum Mc II AMPG-PA 3384/91 Roussiakis, 1996)	49.10	9.50	5.90	5.00	6.00	7.50	7.90
I. viverrinum Mc II (Gaudry, 1862)	48.00	—	—	—	—	—	—
I. viverrinum Mc II NHMUK-M. 9013 (Pilgrim, 1931)	49.00	—	—	—	—	—	—
Mc IV AMPG-PA 4988b/91 (sin)	58.66	9.75	6.53	4.89	6.13	8.47	8.10
I. viverrinum Mc IV AMPG-PA 3381/91 (Roussiakis, 1996)	58.30	9.80	7.00	5.30	5.60	7.70	7.00
I. viverrinum Mc IV AMPG-PA 1062/91 (Roussiakis, 1996)	58.00	9.60	(6.50)	4.90	5.40	7.30	7.00
I. viverrinum Mc IV NHMUK-M. 9013 (Pilgrim, 1931)	55.00	—	—	—	—	—	—
Mc V AMPG-PA 4988c/91 (sin)	48.00	9.53	10.89	5.10	6.52	8.21	9.60
Mc V AMPG-PG 98/24, (sin)	44.55	8.04	8.42	4.65	5.83	(4.86)	7.11
Mc V AMPG-PA 4974/91 (dext)	—	8.30	9.00	—	—	—	—
I. viverrinum Mc V AMPG-PA 3376/91 (Roussiakis, 1996)	46.70	9.10	8.90	5.00	6.60	7.50	(8.50)
I. viverrinum Mc V AMPG-PA 1063/91 (Roussiakis, 1996)	46.80	9.00	8.60	4.80	6.50	7.60	9.00
I. viverrinum Mc V NHMUK-M. 9013 (Pilgrim, 1931)	47.00	—	—	—	—	—	—

Table 16. Femur measurements (mm) of Ictitheriinae from Pikermi.

	L	DAPpr.	DTpr.	DAPdia.	DTdia.	DAPdist.	DTdist.
AMPG-ΠΚ 1311 (dext)	[157.00]	15.31	35.81	9.47	12.45	—	—
AMPG-ΠΚ 1310 (sin)	—	15.35	32.09	—	—	—	—
AMPG-PA 4975/91 (dext)	—	16.15	35.93	—	—	—	—
AMPG-ΠΚ 1314 (sin)	—	—	—	—	—	19.34	24.25
AMPG-ΠG 88/523 (dext)	—	—	—	—	—	23.32	26.03
AMPG-ΠΑ 1304 (dext)	—	—	—	—	—	39.00	31.48
I. viverrinum, Pikermi (Gaudry, 1862)	160.00	—	37.00	—	—	—	31.00

Table 17. Tibia measurements (mm) of Ictitheriinae from Pikermi.

	L	DAPpr.	DTpr.	DAPdia.	DTdia.	DAPdist.	DTdist.
AMPG-PG 98/18 (dext)	168.70	37.80	34.30	15.01	12.96	15.49	22.75
AMPG-ΠG 88/351 (sin)	—	—	—	14.76	11.51	13.30	20.94
I. viverrinum AMPG-PA 2652/91 (Roussiakis, 1996)	—	—	—	—	—	15.20	21.70
I. viverrinum AMPG-PA 3479/91 (Roussiakis, 1996)	—	—	—	—	—	15.20	(20.30)
I. viverrinum AMPG-PA 3399/91 (Roussiakis, 1996)	—	—	—	—	—	14.00	—
I. viverrinum MNHN-PIK. 3129 (Roussiakis, 1996)	(155.60)	—	—	15.00	10.80	14.00	22.00
I. viverrinum MNHN-PIK. 3122 (Roussiakis, 1996)	—	—	—	—	—	15.00	22.00
I. viverrinum MNHN-PIK. 3032 (Roussiakis, 1996)	—	—	—	—	—	—	18.00
I. viverrinum NHMUK-M. 9012 (Pilgrim, 1931)	152.00	—	(24.00)	—	—	—	18.00
I. viverrinum NHMUK-M. 9010 (Pilgrim, 1931)	168.00	—	27.00	—	—	—	20.00

Table 18. Calcaneum measurements (mm) of Ictitheriinae from Pikermi.

	L	DAPpr.	DTpr.	DAPcol.	DTcol.	DAPmax.	DTmax.	DAPdist.	DTdist.
AMPG-PG88/318 (dext)	39.56	10.61	14.73	13.54	8.63	17.45	15.60	10.27	11.80
I. viverrinum, AMPG-PA 3400/91 (Roussiakis, 1996)	—	—	—	—	—	(15.50)	17.30	—	—
I. viverrinum, MNHN-PIK. 3126, Pikermi (Roussiakis, 1996)	—	—	—	14.10	(8.10)	(17.10)	16.60	—	—
I. viverrinum, NHMUK-M. 9010 (Pilgrim, 1931)	41.50	—	—	—	—	—	—	—	—

Table 19. Ectocuneiform measurements (mm) of Ictitheriinae from Pikermi.

	Hmax.	DAPmax.	DTmax.
AMPG-PA 4976/91 (dext)	9.55	17.67	9.40
I. viverrinum AMPG-PA 3403/91 (Roussiakis, 1996)	9.00	14.70	8.50
I. viverrinum AMPG-PA 1058/91 (Roussiakis, 1996)	9.50	14.50	8.70
I. viverrinum NHMUK-M. 9010 (Pilgrim, 1931)	8.50	16.00	9.00

Table 20. Cuboid measurements (mm) of Ictitheriinae from Pikermi.

	Hmax.	DAPmax.	DTmax.	DAPpr.art.	DTpr.art.
AMPG-PA 4977/91 (dext)	12.02	16.08	12.05	8.40	11.38
I. viverrinum AMPG-PA 3402/91 (Roussiakis, 1996)	13.60	10.20	12.00	—	—
I. viverrinum AMPG-PA 1056/91 (Roussiakis, 1996)	13.50	10.40	—	8.00	11.90
I. viverrinum NHMUK-M. 9010 (Pilgrim, 1931)	12.00	11.50	10.00	—	—

Table 21. Navicular measurements (mm) of Ictitheriinae from Pikermi.

	Hmax.	DAPmax.	DTmax.
AMPG-PA 4978/91 (dext)	15.16	11.74	8.50
I. viverrinum AMPG-PA 3401/91 (Roussiakis, 1996)	10.40	13.80	10.80

Table 22. Metatarsal measurements (mm) of Ictitheriinae from Pikermi.

	L	DAPpr.	DTpr.	DAPdia.	DTdia.	DAPdist.	DTdist.
Mt II AMPG-PA 4984a/91 (dext)	—	9.37	6.83	—	—	—	—
Mt II AMPG-PA 5042/91 (dext)	—	(8.90)	6.58	6.38	6.09	—	—
Mt II *I. viverrinum* AMPG-PA 3411/91 (Roussiakis, 1996)	—	(9.80)	6.00	—	—	—	—
Mt II *I. viverrinum* AMPG-PA 3411/91 (Roussiakis, 1996)	60.70	10.40	6.60	5.80	6.60	8.20	8.80
Mt II *I. viverrinum* MNHN-PIK. 3024 (Roussiakis, 1996)	60.40	8.60	(5.80)	—	7.00	—	—
Mt II *I. viverrinum* MNHN-PIK. 3032 (Roussiakis, 1996)	(57.50)	—	7.20	—	5.90	—	—
Mt III AMPG-PA 4984b/91 (dext)	—	13.48	9.31	6.05	7.30	—	—
Mt III AMPG-PA 4979/91 (dext)	—	12.38	8.15	5.37	6.84	—	—
Mt III *I. viverrinum* AMPG-PA 1059/91 (Roussiakis, 1996)	—	12.60	8.60	6.00	7.10	—	—
Mt III *I. viverrinum* AMPG-PA 3406/91 (Roussiakis, 1996)	67.80	12.50	8.40	5.50	6.60	8.70	7.80
Mt III *I. viverrinum* MNHN-PIK. 3024 (Roussiakis, 1996)	66.20	—	7.80	—	7.50	—	—
Mt III *I. viverrinum* MNHN-PIK. 3032 (Roussiakis, 1996)	64.70	—	7.00	—	5.80	—	7.00
Mt IV AMPG-PA 4984c/91 (dext)	70.74	12.13	5.70	6.15	6.09	7.01	7.29
Mt IV AMPG-PA 4980/91 (dext)	—	12.35	6.34	—	—	—	—
Mt IV AMPG-PA 4981/91 (dext)	—	12.15	6.27	—	—	—	—
Mt IV *I. viverrinum* AMPG-PA 1057/91 (Roussiakis, 1996)	—	11.50	(6.90)	(5.40)	(6.40)	—	—
Mt IV *I. viverrinum* AMPG-PA 3408/91 (Roussiakis, 1996)	69.30	11.70	6.70	6.10	6.00	7.90	7.60
Mt IV *I. viverrinum* MNHN-PIK. 3024 (Roussiakis, 1996)	66.90	—	(6.70)	—	6.20	—	—
Mt IV *I. viverrinum* MNHN-PIK. 3032 (Roussiakis, 1996)	64.50	—	—	—	4.90	—	6.00
Mt V AMPG-PA 4984d/91 (dext)	—	10.89	7.85	6.00	5.30	—	—
Mt V AMPG-PA 4982/91 (dext)	—	9.08	6.35	—	—	—	—
Mt V AMPG-PA 4983/91 (dext)	—	9.60	6.20	—	—	—	—
Mt V *I. viverrinum* AMPG-PA 1055/91 (Roussiakis, 1996)	—	9.20	6.90	(5.20)	(6.00)	—	—
Mt V *I. viverrinum* AMPG-PA 3415/91 (Roussiakis, 1996)	(60.50)	9.30	(6.30)	5.70	6.30	7.90	8.00
Mt V *I. viverrinum* MNHN-PIK. 3024 (Roussiakis, 1996)	61.40	9.20	5.30	—	(6.20	—	—
Mt V *I. viverrinum* MNHN-PIK. 3032 (Roussiakis, 1996)	61.90	(7.40)	(4.50)	—	—	—	6.60

Table 23. Metapodial measurements (mm) of various Ictitheriinae from Pikermi.

	DAPdia.	DTdia.	DAPdist.	DTdist.
“Mc III” AMPG-PA 4989/91	5.00	6.06	8.50	8.20
AMPG-PA 5029/91	5.25	6.06	6.25	8.27
AMPG-PA 5030/91	5.47	6.53	6.81	8.54
AMPG-PA 5031/91	—	—	4.96	6.88
AMPG-PA 5032/91	—	—	6.13	6.75
AMPG-PA 5033/91	—	—	7.69	7.31
AMPG-PA 5034/91	—	—	6.00	8.06
AMPG-PA 5035/91	—	—	6.17	8.15
AMPG-PA 5036/91	—	—	4.51	7.03
AMPG-PA 5037/91	—	—	4.68	6.92

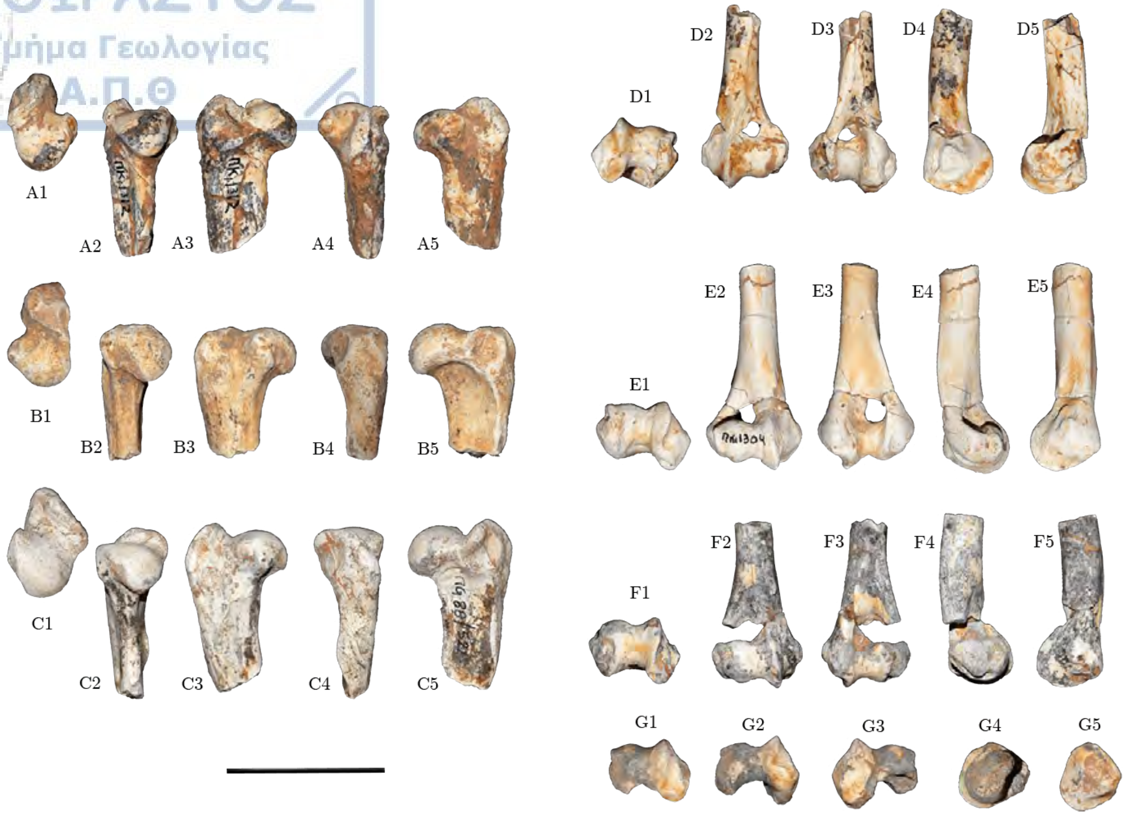

Figure 38. Ictitheriinae humeri. A: AMPG-ΠΚ 1312 (sin), B: AMPG-PA 4963/91 (dext), C: AMPG-ΠΓ 88/521 (dext) in (from the left) proximal (1), posterior (2), lateral (3), anterior (4) and medial (5) views. D: AMPG-PA 4966/91 (sin), E: AMPG-ΠΓ 1304, F: AMPG-PA 4965/91 (dext), G: AMPG-PA 4964/91 (dext) in (from the left) distal (1), anterior (2), posterior (3), medial (4) and lateral (5) views. Scale bar is 5 cm.

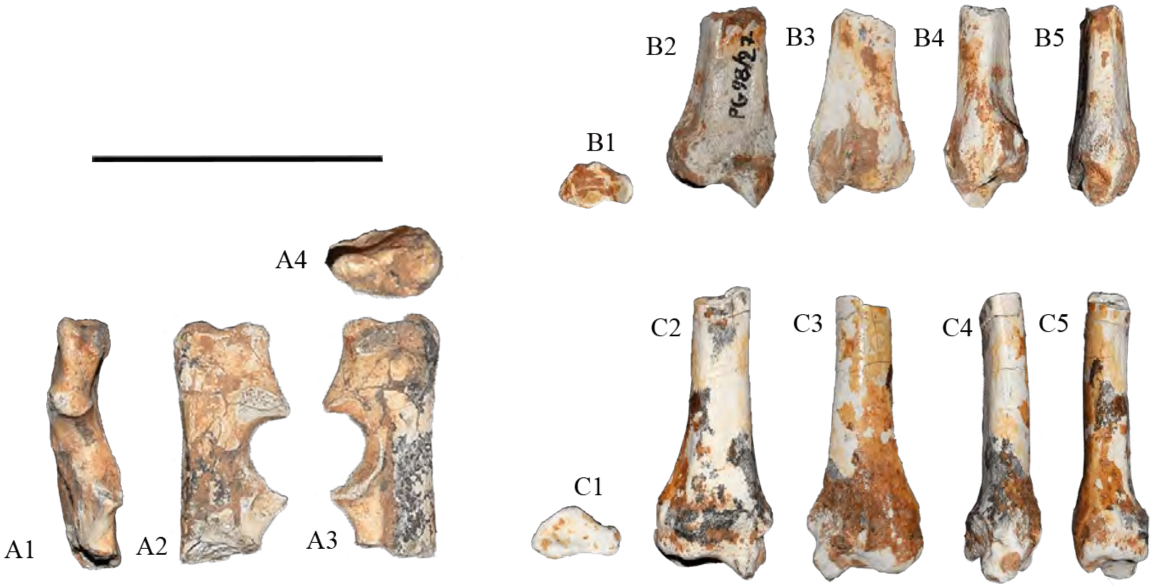

Figure 39. A: proximal end of ulna AMPG-PA 4967/91 (dext) in anterior (1), lateral (2), medial (3) and proximal (4) view. B-C: radii AMPG-PG 98/27 (sin) (B) and AMPG-PA 4968/91 (sin) (C) in distal (1), anterior (2), posterior (3), lateral (4) and medial (5) view. Scale bar is 5 cm.

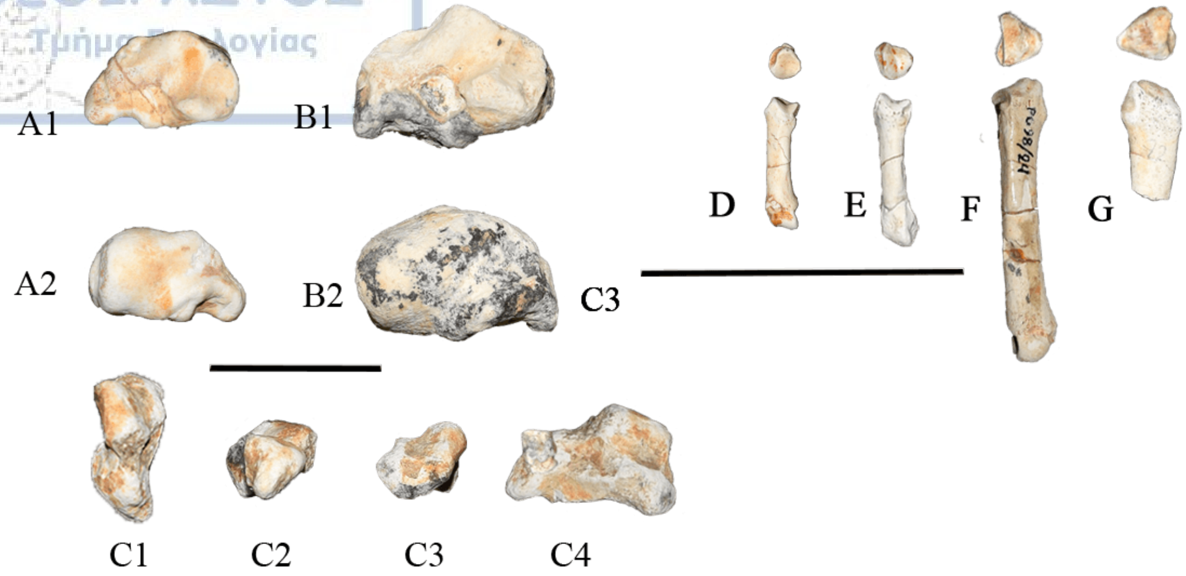

Figure 40. A-B scapholunate AMPG-PA 4969/91 (sin) (A) and AMPG-PA 4970/91 (sin) (B) in palmar (1) and dorsal (2) view. C: magnum AMPG-PA 4971/91 (sin) in proximal (1), dorsal (2), palmar (3) and lateral (4) view. D: Mc I AMPG-PA 4972/91 (sin). E: Mc I AMPG-PA 4973/91 (sin). F: Mc V AMPG-PG 98/24 (sin). G: Mc V AMPG-PA 4974/91 (dext). Left scale bar is 2cm and corresponds to the carpals A, B and C. Right scale bar is 5 cm and corresponds to the metacarpals D, E, F and G.

Figure 41. The questionably restored left Ictitheriinae frontal limb and manus (A-H). All except “Mc III” and G are left. A: humerus AMPG-PA 4985a/91 in lateral (1), medial (2), anterior (3), posterior (4), proximal (5) and distal (6) view. B: ulna AMPG-PA 4985b/91 and radius AMPG-PA 4985c/91 in lateral (1), medial (2), posterior (3), anterior (4), proximal (5) and distal (6) view. C: scapholunate AMPG-PA 4986/91 in palmar (1) and dorsal (2) view. D: unciform AMPG-PA 4987b/91 in proximal view. E: magnum AMPG-PA 4987a/91 in proximal view. F: metacarpals (from the left) Mc II AMPG-PA 4988a/91, “Mc III” AMPG-PA 4989/91, Mc IV AMPG-PA 4988b/91, Mc V AMPG-PA 4988c/91. G: distal epiphysis AMPG-PA 4990/91 that was erroneously restored as a proximal end to “Mc III. H: the restored frontal limb and manus as it was found initially. Scale bar is 5 cm.

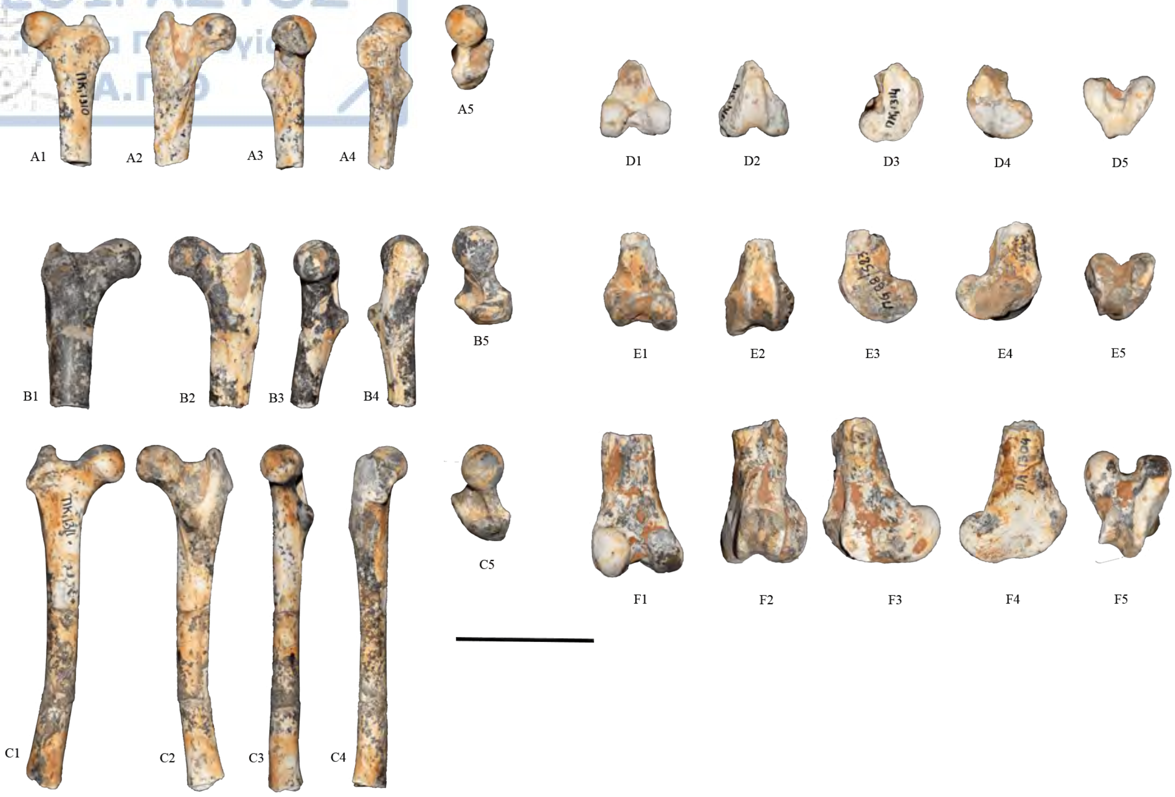

Figure 42. Ictitheriinae femurs. A: AMPG-ΠΚ 1310 (sin), B: AMPG-PA 4975/91 (dext), C: AMPG-ΠΚ 1311 (dext) in anterior (1), posterior (2), medial (3), lateral (4) and proximal (5) view. D: AMPG-ΠΚ 1314 (sin), B: AMPG-ΠG 88/523 (dext), C: AMPG-ΠΑ 1304 (dext) in posterior (1), anterior (2), medial (3), lateral (4) and distal (5) view. Scale bar is 5 cm.

Figure 43. Ictitheriinae tibias. Complete tibia AMPG-PG 98/18 (dext) (left) and tibia preserving its distal half AMPG-ΠG 88/351 (sin) (right) in A: anterior (up) and distal (down), B: lateral, C: posterior, D: medial, E: proximal view. Scale bar is 5 cm.

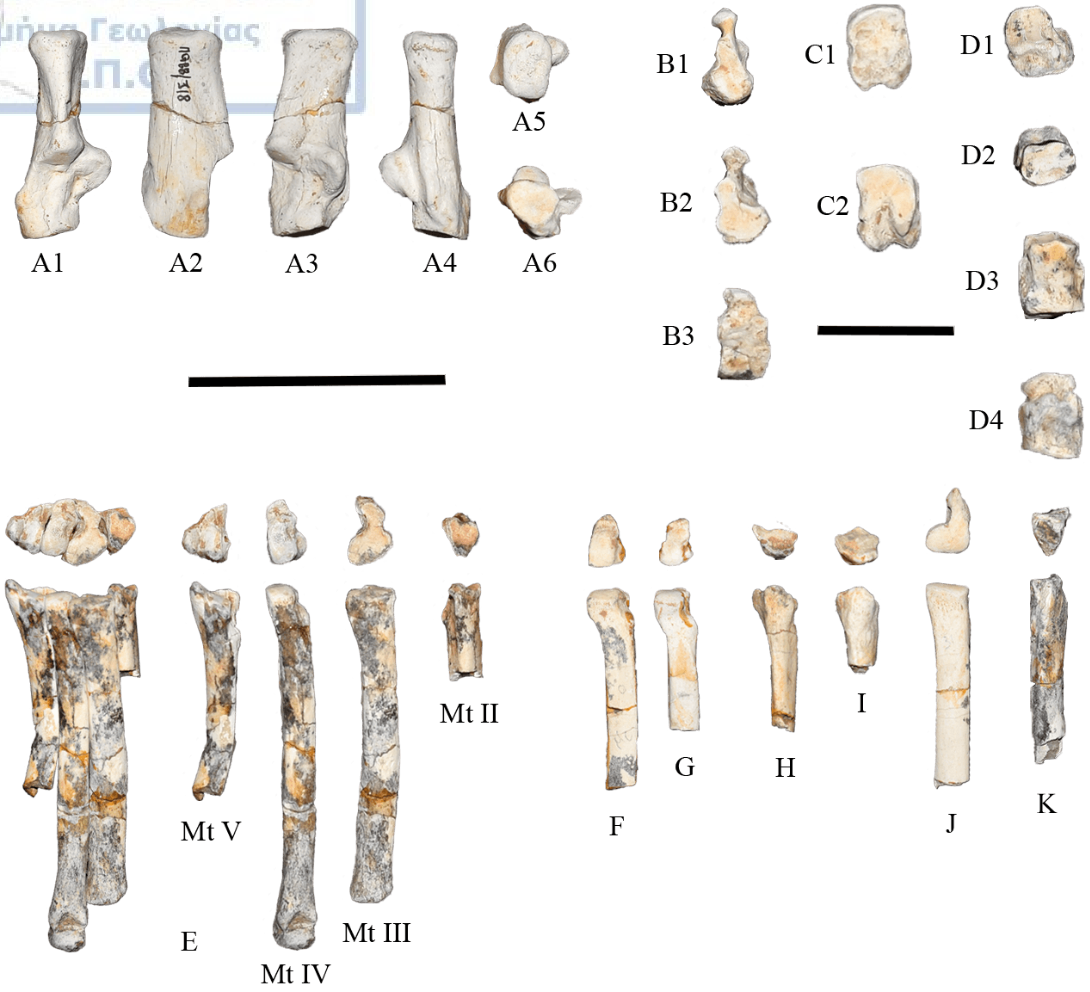

Figure 44. Ictitheriinae tarsals and metatarsals (A-J). A: calcaneum AMPG-ΠG 88/318 (dext) in dorsal (1), lateral (2), medial (3), palmar (4), proximal (5) and distal (6) view. B: 3rd cuneiform (ectocuneiform) AMPG-PA 4976/91 (dext) in dorsal (1), palmar (2) and lateral (3) view. C: navicular AMPG-PA 4978/91 (dext) in palmar (1) and proximal (2) view. D: cuboid AMPG-PA 4977/91 (dext) in distal (1), proximal (2), dorsal (3) and plantar (4) view. E: associated metatarsals articulated (left) and isolated (right) AMPG-PA 4984a-d/91 (dext). F-G: Mt IV AMPG-PA 4980/91 (dext) and AMPG-PA 4981/91(dext) respectively in dorsal view. H-I: Mt V AMPG-PA 4983/91 (dext) and AMPG-PA 4982/91 (dext) respectively in lateral view. J: Mt III AMPG-PA 4979/91 (dext) in dorsal view. K: Mt II (dext) AMPG-PA 5042/91 in dorsal view. The smaller, right scale bar is 2 cm and corresponds to B, C and D. The left, larger scale bar is 5 cm and corresponds to the rest.

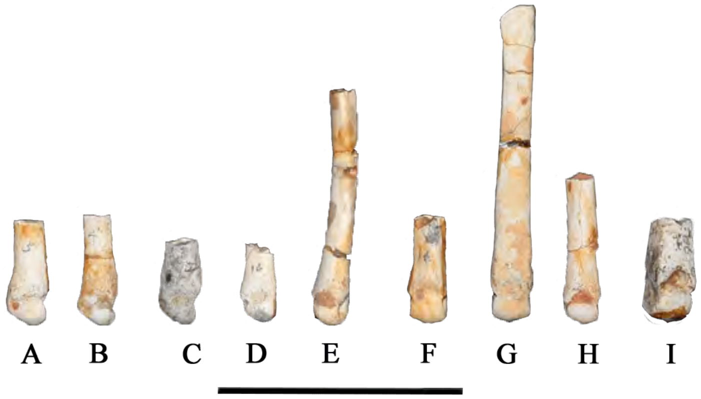

Figure 45. Metapodials of various Ictitheriinae. Scale bar is 5 cm.

Subfamily Hyaeninae (Gray, 1821) Mivart, 1882

Genus *Adcrocuta* Kretzoi, 1938

Adcrocuta eximia (Roth & Wagner, 1854)

(Figs. 46–54, Tables 24–26)

1854 *Hyaena eximia* sp. nov. in Roth & Wagner, pp. 396-398, Pl. 2:6
1924 *Hyaena variabilis* sp. nov. in Zdansky, pp. 93–103 Figs. 11–13, PIs. 18:3–4; 19:3–4; 20:1–4; 21:1–4; 22:1–4
1931 *Crocuta eximia* Roth & Wagner, 1854 in Pilgrim, pp. 116–124, PIs. 1:1–3; 2:1
1938 *Adcrocuta eximia* gen. nov. in Kretzoi, p. 118
1938 *Adcrocuta praecursor* sp. nov. in Kretzoi, p. 118
1938 *Adcrocuta variabilis* Zdansky, 1924 in Kretzoi, p. 118
1957 *Crocuta (Percrocuta) eximia* Roth & Wagner, 1854 in Kurtén, pp. 397–400
1967 *Crocuta miriani* sp. nov. in Meladze, pp. 31–34, Pls. 3:1–2; 4:1-3

Type species: *Hyaena eximia* Roth & Wagner, 1854.

Type locality: Pikermi, Attica, Greece.

Type material: SNSB-BSPG-PIK-105 (holotype): right mandibular ramus with i3-m1 described and figured by Roth & Wagner (1854: 396; Table 8, Fig. 6). Stored in the Bayerische Staatssammlung für Paläontologie und Geologie, Munich, Germany.

Age: Vallesian–Turolian, MN 10–13. For the classical locality of Pikermi: Middle Turolian, MN 12, 7.33–7.29 Ma (Böhme et al., 2017).

Localities: Greece: Xirochori-1, Ravin de la Pluie, Ravin des Zouaves 1, 5, Ravin de la Pluie, Ravin X, Prochoma 1 and Vathylakkos 3 in Axios Valley (Arambourg & Piveteau, 1929; de Bonis et al., 1973; Koufos, 2000; Koufos, 2012; Koufos, 2022c); Mytilinii 1A, Q1, Q4, Q5, A and S3 in Samos Island (Solounias, 1981; Koufos, 2009; Koufos, 2022c); Perivolaki in Thessaly (Koufos, 2006a); Nikiti 2 (Koufos, 2016) and Kryopigi in Chalkidiki (Lazaridis, 2015); Thermopigi in Serres Basin (Geraads et al., 2007; Koufos, 2022c); Halmyropotamos (Melentis, 1967) and Kerassia 4 in Euboea Island (Roussiakis & Theodorou, 2003). Bulgaria: Hadgimidovo and Kalimantsi. France: Mont Luberon. Hungary: Csákvár, Baltavar and Polgárdi. Rumania: Çimislia. Spain: ?Concud, Arquillo de la Fontana, Peña del Macho, Los Aljezares, Masia del Barbo, Los Mansuetos, Piera. Austria: Kohfidisch. North Macedonia: Titov Veles. Moldavia: Chobruchi. Russia: Starokondakovo. Ukraine: Taraklia, Belka, Cherevichnoe, Grebeniki, Novaja Emetovka, Novoukrainka and Novoelisavetovka. Libya: Sahabi. Pakista: Hasnot. Iran: Upper and Middle Maragheh. Georgia: Bazalethi. Kazakhstan: Pavlodar and Kalmakpaj. Turkey: Coban Pinar, ?Amasya, Upper Kavakdere, ?Mugla, Karain, ?Kuyutarla, Kemiklitepe A-B, Kavak Dere, Kinik, Mahmutgazi and Küçükyözgat. China: Chang Chia Chuang, Chao Tsu Kou (Zdansky's Loc. 116v), Chen Chia Mao Kou (Zdansky's Loc. 108), Chin Kou, Chou Chia Kou, Chou Fen Ta, Hsiao Kou Shan, Hsin Yao, Huan Lou Kou (Zdansky's Loc. 109), Kou Chia Ta, Liao Wan Kou, Loc. 110, Loc. 114n, Loc. 115, Loc. 12, Loc. 31, Loc. 44, Ma Chi Liang Kou, Ma Hua Tan (Zdansky's Loc. 114s), Nan Hao Hsia, Nan Ho, Pai Tao Tsun, San Chia Liang Kou (Zdansky's Loc. 43[1]), Ta Tsun, Ta Tung Kou, Tie Chia Kou (Zdansky's Loc. 30), Tung Ta Ling, Van Mu Kou (Zdansky's Loc. 49) and Wang Lou Kou (Werdelin & Solounias, 1991; Turner et al., 2008).

Material: AMPG-PA 3721/91: left maxillary fragment with P2-P3-P4-M1 (sin), AMPG-PG 95/1507: cranium with I1-2(sin, roots)-I3(alveolus)-C(sin)-P2-P3-P4(sin), AMPG-PA 4954/91: cranium with I1(roots)-P2-P3-P4, AMPG-PG 95/1506: mandible with c-p1-p2-p3-p4(dext)-m1, AMPG-PA 3723/91: right hemimandible with ascending ramus and p3-p4, AMPG-PA 3722/91: left hemimandible with i3-c-p1(alveolus)-p2(roots)-p3-p4-m1(distal half), AMPG-PA 4955/91: right hemimandible fragment with erupting p3-p4. (Figs. 48-54).

Remarks: The cranium AMPG-PG 95/1507 and the left hemimandible AMPG-PA 3722/91 might be associated. They have matching degree of wear in their dentition, especially so in their canines and seem to anatomically match.

Description: Cranium: The cranium AMPG-PG 95/1507 (Fig. 48) is almost perfectly preserved aside from some minor deformations, which mainly affect the neurocranium. The orbits are elliptical-shaped with their anterior margins situated above the upper carnassial’s paracone. The frontal bone zygomatic process is relatively prominent and situated approximately above the metastyle blade of P4. The large elliptical-shaped infraorbital foramina open above the distal end of P3. A depression of the maxilla above P2-P3 makes the snout more pronounced. The nasal opening is relatively large and oval-shaped. The nasal bones are sphenoid shaped towards the frontals. A well-developed cranial vault begins above the P3. In-between the nasals a depression develops that continues posteriorly to the frontals until the eventual formation of the sagittal crest. The prominent sagittal crest is well-preserved and extends more posteriorly than the rest of the cranium. In lateral view the sagittal crest curves ventrally as it extends towards the posterior end of the cranium. The strong zygomatic arches are almost completely preserved and reach their maximum width in the anterior part of the neurocranium. The nasal cavity is large, oval-shaped, inclines posteriorly in lateral view and its posterior margin lies above the canine. In ventral view, deformations have created an antero-posteriorly oriented depression in the centre of the palate. Nonetheless, the palate is wider between the carnassials and progressively narrows down towards the anterior part of the cranium. The dentition is straight without imbrications and exhibits a high degree of wear. The choanae is relatively short, with its anterior margin approximately 6 mm from the distal end of P4. The auditory bullae are large, incline posteriorly when viewed from the lateral side and their anterior margins lie slightly behind the posterior margins of the glenoid fossa. The posterior margins of the bullae are flattened. The preserved left occipital condyle is elongated and slightly narrow. The foramen magnum is partially crushed and it probably appears narrower than it would have initially been. The posterior end of the cranium is triangular in dorsal view, due to the nuchal crests’ development.

The cranium AMPG-PA 4954/91 (Fig. 49) was broken in half just posteriorly of the choanae and is not as well-preserved as AMPG-PG 95/1507. Despite that, its general morphology is similar with AMPG-PG 95/1507. In occlusal view, the palatine bone and part of the maxilla is crushed inwards, but otherwise intact. The palatine fissures are also visible, although a bit deformed. The dentition is straight and similarly exhibits a high degree of wear, however in contrast to AMPG-PG 95/1507, slight imbrication of P2 and P3 is observed. Although the short choanae's anterior margin is damaged, it indicates a distance of approximately 6-7 mm from the posterior margin of P4. The depression of the nasal bones is better expressed in AMPG-PA 4954/91, however, the cranial vault is not as pronounced as in AMPG-PG 95/1507. The mesial root of the left P3 can be visibly reaching in height the infraorbital foramen. The posterior half of the cranium partially preserves a distorted and damaged neurocranium. The sagittal crest is also deformed but more or less preserved, with only a piece missing above the neurocranium. The occipital preserves an almost intact foramen magnum without its condyles. It is oval-shaped and its horizontal diameter is larger than its ventral.

AMPG-PA 3721/91 (Fig. 50) preserves only the large, elliptical-shaped infraorbital foramen which is situated above the main cusp of the P3. Its unworn dentition contrasts the aforementioned, older individuals and indicates its young age.

Upper dentition: The cusps of the teeth are rather blunt even on unworn dentition. The main cusps of the premolars incline distally when viewed from the side.

I1-2: Only preserved by some roots in AMPG-PA 4954/91 and AMPG-PG 95/1507. They indicate similarly small, single rooted incisors.

I3: Only the alveolus in AMPG-PG 95/1507 is preserved. It indicates a greatly enlarged incisor.

C: The left canine of AMPG- PG 95/1507 is large in width and length but relatively short. The crown curves slightly distally.

P1: Preserved only by the filled with matrix alveoli in AMPG-PA 4954/91 and AMPG-PG 95/1507. They appear to be small, rounded, single-rooted teeth. They do not seem to form a diastema with P2, but they might form a minute one with the canine.

P2: The tooth is robust and almost square in occlusal view. In place of a mesial cusp there is a slight mesio-lingual swelling of the cingulum. From there, a rather blunt crest begins to form that passes through the main and towards the distal end of the tooth. The main cusp is well-developed, elongated and slightly blunt in AMPG-PA 3721/91 while on the other specimens it is worn. A rudimentary distal cusp is situated in the distal end of the tooth. The cingulum is very strong all around the tooth, except its slightly weaker buccal side.

P3: The morphology is the same with P2, albeit larger in size. The anterior part of P3 is slightly broader than the rest of the tooth. Again, only a mesio-lingual swelling of the cingulum is present instead of a cusp. The low distal cusp is also more developed than P2. The cingulum is strong all around the tooth.

P4: The upper carnassial is large and elongated. The protocone is small and low, projecting lingually of the parastyle in AMPG-PA 3721/91 and AMPG-PG 95/1507, while in AMPG-PA 4954/91 they are either broken or worn out to the point of absence. The larger parastyle connects to the protocone with a small crest. The paracone is well-developed and is situated higher than the other cusps. The elongated metastyle curves slightly buccally towards its distal end, creating a fold in the adamantine in AMPG-PA 3721/91. A mesio-distal crest passes along the parastyle, paracone and metastyle. The cingulum is projected more strongly in the buccal than in the lingual side.

M1: The molar is small, low and almost rudimentary. It is preserved entirely only in AMPG-PA 3721/91. It forms approximately a 90-degree angle with the P4. It extends as far as the distal end of the carnassial. A diastema of approximately 5 mm is formed between the P4 and the M1. The protocone is pointed, lower than the other cusps and is connected with the paracone and metacone distally through two crests. The paracone is situated higher from the other cusps, slightly more buccally and is connected with a crest to the smaller metacone. A valley develops between the protocone and the metacone-paracone. The cingulum is relatively strong.

Mandible: The mandible has a relatively high and robust mandibular corpus. Its margins are almost straight until the distal end of m1, after which they start to ascend. The corpus of the left hemimandible of specimen AMPG-PG 95/1506 is crushed inwards at the p4's level, probably due to taphonomical processes, while the corpus of AMPG-PA 3723/91 is not that well-preserved in general. The mandibles have two mental foramina in their lateral sides, situated approximately below p2's main cuspid and near the border of p2-p3 respectively. Specimen AMPG-PG 95/1506 also bears a taphonomical mark similar to a mental foramen situated above the mesial mental foramen of its left hemimandible. The mandibular symphysis inclines slightly distally. Its ventral margins are situated below p2 while its dorsal margins are situated in the distal part of the canines. The masseteric fossa preserved on AMPG-PA 3723/91 and partially on AMPG-PA 3722/91 is rather deep and its mesial border lies almost below the distal end of m1. The mandibular foramen situated in in the distal part of the ascending ramus is located approximately at the mid-level of the corpus. The ramus ascends almost immediately behind the distal end of m1 and the coronoid process on specimen AMPG-PA 3723/91 curves slightly distally. Also, the condylar process of that specimen is robust and asymmetric. The angular process is not preserved in any specimens.

Lower dentition: The dentition is generally straight besides the slightly more buccally oriented p3 and the slightly more lingually oriented p1 and m1, without major imbrications. The premolars are "squarish" occlusally and their main cusps exhibit a distal inclination in lateral view.

i: A probable i3 is preserved in AMPG-PA 3722/91. It is relatively small, worn and slightly displaced.

c: Preserved in AMPG-PA 3722/91 and without the crown's tip in AMPG-PG 95/1506. It is large and robust with an elliptical cross-section. A crest forms in the disto-lingual side of the left AMPG-PG 95/1506. On specimen AMPG-PA 3722/91 the distal part of the canine is flattened due to extreme wearing.

p1: It is preserved in AMPG-PG 95/1506 and with a filled with matrix alveolus on AMPG-PA 3722/91. It is small, round, monocuspid and single-rooted. A small crest passes through the cuspid in a mesio-distal direction. The cingulum is strong all around the tooth, but more so in its lingual side. A small diastema of approximately 5-8.5 mm is formed with the canine. It is more lingually oriented than the molar and other premolars.

p2: Preserved in specimen AMPG-PG 95/1506 and with its roots in specimen AMPG-PA 3722/91. The maximum width of p2 is at its distal half. It is asymmetrical, double-rooted, has a rudimentary mesial cuspid, a large and high main cuspid and a small and low distal cuspid. A crest passes across the cuspids in a mesio-distal direction. The cingulum is strong all around the tooth, but especially so in the disto-lingual side of p2.

p3: Preserved in AMPG-PA 3723/91, AMPG-PG 95/1506, its distal part in AMPG-PA 3722/91 and erupting in AMPG-PA 4955/91. Its morphology is similar with p2, but overall larger and more robust. A small mesio-lingual cuspid is present in AMPG-PG 95/1506, while in AMPG-PA 3723/91 only a slight swelling of the cingulum occurs. The main cuspid is large and well-developed. A distal cuspid is situated distally, atop a strong cingulum shelf. This shelf is less pronounced in AMPG-PA 3723/91. The cingulum is strong all around the tooth, but especially in the distal part of the tooth. A mesiodistal crest passes along the cuspids in a mesio-lingual to distal direction.

p4: Preserved in AMPG-PG 95/1506 (dext), AMPG-PA 3723/91, worn but otherwise complete in AMPG-PA 3722/91 and erupting in AMPG-PA 4955/91. It is larger than p3 and its well-developed mesial cuspids make it appear more symmetrical. The smaller distal cuspid is situated atop a fold of the distal cingulum. This fold gives the impression of a second distal cuspid and forms a slight crest. The main cuspid is large but otherwise similar with p3. The cingulum is strong all around the tooth, but more so distally. A mesio-distal crest passes across the cuspids.

m1: Preserved in AMPG-PG 95/1506 and with its distal half in AMPG-PA 3722/91. It is larger than the rest of the dentition and mesio-distally elongated. The paraconid and trigonid are approximately of the same height and length. A crest passes across the elongated trigonid mesio-distally from the paraconid to the protoconid. The metaconid is absent. The talonid is low and reduced without a hypoconulid.

Discussion: The systematic position and history of *Adcrocuta eximia* is quite long and complex. Initially it was described as *Hyaena eximia* by Roth & Wagner (1854) based on material from Pikermi. Pilgrim (1931), then transferred it to *Crocuta* under *Crocuta eximia* until sometime later, Kretzoi (1938) erected the genus *Adcrocuta*. However, Kretzoi's work was mostly ignored until Kurtén (1957) resurrected Kretzoi's *Percrocuta*, which included *Adcrocuta* as a subgenus to *Crocuta*. Later, Ficcarelli & Torre (1970) revived both the names of *Percrocuta* and *Adcrocuta*. It wasn't until the work of Schmidt-Kittler (1976) and Chen & Schmidt-Kittler (1983) however, that *A. eximia* was made the sole representative of the genus, essentially separating it from *Percrocuta*. Following these arguments, Howell & Petter (1985), Qiu (1987) and Werdelin & Solounias (1990; 1991) further solidified its taxonomic allocation. Despite the extensive taxonomic work however, the phylogenetic position of *A. eximia* still remained a mystery. A few of the earlier authors (Schmidt-Kittler, 1976; Galiano & Frailey, 1977; Howell & Petter, 1985; Qiu, 1985) considered the genus rather advanced in the Miocene hyaenid evolution and so Werdelin & Solounias (1990) attempted to clarify its status. Their work showed that *A. eximia* is a sister-taxon to *Crocuta*, thus confirming Pilgrim (1931), Kurtén (1957) and Senyürek (1958). It is also worth mentioning however, that one autapomorphy of *A. eximia* (reduced protocone of the upper carnassial), probably indicates an indirect rather a direct ancestry to *Crocuta*. (Werdelin & Solounias, 1991).

A. eximia is characterized by its large size, the derived dentition on the upper carnassial as exemplified by the reduced protocone, the powerful premolars, the retention of a small P1 and a relatively short and broad skull. (Werdelin & Solounias, 1991; Turner et al., 2008). A degree of intraspecific variation is recorded, such as the number (either one or two) and position of the mental foramina (Gaudry, 1863; Werdelin & Solounias, 1991; Koufos, 2000; Roussiakis

& Theodorou, 2003). The mesial cuspid on p2 has also been observed to be either small or entirely absent, while p3 exhibits some variance in its size (Roussiakis & Theodorou, 2003). Lastly, while a metaconid on m1 is usually absent, the presence of a vestigial metaconid has been reported in some cases (de Mecquenem, 1925; Koufos, 2000, Roussiakis, 1996; Roussiakis & Theodorou, 2003).

The morphology of the studied material closely resembles that of *A. eximia*. Metrical comparison of the dental material herein with *A. eximia* both from Pikermi as well as other localities (Figs. 46, 47), further confirms these similarities. Concerning the upper dentition (Fig. 46), the width of AMPG-PA 4954/91's carnassials, appears much lower than it would originally ought to be due to the absence of the protocones, either because of preservation or ontogenetic reasons. Subsequently, this also affects AMPG-PA 4954/91's P4 robusticity index, which is lower (~42) both from the rest of the studied material–that does not display such extreme degree of wear–as well as the comparative sample of *A. eximia* from Pikermi provided by Werdelin & Solounias (1990). Besides that, the rest of the calculated indexes (Table 25) are close in value with the reference sample of *A. eximia* from Pikermi. The M1 of AMPG-PA 3721/91 is also much smaller in size than the minimal value observed for *A. eximia* from Pikermi, but it is rather close in value to the *A. eximia* sample from Samos (Fig. 46). Concerning the lower dentition (Fig. 47), almost all specimens in study are grouped close with one another and are within the observed range of variation of the reference sample. Also, their calculated indexes further serve to confirm that (Table 26). The sole exception would be the slightly larger m1 of AMPG-PA 3722/91 (Fig. 47).

Aside the typical *A. eximia* from Pikermi and other Eurasian localities, de Bonis & Koufos (1981) and Koufos (2000) recognize the subspecies *A. eximia leptoryncha* de Bonis and Koufos, 1981 from the Vallesian locality (MN 10) of Ravin de la Pluie in Axios Valley, Greece. According to these authors this subspecies differs from the typical *A. eximia eximia* with its longer snout, slenderer premolars, narrower palate and a lesser degree of imbrication in the cheek-teeth. Additionally, Koufos (2000) comments that the primitiveness of *A. e. leptoryncha* is reflected with the presence of a strong lingual cingulum on the lower premolars. Roussiakis & Theodorou (2003) note that this last character is absent in the more typical Turolian forms, which seems to also be the case with the specimens studied herein. A couple additional differences between the two subspecies mentioned by Koufos (2009) refer to the longer C-P2 diastema and an index that exemplifies the narrower palate and more elongated muzzle of *A. e. leptoryncha* over the typical *A. eximia*. In that aspect, the two crania in study are more akin to *A. eximia* than *A. e. leptoryncha*. Further comparison with their upper dentition showed that the premolars of *A. e. leptoryncha* are metrically close to the material in study and are well within the observed range of variation for the typical *A. eximia* specimens from Pikermi as well as other Turolian localities (Fig. 46). Additional comparison in their premolar robusticity did not reveal any significant discrepancies in-between them (Tables 25, 26). The only apparent difference observed is *A. e. leptoryncha*'s larger M1, namely its length, which sets it apart from both the material in study as well as the rest of *A. eximia* from Greece. On the other hand, however, when compared with the *A. eximia* sample from China it appears small (Fig. 46). Concerning the lower dentition, Howell & Petter (1985) and Roussiakis & Theodorou (2003) note no significant morphological differences with other *A. eximia* from Pikermi and *A. e. leptoryncha*, which also extends for the specimens herein. Contrasting their metrically similar upper dentition however, comparison of their lower dentition demonstrates the smaller premolars–primarily p2's length and p4's width–of *A. e. leptoryncha* (Fig. 47). Additionally, the robusticity index of p4 in *A. e. leptoryncha* is markedly lower (50.67) from both the *A. eximia* population from Pikermi (62.17) and the material herein, which averages close to 60. Considering the above in addition to the available metrical data, the studied specimens differ from *A. e. leptoryncha* on the basis of their lower dentitions and are closer to the typical Turolian forms of *A. eximia* from Pikermi.

Besides *A. eximia*, two more hyaenids of similar size have been recognized from the Turolian of Greece: *Chasmaporthetes bonisi* Koufos, 1987 from the early Turolian locality of Ravin des Zouaves 5 and the late Turolian of Dytiko 1 and *Hyaenictis graeca* Gaudry 1861 from Pikermi.

The main difference between *A. eximia* and *C. bonisi* lies in their dental morphology. The latter's P2 and P3 are more elliptical in shape and slightly slenderer. Its upper carnassial is also slenderer with a stronger and more developed protocone. Lastly, its M1 is larger than *A. eximia*'s. In the lower dentition, the premolars of *C. bonisi* are also more elliptical contrasting the more rectangular-shaped premolars of *A. eximia*. The rectangular shape of the latter is mainly attributed to the position of its mesial cuspids. Also, the lower carnassial of *C. bonisi* is generally shorter with a monocuspid talonid. Roussiakis & Theodorou (2003) however, comment that the robusticity of the left p2 of *C. bonisi* LGPUT-DTK-126 is close to the minimal observed values of *A. eximia* from Pikermi. Aside from these morphological differences, the metrical comparison with the specimens in study indeed attests to *C. bonisi*'s slenderer P2 and P3, the slightly shorter and broader P4 and the large M1, which distinguishes it both from both *A. eximia* and the studied specimens (Fig. 46). The length of M1 in *C. bonisi*, is, however, close to the mean values of *A. eximia* from China. Comparison of their lower dentition (Fig. 47) showed only some minor differences concerning the width of p3 and p4 with the specimens studied here. However, when examined against the full range of variation exhibited by the reference *A. eximia* sample from Pikermi it is apparent that it is an artefact, since they are either well within or very close to *A. eximia*'s lowest values. In addition, the robusticity index gap for the lower dentition of *C. bonisi* and *A. eximia* from Pikermi is much smaller than it was for their upper dentition (Tables 25, 26).

Hyaenictis graeca is known only by a few scarce remains (Gaudry, 1862–1867; Roussiakis, 1996), but the upper dentition differs from *A. eximia*'s primarily by the larger protocone on P4 and the larger M1. A more in-depth comparison those taxa will be provided in the section of *H. graeca*.

Concluding, the material studied herein exhibits the morphological characters of the typical *A. eximia* from Pikermi allowing its attribution to *Adcrocuta eximia*. The metrical data further serve to back this claim, as the minor discrepancies observed are well within the expected range of variation for the species.

A. eximia is a relatively common and widespread species in the Turolian faunas of Eurasia (Howell & Petter, 1985; Koufos 2000; Turner et al. 2008). It was a large hyaenid, comparable in size to the extant *Crocuta crocuta* and it is the first known member of the family to display a fully developed bone-crunching morphology in its dentition (Turner et al. 2008). Its sudden appearance at the begging of MN 10 (with unknown antecedents) matches its disappearance at the end of MN 13 (Turner et al. 2008).

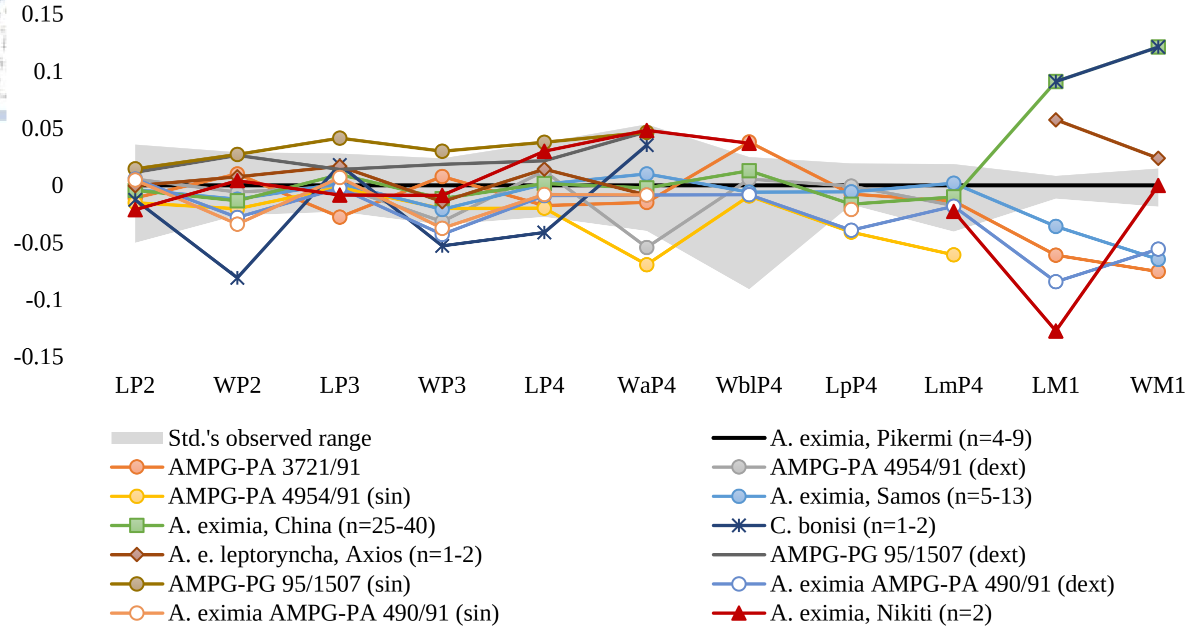

Figure 46. Log ratio diagram comparing the upper dentition of *Adcrocuta eximia* from various Greek localities. The mean values of Werdelin & Solounias (1990) for *A. eximia* (n=4-9) from Pikermi are used as standard. The greyed area indicates the standard’s observed range of variation. Data of *A. eximia* from Samos and China were acquired from Werdelin & Solounias (1990). Data for *A. e. leptoryncha* and *C. bonisi* were acquired from Koufos (2000). Data for *A. eximia* from Nikiti were acquired from Koufos (2016).

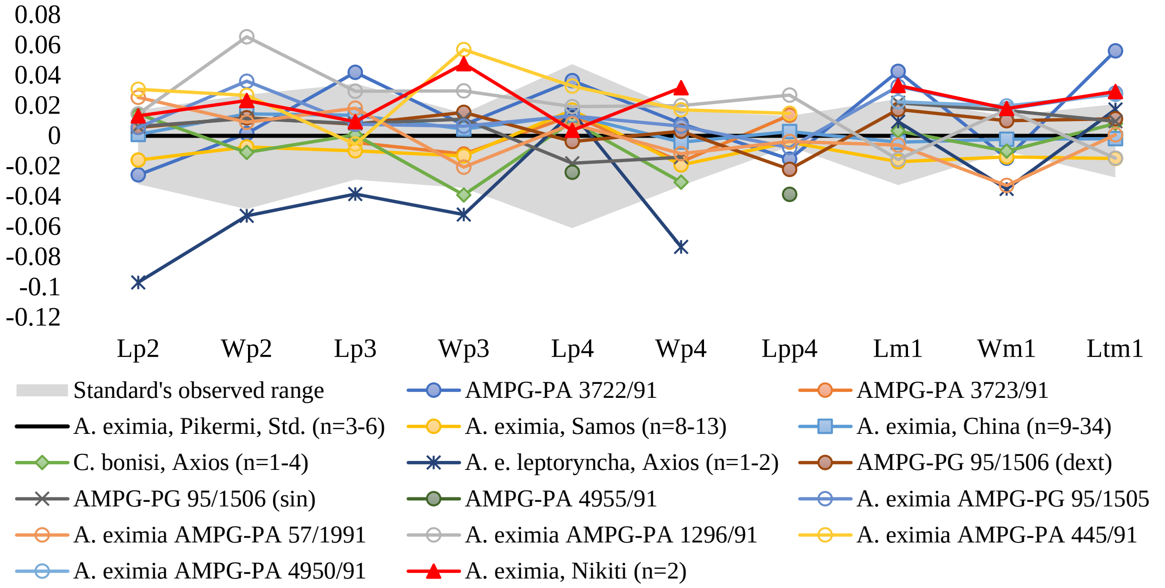

Figure 47. Log ratio diagram comparing the lower dentition of *Adcrocuta eximia* from various Greek localities. The mean values of Werdelin (1990) for *A. eximia* (n=3-6) from Pikermi are used as standard. The greyed area indicates the observed range of variation for *A. eximia* (n=3-6) from Pikermi. Data for *A. eximia* from Samos and China were acquired from Werdelin & Solounias (1990). Data for *A. e. leptoryncha* and *C. bonisi* were acquired from Koufos (2000). Data for *A. eximia* from Nikiti were acquired from Koufos (2016).

Table 24. Cranial measurements (mm) for *Adcrocuta eximia* from Pikermi.

	AMPG-PA 4954/91	AMPG-PG 95/1507
Width of cranium between P4 (buccal) (P–P)	94.69	96.71
Width of cranium between the canines (buccal) (C–C)	(61.7)	66.98
Length of the palate (PL)	132.38	137.63
Maximum width of occipital condyles (CB)	—	61.2
Minimum width between orbits (IOB)	72.45	76.56
Width between postorbital processes (POP)	—	93.12
Postorbital constriction minimum width (POC)	52.45	52.76
Maximum breadth at the zygomatic arches (ZB)	—	191.75
Prosthion-Acrocranion	284.08	296
Prosthion-Basion	236.54	251.87
Prosthion-Choanae	135.68	137.02
Prosthion-middle of the line connected the posterior borders of P4	121.64	126.72
Prosthion-Mandibular fossa	—	(191.36)
Prosthion-middle of the line connecting the anterior borders of bullae	194.54	201.88
Prosthion-anterior border of the orbit	105.98	108.445
Basion-anterior border of choanae	107.06	114.87
Basion-anterior border of the orbit	153.49	164.655
Basion-middle of the line connecting the posterior borders of P4	105.46	107.87
Width at the base of the zygomatic arches	87.3	89.78
Width of foramen magnum	26.17	21.4
Height of foramen magnum	18.86	(9.16)
Height: occipital condyle-occipital protuberance	—	(68.64)
Maximum height: posterior end of choanae-frontal	—	69.95
Length of bullae	—	30.4
Width of bullae	—	32.41

Table 25. Upper dentition measurements (mm) for *Adcrocuta eximia* from Pikermi.

	AMPG-PA 3721/91	AMPG-PA 4954/91		AMPG-PG 95/1507		*Adcrocuta eximia*[1]			*A. e. leptorycha*[2]
						Pikermi	Samos	China	Axios
						(Werdelin & Solounias, 1990)			(Koufos, 2000)
	sin	dext	sin	dext	sin	n=4-9	n=5-13	n=3-45	n=1-2
LI1	—	[8]	[8.19]	[9.96]	[9.04]	—	—	—	—
LI2	—	—	—	[11.94]	—	—	—	—	—
LI3	—	—	—	[16.38]	[13.91]	—	—	13.18	—
WI3	—	—	—	[11.93]	[10.11]	—	—	—	—
LC	—	—	—	[16.7]	18.72	—	—	17.13	17.7
WC	—	—	—	[13.46]	15.03	—	—	13.08	13.85
LP1	—	—	—	[6.98]	[6.93]	—	—	7.33	7.20
WP1	—	—	—	[6.74]	[7.98]	—	—	—	—
LP2	17.51	18.19	17.35	18.44	18.57	17.96	17.81	17.79	17.95
WP2	12.82	12.36	11.95	13.31	13.34	12.53	12.19	12.15	12.75
LP3	20.67	21.98	21.95	22.75	24.24	22.03	22.11	22.51	22.90
WP3	16.10	14.70	15.09	16.50	16.94	15.81	15.06	15.4	15.30
LP4	35.90	38.49	(35.71)	[39.3]	(40.78)	37.39	37.49	37.53	38.65
WaP4	17.69	16.15	15.60	20.39	20.37	18.3	18.73	18.2	17.95
WblP4	12.78	11.86	11.46	—	—	11.71	11.55	12.06	—
LpP4	12.97	13.18	12.01	—	—	13.20	13.03	12.71	—
LmP4	15.31	15.17	(13.74)	—	—	15.80	15.87	15.44	—
HP4	21.36	13.87	14.37	—	—	—	—	—	—
LM1	5.71	—	—	—	—	6.57	6.05	5.89	7.50
WM1	12.02	—	—	—	—	14.30	12.32	13.27	15.10
R.I. P2	73.22	67.95	68.88	72.18	71.84	69.77	68.44	68.30	71.03
R.I. P3	77.98	66.88	68.75	72.53	69.88	71.77	68.11	68.41	66.81
R.I. P4	49.28	41.96	(43.69)	[51.88]	(49.95)	48.94	49.96	48.49	46.44
L(P2–P4)	73.10	78.23	(75.85)	(79.49)	—	—	—	—	—
L(P3/P4)	57.58	57.11	(61.47)	[57.89]	(59.44)	58.92	58.98	59.98	59.25
L(mP4/P4)	42.65	39.41	(38.48)	—	—	42.26	42.33	41.14	—
(LP4/LP3+LP2)	94.03	95.82	90.87	[95.41]	(95.26)	93.50	93.91	93.13	94.61

Table 26. Lower dentition measurements (mm) for *Adcrocuta eximia* from Pikermi.

	AMPG-PA 3722/91	AMPG-PA 3723/91	AMPG-PG 95/1506		AMPG-PA 4955/91	*Adcrocuta eximia*			*A. e. leptoryncha*
						Pikermi	Samos	China	Axios
						(Werdelin & Solounias, 1990)			(Koufos, 2000)
	sin	dext	dext	sin	dext	n=3-6	n=8-13	n=2-34	n=1-2
Li3	—	—	[8.70]	[8.67]	—	—	—	—	—
Wi3	—	—	[6.23]	[6.23]	—	—	—	—	—
Lc	15.98	[15.06]	17.42	15.48	—	—	—	16.90	16.80
Wc	15.48	[11.70]	14.25	13.21	—	—	—	15.10	13.50
Lp1	[6.30]	—	5.59	5.51	—	—	—	5.69	—
Lp2	[15.31]	—	16.46	16.48	—	16.25	15.70	16.30	13.00
Wp2	(11.22)	—	11.49	11.48	—	11.18	11.00	11.60	9.90
Lp3	(21.67)	19.47	20.02	20.04	—	19.67	19.20	20.30	18.00
Wp3	(13.76)	13.16	14.02	13.88	—	13.53	13.10	13.70	12.00
Lp4	23.40	22.19	21.33	[20.64]	20.36	21.52	22.40	22.20	22.30
Wp4	13.63	12.86	13.47	[12.95]	—	13.38	12.80	13.30	11.30
Lpp4	10.30	11.01	10.14	—	9.76	10.67	10.60	10.70	—
Lm1	(30.45)	—	28.73	29.02	—	27.60	26.50	27.30	28.20
Wm1	(12.47)	—	13.20	13.41	—	12.90	12.50	12.80	11.90
Ltm1	(25.70)	—	23.17	23.08	—	22.58	21.80	22.50	23.50
HPC	—	77.21	—	—	—	—	—	85.00	—
Cond-Ang	—	(36.51)	—	—	—	—	—	33.50	—
p2-m1	[89.73]	(81.43)	86.21	84.09	—	—	—	81.90	—
Hdia	48.17	46.79	47.58	47.58	—	—	—	43.40	—
Hbehm1	51.15	42.46	51.76	49.52	—	—	—	46.50	—
Symphysis length	55.60	49.50	49.10		—	—	—	—	—
R.I. p2	(73.29)	—	69.81	69.66	—	68.80	70.18	71.01	76.15
R.I. p3	(63.50)	67.59	70.03	69.26	—	68.78	68.23	67.34	66.67
R.I. p4	58.25	57.95	63.15	(62.74)	—	62.17	57.19	59.68	50.67
R.I. m1	(40.95)	—	45.95	46.21	—	46.74	47.06	46.93	42.20
L (p4/m1)	(76.85)	—	(74.24)	[71.12]	—	77.97	84.33	81.20	79.08

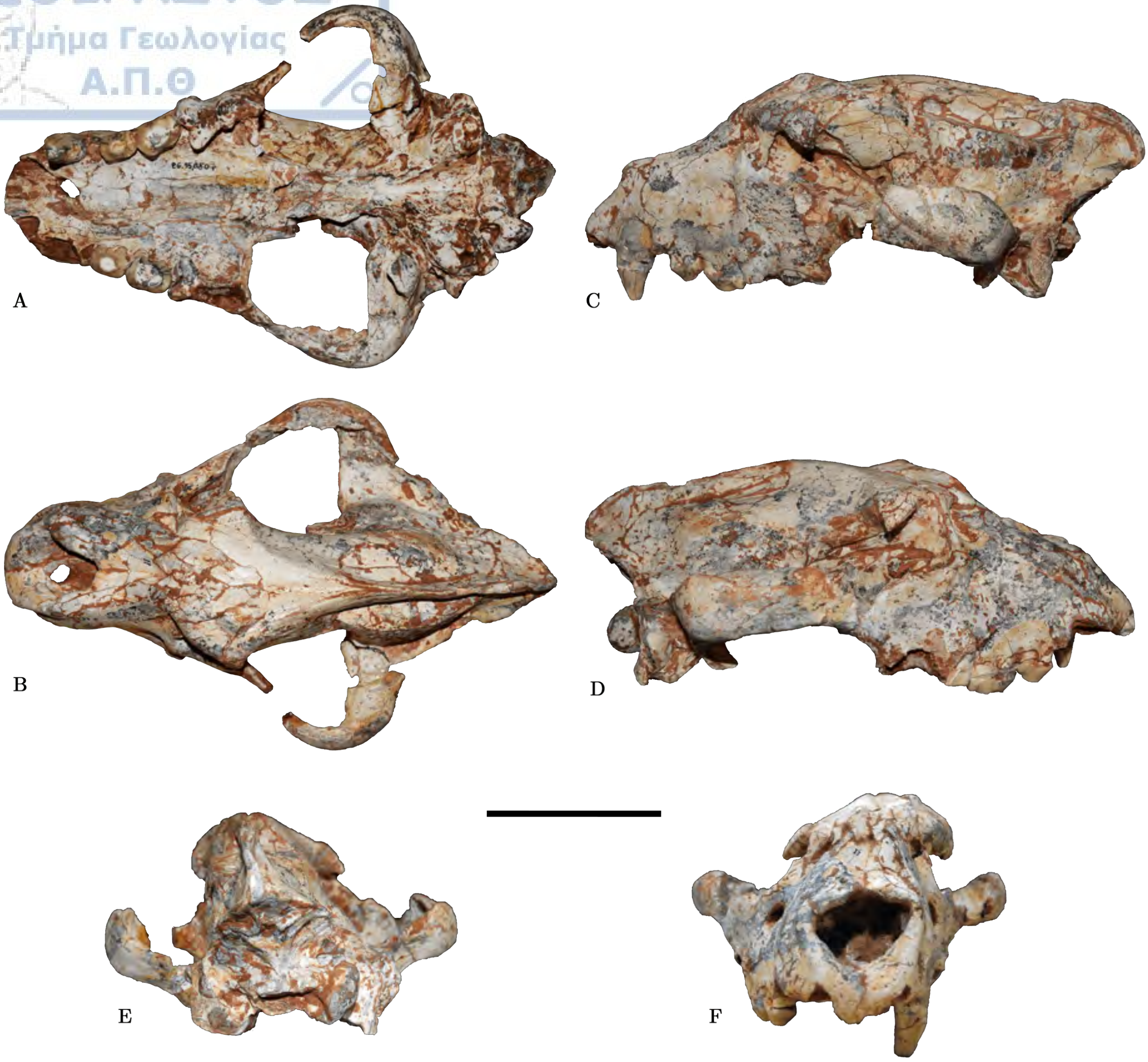

Figure 48. Cranium of *A. eximia* AMPG-PG 95/1507 in A: ventral, B: dorsal, C: lateral (sin), D: lateral (dext), E: posterior and F: anterior view. Scale bar is 10 cm.

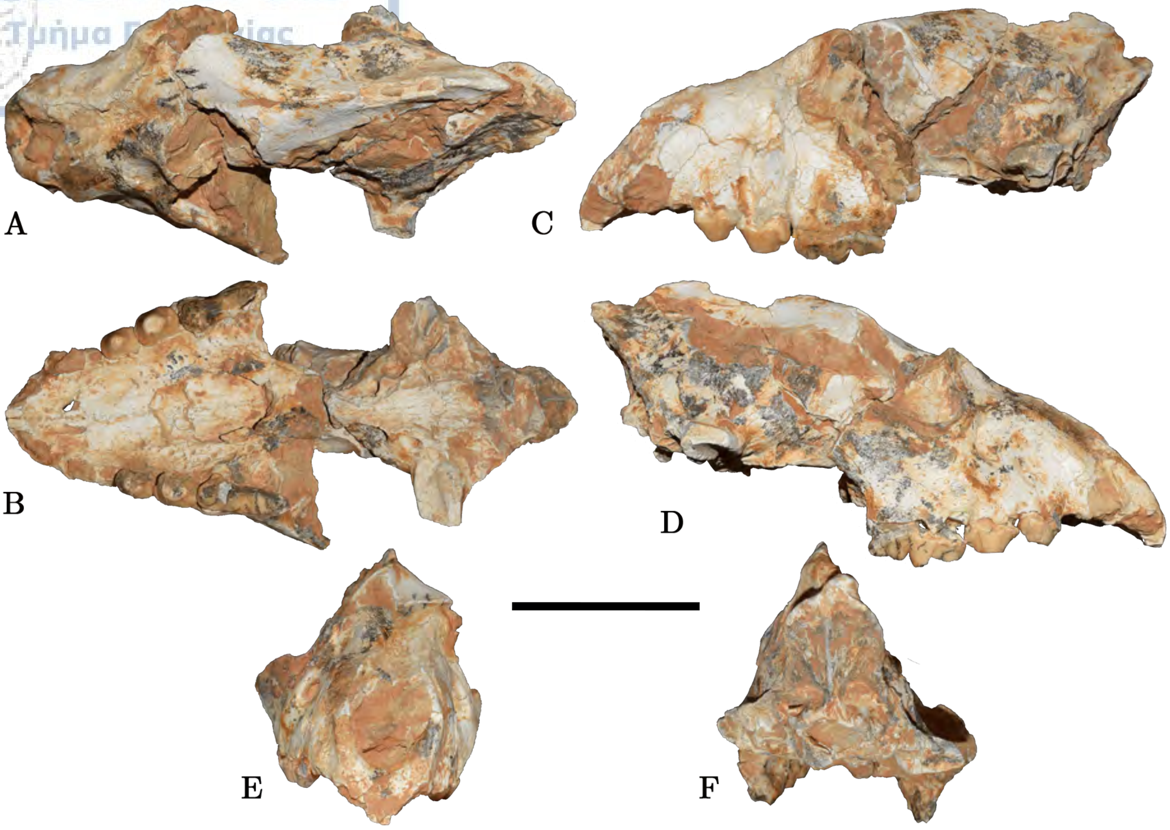

Figure 49. Cranium of *A. eximia* AMPG-PA 4954/91 in A: dorsal, B: ventral, C: lateral (sin), D: lateral (dext), E: anterior and F: posterior view. Scale bar is 10 cm.

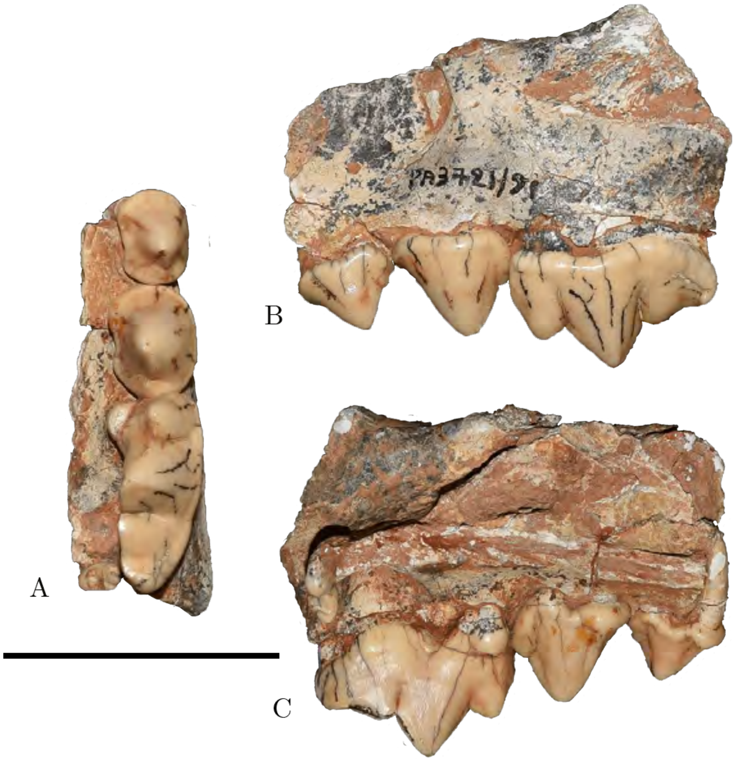

Figure 50. Maxillary fragment of *A. eximia* AMPG-PA 3721/91 in A: occlusal, B: buccal, C: lingual view. Scale bar is 5 cm.

Figure 51. Left hemimandible of *A. eximia* AMPG-PA 3722/91 in A: occlusal, B: medial and C: lateral view. Scale bar is 5 cm.

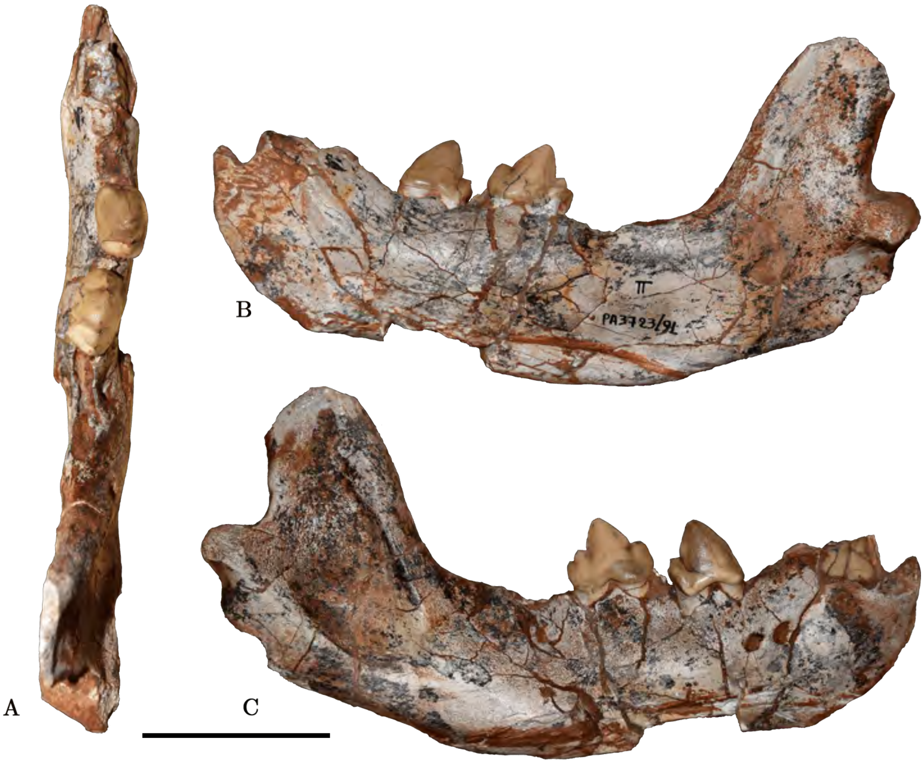

Figure 52. Right hemimandible of *A. eximia* AMPG-PA 3723/91 in A: occlusal, B: medial and C: lateral view. Scale bar is 5 cm.

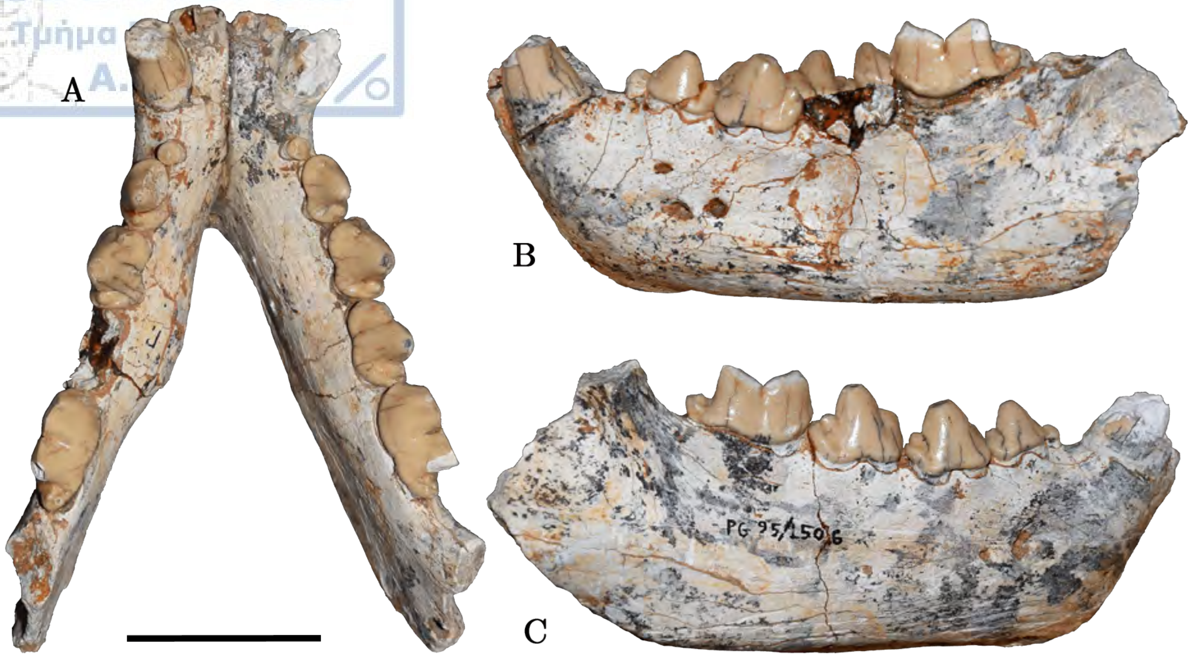

Figure 53. Mandible of *A. eximia* AMPG-PG 95/1506 in A: occlusal, B: lateral (sin) and C: lateral (dext) view. Scale bar is 5 cm.

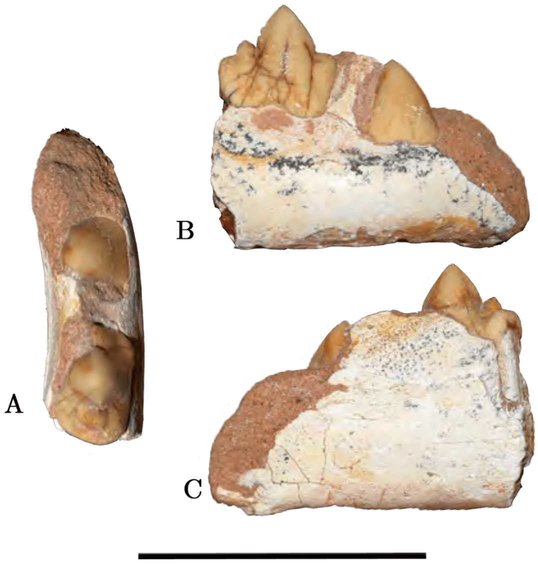

Figure 54. Right hemimandible fragment of *A. eximia* AMPG-PA 4955/91 in A: occlusal, B: lateral and C: medial view. Scale bar is 5 cm.

Genus *Hyaenictis* Gaudry, 1861
Hyaenictis graeca Gaudry, 1861
(Figs. 55–61, Table 27)

Type species: *Hyaenictis graeca* Gaudry, 1861.

Type locality: Pikermi, Attica, Greece.

Type material: MNHN-PIK-3002 (lectotype), left mandibular ramus with dp2– dp4 and P4–M1 (Fig. 2b), described and figured by Gaudry (1861:527; pl. 11, Figs. 1–2) and defined by Pilgrim (1931). Stored in the Museum National d'Histoire Naturelle of Paris, France.

Age: Middle Turolian, MN 12; 7.33–7.29 Ma for the classical locality of Pikermi (Böhme et al., 2017).

Localities: ?Halmyropotamos in Euboea Island (present work), ?Spain: Cerro de la Garrita (Alcalá, 1994).

Material: AMPG-PA 15/91: partially preserved cranium with P2-P3-P4-M1 (sin) and isolated P3-P4 (dext), AMPG-PG 01/110: partially preserved cranium with P3-P4-M1 (dext), AMPG-PG 01/112: isolated P2 (dext), PG 01/109: maxillary fragment with erupting P2-P3 and P4 (sin), AMPG-PG 01/111: maxillary fragment with erupting C-P2-P3 (dext), AMPG-2510: maxillary fragment with P2 (sin) and the roots of I2-I3-C-P1-P3 (sin). (Figs. 56–61)

Remarks: The ontogenetic stages of the specimens included herein vary from young individuals with still erupting permanent dentition to older individuals with visible dental wear.

The isolated right P3-P4 are considered to be associated with AMPG-PA 15/91 as they exhibit the same degree and pattern of wear. Unfortunately, those teeth are damaged and only limited measurements on P4 are possible.

Description: The cranium AMPG-PA 15/91 partially preserves its left side with the maxilla, the anterior orbit and part of the palate. It appears to be slightly crushed in the transversal axis, flattening it a little laterally as a result. In its left lateral side, the large, crescent-shaped infraorbital foramen opens above the distal margin of the P3's main cusp. The anterior margin of the orbit is situated above and in-between the paracone and the parastyle of the P4. The anterior zygomatic bone is strong and thick. A slight depression forms above the main cusp of the carnassial. The nasal bone appears to be straight and narrow. The frontal bone is fragmented and not well preserved. The progress to the forehead appears to be gradual, with no distinct cranial vault. In ventral aspect, the palate is estimated to be relatively narrow with an approximate length of 81mm at the distal margin of the P4. The palatine bone's anterior margin is situated at the projection of P3's main cusp. The choanae's anterior margin, which is not completely preserved, extends ~15mm behind the distal margin of M1. A deep and wide groove opens between P4 and M1.

The cranium of AMPG-PG 01/110 is similar in morphology to AMPG-PA 15/91 but vertically distorted, flattening it vertically as a result. A similar but exaggerated maxillary depression forms above the paracone of the right carnassial. The right infraorbital foramen opens up above P3's main cusp. The orbital socket is elliptical. The lacrimal foramen is observable at the lacrimal bone near the anterior margin of the right orbital socket. The sphenopalatine and caudal palatine foramina are also preserved in the palatine bone inside the right orbital socket. In dorsal view, the frontals are mostly flattened and a slight depression develops in an antero-posterior direction in the middle. In ventral view, the anterior margin of the choanae is broken. Nevertheless, it would have extended at least 10mm behind M1. The postorbital process is relatively small and pointed.

The infraorbital foramen of the young AMPG-PG 01/109 is situated above the main cusp of P3. It opens towards the P2-P3.

AMPG-2510: the left palatine fissure is preserved lingually to the canine and distally of the I2. A depression forms in the lateral side of the maxilla in-between the canine and P2. This results in the formation of an angle between the P1-P2 in occlusal view and the mesial side of P2 being situated lingually and its distal side buccally.

I2: The root from AMPG-2510 is small and mesio-distally elongated.

I3: The greatly enlarged and mesio-distally elongated root from AMPG-2510 probably indicates a similarly enlarged I3.

C: Only the erupting canine of AMPG-PG 01/111 is preserved. It erupts towards the mesial direction. Occlusally, the observable part of the crown inclines slightly buccally. The tip of the crown is rather blunt. The alveolus from AMPG-2510 indicates a large, elliptical to sub-rectangular-shaped canine. In the same specimen it also forms a small diastema of approximately 4.5mm with the root of I3.

P1: Preserved only in AMPG-PA 15/91 and AMPG-2510 with an alveolus and a root respectively. It is relatively small, single-rooted and rounded. Contrasting to AMPG-PA 15/91, AMPG-2510 forms a small diastema of approximately 3mm with P2.

P2: It is mesio-distally elongated. A notch forms in the base of the main cusp's crown. Although the general morphology of P2 is similar across the studied sample, some slight variation in the mesial cusps is present. The mesio-lingual cusps range from very strongly appressed to the main cusp (AMPG-PA 15/91, AMPG-2510, AMPG-PG 01/112, possibly AMPG-PG 01/109) to a slight mesio-lingual swelling of the cingulum (AMPG-PG 01/111). The width of P2 narrows down close to the main cusp, while its maximum width is observed approximately between the main and distal cusp. The cingulum expands disto-lingually through a high and slightly crenulated shelf. The distal cusp is very appressed, although to a lesser degree, to the main cusp. The unworn dentition of AMPG-PG 01/109 and AMPG-PG 01/111 gives the distal cusp a serrated impression. The distal end of the tooth extends slightly towards the buccal direction. The buccal border is relatively straight. Overall, the cingulum is strong lingually and in the distal part of the tooth, but weaker mesially and mesio-buccally. Mesially, there are some crenulations.

P3: The morphology is similar with P2, albeit larger and overall, more robust. P3 imbricates slightly into P2 its mesial side. The buccal border of P3 is straight, the tooth narrows down close to the main cusp and its maximum width is observed in-between the main cusp and the distal cusp. Yet again, some variation in the mesial cusps is observed. The mesio-lingual cusp varies from strongly appressed to the main cusp (AMPG-PA 15/91), to strongly appressed with crenulations (AMPG-PG 01/109, AMPG-PG 01/111), to a simple swelling of the mesio-lingual cingulum (AMPG-PG 01/110). The main cusp is conical, high and slightly distally inclined. The distal cusp is also appressed, although to a lesser degree, to the main cusp. The unworn distal cusps of AMPG-PG 01/109 and AMPG-PG 01/111 give the impression of a low and compressed metastyle blade instead of a typical accessory cusp. The cingulum is strong and well-developed distally as it surrounds the distal part of the tooth. It is particularly strong in its crenulated disto-lingual side. The mesial and mesio-buccal sides are also marked by a cingulum, albeit not as strong. In contrast, the cingulum around the main cusp is either very weak or entirely absent.

P4: The carnassial is large and elongated. The protocone is relatively low but strong, well-separated from the parastyle and situated in its lingual side. In the unworn P4 of AMPG-PG 01/109 a smell crest from its broken protocone fades midway towards the parastyle. The paracone is conical, situated higher than the other cusps and inclines distally. The mesial half of the paracone's crest is longer than its distal half. The metastyle blade is barely longer than the paracone with the exception of the longer metastyle blade of AMPG-PG 01/109. The metastyle blade exhibits a slight inclination buccally towards its distal end. The lingual side of the carnassial is marked by a low but distinct cingulum that extends from the protocone to the metastyle blade. The buccal side is marked by its relatively straight borders and weak cingulum. A crest forms in the mesial side of the parastyle (AMPG-PG 01/109, AMPG-PG 01/110) and then proceeds distally across the cusps of the parastyle, paracone and metastyle blade (AMPG-PA 15/91, AMPG-PG 01/109, AMPG-PG 01/110).

M1: It is relatively large and transversally elongated. It situated almost vertically to the carnassial's metastyle blade. The paracone strongly projects buccally and is the highest of the three cusps. The distally oriented metacone is reduced and appears rudimentary relative to the other cusps. The protocone is the largest and simultaneously the lowest of the three cusps, projecting lingually. The three cusps are interconnected through some small crests near the borders of the crown. A small basin is formed in-between the protocone and paracone-metacone. M1 is only preserved in AMPG-PA 15/91, however, the broken crown of AMPG-PG 01/110 indicates a similar size and morphology.

M2: There is no evidence indicating the presence of a M2 in any of the studied specimens.

Discussion: Contrast to the more complicated history of some other taxa discussed herein, the history of *Hyaenictis graeca* is simpler due to the absence of material. The genus *Hyaenictis* was initially erected by Gaudry (1861) along with its type species, *H. graeca*, on the basis of a juvenile's left hemimandible (MNHN-PIK. 3002) that retained its i1-i2-i3-dc-p1(alveolus)-dp2-dp3-dp4, the unerupted p3-p4 and the erupting m1-m2. A couple of years later, Gaudry (1863) also attributed to the species a right maxillary fragment from a young individual (MNHN-PIK. 3003) with dP3-dP4-P4-M1 and a right hemimandible (MNHN-PIK. 3031) with m1-m2. A young individual's left maxillary fragment (NHMW-PIK-A.4715) with P1-P2-P4-M1 has also been considered to belong to *H. graeca*. Koufos (2011) and de Bonis et al. (2007) have commented that the two maxillary fragments along with the mandible of the type specimen could potentially belong to the same young individual. The otherwise complete absence of additional *H. graeca* remains from Pikermi, combined with the morphology of its m1, drove Solounias (1981) to synonymize *Hyaenictis graeca* with *Adcrocuta eximia.*

Subsequent authors (Howell & Petter, 1985; Qiu, 1987; Werdelin & Solounias, 1990; 1991) however, have since disregarded this notion, essentially proving the validity of *H. graeca* as a taxon while clarifying its differences with *A. eximia*. Werdelin (1996) has hypothesized that the rarity of *H. graeca* material might indicate a specialized ecological niche for the taxon, different from that of the more abundant *A. eximia* and the dog-like "ictitheres".

Besides those four specimens from the type locality, only two other references of *H. graeca* have been made. The first was made by Ginsburg (1977), where he attributed to the species some teeth and postcranial material from Beni Mellal in Morocco, constituting the first reference of *H. graeca* outside its type locality. The p3 of the Beni Mellal material where Ginsburg (1977) based his attribution, however, differs from that of holotype as noted by other authors already (Werdelin & Solounias, 1991; Werdelin & Peigné, 2010; de Bonis et al., 2010). To that, de Bonis et al. (2010) also adds that it could either belong to a percrocutid or an as of yet unidentified Hyaenidae.

The second and most promising specimen was a partially preserved cranium (AMPG-PA 15/91) from the old collections of the classical locality of Pikermi to which Roussiakis (1996) attributed to cf. *Hyaenictis graeca* in his PhD Thesis. He compared it against the other, more commonly found large hyaenid from Pikermi, *Adcrocuta eximia*, the maxillary fragment MNHN-PIK 3003 of *H. graeca*, as well as some other morphologically similar taxa like *Lycyaena* and *Chasmaporthetes*. In his comparison he exemplified both the specimen's similarities with *H. graeca* and its differences with *A. eximia* and other taxa. However, the limited material (both comparative and attributed), their different ontogenetic stages (juvenile vs adult) as well as some authors (e.g., Howell & Petter, 1985) hesitancy to properly acknowledge the initial upper dentition attributed to *H. graeca* by Gaudry (1863) at the time, yet again, due to its limited material and young nature, probably drove Roussiakis (1996) more hesitant to consider a more definite attribution to *H. graeca* at the given time.

As the years passed, more material of similar morphology and size to AMPG-PA 15/91 has been prepared and recognized from the old collections of Pikermi. Additionally, during the recent years, there have been reports of *Hyaenictis* species from African and Spanish localities (e.g., Haile-Selassie & Howell, 2009; Werdelin & Peigné, 2010; Vinuesa et al., 2017). In light of those reasons, it was considered appropriate to review AMPG-PA 15/91 along with the newer specimens and compare them anew against *Hyaenictis graeca* as well as other similar taxa.

The material described herein is of hyaenid morphology and its large size would indicate similarly large individuals. Firstly, considering the classical locality's known fauna, only two species would fit hyaenids of this magnitude: the well-studied *Adcrocuta eximia* and the enigmatic *Hyaenictis graeca*. Secondly, considering the general morphology of its dentition, it seems to alienate from the typical *A. eximia* morphology and resembles more that of the "cursorial" hyaenid lineage of *Lycyaena*-*Hyaenictis*-*Chasmaporthetes*-*Lycyaenops* rather than that of *A. eximia*, but a more in-depth comparison shall be made regardless. The biggest challenge of this study will actually be the comparison with some of the "cursorial" taxa, as most studies that deal with them are focused almost entirely on their lower dentition, mainly due to the absence or scarce material of their upper dentition.

Morphological comparison of the material with *Adcrocuta eximia* exhibits some glaring differences between them. *A. eximia* is characterized by a reduced protocone in its P4, a relatively small M1 along with strong P2 and P3. The material herein however, exhibits a large P4 protocone, a relatively large M1 with a strong parastyle projection, as well as more elongated P2 and P3 (Table 27). Also, in contrast to the higher robusticity values of *A. eximia* in P2 and P3, its upper carnassial is less robust, probably due to its reduced protocone (Table 27). The index (LP4/LP2+LP3) ×100 further exemplifies the premolar's proportional differences between *A. eximia* and the studied sample's (Table 27). Moreover, the cranial remains of *A. eximia* are characterized by a depression in the posterior of their nasals, which forms the anterior part of their cranial vault. As already stressed in the descriptions of AMPG-PA 15/91 and AMPG-PG 110/91, however, this transition occurs gradually without a distinct cranial vault or a nasals depression. In addition, the palate of AMPG-PA 15/91 and AMPG-PG 01/110 appears to be narrower than *A. eximia*, with the choanae of the former extending further back. Some additional, albeit more subtle morphological differences include the appressed cusps, the lingual cingulum in the P4 and the notch in the P2, which are both absent in *A. eximia* specimens.

In stark contrast, comparison with MNHN-PIK. 3003 and NHMW-PIK-A.4715 specimens of *H. graeca*, exhibited some striking similarities. Although the P1 is only preserved by an alveolus and a root in AMPG-PA 15/91 and AMPG-2510 respectively, their size is comparable with the P1 of NHMW-PIK-A.4715. Similarly, the dimensions of P2 in the preserved specimens (Table 27) are similar with those exhibited by NHMW-PIK-A.4715. Additionally, the latter's morphology is almost identical to that of the juvenile's AMPG-PG 01/109. Unfortunately, the presence of a notch similar to that mentioned in the description could not be confirmed in NHMW-PIK-A.4715, as the base of its crown has not fully erupted. P3 has yet to erupt in NHMW-PIK-A.4715, although, its buccal side is revealed. For that matter, its approximate length and buccal morphology seems to be similar to the described P3 for the material above. The carnassials of the material and *H. graeca* specimens are both marked by similarly sized and well-developed protocones. The carnassials total lengths are approximately similar. The primary difference between the studied material and the *H. graeca* specimens, lies in the width of their carnassials. Although, rather than a difference due to their protocones, this is due to the slenderer paracones and metastyle blades of MNHN-PIK. 3003 and NHMW-PIK-A.4715. This difference is also reflected upon their different WblP4 values as well as in their P4 robusticity index (Table 27). The individual dimensions and the relative lengths of the paracone to the metastyle blade of the material are either approximately similar or slightly larger in favour of the latter, as is the case with *H. graeca* MNHN-PIK. 3003 and NHMW-PIK-A.4715 (Table 27). In that regard, the proportionally longer metastyle blade of AMPG-PG 01/109 closely resembles that of MNHN-PIK. 3003. The slightly larger M1 of both AMPG-PA 15/91 and the base of the crown of AMPG-PG 01/110 are comparable to the M1 of both MNHN-PIK. 3003 and NHMW-PIK-A.4715. Morphologically they are both characterized by the strong buccal projection of their parastyle. However, AMPG-PA 15/91 is occlusally more rounded than MNHN-PIK. 3003 that retains a more rectangular shape. In that aspect, NHMW-PIK-A.4715 is morphologically closer to AMPG-PA 15/91 than MNHN-PIK. 3003. Also, the crown of MNHN-PIK. 3003 is marked by a slight groove close to the protocone, that is seemingly absent in both AMPG-PA 15/91 and NHMW-PIK-A.4715. Considering the young age of the two *H. graeca* specimens, as well as the fact the they may well be from the same individual that leaves some room for intraspecific variance. Taking into account the morphological differences (rectangular shape of M1 in MNHN-PIK. 3003 along with a slight groove inside its basin and the slender paracone and metastyle of P4 in both specimens) it is actually very possible that the material belongs to *H. graeca*. Lastly, it is worth to keep in mind that the dental dimensions of MNHN-PIK. 3003 and NHMW-PIK-A.4715 are based on casts and not the original specimens and some values may slightly vary (e.g., noticeably the WblP4 in MNHN-PIK. 3003).

Besides *Hyaenictis graeca*, another, more basal and slightly better-known member of the "cursorial" lineage is known from Pikermi: *Lycyaena* Hensel, 1863 represented with the species *L. chaeretis*. Unlike *H. graeca*, the material does show some morphological, but not metrical, similarities. Both the studied and *L. chaeretis* specimens from the Turolian of Pikermi and Samos in Greece exhibit large, well-separated protocones in their upper carnassials, appressed accessory cusps in their premolars, relatively large M1 and more or less similar dental proportions. Besides the smaller size of *L. chaeretis* however (Fig. 55), there are also some morphological differences. In *L. chaeretis* specimens from Pikermi in particular, the premolars form small diastemata in-between and do not exhibit the imbrication observed in the studied material's premolars. In contrast, *L. chaeretis* NHMW-SAM-A.4744 from Samos exhibits a slightly different morphology and in some regards is more similar to the described material. NHMW-SAM-A.4744 does not form any diastemata between its P2-P4 and its P3 even imbricates within P2. However, NHMW-SAM-A.4744's P3 is strongly angled, pushing its mesio-lingual cusp towards the palate, something not observed in neither other *Lycyaena* specimens nor the described material. The disto-lingual expansion of the cingulum described for the material above, is also present, albeit slightly weaker, both in NHMW-SAM-A.4744 from Samos and NHMUK-M8978 from Pikermi described by Pilgrim (1931). The morphology of *L. chaeretis* M1 slightly differs from the morphology of AMPG-PA 15/91 (Fig. 5 in de Bonis & Koufos, 1994; Fig. 16, a2 in Koufos, 2021) and is sub-triangular shaped in occlusal view. Also, the length between the choane's anterior margin and M1 is shorter than that of AMPG-PA 15/91 and probably AMPG-PG 01/110 too.

Another, better-known member of *Lycyaena*, *L. dubia* Zdansky, 1924 from China, exhibits, for the most part, the same similarities and differences as *L. chaeretis*. The upper dentition of *L. dubia* is relatively similar in proportion to that of the material's, but its dental dimensions are similar to those of *L. chaeretis* (Fig. 55). Besides that, some morphological differences were noted as well. The holotype of *L. dubia* figured in Werdelin (1988a) exhibits a rounded distal end in its P2, while the studied sample's distal P2 margin (AMPG-PA 15/91, AMPG-PG 01/109, AMPG-PG 01/111) is sharper and more angular towards the disto-buccal direction. Additionally, the P2 and P3 in the holotype of *L. dubia* lack the disto-lingual expansion of the cingulum that characterizes the material in study. Lastly, the P2 of *L. dubia*'s holotype forms a small diastema with P3, instead of minor imbrication as expressed in the material herein.

The material also shares similar traits, both morphological and metrical, with representatives of the genus *Chasmaporthetes*. Although most representatives of this genus are known from the Plio-Pleistocene, its first occurrence is marked during the Miocene. Representatives of this genus have also been reported in Greece (Koufos 1987; 1993) According to Qiu et al. (2004) and more recently also reported by Tseng et al. (2013), the maxilla of *Chasmaporthetes* seems to be marked by a "thumbprint fossa" above their P4. Such a depression was similarly observed both in AMPG-PA 15/91 and AMPG-PG 01/110, however, it also seems present in *L. chaeretis* craniums as well. Whether it is a character shared amongst other cursorial hyaenids however is still unknown. In regards to the *Chasmaporthetes* upper dentition, it is generally characterized by slender and trenchant premolars, relatively well-developed distal cusps and variable mesial cusps. The P1 is large but is often shedded during the early adult life of some species. The upper carnassial's protocone is strong and usually well-developed, the parastyle is relatively elongated, while the paracone somewhat reduced. The metastyle blade is elongated and its length varies from longer to approximately similar to its paracone. The more elongated metastyle blade is usually a trait of the more primitive, Miocene species (Kurtén & Werdelin, 1988; Werdelin et al., 1994; Werdelin & Peigné, 2010; Tseng et al., 2013). *Chasmaporthetes* differs from *Hyaenictis* and *Lycyaena* through some more derived dental traits. These, however, either regard their lower dentition (e.g., loss of M2 in *Chasmaporthetes*), or the proportions of P4. The proportional differences of the upper carnassial however, refer exclusively to the more primitive representatives of the genus from the Miocene, such as *C. borissiaki* (Khomenko, 1932) and *C. exitelus* Kurtén and Werdelin, 1988. In the more derived *Chamaporthetes*, such as *C. lunensis* Del Campana, 1914 and *C. australis* (Hendey, 1978), the metastyle blade is still elongated, but proportionally closer to that of *Hyaenictis* (Werdelin et al., 1994).

C. bonisi Koufos, 1987 from the Late Miocene (MN 13) of Ravin des Zouaves 5 of Axios Valley, Greece from the Late Miocene has, overall, smaller dentition than the material in study (Fig. 55). The morphology of the studied material's P2 and P3 however resemble those of *C. bonisi*. Also, the P3 of *C. bonisi* slightly imbricates within P2 in a similar way. The morphology of their upper carnassials is similar, even though the protocone of *C. bonisi* is slightly more mesially oriented. The most striking difference between the them, aside from their size, lies in the morphology of M1. The length between the paracone and the metacone in the M1 of *C. bonisi* is greater than the length of its protocone, which gives the crown a rather sub-triangular impression in occlusal view. In the preserved M1 of AMPG-PA 15/91 however, the aforementioned values are approximately equal.

C. exitelus from the Turolian (MN 12) Loc. 116w (Zdansky's locality) in China was initially erected by Kurtén & Werdelin (1988). De Bonis & Koufos (1994) consider it a probable synonym of *C. bonisi*, while Tseng et al. (2013) argue that *C. exitelus* might actually be conspecific with *C. lunensis*. In any case, based on the available material regarding *C. exitelus* and *C. bonisi*, their morphological and metrical resemblance is striking and by extension, the same similarities and differences that applied to the latter apply here as well. Additionally, the length of the paracone in *C. exitelus* provided by Kurtén & Werdelin (1988) is greatly reduced compared to its elongated metastyle blade. As stated in the description, the relative lengths of those values for the material herein are either approximately equal or only slightly in favour of the metastyle blade. Lastly, the distance between the choanae and M1 in the holotype of *C. exitelus* appears to be very small (Fig. 2 in Kurtén & Werdelin, 1988), which contrasts the longer length observed in AMPG-PA 15/91 and AMPG-PG 01/110. It is also interesting that *C. exitelus* has been characterized by Werdelin & Solounias (1996) as a vicariant of *H. graeca*, similarly to *L. chaeretis*-*L. dubia*.

C. borissiaki is known from the lower Pliocene (MN 15) of Dermedzhi in Moldova and Perpignan in France. As a primitive *Chasmaporthetes* it differs from the material herein with its very elongated metastyle blade relative to its paracone. Also, its overall dental dimensions are smaller than those of the studied sample (Fig. 55). Its morphology and metrical values resemble those of the European *C. lunensis* and it has been hypothesized that they could, potentially be conspecific (Rook et al., 2004).

C. lunensis (Del Campana, 1914) from the Late Pliocene-Early Pleistocene (?MN 13–17) ranged across numerous Eurasian localities, including the Middle Villafranchian (MN 17) locality of Dafnero 1 in Western Macedonia, Greece (Koufos, 1993), exhibiting the greatest geochronological dispersal encountered within the genus. This species has been debated extensively (Kurtén & Werdelin, 1988; Werdelin & Solounias, 1991 and references therein) and essentially separated by those authors between *C. l. lunensis* (Europe) and *C. l. honanensis* (Asia). The metrical and morphological differences between the two populations, that chiefly concern the mesial cusps of $P^2/_2$ and $P^3/_3$, were attributed to intraspecific variation rather than a taxonomic indicator (Galiano & Frailey, 1977; Kurtén & Werdelin, 1988; Rook et al., 2004 and references therein). In any case, comparison of the material with the larger *C. lunensis* from China (=*C. kani* in Galiano & Frailey, 1977; Qiu, 1987), showed some morphological similarities. The P3 of the specimens from China exhibit a similar imbrication with their P2-P3. Their carnassials and its cusps are also morphologically and proportionally similar to that of the studied material. Their M1 morphology, however, differs from AMPG-PA 15/91 (Fig. 5 in de Bonis & Koufos, 1994). From a more recently published complete cranium of *C. lunensis* from the middle Villafranchian locality of La Puebla de Valverde in Spain (Anton et al., 2006), the distance between its M1 and its anterior margin of the choanae is smaller than AMPG-PA 15/91 and AMPG-PG 01/110. Also, even though that cranium's P2 and P3 morphology resemble those of the studied sample, they differ in their P4 and M1. The P4's protocone in the Spanish *C. lunensis* is not as well-separated and has a much longer metastyle blade than its paracone. Also, the general morphology of its M1 does not resemble that of AMPG-PA 15/91. Lastly, *C. lunensis* both from Asia and Europe have smaller dental dimensions than the material herein (Fig. 55).

C. gangriensis Tseng et al., 2013 was erected from the lower Pliocene (Ruscinian) of Tibet. Although its premolars morphology has some resemblance in a similar way with other *Chasmaporthetes* compared here, it has much smaller dental dimensions, only slightly larger than *L. dubia* (Fig. 55).

C. australis from the Latest Miocene-Early Pliocene (MN 14) of Langebaanweg in South Africa (Werdelin et al., 1994; Rook et al., 2004). This large-sized *Chasmaporthetes* has been treated in Werdelin et al. (1994) and has been considered a member of that genus ever since. In his original description of the taxon, Hendey (1974) noted that its protocone is relatively small, while the metastyle blade, paracone and parastyle are approximately equal in length. The dental dimensions of this species are comparable to the material herein (Fig. 55), although its P4 is slightly more elongated and slenderer at its protocone. Proportionally, the material in study also has a parastyle which is smaller than its paracone and metastyle blade. Unfortunately, there are no figures of its upper dentition, plus, its M1, if present, is of unknown morphology and dimensions.

C. nitidula (Ewer, 1955) from the Lower Pleistocene locality of Swartkrans, Africa. Its dental dimensions are smaller, similar in size to those of *C. lunensis* (Fig. 55). In addition, its dental morphology is very different from that of the studied sample. The mesial cusps of P2 and P3 are very large and well-developed, creating symmetrical premolars as seen in the initial figures of the taxon by Ewer (1955).

Finally, the most recent member of the cursorial hyaenid lineage would be that of *Lycyaenops* Kretzoi, 1938. From *L. rhomboideae* Kretzoi, 1938 only its lower dentition is known and it has been shown (Werdelin, 1999) to be very different from that of *Hyaenictis*. The known upper dentition the other attributed member to the genus, *L. silberbergi* (Broom in Broom & Schepers, 1946), differs greatly from the studied sample. Its P3 has a distal cusp that is better separated and the mesial cusp is apparently absent. It does exhibit however a similar disto-lingual expansion of the cingulum. The size of this taxon's P3 is slightly smaller than that of the described material according to the data provided by Adams et al. (2016) (Fig. 55).

Besides the type species, some other species of *Hyaenictis* have either been erected or disproven (e.g., Turner, 1988) during the recent years:

H. hendeyi Werdelin et al., 1994 from the latest Miocene-Early Pliocene (MN 14) of Langebaanweg in Africa is probably one of the best-studied species attributed to *Hyaenictis* thus far, indicating a more central and perhaps different ecological niche than that of *H. graeca* (Werdelin, 1996). Since its erection there have also been reports of this taxon from more African localities (e.g., Morales et al., 2005; Howell & Garcia, 2007), but almost exclusively from its lower dentition. Werdelin et al. (1994) focused their discussion and comparison primarily in the lower dentition, despite the presence of a maxillary fragment with upper dentition. From its upper dentition, only the dimensions of the premolars are known, as neither Hendey (1978) nor Werdelin et al. (1994) provide any figures or discuss their morphology. Thus, the upper dental morphology as well as the dimensions and status of M1 are unknown. However, based on the description by Werdelin et al. (1994) its lower dentition appears to differ quite a bit from that of *H. graeca*. Concerning the material herein, the metrical comparison of their upper dentition did not reveal any glaring differences (Fig. 55).

H. wehaietu Haile-Selassie and Howell, 2009 from the Amba East Vertebrate Locality 1 in the Kuseralee Member of the Sagantole Formation in Middle Awash, Africa. The locality dates approximately 5.2 Ma. *H. wehaietu* is the smallest taxon attributed to *Hyaenictis* thus far. Its P2 lacks a mesial cusp and has a well-developed distal one. The distal end of its P2 is rounded. Its P3 is similar in morphology to P2 but has mesio-lingual cusp and is overall larger. The protocone of the P4 is situated lingually of the parastyle and its metastyle blade is much longer than the parastyle. The paracone is the largest cusp. Its P4 is relatively similar with that of *H. hendeyi*. Comparison with the material in question exemplified *H. wehaietu*'s much smaller premolar size. This contrasts slightly its relatively greatly enlarged length on its M1 which approximates that of larger specimens (Fig. 55). Morphological differences with the material include the absence of the disto-lingual expansion of the cingulum in the P2 and P3 of *H. wehaietu*. Also, in that taxon those two teeth are straight instead mildly imbricated. The paracone of *H. wehaietu*'s M1 appears to be slenderer than that of AMPG-PA 15/91 and overall, more distally projected than the distal margin of M1.

More recently, Suwa et al. (2015) referred a small and much older (~8.5 Ma) P3 to cf. *Hyaenictis* with possible affinities to *H. wehaietu* from the Chorora Formation in Ethiopia, Africa. Despite its small size (19.00 x 10.50mm) its morphology has some resemblance with the material herein. It does have an appressed distal cusp and a minor, strongly appressed mesio-lingual cusp that forms a thick crest towards the distal side of the tooth. The mesio-distal expansion of the cingulum is, however, absent. This morphology is generic enough however that could very well be attributed to almost any other cursorial hyaenid genera. Lastly, it is worth noting that with this morphology, the tooth resembles more a P2 rather than a P3.

Besides these, there have also been reports of a possible third *Hyaenictis* in Africa, referred to only as *Hyaenictis* sp. (Morales et al., 2005; Howell & Garcia, 2007; Werdelin & Peigné, 2010).

Hyaenictis almerai Villalta Comella & Crusafont Pairó, 1945 is known only from some scarce mandibular material from the late Vallesian-early Turolian (MN 10–11) of San Miquel del Taudell in Spain. It differs from both *H. graeca* and *H. hendeyi* in the shape of the lower premolars (Werdelin et al., 1994). Similar to the other *Hyaenictis* though, its metaconid is absent while the m2 is present. Werdelin & Solounias (1991) had argued that further study needed to be done, as it characters do not fit those of *Hyaenictis*. A few years ago, Vinuesa et al. (2017) published a cranium with an associated mandible from the late Vallesian-early Turolian (MN 10–11) sites of Ronda Oest Sabadell in Spain which they attributed to *Hyaenictis* aff. *almerai*. The authors focused their work almost exclusively to the comparison of the lower dentition and for the most part ignored the upper teeth. Based on their description and figures, the P2 of this specimen seems to be similarly angled distally towards the disto-buccal side. In general, the premolar morphology does not indicate important differences with the material in study and their metrical values are similar, aside from the slightly longer P4 of *H.* aff. *almerai*. The most striking difference between them would actually be the M1 of the latter species, which is very small compared to both the material and the other *H. graeca* specimens (Fig. 55).

Lastly, Koufos (2012) mentioned a right P2 from the Late Vallesian (~9.3 Ma) locality of Ravin de la Pluie in Axios Valley under ?*Hyaenictis* sp. to which he noted the metrical and morphological resemblance to NHMW-PIK-A.4715 over other, similar taxa. The metrical and morphological similarities he noted do exist with the studied material as well, but other than that there is nothing new to add to his initial allocation.

Concluding, the comparison of the material described with various similar hyaenids served to exemplify its metrical and morphological similarities with *H. graeca*. Additionally, the diagnostics provided for the species (Werdelin et al., 1994; Koufos, 2022c) further support this. As mentioned in the beginning of this section, the scarcity and young ontogenetic stage of the *H. graeca* material initially attributed by Gaudry (1863) makes both comparison and attribution to the species difficult, as there are still many unknown aspects concerning this taxon, such as its range of intraspecific variation. Again, the most important difference observed between the material and *H. graeca* specimens NHMW-PIK-A.4715 and particularly MNHN-PIK. 3003, is the width in their paracones and metastyle blades. Although the exact causation of this is not known, it is probably due to individual variation within the species level that is exaggerated by the limited comparative material rather than a taxonomic difference. Also, from an ecological aspect, the attribution of the material to *H. graeca* rather than another, novel species to Pikermi seems more logical, as when one considers the already well-studied and large carnivore fauna from that locality, the addition of yet another large predator in its already “overpopulated” guild wouldn’t make much sense. Lastly, taking into consideration the know expanded *H. graeca* material, its mesial cusps of P2 and P3 seem to exhibit some degree of variance, similarly with *Chasmaporthetes*.

AMPG-2510 is the sole specimen included that is probably not from the classical locality of Pikermi, but from the approximately similarly dated locality of Halmyropotamos in Euboea Island. The last to study the carnivore guild of Halmyropotamos extensively was Melentis (1967). During some more recent preparation of material from that site that was stored in the AMPG, this maxillary fragment, that does not comfortably fit any known carnivorans from that locality, was recovered. The size and morphology of its sole tooth (P2) though, exhibits similar morphology and dimensions with the rest of the material described herein, and by extension, *H. graeca*. Some differences from the material herein however were noted. The most striking difference concerns the mesial side of P2, which is highly directed lingually and creates an angle with the root of P1, essentially narrowing the snout, something not observed in neither AMPG-PA 15/91 nor NHMW-PIK-A.4715 which are straight. Also, the characteristic notch under the main cusp of P2 described is milder. Whether that is the result of taphonomical processes or individual variation is unknown. An attribution to other genera such as *Chasmaporthetes* is not considered as likely, both due to metrical (Fig. 55) but also faunal reasons. If this specimen does indeed belong to *H. graeca*, which, considering the localities similar faunas and age does seem likely, that would make it the first recorded *H. graeca* specimen outside its type locality.

Besides the maxillary fragment AMPG-2510, there is one more specimen to consider. Alcalá (1994), is his PhD Thesis attributed the P3 MNCN-CD-913 from the Turolian (~7 Ma, MN 12) locality of Cerro de la Garrita in Concud, Spain to *L. chaeretis*. Based both on the scale of its figure (p. 491, Pl. VII-j) and Alcalá's measurements however, the tooth is far too large to be considered for that taxon (~24.10 x 14.20 mm). The most interesting part besides its size is its morphology, as it is identical to that of AMPG-PA 15/91. Whether that could indicate the presence of *H. graeca* or another taxon, of similar size and morphology in Cerro de la Garrita of Spain is worth to be further explored.

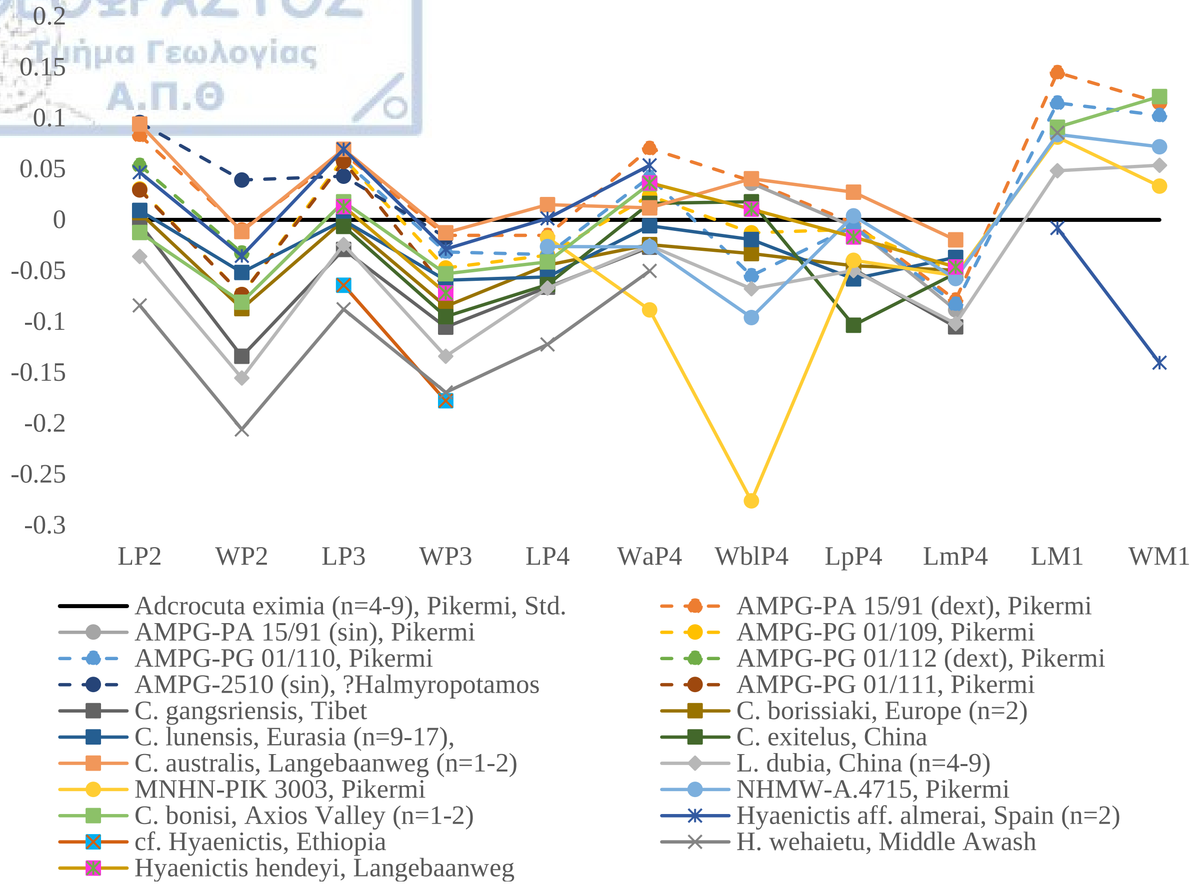

Figure 55. Log-ratio diagram for the upper dentition of *Hyaenictis graeca*. *Adcrocuta eximia* (n=4-9) from Pikermi was used as standard. Data for the standard were acquired from Werdelin & Solounias, 1990. Data for the various *Chasmaporthetes* were acquired from Kurtén & Werdelin (1988), Werdelin et al. (1994), Koufos (2000) and Tseng et al. (2013). Data for *Lycyaena* were acquired from Werdelin (1988a). Data for the various *Hyaenictis* were acquired from Werdelin et al. (1994), Haile-Selassie & Howell (2009), Suwa et al. (2015), Vinuesa et al. (2017).

Table 27. Upper dentition measurements (mm) of *Hyaenictis graeca*.

	AMPG-PA 15/91		AMPG-PG 01/109	AMPG-PG 01/110	AMPG-PG 01/111	AMPG-PG 01/112	AMPG-2510	MNHN-PIK. 3003	NHMW-A.4715
	Pikermi		Pikermi	Pikermi	Pikermi	Pikermi	?Halmyropotamos	Pikermi	Pikermi
	dext	sin	sin	dext	dext	dext	sin	dext (cast)	sin (cast)
LI2	—	—	—	—	—	—	[6.81]	—	—
WI2	—	—	—	—	—	—	[3.21]	—	—
LI3	—	—	—	—	—	—	[13.73]	—	—
WI3	—	—	—	—	—	—	[8.53]	—	—
LC	—	—	—	—	—	—	[23.18]	—	—
WC	—	—	—	—	—	—	[15.70]	—	—
LP1	—	[6.97]	—	—	—	—	[7.10]	—	8.88
WP1	—	[6.87]	—	—	—	—	[8.14]	—	6.60
LP2	—	(21.75)	(19.26)	—	19.22	20.32	22.38	—	19.74
WP2	—	12.25	10.58	—	10.58	11.63	13.71	—	10.32
LP3	—	25.59	25.32	25.22	25.15	—	[23.68]	—	—
WP3	[14.51]	15.27	14.18	14.70	13.52	—	[15.20]	—	—
LP4	(34.55)	36.10	34.52	(34.57)	—	—	—	35.91	35.20
WaP4	—	21.51	(19.33)	(20.16)	—	—	—	14.93	17.22
WblP4	12.72	12.79	11.37	(10.32)	—	—	—	6.20	9.39
LpP4	13.00	13.10	12.92	13.01	—	—	—	12.05	13.32
LmP4	(12.83)	13.18	14.03	(13.06)	—	—	—	13.93	13.84
HP4	18.87	18.53	19.68	16.63	—	—	—	19.15	(18.94)
LM1	—	9.17	—	[8.56]	—	—	—	7.92	7.97
WM1	—	18.65	—	[18.11]	—	—	—	15.44	16.87
L(P2–P4)	—	(81.90)	[76.68]	—	—	—	—	—	(72.37)
R.I. P2	—	(56.32)	54.93	—	55.05	57.23	61.26	—	52.28
R.I. P3	—	59.67	56.00	58.29	53.76	—	[62.50]	—	—
R.I. P4	—	59.58	(56.00)	(58.32)		—	—	41.58	49.92
W(P3/P4)	—	70.99	(73.36)	(72.92)	—	—	—	—	—
L(P3/P4)	—	70.89	(73.35)	(72.95)	—	—	—	—	—
L(mP4/P4)	(36.09)	36.40	37.46	(35.93)	—	—	—	38.79	39.32
LP4/(LP2+LP3)	—	(76.26)	(77.43)	—	—	—	—	—	—

Table 27. (Continued).

	H. hendeyi	*H.* aff. *almerai*	*H. wehaietu*	*L. chaeretis*	L. dubia	*C. bonisi*	*C. exitelus*	*C. borissiaki*	*C. lunensis*	*C. australis*	*C. gangsriensis*
	Langebaanweg	Spain	Ethiopia	Pikermi	China	Axios	China	Moldavia & France	Eurasia	Langebaanweg	Tibet
	(Werdelin et al., 1994)	(Vinuesa et al., 2017)	(Haile-Selassie & Howell, 2009)	(Author; Koufos, 2021)	(Werdelin, 1988a)	(Koufos, 2000)	(Kurtén & Werdelin, 1988)			(Werdelin et al., 1994)	(Tseng et al., 2013)
	SAM PQ-L21000	ICP-IPS62078	AME-VP-1/114	n=1-4	n=4-9	n=1-2	AMNH 26369	n=2	n=9-17	n=1-2	IVPP-V18566.1
LP2	—	20.00	14.80	16.51	16.53	17.45	—	18.25	18.34	22.30	17.80
WP2	—	11.55	7.80	9.42	8.76	10.4	—	10.25	11.13	12.20	9.20
LP3	22.70	25.85	18.00	20.24	20.83	22.95	21.70	22.00	22.00	25.85	20.60
WP3	13.40	14.80	10.70	12.61	11.61	14	12.70	13.00	13.79	15.35	12.40
LP4	—	37.50	28.20	32.04	32.03	34	32.30	33.75	32.85	38.70	32.10
WaP4	19.90	20.70	16.30	17.09	17.27	19.85	19.00	17.30	18.05	18.80	17.20
WblP4	12.00	—	—	10.66	10.02	—	12.20	10.85	11.20	12.85	—
LpP4	12.70	—	—	12.02	11.77	—	10.40	11.90	11.55	14.05	11.80
LmP4	14.20	—	—	11.73	12.49	—	14.00	14.10	14.51	15.10	12.40
LM1	—	6.45	8.00	7.13	7.34	8.1	—	—	—	—	—
WM1	—	10.35		15.93	16.18	18.9	—	—	—	—	—
RI P2	—	57.74	52.70	57.54	52.99	59.60	—	56.16	60.66	54.71	51.69
RI P3	59.03	57.24	59.44	62.39	55.74	61.00	58.53	59.09	62.70	59.38	60.19
RI P4	—	55.20	57.80	53.40	53.92	58.38	58.82	51.26	54.96	48.58	53.58
W(P3/P4)	67.34	71.48	65.64	73.49	67.23	70.53	66.84	75.14	76.40	81.65	72.09
L(P3/P4)		68.93	63.83	64.29	65.03	67.50	67.18	65.19	66.97	66.80	64.17
L(mP4/P4)	—	—	—	36.63	38.99		43.34	41.78	44.17	39.02	38.63
LP4/(LP2+LP3)	—	81.79	85.98	86.29	85.73	84.16	—	83.85	81.42	80.37	83.59

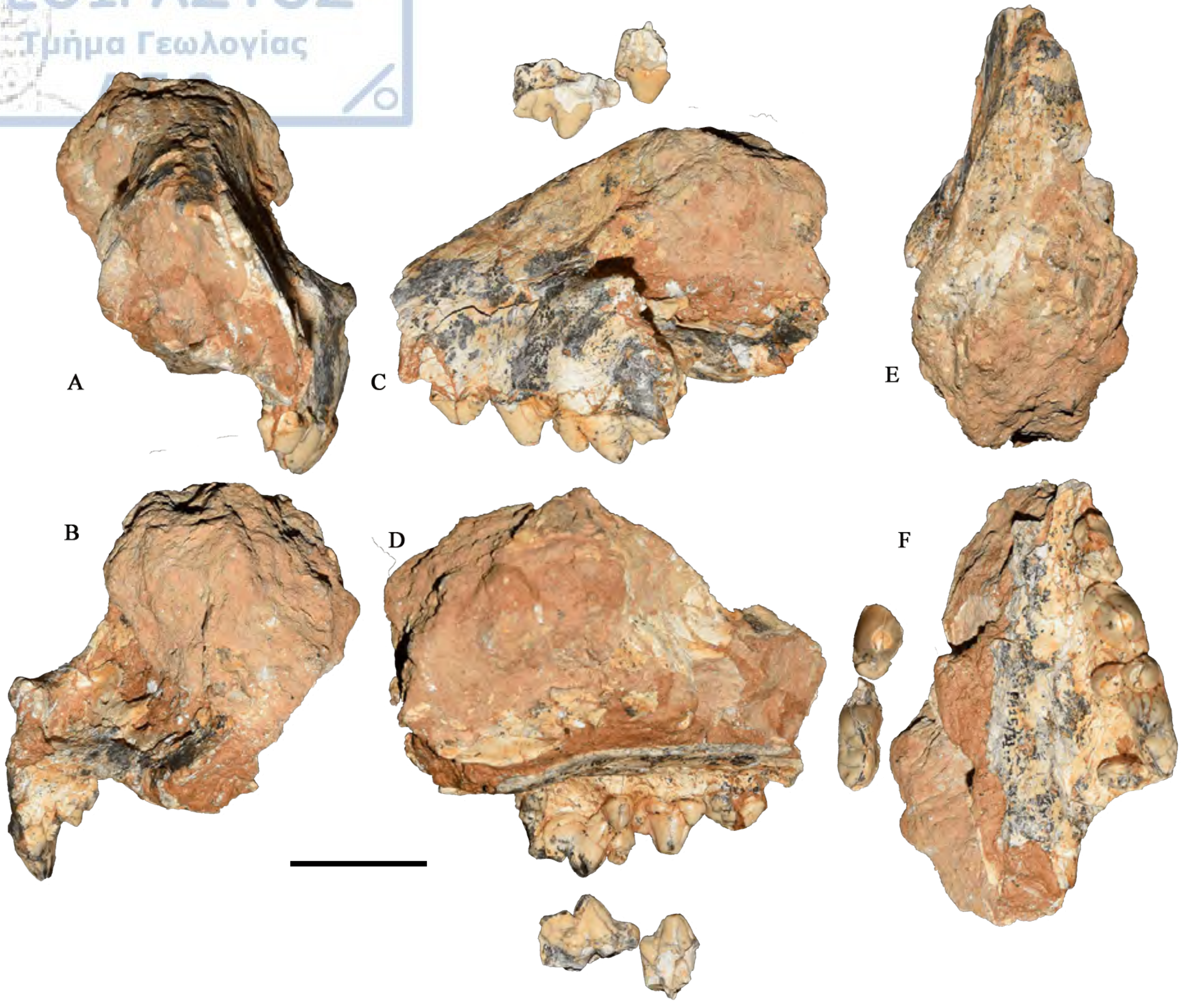

Figure 56. Partially preserved left cranium of *H. graeca* AMPG-PA 15/91 in A: mesial, B: distal, C: lateral, D: lingual, E: dorsal and F: occlusal view. Scale bar is 5 cm.

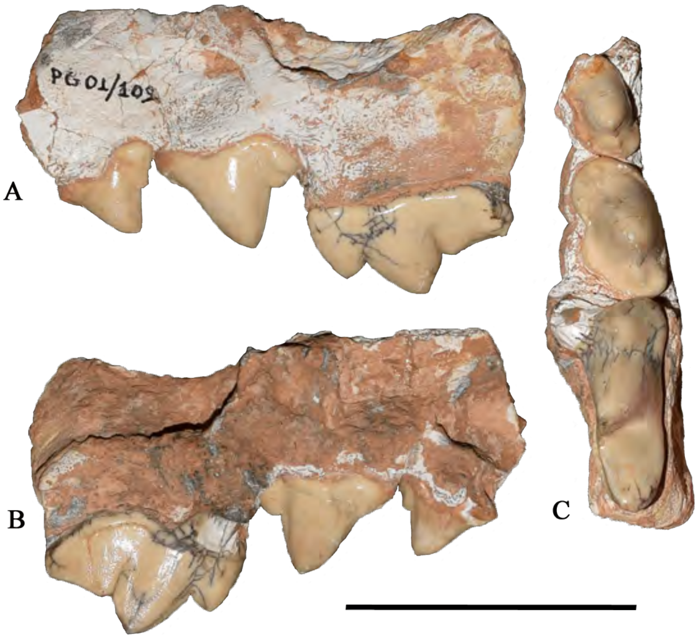

Figure 57. Left maxillary hemimandible of *H. graeca* AMPG-PG 01/109 in A: lateral, B: lingual and C: occlusal view. Scale bar is 5 cm.

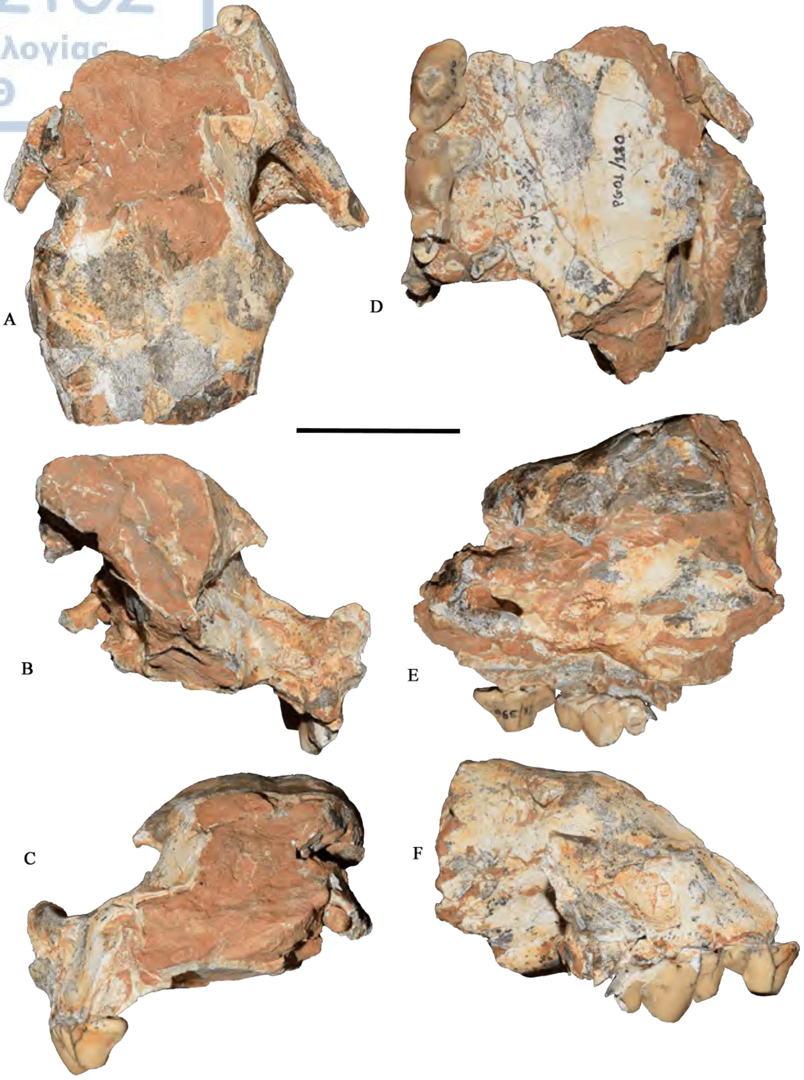

Figure 58. Partially preserved cranium of *H. graeca* AMPG-PG 01/110 in A: dorsal, B: posterior, C: anterior, D: ventral, E: lateral (sin) and F: lateral (dext) view. Scale bar is 5 cm.

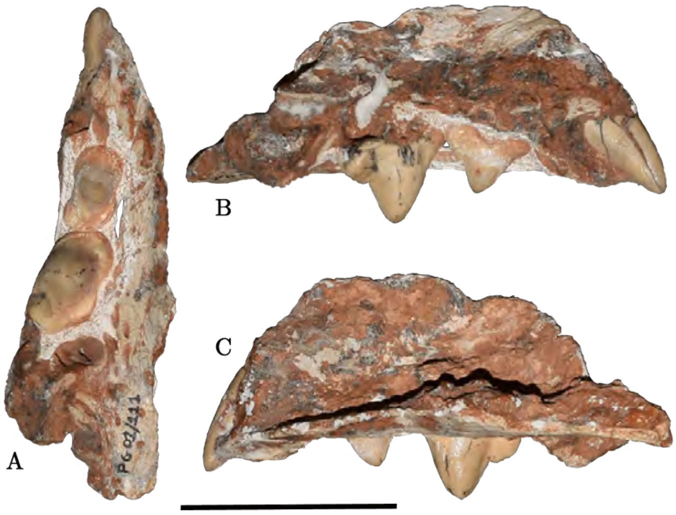

Figure 59. Right maxillary fragment of *H. graeca* AMPG-PG 01/111 in A: occlusal, B: lateral and C: lingual view. Scale bar is 5 cm.

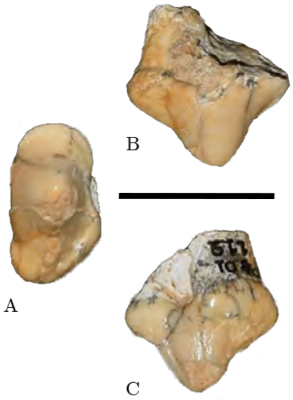

Figure 60. Isolated P2 (dext) of *H. graeca* AMPG-PG 01/112 in A: occlusal, B: lateral and C: lingual view. Scale bar is 2 cm.

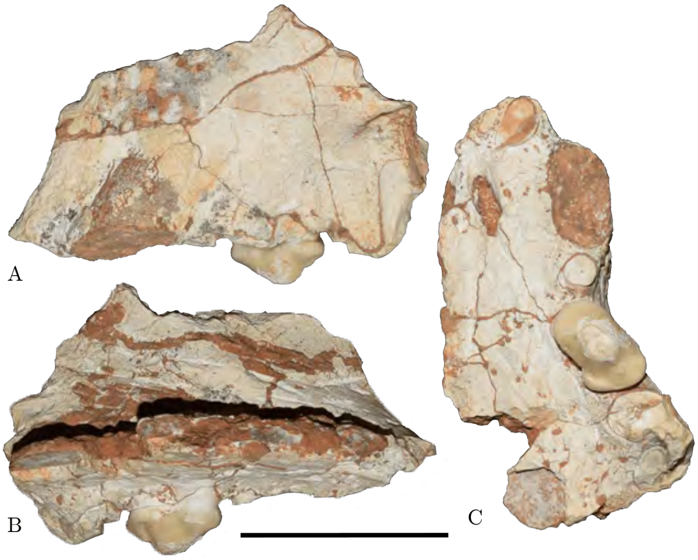

Figure 61. Left maxillary fragment of *H. graeca* AMPG-2510 possibly from the locality of Halmyropotamos in A: lateral, B: lingual and C: occlusal view. Scale bar is 5 cm.

Genus *Lycyaena* Hensel, 1862
Lycyaena chaeretis Gaudry, 1861
(Figs. 62–64, Table 28)

1861 *Hyaena chaeretis* n. sp. Gaudry, p. 534, Pl. 9, Figs. 3–6.
1862 *Lycyaena chaeretis* n. g. Hensel, p. 567.
1981 *Thalassictis chaeretis* (Gaudry) - Solounias, p. 74, Fig. 18.
1981 *Thalassictis* n. sp. Solounias, p. 76, Fig. 19.
1981 *Thalassictis (Lycyaena) chaeretis* (Gaudry) - Solounias & de Beaumont, p. 299.
1988 *Thalassictis (Lycyaena) chaeretis* (Gaudry) - Werdelin, p. 246.
1991 *Lycyaena chaeretis* (Gaudry) - Werdelin & Solounias, p. 25.

Type species: *Hyaena chaeretis* Gaudry, 1861.

Type locality: Pikermi, Attica, Greece.

Type material: MNHN-PIK-3383 (holotype); mandibular fragment with right c–p2 and left p2–m1 described and figured by Gaudry (1861:534; pl. 11, Figs, 3–6). Stored in Museum nationale d’Histoire naturelle, Paris, France.

Localities: A in Samos Island (Solounias, 1981).

Age: Middle Turolian, MN 12, 7.33–7.29 Ma for the classical locality of Pikermi (Böhme et al., 2017).

Material: AMPG-PG 95/1531: left maxillary fragment with P1-P2-P3-P4-M1 (sin) (Fig. 63).

Description: An oval-shaped taphonomical mark is located on the lateral side of the maxilla above P2. The infraorbital foramen is situated above the P3’s distal cusp. Two slight depressions of the maxilla are formed above the P2 and the carnassial’s paracone respectively. A deep groove is observed in the palate region between the P4 and M1. The dentition is straight in occlusal view and there is minor imbrication of P3 in P4. The other premolars are generally well-spaced and form short diastemata. The main cusps of P2-P3-P4 incline distally when viewed from the lateral side. The dentition has visible signs of wear.

P1: The single-rooted P1 is simple without mesial or distal cusps. A slight mesio-distal marks the cusp. The lingual cingulum is well-developed. The tooth forms a diastema with P2 of approximately 2.85 mm.

P2: The mesial cusp is absent. Instead, there is a swelling of the cingulum situated mesio-lingually. The main cusp is high and well-developed. The distal cusp is low and slightly appressed to the main cusp. A shelf marks the lingua side of P2. A thick crest forms at the mesio-lingual cingulum projection and passes across the main cusp towards the distal cusp. A small diastema of approximately 1.20 mm separates P2 from P3.

P3: The general morphology of the P3 is the same as with P2, but it is overall, larger. P3 has a small mesio-lingual cusp strongly appressed to its main cusp. A low but well-developed distal cusp is situated in the distal end of the tooth. The main cusp is well-developed;

however, the tip of its crown is missing. The cingulum is strong all around P3, but especially so at the main cusp's lingual side, where it forms a slightly lingually projecting shelf. Although the crest is not preserved, it would have a mesio-lingual to distal direction.

P4: It is elongated and slender. The protocone is situated lingually of the parastyle. It is slightly broken, well-developed and well-separated from the small parastyle. The paracone is high, pointed and its mesial half is slightly longer than its distal half. The metastyle blade curves slightly buccally towards its distal end. A crest forms at the mesial side of the parastyle and traces mesio-distally across the parastyle, paracone and metastyle blade. The cingulum is strong around the tooth and forms a small shelf in the lingual side. In lateral view, the large distal root of the carnassial is visible.

M1: It is small, low and lingo-buccally elongated, forming an almost 90^o angle with the carnassial. It is slightly broken and the metacone is missing. A central basin is formed between the lingually projecting protocone and paracone. The paracone is situated close to the middle of the carnassial's metastyle blade and probably projected more buccally than the metacone. Also, the paracone is situated higher than the protocone. The metacone was probably the distal-most cusp of the tooth, giving the tooth a sub-triangular appearance.

Discussion: Members of the genus *Lycyaena* are rare in Eurasian localities. *L. chaeretis* is a species with a rather long nomenclature and taxonomic history which has been thoroughly discussed by other authors (Werdelin, 1988a; Werdelin & Solounias, 1991; Koufos, 2021). Initially it was described as *Hyaena chaeretis* by Gaudry (1861), while the genus *Lycyaena* was erected one year later by Hensel (1862). After a period of turmoil regarding the status of the genus and its affinities (e.g., Solounias, 1981; Solounias & de Beaumont, 1981; Qui, 1985; Werdelin, 1988a), Hensel's name for the genus was restored by Werdelin & Solounias (1991) and has been established ever since.

The material described herein shares a lot of morphological similarities with *L. chaeretis* (Pilgrim, 1931; Werdelin, 1988a; Werdelin & Solounias, 1991; Koufos, 2021). Their similar dental morphology is further supported by the metric comparison with *L. chaeretis* specimens from Pikermi and Samos (Fig.62). The most striking difference noticed from the other *L. chaeretis* specimens however, was the smaller M1 size of AMPG-PG 95/1531. While the slightly damaged nature may serve to partially justify this, there seems to be some discrepancy between the M1 of NHMUK-PIK-M.8978 which, according to Koufos (2021) is 18.3 mm, while according to Pilgrim (1931) it is 14 mm.

Except *L. chaeretis* two additional large hyaenids have been described from Pikermi: *Adcrocuta eximia* and *Hyaenictis graeca*. The former's dental morphology (e.g., size of the protocone) and overall dental size differ a lot (Fig. 62), and while the dental morphology of AMPG-PG 95/1531 and *H. graeca* share similarities, its dimensions are too small to consider (Fig. 62).

Although *L. chaeretis* has only be recognized in Greece, other *Lycyaena* species have been recognized amongst other Eurasian localities:

L. dubia was erected on the basis of material from the locality Loc. 49, China. The morphology between the Chinese and Greek *Lycyaena* are very similar, to the point where they might be conspecific as it has been suggested by Werdelin (1988a). However, mainly due to the absence of material on the Greek specimens, such conclusions cannot be safely drawn at this time being and thus the species are kept separate. In any case, as far as the material of this study is concerned the *L. chaeretis* specimens from Pikermi are metrically (Fig.62). and morphologically (Fig. 64) similar. One difference between them is the almost straight dentition of AMPG-PG 95/1531, whereas P2 and P3 in *L. dubia* PMU-M3856 are placed at an angle. This difference, however, might just as well be the case of taphonomical processes or simply individual variation.

L. macrostoma (Lydekker, 1884) from Dhok Pathan, Siwaliks was erected on the basis of material from Siwaliks and shares similarities with *L. chaeretis* and *L. dubia*. Overall, *L macrostoma* is larger than *L. dubia* and *L. chaeretis* and has a broader m1 (Pilgrim, 1931; Werdelin & Solounias, 1991; Koufos, 2021). Whether that is true and it constitutes a different species or they are conspecific with *L. dubia* and *L. chaeretis* and this is an artefact due to the absence of additional material is still unclear. As far as this study is concerned, the upper dentition of *L. macrostoma* differs from other the aforementioned taxa only by its slightly elongated P3 (Fig.62).

L. crusafonti Kurtén, 1976 is known only by some mandibular remains from Tunisia. It the largest known representative of the genus. According to Werdelin & Solounias (1991) the limited material of this species does not allow safe or more specific conclusions.

The taxonomic status of other *Lycyaena* species such as *L. proava* Pilgrim, 1932 and *L. chinjiensis* Pilgrim, 1932 from Siwaliks, Pakistan have generally been disregarded by Werdelin (1988a) as probably associated with members of either *Thalassictis* or *L. macrostoma*.

Concluding, the morphological and metrical comparisons allow the attribution of the studied specimen to *Lycyaena chaeretis*. The observed metrical differences, chiefly M1’s width, are not of significant importance and are considered to be within the expected intraspecific range of variation for the, so-far, small sample of *L. chaeretis*.

Phylogenetically *Lycyaena* is considered the oldest member of the *Lycyaena-Hyaenictis–Chasmaporthetes-Lycyaenops* clade (Werdelin & Solounias, 1991). In regards to its ecological niche, it is placed within the cursorial meat and bone eaters, which are characterized by a reduction in molars and a slenderer postcranial skeleton, exhibiting thus, more cursorial traits (Turner et al., 2008).

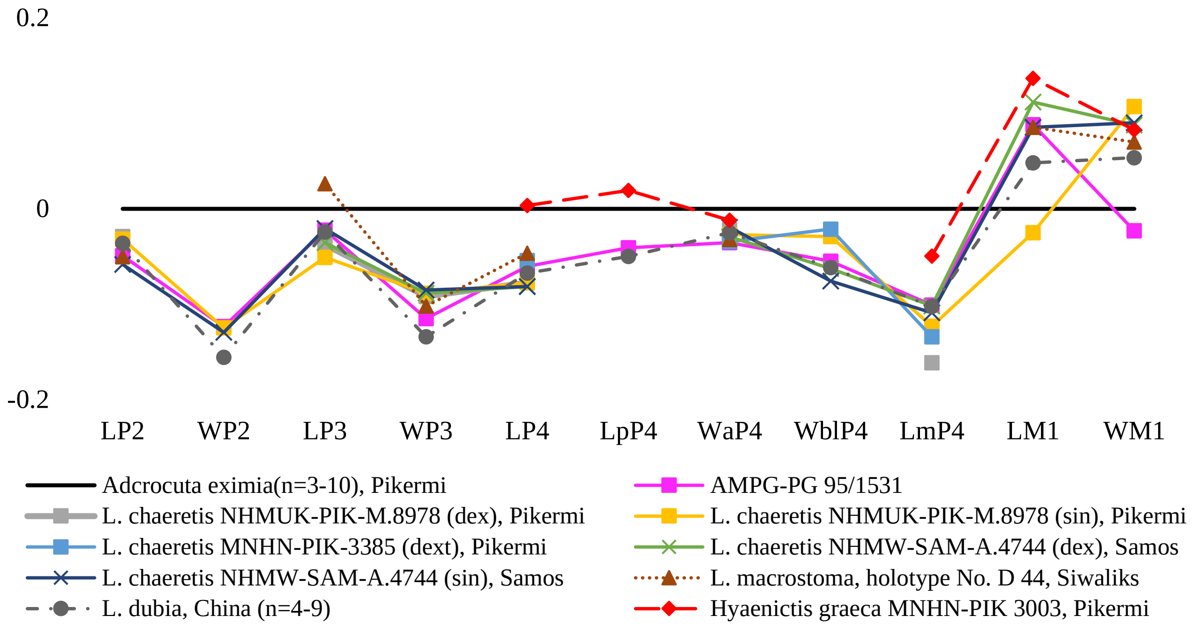

Figure 62. Log-ratio diagram for *Lycyaena chaeretis*. *Adcrocuta eximia* (n=3-9) from Pikermi was used as standard. Data for the standard were acquired from Werdelin & Solounias (1990). Data for *L. macrostoma* from Siwaliks were acquired from Pilgrim (1931). Data for *L. dubia* from China were acquired from Werdelin (1988a). Data for *L. chaeretis* from Pikermi and Samos were acquired from Koufos (2021). Data for *H. graeca* from Greece were acquired from Roussiakis (1996)

Table 28. Upper dentition measurements (mm) for various *Lycyaena* species.

	L. chaeretis						*L. macrostoma*	*L. dubia*
	Pikermi				Samos		Siwaliks	China
	AMPG-PG 95/1531	NHMUK-PIK-M.8978		MNHN-PIK-3385	NHMW-SAM-A.4744			
		(Koufos, 2021)					(Pilgrim, 1931)	(Werdelin, 1988a)
	sin	dext	sin	dext	dext	sin		n=4-8
LP1	7.34	—	—	—	7.00	7.20	—	—
WP1	6.08	—	5.80	—	6.00	6.10	—	—
LP2	16.04	16.80	16.70	—	—	15.70	16.00	16.53
WP2	9.43	—	9.40	—	—	9.30	—	8.76
LP3	20.92	20.20	19.60	—	20.30	21.00	23.40	20.83
WP3	12.13	12.80	12.90	—	12.90	13.00	12.50	11.61
LP4	32.54	31.30	31.30	33.00	31.00	31.00	33.60	32.03
WaP4	16.87	17.40	17.20	16.90	17.10	17.50	17.00	17.27
WblP4	10.18	—	10.80	11.00	10.00	9.70	—	10.02
LpP4	12.53	—	—	—	—	—	—	11.77
LmP4	12.02	10.90	11.90	11.60	12.50	12.30	—	12.49
HP4	16.15	—	—	—	—	—	—	—
LM1	(8.05)	6.20	—	—	8.50	8.00	8.00	7.34
WM1	13.56	18.30	—	—	17.50	17.70	16.80	16.18
R.I. P2	58.79	—	56.29	—	—	59.24	—	52.99
R.I. P3	57.98	63.37	65.82		63.55	61.90	—	55.74
R.I. P4	51.84	55.59	54.95	51.21	55.16	56.45	—	53.92
L(P3/P4) ×100	58.86	64.54	62.62		65.48	67.74	—	65.03
L(P2–P4) ×100	67.95	—	—	—	—	—	—	—
L(mP4/P4) ×100	38.51	—	—	—	—	—	—	—
L(P4/P2+P3) ×100	88.04	—	—	—	—	—	—	—

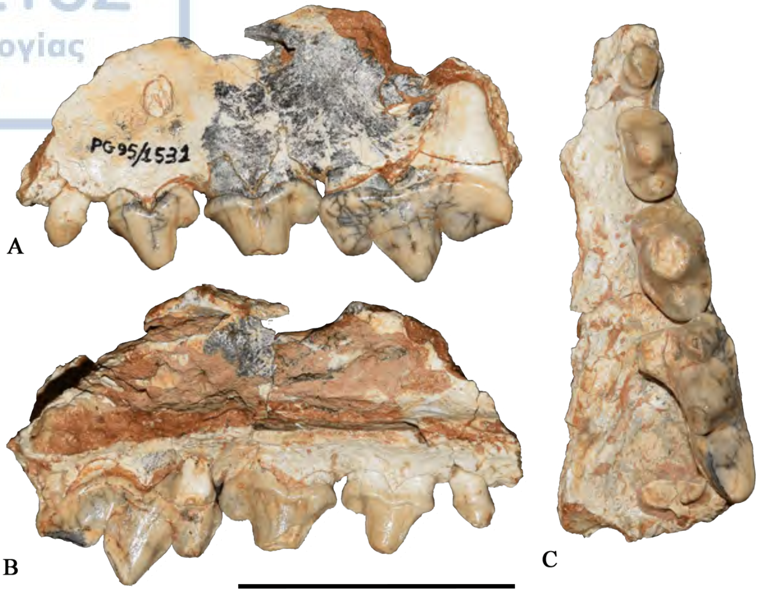

Figure 63. Left maxillary fragment of *Lycyaena chaeretis* AMPG-PG 95/1531 in A: lateral, B: medial and C: occlusal view. Scale bar is 5 cm.

Figure 64. Dental comparison of *L. chaeretis* AMPG-PG 95/1531 (right) with *L. dubia* holotype PMU-M3856 from Loc. 49, China (left). *L. dubia* photo source: Werdelin (1988a). Scale bar is 5 cm.

Hyaeninae indet.

(Figs. 65–67, Tables 29–37)

The bulk of the material attributed to this section probably belongs, with a few exceptions which will be noted in their appropriate sections, to the larger hyaenids of Pikermi, namely *Adcrocuta eximia* and *Hyaenictis graeca*. Granted that the postcranial skeleton of *Hyaenictis graeca* is virtually unknown, with the added the intraspecific variation of *Adcrocuta eximia*, separation between the two is difficult at the given time. It is, however, acknowledged that simply due to the sheer abundance of *A. eximia* craniodental material over *H. graeca*, the material herein would, by extension, potentially be attributed to *Adcrocuta eximia* rather than *Hyaenictis graeca*.

Material: AMPG-PA 4991/91: left hemimandible fragment with dp2-dp3, AMPG-PA 2989/91: distal part of a right humerus, AMPG-PA 3042/91: distal part of a left humerus, AMPG-PG 98/29: right proximal end of ulna with olecranon, AMPG-PA 4992/91: right ulna without the olecranon, AMPG-PA 4993/91: right radius, AMPG-PA 1019/91: proximal and distal ends of a left radius, AMPG-PA 4994/91: left proximal radius, AMPG-PA 4995/91: right radius without the proximal epiphysis, AMPG-PA 4996a/91: right scapholunate, AMPG-PA 4996b/91: right Pyramidal, AMPG-PA 4996c/91: right trapezium, AMPG-PA 4996d/91: right trapezoid, AMPG-PA 4996e/91: right magnum, AMPG-PA 4996f/91: right unciform, AMPG-PA 4996g/91: right proximal half of Mc I, AMPG-PA 4996h/91: right Mc II, AMPG-PA 4996i/91: right Mc III, AMPG-PA 4996j/91: right Mc IV, AMPG-PA 4996k/91: right Mc V, AMPG-PA 4996l/91: sesamoid, AMPG-PA 4997a/91: right Mc II, AMPG-PA 4997b/91: right Mc III, AMPG-PA 4997c/91: right Mc IV, AMPG-PA 4997d/91: right Mc V, AMPG-PA 4998a/91: left Mc II, AMPG-PA 4998b/91: left Mc III, AMPG-PA 4998c/91: left Mc IV, AMPG-PA 4998d/9: left Mc V, AMPG-PA 4999/91: right proximal phalange from a Mc I, AMPG-PA 5000/91: left proximal phalange from a Mc I, AMPG-PA 5001/91: right navicular, AMPG-PA 5002/91: right cuboid, AMPG-PA 5040/91: isolated metapodial without the proximal epihysis. (Figs. 65-67).

Remarks: The right carpals and metacarpals AMPG-PA 4996a-l/91 belong to the same individual. The right metacarpals AMPG-PA 4997a-d/91 belong to the same individual. The left metacarpals AMPG-PA 4998a-d/91 belong to the same individual.

Hemimandible with dp2-dp3: The mandibular corpus of the hemimandible fragment is very high and robust relative to its deciduous dentition and its margins appear straight. The mesial and distal sides of dp2 are damaged making it difficult to ascertain the presence or absence of cuspids. However, distally, a small cuspid seems to be present. dp3 is more elongated with a well-separated mesial cuspid that projects lingually. The distal side of the tooth is slightly damaged, but even so, the distal cuspid which is situated atop a cingulum projection is relatively elongated, being approximately equal with its main cusp.

Discussion: The large size of this young individual's hemimandible indicates that it would have grown to be a relatively large Hyaenidae. Further metrical comparison of its deciduous dentition with the deciduous dentition of *Adcrocuta eximia* and *Hyaenictis graeca* showed the material's metrical similarity with *A. eximia* over *H. graeca*, as the latter's deciduous dentition is even more elongated. Comparison with *Lycyaena chaeretis* AMPG-PA 31/1991 described by Roussiakis (1996) showed that AMPG-PA 4991/91 has a higher mandibular corpus (~33mm for the studied specimen and ~25mm for that of *L. chaeretis* at dp3). Their overall morphology in dp3 differs as well, as the main cusp in AMPG-PA 4991/91 is larger compared to that of *L. chaeretis*. In addition, the distal end of *L. chaeretis* dp3 extends way past its distal cusp, giving the tooth a talonid-like impression, while the studied specimen exhibits a fold of the distal cingulum which gives the tooth a serrated impression.

Humerus: Both humeri preserve only the distal epiphysis and part of their distal diaphysis. The lateral margins of the distal articulation surface are almost vertically oriented. The supratrochlear foramen is situated above the trochlea. Inside the foramen, the supracondylare foramen is present. The studied material preserves the bases of the bar, whether they completely ossified or not however, cannot be ascertained.

Discussion: Concerning the ossification of the bar, Pilgrim (1931) notes that in *Adcrocuta eximia* and *Crocuta crocuta*, although the bases of the bar are present, they don't completely ossify. This was later also confirmed by Roussiakis (1996) in regards to another specimen of *A. eximia*.

The material resembles morphologically the humerus described under *Adcrocuta eximia* by Roussiakis (1996) and more recently Kovachev (2012). Their size however is smaller than the humeri of *A. eximia* and probably indicates a different species. Even though *H. graeca*'s postcranial skeleton is unknown, its size would probably approximate that of *A. eximia* and for that reason it is also excluded. On the other hand, their size is just too large to consider either *I. viverrinum* or *H. wongii*. That leaves only one taxon to consider, *Lycyaena chaeretis*. Even though its postcranial skeleton is not sufficiently known, based on its craniodental material its humerus would probably approximate the size of the studied humeri. Thus, their attribution to *L. chaeretis* is considered to be the more likely.

Ulna: The AMPG-PG 98/29 olecranon is rectangular-shaped. The anconeal process extends slightly more anteriorly than the olecranon tuberosity and the height distance between them is moderate. As a result, the olecranon appears antero-posteriorly straight. Its proximal projection in the middle of the trochlear notch would pass in-between the lateral and medial olecranon tuberosities. The lateral olecranon tuberosity is slightly damaged. Even so, it is situated almost at the middle of the olecranon, way posteriorly of the medial olecranon tuberosity, which is situated at the anterior margin of the olecranon's head. The trochlear notch is not particularly deep. Distal of the trochlear notch, the radial notch is situated on the lateral side while the coronoid process is situated on the medial side. Both are worn and not very well preserved which probably results in the more anterior extension of the anconeal process. In the lateral side and between the trochlear notch and the lateral olecranon tuberosity, a rather deep, well-developed groove is developed.

AMPG-PA 4992/91's dimensions fit with the dimensions of the aforementioned proximal end of ulna with olecranon. Whether they belonged to same species however, cannot be ascertained presently. The shaft of the ulna is broader proximally and gradually tapers down until the middle of the shaft. In its posterior side, linear markings for muscle attachments, most likely for the flexor digitorum profundus, can be observed which trace down the shaft of the ulna distally. The anterior side of the ulna is slightly more convex and the interosseous crest of the ulna can be discerned. In the head of the ulna in the distal part, the styloid process of the ulna can would articulate to the ulnar notch of the radius.

Discussion: Comparison with the *A. eximia* from Hadzhidimovo (Kovachev, 2012) showed similar transversal dimensions. The antero-posterior dimensions however, are larger in AMPG-PG 98/29. The antero-posterior length of the styloid process of AMPG-PA 4992/91 is approximately similar with a styloid process attributed to *A. eximia* by Roussiakis (1996).

Radius: The proximal articular surface is elliptical and concave. The neck of the radius is about the same size as its proximal articular surface and curves slightly medially. In the medial side of its neck, there is a prominent oval-shaped radial tuberosity for insertion of the biceps brachii muscle. The shaft is elliptical to sub-triangular in cross-section and curves slightly towards the lateral side close to its middle. The shaft gradually thickens towards the distal end, especially so at the medio-lateral direction. Anteriorly, the distal end of the radius is almost triangular in shape and convex. In its medial side, the almost vertical and oval-shaped ulnar notch is observed, where the radius articulates to the ulna. The lateral side is rougher and more convex, with the styloid process extending more distally than the distal articular surface. In the posterior side, three distinct grooves are observed where the external abductor pollicis longus (medially), the external carpi radialis (middle) and the external digitalis communis (laterally) attached. The distal articular surface is elongated, elliptical to sub-triangular in shape and concave. The articulation to the scapholunate can also be observed, in the lateral side of the distal articular surface.

AMPG-PA 1019/91 is similar, albeit slightly more robust than AMPG-PA 4993/91. In its distal part, the anterior surface is more flattened as opposed to the slightly more convex AMPG-PA 4993/91. The three grooves for the external abductor pollicis longus (medially), the external carpi radialis (middle) and the external digitalis communis (laterally) are better preserved in AMPG-PA 1019/91. Especially for the external digitalis communis, the prominent and perfectly preserved concave groove can be observed.

AMPG-PA 4994/91 preserves only its proximal part and its general morphology resembles those described above. A few differences are noted however. Contrasting the straighter neck of the aforementioned radii, the neck of AMPG-PA 4994/91 gently curves medially. The radial tuberosity is proximo-distally elongated and is less projected. A small notch marks the area above the radial tuberosity. Lastly, its size is smaller.

AMPG-PA 4995/91 is missing its proximal epiphysis. The general morphology is the same as described for the AMPG-PA 4993/91 and AMPG-PA 1019/91. Again, however, some differences were noted. It is slightly smaller, with a slenderer shaft that is more strongly curved laterally. In addition to that, in the lateral side of its anterior surface the groove developed there is more prominent. As a result, the lateral side of the shaft has developed a thin and sharp edge.

Discussion: Based on their morphology and dimensions, the radii described here would probably belong to two different species. The larger in dimensions AMPG-PA 1019/91 and AMPG-PA 4993/91 and similar morphologies would probably justify their allocation to one species. The smaller and slightly different morphologically AMPG-PA 4994/91 and AMPG-PA 4995/91 would probably belong to another, slightly smaller species.

Further comparison of the two larger radii with radii attributed to *A. eximia* (Pilgrim, 1931; Orlov, 1941; Roussiakis, 1996; Kovachev, 2012; Lazaridis, 2015) showed morphological similarities. The studied radii, however, although comparable with some specimens, are generally on the larger end than many of the radii attributed to that species. As *A. eximia* apparently exhibits at least some degree of intraspecific variation, the possibility that AMPG-PA 1019/91 and AMPG-PA 4993/91, could potentially belong to larger *A. eximia* individuals is probable.

The smaller AMPG-PA 4994/91 and AMPG-PA 4995/91 are comparable as well with some of the radii attributed to *A. eximia*. However, due to their morphological differences, they probably belong to a different taxon. That essentially leaves *H. graeca* and *L. chaeretis* to consider. In both cases their postcranial skeleton varies from completely to almost completely unknown respectively. *H. graeca* would probably be too large for a radius of that size, however, since its postcranial skeleton is virtually unknown and its craniodental material is rather limited, then by extension so are its intraspecific variation limits. Considering *L. chaeretis*, Pilgrim (1931) had provisionally attributed a radius to that species, but, both its distal and proximal end's width were much smaller than both AMPG-PA 4994/91 and AMPG-PA 4995/91. As with *H. graeca*, the intraspecific variation range of *L. chaeretis* is also relatively unknown, as its craniodental material is also limited. Also, as Pilgrim doesn't provide a description of the attributed radius's morphology, its currently unknown whether it would actually fit the morphology of the radii examined here. Considering the above, a more specific attribution cannot be given at the current time, although, the attribution to *L. chaeretis* instead of *H. graeca* seems more plausible, simply due to their size difference.

Carpals: Consists of the trapezium, trapezoid, magnum, unciform distally and the scapholunate and pyramidal proximally.

Scapholunate: it is the largest of the carpals. It is medio-laterally elongated. Proximally it would articulate with the radius through its dorso-plantarly convex surface. The medio-plantar side of the scapholunate is marked by the flexor carpi radialis groove. The plantar tubercle is short but strong and curves towards the plantar direction. The distal articular surface articulates through some concave facets, from medial to lateral, with the trapezoid, magnum and unciform. These articular surfaces are divided by some small ridges in-between. The articular surface for the unciform is the largest. The trapezium might have articulated slightly in the medial-most side of the scapholunate, but a distinct surface was not observed. Compared to the scapholunates described in the Ictitheriinae section, this one has a relatively weaker and less expanded palmar tubercle. Also, the articular surface for the trapezoid in this one is markedly concave, while in the one described in the Ictitheriinae section is shallow and simply marked by an oblique edge.

Pyramidal: the most laterally situated carpal. It is sub-triangular and articulates distally with the unciform and medially with the scapholunate through its concave facets. Its lateral side is convex. It should have also articulated laterally with the pisiform.

Trapezium: The smallest of the carpal bones. It is elongated in the dorso-palmar direction. Distally it articulates with Mc I through a dorso-palmarly concave articular surface. It is the most medially oriented carpal. It articulates laterally with the trapezoid through a dorso-palmarly elongated concave surface. Dorsally it might also articulate slightly with the scapholunate.

Trapezoid: Dorsally it is slightly rounded to quadratic-shaped. Distally it articulates through a convex ridge-bearing facet with Mc II. Its proximal articular surface articulates with the scapholunate and is marked by a dorso-plantar ridge.

Magnum: It is elongated in the dorso-plantar direction. Its proximal articular surface is convex due to a laterally oriented ridge that articulates with the scapholunate. The distal surface is concave and articulates with Mc III. On its medial surface it articulates with the trapezoid through a slightly convex to flat facet, while on its lateral surface it articulates with the unciform through an elongated but narrow surface close to its dorsal side. Compared to the magnums described in the Ictitheriinae section, this is characterized by a relatively broader dorsal margin and a larger proximal articular surface.

Unciform: It is quadrangular-shaped and dorso-plantarly elongated. Its proximal surface is convex due to the presence of a ridge. Medially of the ridge it articulates with the scapholunate and laterally of the ridge with the pyramidal. A surface that would articulate it with the pisiform is located in plantar side. Its distal articular surface is separated by a small ridge into two facets: the lateral that articulates with Mc V and the medial that articulates with Mc IV. Compared to the unciform described in the Ictitheriinae section this unciform is relatively higher.

Metacarpals: The general morphology is relatively similar to the metacarpals described in the Ictitheriinae section.

Mc I: only its proximal half is preserved. It is the smallest of the metacarpals. It articulates with the trapezium through its smooth, cylindrical and laterally inclined proximal epiphysis. In contrast to the rest of the metacarpals, a distinct articular surface with another metacarpal was not observed.

Mc II: Proximally it articulates with the trapezoid. Laterally it articulates with Mc III while also slightly overlapping its proximal epiphysis. The proximal articular surface is elongated and concave in the dorso-plantar direction. In articulation, its proximal epiphysis faces slightly towards the medial side and is situated more proximally than the other metacarpals. The almost square-shaped distal epiphysis indicates the probable articulation with the proximal phalange via a symmetrical cylindrical trochlea. The shaft is slightly curved towards the lateral side and is sub-triangular in cross-section.

Mc III: The longest of the metacarpals. It is similar to Mc II. The only difference is that its straight and its proximal and distal epiphysis are slightly larger. Laterally it articulates with Mc IV while slightly overlapping its proximal epiphysis. The proximal articular surface is strongly elongated, slightly concave in the dorsal-palmar direction and articulates proximally with the magnum. Towards its plantar margin a tubercle is developed. The shaft is slightly elliptical in cross-section. The distal epiphysis is almost square-shaped.

Mc IV: The second shortest metacarpal after Mc I. The proximal epiphysis is convex and articulates with the unciform. The shaft is straight like Mc III and is sub-triangular to elliptical in cross-section. Mc IV articulates laterally with Mc V through a latero-proximal articular surface and a notch below that. Medially it articulates with Mc III through a medially projecting articular facet. Mc IV and V articulate without overlaps in their proximal epiphysis.

Mc V: It is the shortest metacarpal after Mc I. The shaft is thicker proximally and slightly narrows and straightens down just above the mid-shaft. It also curves towards the medial side and it is sub-triangular in cross-section. The proximal articular surface is convex and articulates with Mc IV through a small articular facet. The proximal articular surface forms a tubercle in its lateral side for insertion of the extensor carpi ulnaris muscle. The distal epiphysis is more rounded compared to the rest of the metacarpals.

Mc I proximal phalange: It is straight in lateral view. The proximal articular surface is slightly concave. The distal articular surface exhibits slight latero-plantar inclination.

Sesamoid: a small crescent-shaped bone which articulates in the distal end of the metacarpals.

Discussion: The only difference noted in the studied material concerns the metacarpals of AMPG-PA 4997a-d/9 that are slightly larger in dimensions. Also, it is interesting that the distal half of Mc V AMPG-PA 4997d/91 from that manus is pathological. Their only slightly large dimensions and otherwise identical morphology rather indicate intraspecific variation than a different species.

Morphologically and metrically, the carpals, metacarpals and proximal phalanges of Mc I described are similar to a manus described by Roussiakis (1996) which he attributed to *Adcrocuta eximia*. Further comparison of the material with the *A. eximia* from Hadzhidimovo (Kovachev, 2012) showed that the material from Pikermi is slightly larger in its dimensions. Considering the striking similarity with the manus described by Roussiakis (1996), the material studied herein probably belongs to the same species. Whether that is *A. eximia* or *H. graeca* however, cannot be confirmed yet.

Status of Mc I in Hyaenidae: Metacarpal I, with the exception of *Proteles cristatus*, is atrophic and not functional in extant Hyaenidae. Unfortunately, the status on its presence or absence in extinct Hyaenidae is not sufficiently studied. Kovachev (2012) notes that Mc I is not developed in the *A. eximia* skeleton from Hadzhidimovo he described and doesn't even make a mention about the presence or absence of a trapezium. Contrariwise, Roussiakis (1996) describes a manus from Pikermi which was found in anatomical position with a functional Mc I–including its distal epiphysis and associated proximal phalange–which he attributed to *A. eximia*.

Gaudry (1863) described and figured an atrophic Mc I amongst some other frontal limb fossils which he all attributed to *A. eximia*, based on the fact that a skull of the aforementioned taxon was found on the same fossiliferous block. What is not clearly stated though, is whether that Mc I was from the same fossiliferous block, as it is depicted outside of the matrix that contain the anatomically positioned fossils. Roussiakis (1996) considers that it may as well be a Mt I instead of Mc I, which is also atrophic in the extant hyaenids.

Besides *A. eximia*, Hendey (1974) has reported a functional Mc I from *Ikelohyaena abronia* (Hendey, 1974), approximately half the size of its Mc II, and from *Chasmaporthetes australis* (Hendey, 1974). The Mc I and distal epiphysis of Mc V of the latter taxon is of similar proportions with that of *Proteles cristatus* according to Hendey (1974). Lastly, he also made a note that the morphology of both species' Mc I are similar to that of *Proteles cristatus* (Hendey, 1974).

Navicular: The navicular is elongated in the dorso-plantar direction. The dorsal articular surface is concave and articulates with the talus. The plantar articular surface is slightly convex and articulates antero-lateral with the 3rd cuneiform, antero-medial with the 2nd cuneiform and dorso-lateral with the 1st cuneiform. The lateral side of the navicular articulates with the cuboid.

Discussion: It is provisionally attributed to this section based on its size and hyaenid morphology. Subsequent comparisons are limited due to the absence of comparative material. Judging from its large size it would have probably belonged to one of the larger hyaenids of Pikermi, either *A. eximia* or *H. graeca*.

Cuboid: The morphology of AMPG-PA 5002/91 is similar as described for the cuboid AMPG-PA 4977/91 described in the Ictitheriinae section. Aside from AMPG-PA 5002/91's larger size, the only other difference noted is the semi-circular rather than rectangular-shaped proximal articular surface.

Discussion: It is provisionally attributed to this section based on its size and hyaenid morphology. Subsequent comparisons are limited by the absence of comparative material. Judging from its large size it would have probably belonged to one of the larger hyaenids of Pikermi, either *A. eximia* or *H. graeca*.

Metapodial: a metapodial that lacks its proximal epiphysis. Aside from its size, morphology which place it in Hyaeninae and probably the fact that it is a central (III or IV), further identification is not possible

Table 29. Lower deciduous tooth measurements (mm) of Hyaeninae from Pikermi.

	AMPG-PA 4991/91	*Adcrocuta eximia*					*Hyaenictis graeca*	*Lycyaena chaeretis*
		Pikermi				Perivolaki	Pikermi	Pikermi
		(Gaudry, 1862–1867; Pilgrim, 1931)				(Koufos, 2006a)		(Roussiakis, 1996)
		NHMUK- M. 8973		NHMUK-M. 9880	NHMUK-M. 8974	LGPUT-PER-1240	MNHN-PIK-3002-3 (cast)	AMPG- 31/1991
	sin	sin	dext	sin	sin	dext	dext	dext
Ldp2	(8.90)	11.00	11.00	9.00	11.00	10.50	13.60	—
Wdp2	4.95	—	5.50	5.00	—	5.00	5.00	—
Ldp3	13.83	13.00	14.00	13.00	13.00	13.40	17.50	15.00
Wdp3	6.10	—	6.50	6.00	—	6.50	7.00	6.40

Table 30. Humerus measurements (mm) of Hyaeninae.

	DAPdist.	DTdist.	DTdist.art.
AMPG-PA 3042/91 (sin), Pikermi	37.95	34.92	29.91
AMPG-PA 2989/91 (dext), Pikermi	30.13	41.05	31.82
A. eximia AMPG-PA 3466/91, Pikermi (Roussiakis, 1996)	42.70	57.70	—
A. eximia MNHN-PIK. 3355, Pikermi (Roussiakis, 1996)	40.60	53.50	—
A. eximia NHMUK-M. 8997, Pikermi (Pilgrim, 1931)	—	55.00	—
A. eximia, Hadzhidimovo (Kovachev, 2012) (sin)	35.00	53.00	45.00
A. eximia, Hadzhidimovo (Kovachev, 2012) (dext)	40.00	53.00	45.00

Table 31. Ulna measurements (mm) of Hyaeninae from Pikermi and other localities.

	DAPpr.	DTpr.	DAPanc.	OH	DAPt.n	Ht.n	DAPdia.	DTdia.	DAPdist.	DTdist.
AMPG-PG 98/29 (dext)	40.44	24.67	46.23	28.30	28.67	34.38	—	—	—	—
AMPG-PA 4992/91 (dext)	—	—	—	—	—	—	15.54	17.52	18.67	12.32
A. eximia AMPG-PA 3137/91 Pikermi (Roussiakis, 1996)	—	—	—	—	—	—	—	—	17.50	—
A. eximia (dext) Hadzhidimovo (Kovachev, 2012)	42.00	17.00	—	—	—	—	15.00	12.00	26.00	31.00
A. eximia (sin) Hadzhidimovo (Kovachev, 2012)	41.00	16.00	—	—	—	—	14.00	11.00	24.00	31.00
A. eximia LGPUT-KRY 5295, Kryopigi (Lazaridis, 2015)	—	—	45,20	—	—	32.85	—	—	—	—
A. eximia LGPUT-KRY 6295, Kryopigi (Lazaridis, 2015)	—	—	44.77	—	—	—	—	—	—	—

Table 32. Radius measurements (mm) of Hyaeninae.

	L	DAPpr.	DTpr.	DTcol.	DAPdia.	DTdia.	DAPdist.	DTdist.
AMPG-PA 4993/91 (dext), Pikermi	261.63	23.52	34.00	26.73	17.31	24.75	26.77	44.55
AMPG-PA 1019/91 (sin), Pikermi	—	23.88	34.91	28.45	—	—	27.15	47.96
AMPG-PA 4994/91 (sin), Pikermi	—	18.41	26.15	17.66	—	—	—	—
AMPG-PA 4995/91 (dext), Pikermi	—	—	—	—	14.79	20.29	24.14	39.00
L. chaeretis NHMUK-M. 9007, Pikermi (Pilgrim, 1931)	193.00	—	17.00	—	—	—	—	30.50
A. eximia NHMUK-M. 8997, Pikermi (Pilgrim, 1931)	—	—	31.00	—	—	—	—	—
A. eximia (dext), Hadzhidimovo (Kovachev, 2012)	190.00	23.00	23.00	—	16.00	18.00	28.00	40.00
A. eximia (sin), Hadzhidimovo (Kovachev, 2012)	188.00	22.00	27.00	—	14.00	20.00	30.00	42.00
A. eximia, Pavlodar (Orlov, 1941)	232.00	20.70	28.80	—	18.00	21.40	23.30	41.00
A. eximia AMPG-PA 3146/91, Pikermi (Roussiakis, 1996)	—	—	—	—	(15.10)	(22.50)	26.20	44.50
A. eximia MNHN-PIK 3036a, Pikermi (Roussiakis, 1996)	—	22.40	29.50	23.60	(16.20)	(20.40)	—	—
A. eximia MNHN-PIK 3354, Pikermi (Roussiakis, 1996)	—	—	—	—	(13.20)	(20.70)	22.90	39.00
A. eximia LGPUT-KRY6296, Kryopigi (Lazaridis, 2015)	—	(13.48)	(23.00)	—	—	—	—	—
A. eximia LGPUT-NIK-1553, Nikiti (Koufos, 2016)	223.00?	20.00?	28.70	—	12.90	21.50	26.20?	44.50
A. eximia MNHN-PIK. 3006a, Pikermi (Koufos, 2016)	—	22.60	30.00	—	—	—	—	—
A. eximia MNHN-PIK. 3006b, Pikermi (Koufos, 2016)	—	21.10	30.50	—	—	—	—	—

Table 33. Carpal measurements (mm) of Hyaeninae from Pikermi and other localities.

	Hmax.	DAPmax.	DTmax.
Scapholunate AMPG-PA 4996a/91 (dext)	24.51	21.13	36.05
Scapholunate *A. eximia* AMPG-PA 3140/91, Pikermi (Roussiakis, 1996)	—	23.00	35.40
Scapholunate *A. eximia* MNHN-PIK 3296, Pikermi (Roussiakis, 1996)	—	24.90	35.30
Scapholunate *A. eximia*, Karain (Schmidt-Kittler, 1976)	—	26.40	40.00
Unciform AMPG-PA 4996f/91 (dext)	18.24	23.08	17.97
Unciform *A. eximia* AMPG-PA 3140/91, Pikermi (Roussiakis, 1996)	18.80	21.50	18.40
Unciform *A. eximia*, Karain (Schmidt-Kittler, 1976)	—	21.80	20.40
Unciform *A. eximia*, Pavlodar (Orlov, 1941)	19.50	22.50	18.00
Trapezium AMPG-PA 4996c/91 (dext)	8.00	17.46	8.87
Trapezium *A. eximia* AMPG-PA 3139/91, Pikermi (Roussiakis, 1996)	9.90	15.50	9.00
Trapezium *A. eximia*, Karisruhe (Schmidt-Kittler, 1976)	—	19.00	14.50
Trapezoid AMPG-PA 4996d/91 (dext)	10.22	17.06	10.37
Trapezoid *A. eximia* AMPG-PA 3142/91, Pikermi (Roussiakis, 1996)	10.10	17.10	14.50
Trapezoid *A. eximia* MNHN-PIK 3364, Pikermi (Roussiakis, 1996)	11.50	19.10	15.70
Magnum AMPG-PA 4996e/91 (dext)	13.45	23.70	13.94
Magnum *A. eximia* AMPG-PA 3141/91, Pikermi (Roussiakis,1996)	15.00	21.00	12.80
Magnum *A. eximia* MNHN-PIK 3363, Pikermi (Roussiakis, 1996)	15.80	23.80	13.60
Pyramidal AMPG-PA 4996b/91 (dext)	14.76	22.06	14.15
Pyramidal *A. eximia* AMPG-PA 3144.91, Pikermi (Roussiakis, 1996)	14.80	22.20	13.60
Sesamoid AMPG-PA 4996l/91	3.76	8.21	5.39

Table 34. Metacarpal measurements (mm) of Hyaeninae from Pikermi.

	L	DAPpr.	DTpr.	DAPdia.	DTdia.	DAPdist.	DTdist.
Mc I AMPG-PA 4996g/91 (dext), Pikermi	—	7.95	8.80	—	—	—	—
Mc I *A. eximia* AMPG-PA 3145/91, Pikermi (Roussiakis, 1996)	39.50	8.20	7.20	5.30	6.50	8.50	8.20
Mc II AMPG-PA 4996h/91 (dext)	84.52	19.36	14.30	10.14	11.38	13.18	13.87
Mc II AMPG-PA 4997a/91 (dext)	92.27	21.86	15.90	13.78	11.00	14.02	16.45
Mc II AMPG-PA 4998a/91 (sin)	85.52	20.58	14.87	10.96	11.34	13.67	14.22
Mc II *A. eximia* AMPG-PA 3133/91, Pikermi (Roussiakis, 1996)	87.10	19.60	(12.80)	11.60	10.10	12.20	16.50
Mc II *A. eximia*, Karlsruhe (Schmidt-Kittler, 1976)	—	11.10	11.00	—	—	—	—
Mc II *A. eximia* (dext), Hadzhidimovo (Kovachev, 2012)	77.00	19.00	12.00	—	11.00	12.00	12.00
Mc II *A. eximia* (sin), Hadzhidimovo (Kovachev, 2012)	—	14.00	12.00	(11.00)	—	15.00	—
Mc III AMPG-PA 4996i/91 (dext)	99.39	23.48	16.37	8.68	10.29	13.36	13.73
Mc III AMPG-PA 4997b/91 (dext)	106.56	22.41	18.23	12.36	12.74	14.08	15.54
Mc III AMPG-PA 4998b/91 (sin)	99.97	20.70	15.66	9.00	10.71	14.27	13.31
Mc III *A. eximia* AMPG-PA 3121/91, Pikermi (Roussiakis, 1996)	101.80	20.30	17.20	10.40	11.50	13.40	15.00
Mc III *A. eximia* MNHN-PIK. 3352, Pikermi (Roussiakis, 1996)	(103.00)	21.00	17.00	(12.00)	(11.70)	14.80	(13.60)
Mc III *A. eximia*, Pavlodar (Orlov, 1941)	—	—	—	8.70	11.70	15.70	15.70
Mc III *A. eximia*, Pavlodar (Orlov, 1941)	—	21.00	16.40	9.00	11.20	—	—
Mc III *A. eximia*, Pavlodar (Orlov, 1941)	—	20.50	16.00	9.00	11.50	—	—
Mc III *A. eximia*, Karlsruhe (Schmidt-Kittler, 1976)	106.70	—	16.90	—	—	—	—
Mc III *A. eximia*, Kinic (Schmidt-Kittler, 1976)	—	—	18.00	—	—	—	—
Mc III *A. eximia* (dext), Hadzhidimovo (Kovachev, 2012)	89.00	22.00	15.00	—	13.00	—	16.00
Mc III *A. eximia* (sin), Hadzhidimovo (Kovachev, 2012)	87.00	23.50	16.00	—	(11.00)	12.00	16.00

Table 34. (Continued).

	L	DAPpr.	DTpr.	DAPdia.	DTdia.	DAPdist.	DTdist.
Mc IV AMPG-PA 4996j/91 (dext)	95.52	19.42	14.35	8.85	9.70	13.45	13.12
Mc IV AMPG-PA 4997c/91 (dext)	104.82	21.85	16.60	10.93	11.58	16.00	15.13
Mc IV AMPG-PA 4998c/91 (sin)	95.97	20.52	13.02	9.34	10.84	14.09	13.00
Mc IV *A. eximia* AMPG-PA 3129/91, Pikermi (Roussiakis, 1996)	98.30	20.00	13.00	10.00	11.60	—	14.30
Mc IV *A. eximia* MNHN-PIK. 3352, Pikermi (Roussiakis, 1996)	99.30	17.10	>14.00	(11.00)	(12.50)	15.40	13.00
Mc IV *A. eximia* NHMUK-M. 8998, Pikermi (Pilgrim, 1931)	97.00	—	—	—	—	—	—
Mc IV *A. eximia*, Karlsruhe (Schmidt-Kittler, 1976)	103.00	—	14.50	—	—	—	—
Mc IV *A. eximia* (dext), Hadzhidimovo (Kovachev, 2012)	84.00	18.00	14.00	—	14.00	—	14.00
Mc IV *A. eximia* (sin), Hadzhidimovo (Kovachev, 2012)	84.00	19.00	—	—	11.00	—	12.00
Mc IV *A. eximia* LGPUT-KRY3711, Kryopigi (Lazaridis, 2015)	>63.70	20.08	14.60	9.50	12.45	—	—
Mc IV *A. eximia* LGPUT-NIK-1916, Nikiti (Koufos, 2016)	94.50	19.00	13.00	9.30	11.20	14.10	14.00
Mc V AMPG-PA 4996k/91 (dext)	79.44	16.64	16.72	9.34	10.30	12.31	14.65
Mc V AMPG-PA 4997d/91 (dext)	85.93	18.01	16.95	12.28	12.16	14.45	[20.17]
Mc V AMPG-PA 4998d/91 (sin)	78.82	16.39	18.47	10.09	10.49	12.39	13.78
Mc V *A. eximia* AMPG-PA 3125/91, Pikermi (Roussiakis, 1996)	80.20	16.00	18.00	9.50	10.40	(12.00)	14.20
Mc V *A. eximia* MNHN-PIK.3352, Pikermi (Roussiakis, 1996)	(85.80)	16.80	(21.00)	9.60	(12.00)	(12.00)	12.00
Mc V *A. eximia* NHMUK-M. 8997, Pikermi (Pilgrim, 1931)	83.00	—	—	—	—	—	—
Mc V *A. eximia*, Pavlodar (Orlov, 1941)	77.20	15.80	18.50	9.20	11.20	14.00	15.20
Mc V *A. eximia*, Pavlodar (Orlov, 1941)	80.20	16.00	18.00	10.80	11.30	13.50	15.00
Mc V *A. eximia* (dext), Hadzhidimovo (Kovachev, 2012)	71.00	16.00	18.00	—	10.00	12.00	14.00
Mc V *A. eximia* (sin), Hadzhidimovo (Kovachev, 2012)	81.00	16.00	17.00	8.50	10.00	13.00	14.00
Mc V *A. eximia* LGPUT-KRY8814, Kryopigi (Lazaridis, 2015)	—	15.50	17.00	—	(<12.80)	—	—
Mc V *A. eximia* LGPUT-KRY7954, Kryopigi (Lazaridis, 2015)	—	15.80	17.00	8.03	10.91	—	—
Mc V *A. eximia* LGPUT-NIK-1917, Nikiti (Koufos, 2016)	—	—	—	9.60	11.00	13.60	14.50

Table 35. Phalange measurements (mm) of Hyaeninae from Pikermi.

	L	DAPpr.	DTpr.	DAPdia.	DTdia.	DAPdist.	DTdist.
Proximal phalange of Mc I AMPG-PA 4999/91 (dext)	18.34	8.00	9.00	5.87	6.88	6.19	8.70
Proximal phalange of Mc I AMPG-PA 5000/91 (sin)	19.74	7.91	9.33	5.50	7.14	6.12	8.60
Proximal phalange of Mc I *A. eximia* AMPG-PA 3138/91 (Roussiakis, 1996)	17.90	10.10	9.70	6.10	7.90	6.40	8.60

Table 36. Tarsal measurements (mm) of Hyaeninae from Pikermi.

	Hmax.	DAPmax.	DTmax.	DTpr.art.	DAPpr.art.
Navicular AMPG-PA 5001/91 (dext)	24.29	15.69	17.52	—	—
Cuboid AMPG-PA 5002/91 (dext)	18.73	23.68	15.34	15.80	12.77

Table 37. Metapodial measurements (mm) of Hyaeninae from Pikermi.

	DAPdia.	DTdia.	DAPdist.	DTdist.
AMPG-PA 5040/91	8.95	12.67	9.40	13.40

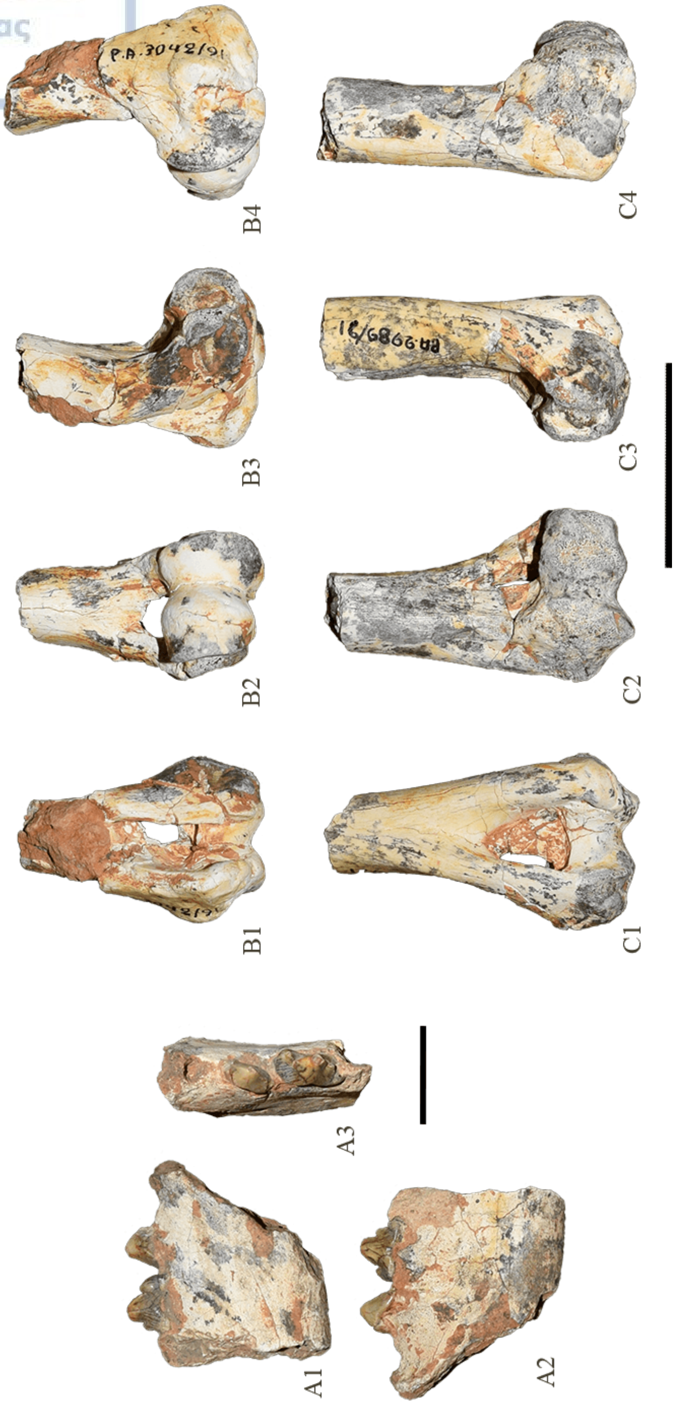

Figure 65. A: left hemimandible with deciduous dentition dp2-dp3 AMPG-PA 4991/91 in lingual (1), buccal (2) and occlusal (3) view. B-C: distal end of humeri AMPG-PA 3042/91 (sin) (B) and AMPG-PA 2989/91 (dext) (C) in posterior (1), anterior (2), medial (3) and lateral (4) view. Left scale bar is 2 cm and corresponds to the hemimandible. The right, larger scale bar is 5 cm and corresponds to the humeri. The smaller, left scale bar is 2 cm and corresponds to the hemimandible.

Figure 66. A: olecranon AMPG-PG 98/29 (dext) in lateral (1), medial (2), anterior (3) and proximal (4) view. B: ulna without olecranon AMPG-PA 4992/91 (dext) in medial (1) and lateral (2) view. C: proximal end of radius AMPG-PA 4994/91 (sin) in posterior (1), anterior (2), lateral (3), medial (4) and proximal (5) view. D: radius without proximal epiphysis AMPG-PA 4995/91 (dext) in anterior (1), posterior (2), lateral (3), medial (4) and distal (5) view. E-F: radius without shaft AMPG-PA 1019/91 (sin) (E) and complete radius AMPG-PA 4993/91 (dext) (F) in posterior (1), anterior (2), medial (3), lateral (4), proximal (5) and distal (6) view. Scale bar is 5 cm.

Figure 67. A: associated carpals and metacarpals Mc I-V AMPG-PA 4996a-l/91 (dext) articulated (1, 2) and isolated (3-21). A3-A6: associated Mc V-Mc II AMPG-PA 4996k-h/91 (dext) in dorsal view. A7-A8: pyramidal AMPG-PA 4996b/91 (dext) in dorsal (7) and proximal (8) view. A9-A12: scapholunate AMPG-PA 4996a/91 (dext) in palmar (9), dorsal (10), proximal (11) and distal (12) view. A13, A17: unciform AMPG-PA 4996f/91 (dext) in proximal (13) and dorsal (17) view. A14, A18: magnum AMPG- PA 4996e/91 (dext) in proximal (14) and dorsal (18) view. A15, A19: trapezoid AMPG-PA 4996d/91 (dext) in proximal (15) and dorsal (19) view. A16, A20: trapezium AMPG-PA 4996c/91 (dext) in proximal (16) and dorsal (20) view. A21: sesamoid bone AMPG-PA 4996l/91. B: associated metacarpals Mc II-V AMPG-PA 4997a-d/91 (dext) articulated (1, 2) and isolated (3-6). C: associated metacarpals Mc II-V AMPG-PA 4998-d/91 (sin) articulated (1, 2) in their original, erroneous restoration (3, 4) along with their “associated” phalanges. D: isolated Mc I proximal phalanges AMPG-PA 4999/91 (dext) (1) and AMPG-PA 5000/91 (sin) (2). E: phalanges found erroneously restored in metacarpals of (B) AMPG-PA 4997-d/91. F: navicular AMPG-PA 5001/91 (dext) in palmar (1) and dorsal (2) view. G: cuboid AMPG-PA 5002/91 (dext) in distal (1), proximal (2), lateral (3) and medial (4) view. H: isolated Hyaeninae metapodial. The smaller scale bar is 2 cm and corresponds to D, F and G. The larger scale bar is 5 cm and corresponds to the rest.

Family Felidae Gray, 1821

The family of Felidae, often referred to simply as "cats" or felids, are a group of obligatory carnivores. The family consists of 41 extant species (Kitchener et al., 2017) and it includes members of various sizes, from the domestic cat *Felis catus* to larger felids like the lynx, the puma, the tiger, the lion and many other less known species. They inhabit continental environments for the most part and exhibit an almost worldwide distribution, except Antarctica, Australia and New Zealand (Koufos, 2022b). The domesticated cat is the sole exception to this, as it generally lives wherever humans do. Cats have been studied for over 200 years in aspects regarding their ecology, functional morphology, behaviour, phylogeny and their interrelationships (Werdelin et al., 2010 and references therein). In addition, the fossil record of the family is quite extensive, displaying some of the most recognizable extinct animals recorded: the sabre-toothed cats (Werdelin et al., 2010).

The family's origins lie in Europe and the first true-felid is attributed to the bobcat-sized *Proailurus lemanensis*, that lived ~27 Ma. Granted the fossil record's scarcity, it has been estimated that the earliest felids could have potentially appeared earlier, between 35 Ma and 28.5 Ma (Werdelin et al., 2010 and references therein). The morphology of *Proailurus* resembles that of a modern felid aside from a few primitive characters (e.g., dentition, auditory bulla, shorter limbs) that are absent in derived felids (Werdelin et al., 2010). The next step in felid evolution was marked by the *Pseudaelurus*-grade complex ~22 Ma, which is considered the ancestor to all subsequent felids. The first migration of felids into North America took place shortly after that, around 19 Ma, with a *Proailurus*-grade species that gave rise to the North America *'Pseudaelurus'* (Werdelin et al., 2010 and references therein). More migrations by more derived species from Eurasia to America have been recorded (Werdelin et al., 2010). Approximately 14-13 Ma the evolution of felids split into two sub-families: the extinct Machairodontinae (sabretooths) of European origin and the extant Felinae (conical toothed cats) of Eurasian origin (Werdelin et al., 2010 and references therein). The sabretooth evolution gave rise to many different lineages from the Miocene to Pleistocene both in the Old and the New World and is relatively well-recorded (Werdelin et al., 2010). The fossil history of Felinae however, is not as well-known as that of the sabretooths (Werdelin et al., 2010). Nevertheless, molecular studies have shown eight lineages amongst extant felids. These derived lineages split from other felids in short intervals in the span of approximately 6.3 Ma during the Late Miocene due to as of yet unknown ecological or functional reasons (Johnson et al., 2006). The first lineage to split was *Panthera* (~10.8), followed by the bay cat lineage (~9.4), *Caracal* lineage (~8.5), ocelot lineage (~8.0), *Lynx* lineage (~7.2), *Puma* and *Acinonyx* lineage (~6.7), and lastly, the leopard lineage from the domestic cat lineage (~6.2) (Johnson et al., 2006).

Felids are represented in the Greek fossil record with 10 valid genera, 13 species and *"Metailurus parvulus"*, whose systematic position is still unclear. (Koufos, 2022b). Their presence has been recorded as early as the 19th century from the localities of Pikermi and Samos (e.g., Gaudry, 1862–1867; Forsyth Major, 1894). Since then, new felid remains have been found and described from various other Greek localities (e.g., Arambourg and Piveteau, 1929; Melentis, 1967; Koufos, 2000; 2006b; 2009; Roussiakis et al., 2006). The oldest felid remains are attributed to *Pseudaelurus* from the Early/Middle Miocene locality of Antonios locality in Chalkidiki (Koufos 2008). The late Miocene and Quaternary are relatively rich with several species described, while the Pliocene record is rather poor (Koufos, 2022b and references therein). The extant felid community in Greece today includes, besides the domesticated cat, *Felis silvestris* and probably *Lynx lynx* (Koufos, 2022b).

Subfamily Machairodontinae Gill, 1872
Genus *Amphimachairodus* Kretzoi, 1929
Amphimachairodus giganteus (Wagner, 1848)
(Fig. 68, Table 38)

1848 *Felis gigantea* in Wagner, Pl. 6, Fig. 10.
1857 *Machaerodus leoninus* in Wagner, p.121, Pl. v, Fig. II; *non Machaerodus leoninus* Roth & Wagner, p. 400, Pl. ix, Figs. 1–4.
1863 *Machairodus cultridens* (Cuv.) in Gaudry, p. 109, Pl. xvi., Figs. 1–6
1924 *Machairodus palanderi* in Zdansky, pp. 108–116, Table XXIV, Figs. 4–9; Table XXV, Figs. 1–2; Table XXVI, Figs. 1–4, Table XXVII, Figs. 1–2.
1924 *Machairodus tingii* in Zdansky, pp. 116–120, Table XXVII, Figs. 3–4; Table XXVIII, Figs. 1–2.
1929 *Machairodus aphanistus* var. *taracliensis* in Riabinin, pp. 100, 127, Pls. vii, viii, ix
1931 *Epimachairodus (?) taracliensis* (Riabinin) in Pilgrim, p. 132
1975 *Machairodus giganteus* in de Beaumont, Fig. 6a.

Type species: *Machairodus palanderi* Zdansky, 1924, Loc. 113, China, Late Miocene.

Type locality: Pikermi, Attica, Greece.

Type material: SNSB-BSPG-AS II 127 (holotype), olecranon described and figured by Wagner (1848, Pl. 10, Fig. 6). Stored in the: Bayrische Staatssamlung für Paläontologie und historische Geologie, Munich, Germany.

Age: MN 10–13; For the classical locality of Pikermi: Middle Turolian, MN 12, 7.33–7.29 Ma (Böhme et al., 2017).

Localities: Greece: Ravin Zouaves 5, Ravin X in Axios Valley; Kryopigi in Chalkidiki; Halmyropotamos, Kerassia 4 in Evia Island; Mytilinii-1 in Samos Island. Spain: Crevillente-2, d Crevillente-16, Venta del Moro, Cerro de la Garita, Los Mansuetos, El Arquillo, Milagros. France: Mont Luberon. Italy: Baccinelo V3. Hungary: Baltavar. Bulgaria: Kalimanchi. Ukraine: Grebeniki, Cherevichnoe, Novoukrainka 1, Belka. Moldavia: Taraklia. Kazakhstan: Kalmakpai. China: several localities. (Salesa et al., 2012 and references therein; Koufos, 2022b).

Material: AMPG-PA 420/91: left ulna with olecranon missing the distal half of its trochlear notch. (Fig. 68).

Description: The specimen preserves the olecranon, the upper half of the trochlear notch and the posterior part of its proximal diaphysis. The olecranon tuberosity is very well developed and protrudes in the medio-lateral direction towards the posterior part of the ulna. The anconeal process extends far anteriorly the olecranon. In medial side, a well-developed crest, which forms near the postero-medial margin of the olecranon, serves as muscle insertion for the triceps. The crest ends abruptly though, as the ulna is damaged more distally. Also, in the same side, the anterior olecranon tuberosity which serves as insertion for the anconeous muscle is well-developed. In lateral side, the insertion of the triceps is situated more anteriorly and higher than the medial side. Additionally, the insertion for the anconeous muscle is situated towards the distal part of the ulna, approximately between the anconeal process and the proximal end of the ulna. A groove marks the superomedial edge of the ulna’s trochlear notch. Lastly, the proximal projection of the distalmost point preserved in trochlear notch would pass through the lateral olecranon tuberosity.

Discussion: The size of this ulna indicates a large individual. Few such carnivorans however are known from Pikermi. Considering its morphology, it was compared with two olecrana of *Amphimachairodus giganteus* from Pikermi that were figured and described by Wagner (1848) and Gaudry (1862) under *Felis gigantea* and *Machairodus cultridens* respectively. As it also happens, the ulnar remains of the former author are regarded as the holotype for the species. The comparison between them only exemplified their remarkable morphological similarities. Regarding their size, based on the scale of a recent photograph (Kargopoulos, pers. commun.) from the holotype that is stored in the SNSB-BSPG in Munich the size of AMPG-PA 420/91 seems to be approximately equal to that of the holotype. Thus, considering the above, the studied ulna can be attributed to *Amphimachairodus giganteus*.

A. giganteus is the largest known carnivore from Pikermi and probably was an apex predator. Remains of this taxon have been found in several Eurasian localities (Sardella et al., 2012 and references therein; Koufos, 2022b and references therein). The systematic position of this taxon has often been debated and multiple hypotheses have been voiced (e.g., de Beaumont, 1975; Morlo & Semenov, 2004; Christiansen, 2013; Geraads & Spassov, 2020). The most recent arguments concern whether it should be kept within the genus *Machairodus*, along with *M. aphanistus*, or transferred to a separate genus, *Amphimachairodus* (Christiansen, 2013; Geraads & Spassov, 2020).

Table 38. Ulna with olecranon measurements (mm) of *Amphimachairodus giganteus* from Pikermi.

	DAPpr.	DTpr.	DAPanc.	OH	DAPt.n
AMPG-PA 420/91 (sin)	45.03	31.03	67.16	51.19	(37.61)

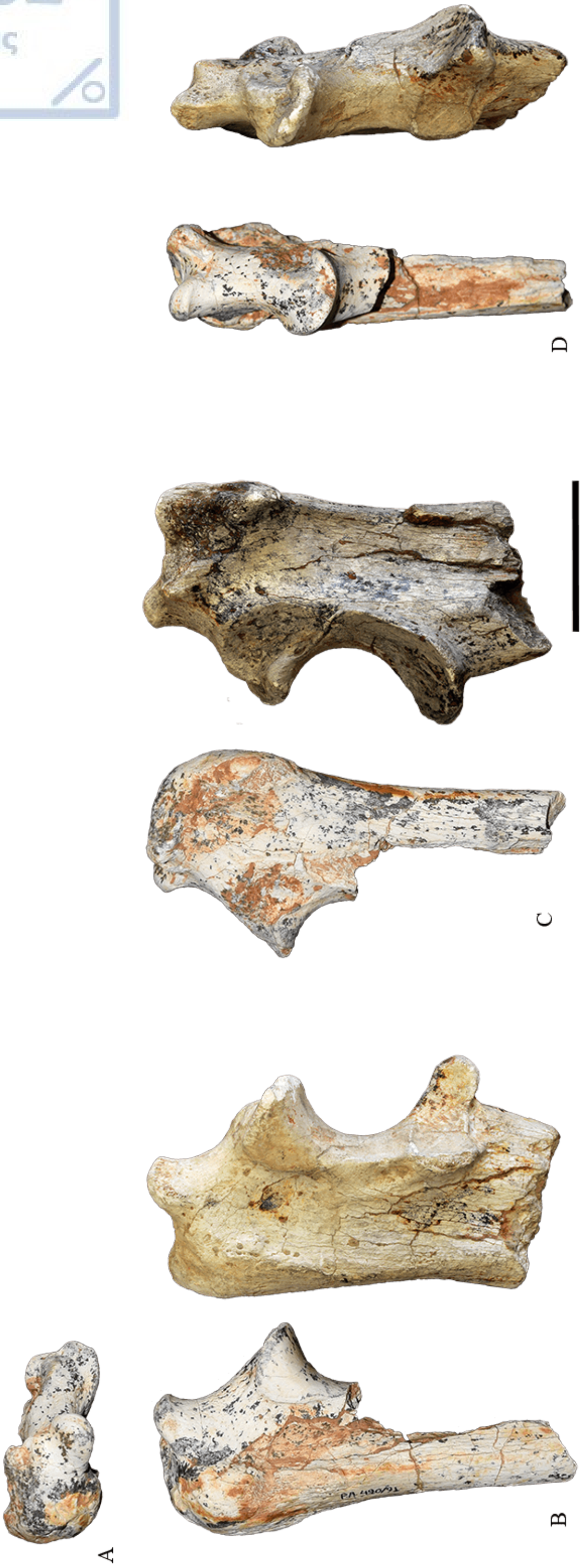

Figure 68. Ulna with olecranon AMPG-PA 420/91 (sin) (left) compared to the holotype of *A. giganteus* SNSB-BSPG-AS II 127 from Pikermi (right) in A: proximal (only AMPG-PA 420/91), B: medial, C: lateral, D: anterior view. The originally right holotype of *A. giganteus* was mirrored to match the left AMPG-PA 420/91. The scale bar is 5 cm. Holotype photograph: Kargopoulos N.

Genus *Pontosmilus* Kretzoi, 1929

Pontosmilus orientalis (Kittl, 1887)

(Figs. 69–73, Tables 39–40)

1887 *Machairodus orientalis* Kittl, p. 329, Pl. 14, Figs. 15, Pl. 15, Fig. 12.
1888 *Machairodus schlosseri* Weithofer, p. 233, Pl. 11, Fig. 17.
1901 *Felis orientalis* Boule, p. 569.
1901 *Felis schlosseri* Boule, p. 569.
1911 *Machairodus hungaricus* Kormos, p. 182, Pl. 17.
1913 *Paramachaerodus orientalis* Pilgrim, p. 291.
1929 *Pontosmilus indicus* Kretzoi, p. 1300.
1929 *Machaerodus sivalensis* Matthew, p. 506.
1930 *Propontosmilus matthewi* Kadic and Kretzoi, p. 48.
1932 *Paramachaerodus indicus* Pilgrim, p. 189, Pl. 8, Fig. 7.
1938 *Paramachaerodus schlosseri* Kretzoi, p. 108.
1938 *Paramachaerodus hungaricus* Kretzoi, p. 108.
1938 *Propontosmilus matthewi* Kretzoi, p. 108.
1938 *Pontosmilus orientalis* Kretzoi, p. 109.
1951 *Paramachaerodus matthewi* Kretzoi, p. 409.
1952 *Paramachaerodus schlosseri hungaricus* Kretzoi, p. 24, Pl. 1, Fig. 1; Pl. 2, Fig. 4.
1952 *Pontosmilus orientalis* Kretzoi, p. 24.
1976 *Megantereon orientalis* Kurtén, p. 192.
1994 *Paramachairodus orientalis* Alcalá, p. 150, Pl. 8, Fig. k–n.

Type species: *Machairodus orientalis* Kittl, 1887.

Type locality: Maragheh, Iran, Late Miocene, MN 11–12 (Kittl, 1887).

Type material: NHMW-2007z0172/0001 (holotype), frontal part of the cranium with the tooth rows described and figured by Kittl (1887: p. 329; Table 14, Figs. 1–5). Stored in the Naturhistorisches Museum in Wien, Austria.

Age: 7.33–7.29 Ma for the classical locality of Pikermi (Böhme et al., 2017). MN 11–13 for other localities (Salesa et al., 2012).

Localities: Greece: Pikermi in Attica (Weithofer, 1888); ?Nea Silata in Chalkidiki (Koufos, 2006b). Spain: Puente Minero, Concud, Crevillente-15, Crevillente-16, Las Casiones (Salesa et al., 2012). Germany: Dorn-Dürkheim 1 (Morlo, 1997). Hungary: Csákvár and Polgardi (Kormos, 1911; Kadic & Kretzoi, 1927). Bulgaria: Gorna Sushitsa (Spassov et al., 2019). North Macedonia: Veles (Schlosser, 1921). Turkey: Çobanpinar and Gulpinar (Koufos et al., 2018b).

Material: AMPG-PA 4959/91: left maxillary fragment with the alveoli of I3-C and P3-P4 dentition, AMPG-PA 4953/91: left hemimandible with i2(root)-i3-c-p2(root)-p3(root)-p4(alveolus)-m1. (Figs. 72–73).

Description: The maxillary fragment AMPG-PA 4959/91 preserves the elliptical infraorbital foramen which opens above the distal end of P3. In occlusal view, a small groove between the metastyle blade and the alveolus of M1 is formed.

I3: Only part of its alveolus is preserved. Based on its size it indicates a relatively large and robust incisor. A small diastema of approximately 5 mm forms between the alveolus of I3 and the alveolus of the canine.

C: Only the alveolus is preserved. Its cross section indicates a relatively large and laterally flattened canine. A small diastema of approximately 7 mm forms between the canine's alveolus and P3.

P3: It is relatively flattened transversally. A low vestigial mesial cusp is situated mesiolingually, atop a cingulum projection. The main cusp is conical and high. The small distal cusp is situated atop a cingulum projection. The tooth expands lingually at the main's cusp distal half. A crest runs through the top of the cusps. The cingulum is generally weak, with the exception of the mesial and distal Part of the tooth.

P4: The upper carnassial is elongated. The slightly broken protocone appears to have been relatively low and in close proximity to the P4. It is situated lingually of the parastyle, without projecting mesially. A blunt crest traces from the protocone to the top of the paracone's cusp. An ectostyle at the mesial margin of P4 is not developed. The paracone and parastyle are conical. The paracone is situated higher than the other cusps. The metastyle blade is broken, but its length would have probably been close to the paracone's. A crest traces from the mesial side of the parastyle to the distal part of the paracone. The cingulum is strong on the buccal side and weak in the lingual side.

M1: Only a small and slightly buccolingually elongated alveolus is present. It forms a slightly larger than 90^{o} angle with the carnassial.

Mandible: The mandible AMPG-PA 4953/91 has a relatively low but robust mandibular corpus. The dorsal corpus is concave, while the ventral margin is almost horizontal. On the buccal side of the hemimandible, just distally of the canine, a mental crest develops. The ascending ramus is not preserved; however, it can be discerned that the ramus starts ascending near the carnassial's distal margin. The mesially preserved masseteric fossa is relatively deep. The mandibular symphysis is almost vertical. Two mental foramina are observed in close proximity to each other on the buccal side of the hemimandible. The first is situated below the vestigial p2 and the second below the mesial half of the p3. A diastema develops between c-p2 and a smaller p2-p3.

i2: Only the elliptical-shaped root of a small, single-rooted tooth remains.

i3: Caniform in shape and larger than i2. The crest traces almost bucco-lingually. The cingulum projects in its distal part and creates a small shelf.

c: The tip of the crown and its base are damaged. The canine is slightly compressed buccolingually and its lingual side is flattened. Its cross-section is elliptical. No crenulations were observed, maybe because of the damaged base the crown.

p2: A small, almost round single-root of a vestigial p2 is observed. It forms a diastema of approximately 10mm with the canine and a smaller one of approximately 3 mm with p3.

p3: Only the roots remain. The mesial half is slenderer, while the distal half is wider and more robust. The diastema between the canine and p2 is approximately 15 mm.

p4: Only the filled with matrix alveolus remains. The morphology appears similar with p3, albeit slightly larger.

m1: The lower carnassial is elongated. The paraconid and the protoconid are of approximately equal length. The latter is situated higher and is less robust than the former. The two cuspids are separated by a valley in the lingual side. The talonid is rudimentary and lacks any observable cuspids. A slightly serrated crest traces from the tip of the paraconid, through the protoconid and ends up in the vestigial talonid.

Discussion: This taxon was initially erected by Kittl (1887) based on some craniodental remains from Maragheh in Iran under *Machairodus orientalis*. Weithofer (1888) described some mandibular and postcranial elements from Pikermi which he assigned to *Machairodus schlosseri*. Pilgrim (1913) transferred Weithofer's taxon to *Paramachaerodus*, without, however, assigning a type species for the genus. Matthew (1929) was the first to synonymize the two taxa from Pikermi and Maragheh, a notion which was later also followed by Pilgrim (1931), as he identified both *Machairodus schlosseri* from Pikermi and *Machairodus orientalis* from Maragheh as genosyntypes – with the latter as genolectotype – as well as most recent authors (e.g., Salesa et al., 2010; 2012; Koufos, 2011; Li & Spassov, 2017). Just recently, the systematic status of some metailurine felids was reviewed once more by Jiangzuo et al. (2022). Amongst other changes, they transferred the craniodental material of *Pa. orientalis* from Maragheh to *Pontosmilus*, under *Pontosmilus orientalis* and the craniodental remains of "*Metailurus major"* from Europe under the resurrected *Paramachaerodus schlosseri* (Weithofer, 1888). Although their work is certainly interesting, it also begs some questions, and despite their answers lying beyond the scope of this study, they deserve a more in-depth exploration in the future.

Through their work, Jiangzuo et al. (2022) seem to imply that there is only one large metailurine felid in Pikermi and that there is little reason for the cranial remains of *Paramachaerodus schlossseri* (=*Metailurus major*) from Greece (Melentis, 1967; Roussiakis, 2001b) and the mandibular remains of *Pontosmilus orientalis* (=*Paramachaerodus orientalis*) from Pikermi (Weithofer, 1888) to remain separate. Albeit simplistic this could be true, if not for the presence of at least two distinct metailurine felids in Pikermi: (1) *Pontosmilus orientalis* (=*Paramachaerodus orientalis*) and (2) *Paramachaerodus schlosseri* (=*Metailurus major*). The second point, which was not entirely clarified in their work, concerns whether the rest of *Pontosmilus orientalis* (=*Paramachaerodus orientalis*) remains recorded in other Eurasian localities such as Turkey (Koufos et al., 2018b), Spain (Salesa et al., 2010; 2012) and Bulgaria (Spassov et al., 2019) are similarly attributed to *Pontosmilus orientalis*. Nevertheless, for the purposes of this study, the recent taxonomic allocation proposed by Jiangzuo et al. (2022) shall be followed, treating *Paramachaerodus orientalis* and *Metailurus major* from Europe as *Pontosmilus orientalis* and *Paramachaerodus schlosseri* respectively.

The morphology of the available material shows machairodont adaptations. Two such felids have been recognized from Pikermi that could potentially meet the criteria of the material's size and morphology: *Pontosmilus orientalis* and *Paramachaerodus schlosseri*. Between them, the former is considered to have evolved more "machairodont" adaptations than the latter, indicating a closer morphological affinity with the material in study.

The reviewed systematics of the genus *Paramachaerodus*, *Pontosmilus orientalis* included, by Salesa et al. (2010) fit for the most part with the morphology of the described specimens from Pikermi and other localities by other authors. Despite their similarities a few differences were observed, such as the absence of crenulations in the lower canine. Though, as already noted in the description, their absence may be due to the canine's poor preservation status. Additionally, the presence of a vestigial p2 that was noted in the mandible seems to be generally absent in *Po. orientalis*. Regarding the upper dentition, the usually present ectostyle (Salesa et al., 2010) is absent from the upper carnassial and P3 exhibits a small mesial cusp which, according to Jiangzuo et al. (2022) is absent. Lastly, although only the filled with matrix alveolus of AMPG-PA 4959/91's M1 remains, its shape indicates a relative bucco-lingual elongation instead of the typically (Salesa et al., 2010) rounded size. Furthermore, the metrical comparisons of AMPG-PA 4959/91's upper dentition with *Po. orientalis* specimens (Fig. 69) did not reveal any significant size differences aside from the slightly larger P3 of the former. Mandibular comparisons showed similar sizes with the specimens from Gulpinar, Turkey (Koufos et al., 2018b) and Gorna Sushitsa, Bulgaria (Spassov et al., 2019). The lower canine and m1 range on the lower spectrum (Fig. 70-71) of *Po. orientalis* specimens, with the m1's dimensions being almost identical with the material from Turkey (Fig. 71).

Paramachaerodus schlosseri is a more widely known metailurine felid in Eurasia (e.g., Roussiakis, 2001b; Jiangzuo et al., 2022). Considering the characters of the genus and the species (Roussiakis, 2001b; Jiangzuo et al., 2022), the upper dentition of AMPG-PA 4959/91 and *Pa. schlosseri* differ quite a bit in their morphology (Fig. 74). Moreover, direct comparison of AMPG-PA 4959/91 with *Pa. schlosseri* specimens AMPG-PA 1257/91 and AMPG-PG 95/1532 from Pikermi that were described by Roussiakis (2001b) further exemplified these differences. AMPG-PA 4959/91 has a more powerful lateral flattening in its canine in relation to *Pa. schlosseri* specimens (Table 1). The carnassial morphology of AMPG-PA 4959/91 also differs from *Pa. schlosseri*, with the former having a more reduced protocone that is situated closer to P4 as opposed to the well-developed and more lingually extending protocone of the latter. In addition, the former's buccal border is less undulated than in *Pa. schlossseri*. Although M1 is preserved only by its matrix-filled alveolus in AMPG-PA 4959/91, it nonetheless indicates a smaller tooth, whereas the M1 of *Pa. schlossseri* is clearly larger and more elongated lingo-buccally. The size of P3 and P4 of AMPG-PA 4959/91 is also smaller than *Pa. schlosseri* material (Fig. 69). In terms of the maximum width of P3, in *Pa. schlosseri* it lies near the distal cusp, while in AMPG-PA 4953/91 it is situated approximately in the middle of the tooth. The mandibular and lower dental comparison is more difficult, due to the fragmentary nature of AMPG-PA 4953/91. The characters which probably serve to effectively distinguish AMPG-PA 4953/91 from *Pa. schlosseri* is the presence of a mental crest (mandibular flange). Such a trait is common in "machairodonts", whilst it is absent in *Pa. schlossseri* whose mandibular morphology is closer to that of Felinae (Roussiakis, 2001b). Also, the lower carnassial of AMPG-PA 4953/91 is slightly serrated along its crest, which also seems to match the diagnostics of *Pontosmilus* provided by Jiangzuo et al. (2022). The lower carnassial's morphology is also similar to that of *M. major* from Baode, although smaller in size (Fig. 71). Their difference in size is not very important though since the holotype of *Po. orientalis* is similar in size with *M. major* from Baode (Fig. 71).

Besides *Po. orientalis*, other species of *Paramachaerodus* and *Pontosmilus* have been recognized, which will shall also be compared against AMPG-PA 4953/91 and AMPG-PA 4959/91 below:

Pontosmilus maximiliani (Zdansky, 1924) known from MN 12 of China and MN 13 of Spain. It is larger than *Po. orientalis* and despite some common traits which they share (e.g., small protocone and serrated cheek teeth) they have some fundamental differences. *Po. maximiliani* differs from both AMPG-PA 4959/91 and *Po. orientalis* from its aligning P3 and P4 in occlusal view and the greater diastema formed between C-P3. Its lower dentition differs from AMPG-PA 4953/91 and *Po. orientalis* in the lower carnassial. Its talonid is absent, whereas in AMPG-PA 4953/91 and *Po. orientalis* is greatly reduced but still present.

Paramachaerodus ogygia (Kaup, 1832) – or *Promegantereon ogygia* according to Li & Spassov (2017) – from MN 9 of Germany and MN 10–11 in Spain (Salesa et al., 2010). It is considered the most primitive taxon of the *Paramachaerodus* lineage (Salesa et al., 2010; Li & Spassov, 2017). It is distinguished from *Po. orientalis* by the absence of crenulations in the canines, the less laterally compressed upper canines, the more elongated P3 that expands disto-lingually. The upper carnassial lacks an ectostyle and the protocone is not as reduced and its oriented more mesially. Occlusally, P3-P4 align and M1 is larger. In the lower dentition p2 is present and the crown of p4 does not expand mesio-buccally. The talonid of the lower carnassial is not as reduced. The mandibular symphysis is less derived, not as high and lacks a mandibular flange (Salesa et al., 2010). While for the most part both AMPG-PA 4959/91 and AMPG-PA 4953/91 differ from *Pr. ogygia* and align with the characters of *Po. orientalis*, a couple of characters are shared with the former. In the upper dentition, AMPG-PA 4959/91 is similarly marked by the absence of ectostyle. The lower dentition of AMPG-PA4953/91 is also marked by the presence of p2. Although, unlike *Pr. ogygia*, it appears vestigial.

The recently erected *Paramachaerodus transasiaticus* Li & Spassov, 2017 from MN 11 localities of Bulgaria and China. It was considered by its authors as the intermediate evolutionary stage between *Pr. ogygia* and *Po. orientalis*. According to Li & Spassov (2017), it differs from *Po. orientalis* by its weaker crenulations and the disto-lingual expansion of the P3. The upper carnassial has a less developed ectostyle in its P4, its buccal border is sinusoidal instead of straight and the protocone is reduced. M1 is also longer and two-rooted., The lower dentition has a shorter c-pm3 diastema and the lower carnassial has a more developed and elongated talonid with a metaconid. (Li & Spassov, 2017). Further comparison with the material in study showed a few common traits. AMPG-PA 4959/91 similarly lacks an ectostyle in its P4. Interestingly, AMPG-PA 4959/91's P4 buccal border appears to be morphologically in-between that of *Pa. transasiaticus* and the holotype of *Po. orientalis* (NHMW-2007z0172/0001). Based on the figures of Li & Spassov (2017) the protocone appears rather similar both to other *Po. orientalis* and AMPG-PA 4959/91. Unfortunately, the number of roots in M1 of AMPG-PA 4959/91cannot be ascertained, but, based on the small size of its alveolus it would much likely be single rooted, similar to *Po. orientalis*. Concerning the lower dentition, both AMPG-PA 4953/91 and *Pa. transasiatius* exhibit a p2, however, unlike *Pa. transasiatius*, the p2 of AMPG-PA 4953/91 is vestigial.

Concluding, both AMPG-PA 4953/91 and AMPG-PA 4959/91 exhibit the morphological traits to justify their attribution to *Po. orientalis*. Also, the size differences don't indicate any significant variance and are within the expected intraspecific variation levels for that species. Nonetheless, the presence of some probably more primitive characters in the studied specimens are acknowledged, namely the absence of an ectostyle in P4 and the presence of a vestigial p2, which is not typical for *Po. orientalis*. Whether that represents an as of yet unknown intraspecific variation or just individual variation is yet to be uncovered, as the available *Po. orientalis* material is still limited.

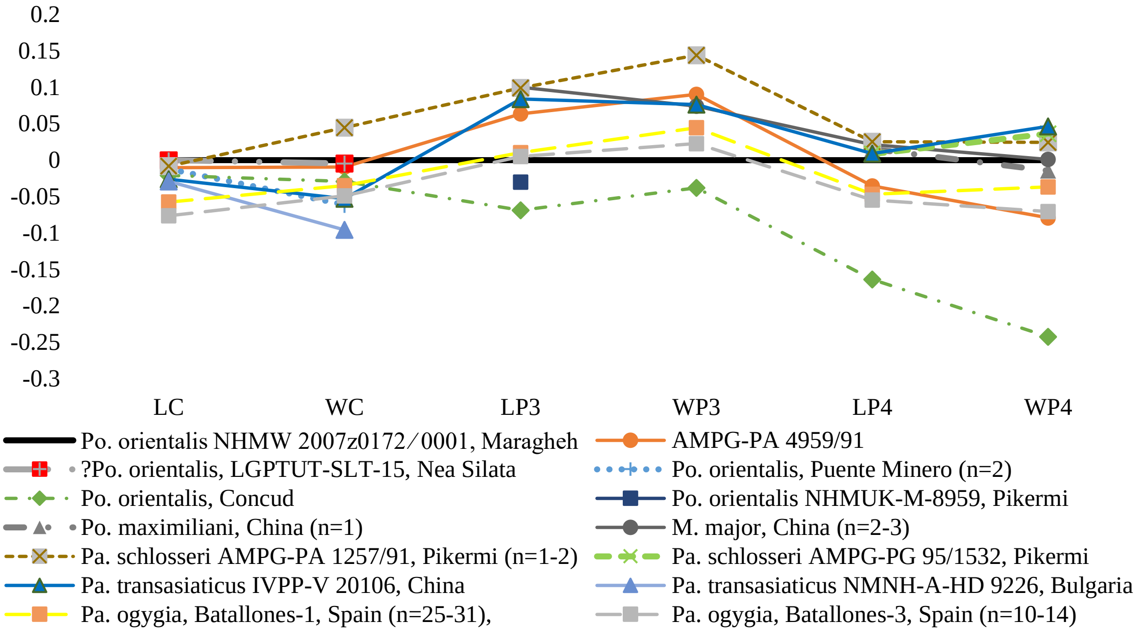

Figure 69. Log-ratio diagram for the upper dentition of *Po. orientalis*. The dental values of the holotype were used as standard. Data were acquired from Kittl (1887), Zdansky (1924), Koufos (2006b), Pilgrim (1931), Salesa et al. (2010; 2012), Siliceo et al. (2014) and Li & Spassov (2017).

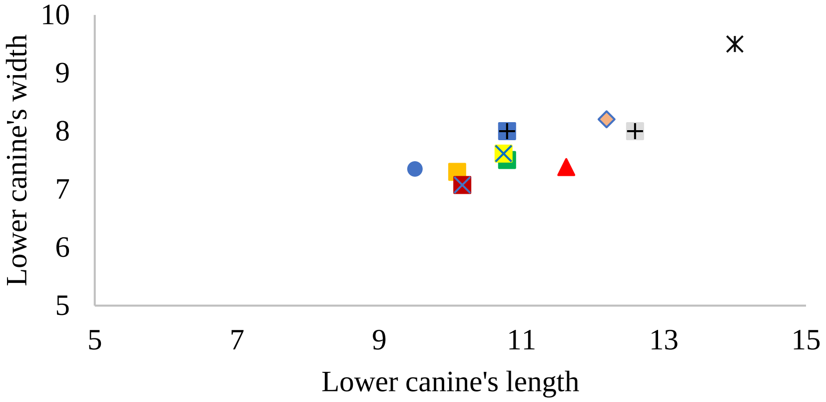

Figure 70. Bivariate plot for the lower canine of *Po. orientalis*. ●: *Po. orientalis* AMPG-PA 4953/91 from Pikermi. ▲: *Po. orientalis* C-26 from Spain. ✳ : *Po. orientalis* M-8959 from Pikermi. ⊞: *Pa. transasiaticus*, China. ⊞: *Pa. transasiaticus*, Bulgaria. ■ : *Po. orientalis* PV-2702 Çobanpinar, Turkey. ■ : *Po. orientalis* PV-730 Gulpinar, Turkey. ◇: *Po. orientalis* GS2-3157 Bulgaria. ☒: *Pa. ogyria* (n=32), Batallones-, Spain. ⊠: *Pa. ogyria* (n=4), Batallones-3, Spain. Data for the specimens from Spain and M-8959 from Pikermi were acquired from Salesa et al. (2010). Data for the specimens from Turkey were acquired from Koufos et al. (2018b). Data for the specimens from China and Bulgaria were acquired from Spassov et al. (2019) Data for *Pa. ogygia* were acquired from Siliceo et al. (2014).

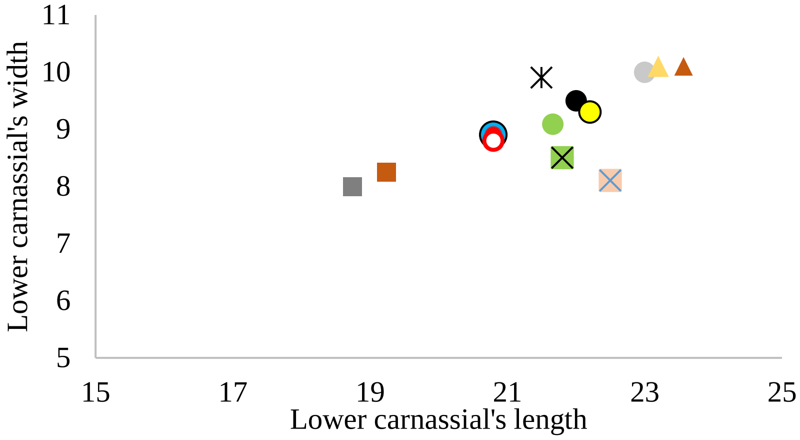

Figure 71. Bivariate plot for the lower carnassial of *Po. orientalis*. ●: *Po. orientalis* AMPG-PA 4953/91 from Pikermi. ●: *Po. orientalis* from Spain. ●: *Po. orientalis* NHMUK-M. 8959 from Pikermi. ●: *Po. orientalis* NHMUK-M. 3829 from Maragheh. ●: *Po. orientalis* GS2-3157 from Bulgaria. ▲: *M. major* from Baode. ▲: *Pa. schlosseri* from Spain. ☒: *Pa. transasiaticus* from China. ☒ : *Pa. transasiaticus* from Bulgaria. ×: *Po. maximiliani* PMU-M7260 from Spain. ○: *Po. orientalis* PV-730 from Gulpinar, Turkey. ●: *Po. orientalis* PV-2691 from Çobanpinar, Turkey. ■: *Pa. ogygia* (n=23) Batallones-1, Spain. ■: *Pa. ogygia* (n=11), Batallones-3, Spain. Data for the specimens from Spain were acquired from Salesa et al (2010; 2012). Data for the specimens from China were acquired from Zdansky (1924) and Spassov et al. (2019). Data for the specimens from Turkey were acquired from Koufos et al. (2018b). Data for *Pa. ogygia* were acquired from Siliceo et al. (2014).

Table 39. Upper dentition measurements (mm) of *Po. orientalis* and *Pa. schlosseri*.

	Po. orientalis								*Pa. schlosseri*		
	AMPG-PA 4959/91	NHMW-2007z0172 ⁄ 0001	NHMUK-M. 3828	CPT-PM-575	CPT-PM-576	MNCN-CSIC-C-25	MNCN-CSIC-CRA C-1	MNCN-CSIC-CRA C-2	AMPG-PA 1257/91 [1]		AMPG-PG 95/1532 [1]
		(Salesa et al. 2010)	(Pilgrim, 1931)	(Salesa et al. 2010)					(Roussiakis, 2001b)		
	Pikermi	Maragheh		Puento Minero			Concud		Pikermi		
	sin								dext	sin	
LC	(16.61)	17.00	—	16.71	16.35	16.2	—	—	16.68	—	(18.11)
WC	(9.39)	9.60	—	8.06	8.62	8.98	—	—	10.64	—	(11.00)
LP3	17.36	15.00	—	—	—	—	12.80	—	18.57	19.12	[19.69]
WP3	8.68	7.05	—	—	—	—	6.46	—	9.73	9.92	[7.00]
LP4	(25.82)	28.00	28.50	—	—	—	—	19.20	29.68	—	28.55
WaP4	11.46	13.75	14.00	—	—	—	—	7.87	14.54	—	14.95
WblP4	8.24	—	—	—	—	—	—	—	9.67	—	8.29
LpP4	9.96	—	—	—	—	—	—	—	10.57	—	10.44
LmtP4	9.34	—	—	—	—	—	—	—	11.4	—	11.04
HP4	13.85	—	—	—	—	—	—	—		—	
LM1	[3.60]	—	—	—	—	—	—	—	5.60	5.60	(4.74)
WM1	[6.52]	—	—	—	—	—	—	—	12.35	12.26	(12.29)
R.I. C	(56.53)	56.47	—	48.23	52.72	55.43	—	—	63.79	—	(60.74)
R.I. P3	50.00	47.00	—	—	—	—	50.46	—	52.40	51.88	—
R.I. P4	48.00	49.10	49.12	—	—	—	—	40.99	48.99	—	52.36
(LP3/LP4) ×100	67.23	53.57	—	—	—	—	—	—	62.58	—	—

[1]: Measurements taken by the author.

Table 40. Mandibular and lower dentition measurements (mm) of *Po. orientalis* from Pikermi.

	AMPG-PA 4953/91	NHMUK-M. 8959[1]	NHMUK-M. 3829[1]	MNCN-CSIC-C-26[1]	Mean values n=1-2	Isolated teeth	EUNHM- PV-730	NMNHS-GS2-3157
		(Salesa et al., 2010)			(Salesa et al., 2012)	(Koufos et al., 2018b)		(Spassov et al., 2019)
	Pikermi		Maragheh	Concud	Las Casiones	Çobanpinar	Gulpinar	Gorna Sushitsa
Li3	4.6	—	—	—	—	—	—	—
Wi3	4.15	—	—	—	—	—	—	—
Lc	9.73	14	—	11.63	—	10.1	10.8	12.2
Wc	7.14	9.5	—	7.38	—	7.3	7.5	8.2
Lp1	[2.25]	—	—	—	—	—	—	—
Wp1	[1.79]	—	—	—	—	—	—	—
Lp3	[14.11]	—	—	—	14.39	12.1	11.7	13.8
Wp3	[5.93]	—	—	—	7.1	5.8	5.7	6.2
Lp4	[16.54]	19	—	—	19.45	17.0	18.3	
Wp4	[6.48]	—	—	—	8.3	7.4	7.9	
Lm1	20.8	22	23		21.66	20.8	20.8	22.2
Wm1	8.9	9.5	10	—	9.09	8.9	8.8	9.3
Ltm1	19.12	—	—	—	—	—	—	—
Ltalm1	1.68	—	—	—	—	—	—	—
Hm1	13.82	—	—	—	11.03	—	—	12.9
R.I. c	43.68	67.86	—	63.46	—	72.28	69.44	67.21
R.I. m1	42.79	43.18	43.48	—	41.97	42.79	42.31	41.89
Hdia	25.57	—	—	—	—	—	27.7	—
Symphysis length	28.72	—	—	—	—	—	—	28.6
Hbehm1	28.23	—	—	—	—	—	24.0	—
L(c–m1)	76.37	—	—	—	—	—	74.9	—

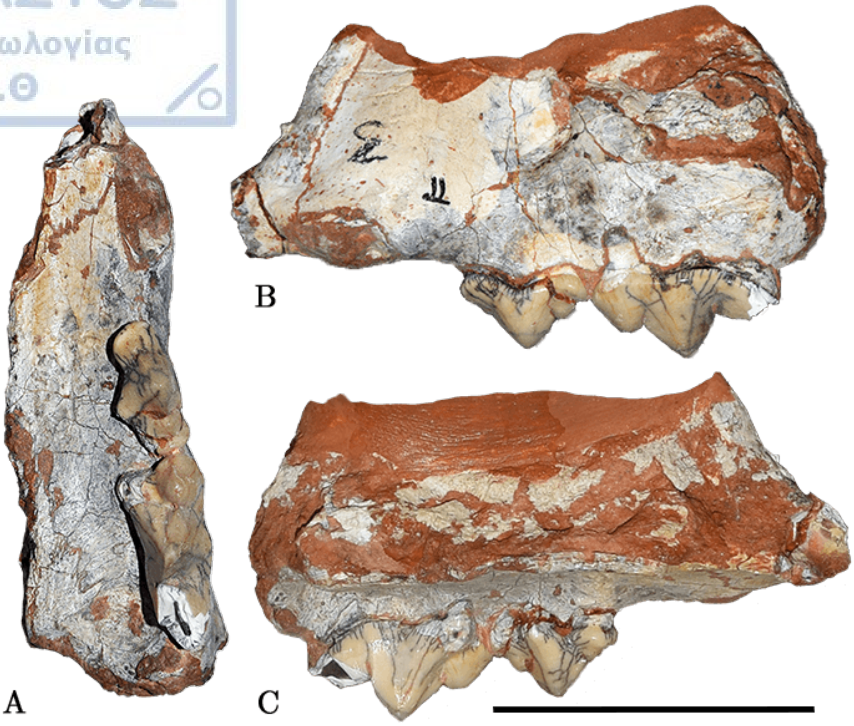

Figure 72. Left maxillary fragment of *Pontosmilus orientalis* AMPG-PA 4959/91 in A: occlusal, B: lateral and C: medial view. Scale bar is 5 cm.

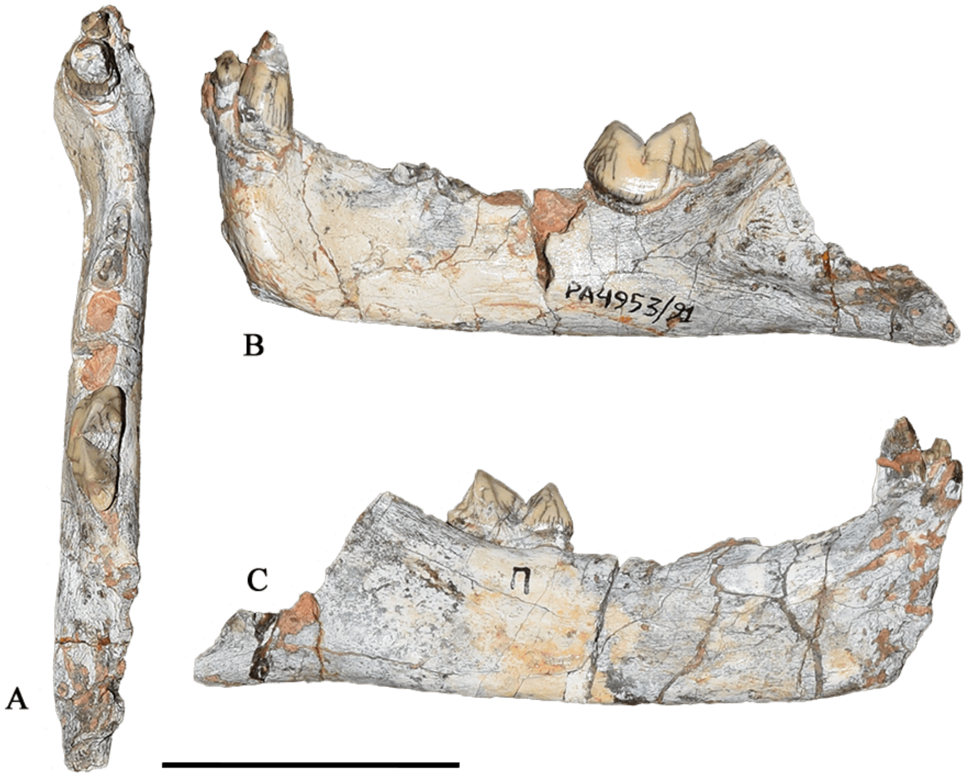

Figure 73. Left hemimandible of *Pontosmilus orientalis* AMPG-PA 4953/91 in A: occlusal, B: lateral and C: medial view. Scale bar is 5 cm.

Pa. transasiaticus, China (Jiangzuo et al., 2022) *M. major*, Baode (Jiangzuo et al., 2022)

Pa. schlosseri, China (Jiangzuo et al., 2022) *Pa. schlosseri*, Pikermi (Roussiakis, 2001b)

AMPG-PA 4959/91 *Pa. schlosseri* PG 95/1532 (Roussiakis, 2001b)

Figure 74. Upper dental comparison (P3-M1) of *Pa. schlosseri* with the studied AMPG-PA 4959/91 *Po. orientalis* specimen. Source is listed above each specimen. Scale is 3 cm.

Felidae indet.

(Fig. 75, Tables 41–43)

The material attributed to this section exhibits Felidae characteristics. Unfortunately, the scarcity of felid remains in the fossiliferous record limits the available comparative material which in turn limits more specific attributions of these specimens. Aside from some exceptions (e.g., Roussiakis et al., 2006) the postcranial skeleton of some of these animals (e.g., *Po. orientalis*) are for the most part still unknown.

Material: AMPG-PA 5003/91: proximal end of left ulna with the olecranon, AMPG-PA 5004/91: left magnum, AMPG-PA 5005/91: left Mc I, AMPG-PA 5006/91: left Mc II, AMPG-ΠΚ 1/395: left Mc III, AMPG-PA 5007/91: left Mc V. (Fig. 75).

Olecranon: The olecranon process has a proximally straight border and its inclination towards the posterior is very slight. As a result, the olecranon process is almost square-shaped in side view. The coronoid process projects slightly more anteriorly than the anconeal process. The well-developed olecranon process's posteromedial crest marks the insertion of a probably equally well-developed head of the triceps. The crest extends distally, almost reaching the trochlear notch's proximal margin. The lateral olecranon tuberosity is slightly thicker and located slightly more posteriorly than the thinner but slightly higher medial olecranon tuberosity. The former tuberosity serves as insertion for the anconeous muscle, while the latter serves as insertion for the medial head of the triceps. The laterally directed radial notch has a smooth and rounded border. If the proximo-distal ridge of the trochlear notch were to be extended proximally, the line would pass through the lateral tuberosity of the olecranon.

Discussion: The sheer size of the ulna alone is enough to exclude most known felids from Pikermi, as it is too small to consider for taxa like *Po. orientalis* or *Pa. schlosseri* and even for *"M. parvulus"*. Contrasting the size difference, its morphology exhibits similarities with the ulna of "*M. parvulus"* from Kerassia 1 in Euboea Island described by Roussiakis et al. (2006). Despite their similarities however, a couple morphological differences were observed. The coronoid process of AMPG-PA 5003/91 projects slightly more anteriorly than the anconeal process, whereas in "*M. parvulus"* from Kerassia they are approximately at the same level. Also, the lateral olecranon tuberosity of AMPG-PA 5003/91 is located slightly more posteriorly than the medial one, whereas in "*M. parvulus"* from Kerassia the opposite is observed. In any case, it should be noted that since there were no other available ulnas from *"M. parvulus"*, its intraspecific variation is practically unknown. Also, as with "*M. parvulus"* from Kerassia, the superomedial edge of the trochlear notch lacks a groove, which according to Werdelin & Lewis (2001) is present in machairodonts with the exception of *Homotherium* Fabrini, 1890. Perhaps its absence in "*M. parvulus"* and AMPG-PA 5003/91 is due to their lesser degree of machairodont adaptations compared to other machairodontines (e.g., *Paramachaerodus*, *Amphimachairodus*, etc.). On the other hand, the olecranon's resemblance to those of extant Felinae make a possible attribution to *Pristifelis attica* more than likely, as both its size – albeit slightly smaller, but more or less within the expected range of intraspecific variation – and morphology fit well with the *Pr. attica* material described from Pikermi by Roussiakis (2002) and from Spain by Salesa et al. (2012) (Table 41, Fig. 75; A1-A3).

Magnum: The articular surface to the trapezoid is narrow and located proximo-dorsally to the concave articular surface for the Mc II. Distally, the sub-triangular concave facet probably serves as articulation for Mc III and IV. The well-developed palmar tubercle is oblique. Proximally it articulates with the scapholunate through a laterally compressed convex surface.

Discussion: The magnum exhibits Felidae characteristics and based on its size probably belonged to a medium to small sized individual. The size and morphology are close to the magnum described by Roussiakis et al. (2006) for *"M. parvulus"* from Kerassia. Based on that and on the absence of similarly sized Felidae from Pikermi it can potentially be attributed to that taxon.

Mc I: It is short, robust and transversally elongated. The proximal articular surface that articulates with the trapezium slopes laterally and is elliptical-shaped in proximal view. Also, the proximal articular surface takes up approximately 2/3 of the proximal ends width and extends towards the dorsal side of the shaft. The projecting tuberosity of the proximo-medial side, which serves as attachment for the extensor ossis metacarpi pollicis tendon, is situated at a slightly lower level than the surface that articulates with the trapezium. The distal articular surface is oblique, sloping towards the lateral side and in its middle a groove is formed.

Discussion: The metacarpal's size indicates a medium to small sized individual. Further comparison with *"M. parvulus"* from Kerassia 1 indicates similar morphology and size. Based on that and in the absence of other similarly sized felids from Pikermi, it could potentially be attributed to that taxon.

Mc II: The proximal articular surface is medio-laterally concave and elongated in the dorso-plantar axis. The articular surface for the trapezium is elliptical-shaped. The radial artery groove on the proximo-dorsal surface of the shaft is well-developed. The shaft turns oblique towards the medial side just distal of the proximal epiphysis but then straightens down. The shaft's cross-section is sub-triangular to elliptical. The distal epiphysis is rounded.

Discussion: The well-marked radial artery groove in Mc II indicates a machairodont rather than a Felinae (Werdelin & Lewis, 2001; Roussiakis et al., 2006), with the only exception being the *Homotherium* from Senèze (Ballesio, 1963). A similar groove is also present in *"M. parvulus"* from Kerassia 1 (Roussiakis et al., 2006) and in *Po. orientalis* from Pikermi figured by Weithofer (1888). Further comparison with *"M. parvulus"* from Kerassia 1 showed morphological similarities but the length of AMPG-PA 5006/91 is greater. Although their proximal articular surfaces are similar, that of AMPG-PA 5006/91 appears to be slightly more compressed transversally. As the morphology and size of larger felids such as *Po. orientalis* and *Pa. schlosseri* are not known, further comparison that would perhaps allow a more definite attribution is currently impossible. Just based on their size difference, the allocation to either *Po. orientalis* or *Pa. schlosseri*, would seem more probable.

Mc III: Only its proximal epiphysis is preserved. It is medio-laterally concave. Its sub-triangular and dorso-palmarly elongated proximal articular surface would probably articulate with the magnum.

Discussion: Its morphology is felid-like and it greatly resembles both in morphology and dimensions the Mc III of *"M. parvulus"* from Kerassia 1 (Roussiakis et al., 2006). Granted that the Mc III of *Po. orientalis*, and by extension that of *Pa. schlosseri*, are slightly larger (Weithofer, 1888) while that of *P. attica* is generally smaller, it could potentially belong to *"M. parvulus"*.

Mc V: The proximal articular surface articulates with the unciform. It is smooth, strongly convex in the dorso-plantar direction and slightly slopes medially. It articulates with Mc IV through a medially projecting facet just distal of the proximal epiphysis. The lateral tuberosity for the attachment of the extensor ulnaris muscle does not extend laterally of the proximal epiphysis. The shaft is relatively straight, exhibiting only a very minor curvature medially and its sub-triangular in cross-section. The distal epiphysis is rounded.

Discussion: Comparison with *"M. parvulus"* from Kerassia 1 exemplified their morphological similarities but also a couple of differences. Unlike *"M. parvulus"* from Kerassia 1, AMPG-PA 5007/91 is slightly longer and its shaft's dorso-plantar length is greater than its medio-lateral. Also, AMPG-PA 5007/91 has a broader proximal articular surface. The Mc V of a *Po. orientalis* figured by Weithofer (1888) is slightly longer (55mm) than that of AMPG-PA 5007/91. Their morphology however is as similar as with *"M. parvulus"*. Since the intraspecific variation of those two species remain currently unknown, the studied Mc V could just as well belong to a smaller *Po. orientalis* or a larger *"M. parvulus"*.

Table 41. Olecranon measurements (mm) of Felidae from Pikermi.

	DAPpr.	DTpr.	DAPanc.	DAPr.n	DTr.n	OH	Ht.n
AMPG-PA 5003/91 (sin)	11.72	6.55	12.95	14.04	9.95	14.06	11.50
AMPG-PA 2804/91 (sin), Pikermi (Roussiakis, 1996) [1]	13.51	7.82	15.80	—	—	17.28	—
FCPT-KS-3279 (sin), Las Casiones (Salesa et al., 2012)	—	8.41	—	—	11.40	18.04	12.50

[1]: measuremens after the author.

Table 42. Magnum measurements (mm) of Felidae from Pikermi.

	Hmax.	DAPmax.	DTmax.
AMPG-PA 5004/91 (sin)	10.32	14.89	10.36
“M. parvulus” AMPG-K1/258/6 (sin), Kerassia 1 (Roussiakis et al., 2006)	10.40	14.00	9.00

Table 43. Metacarpal measurements (mm) of Felidae from Pikermi.

	L	DTprox.	DAPprox.	DTdia.	DAPdia.	DTdist.	DAPdist.
Mc I AMPG-PA 5005/91 (sin)	20.37	12.45	7.84	8.98	6.58	9.17	8.93
Mc I *“M. parvulus”* AMPG-K1/258/9 (sin), Kerassia 1 (Roussiakis et al., 2006)	18.10	11.50	7.30	—	—	9.10	8.60
Mc II AMPG-PA 5006/91 (sin)	59.10	13.41	10.35	7.54	7.09	11.75	11.49
Mc II *“M. parvulus”* AMPG-K1/258/10 (sin), Kerassia 1 (Roussiakis et al., 2006)	55.70	10.60	13.00	7.00	6.50	10.70	10.60
Mc III AMPG-ΠΚ 1/395 (sin)	—	10.68	10.90	—	—	—	—
Mc III *“M. parvulus”* AMPG-K1/258/11 (sin), Kerassia 1 (Roussiakis et al., 2006)	66.50	11.80	11.60	7.20	6.40	10.90	10.10
Mc III *Po. orientalis*, Pikermi (Weithofer, 1888)	73.00	—	—	—	—	—	—
Mc V AMPG-PA 5007/91 (sin)	51.51	10.49	10.10	6.04	6.70	9.79	10.72
Mc V *“M. parvulus”* AMPG-K1/258/13 (sin), Kerassia 1 (Roussiakis et al., 2006)	48.20	9.80	10.70	6.30	5.50	9.70	9.60
Mc V *Po. orientalis*, Pikermi (Weithofer, 1888)	55.00	—	—	—	—	—	—

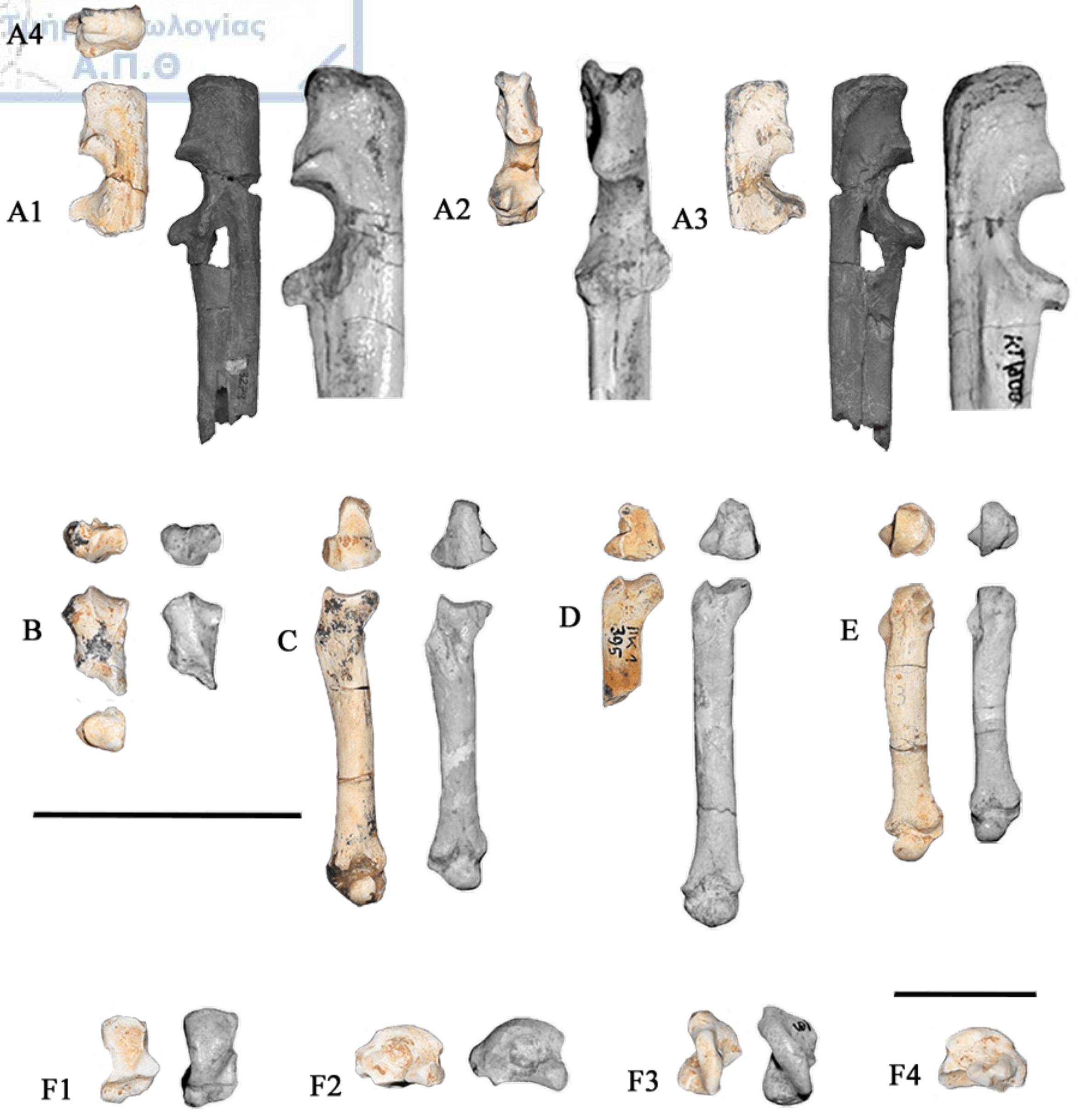

Figure 75. Felidae material (left, in colour) compared against the left olecranon of *Pr. attica* from Las Casiones in Spain (middle, in darker greyscale) (Salesa et al. 2012) and various *"M. parvulus"* postcranial material (on the right, in lighter greyscale) from Kerassia 1 in Euboea Island (Roussiakis et al., 2006). A: Felidae olecranon AMPG-PA 5003/91 (sin) in medial (1), anterior (2), lateral (3) and proximal (4) view. The ulna from Kerassia 1 is right but was mirrored to match the left olecranon of the study. B: Mc I AMPG-PA 5005/91 (sin) in dorsal view along with its proximal and distal articular surfaces. C: Mc II AMPG-PA 5006/91 (sin) in dorsal view. D: proximal end of Mc III AMPG-ΠΚ 1/395 (sin) in dorsal view. E: Mc V AMPG-PA 5007/91 (sin) in dorsal view. F: magnum AMPG-PA 5004/91 (sin) in distal (1), medial (2), proximal (3) and lateral (4) view. The larger scale bar is 5 cm and corresponds to A-E. The smaller scale bar is 2 cm and corresponds to F.

Carnivora indet.

(Fig. 76, Tables 44–50)

The material herein belongs to carnivorans, but a more specific attribution to family or genus was impossible at the time, either due to the absence of sufficient comparative material or due to the fossil's preservation status.

Material: AMPG-PA 5008/91: axis preserving only the body, AMPG-PA 5043/91: distal end of a right fibula, AMPG-PA 5009/91: right navicular, AMPG-PA 5010/91: left navicular, AMPG-PA 5011a/91: left metacarpal II, AMPG-PA 5011a/91: left metacarpal III, AMPG-PA 5011a/91: left metacarpal IV, AMPG-PA 5038/91: distal end of a metapodial, AMPG-PA 5039/91: distal end of a metapodial, AMPG-PA 5012/91: proximal phalange, AMPG-PA 5014/91: proximal phalange, AMPG-PA 5018/91: proximal phalange, AMPG-PA 5019/91: proximal phalange, AMPG-PA 5020/91: proximal phalange, AMPG-PA 5021/91: proximal phalange, AMPG-PA 5022/91: middle phalange, AMPG-PA 5023/91: middle phalange, AMPG-PA 5024/91: middle phalange, AMPG-PA 5025/91: middle phalange, AMPG-PA 5013/91: middle phalange, AMPG-PA 5015/91: middle phalange, AMPG-PA 5016/91: distal phalange, AMPG-PA 5017/91: distal phalange, AMPG-PA 5026/91: distal phalange, AMPG-PA 5027/91: distal phalange, AMPG-PA 5028/91: distal phalange.

Remarks: The metacarpals AMPG-PA 5011a-c/91 are associated and belong to the same individual.

Axis: An axis from a relatively small carnivoran that preserves only the body. The superior articular facets for the atlas are sub-triangular and more elongated along the rostro-caudal axis. The centrum is elliptical, elongated transversally and slightly concave. The rounded odontoid process is broken. Although its overall size is similar to the axis described by Roussiakis et al. (2006) for *"M. parvulus"* from Kerassia, its morphology and proportions differ substantially, suggesting a different family.

Fibula: a distal end of a fibula. Based on its size it would have probably belonged to a medium to large sized carnivoran. The articular surface with the tibia on its medial side is elliptical shaped and extends towards the anterior side. The malleolar fossa is almost round and relatively large. The lateral malleolus is almost at the same level as the articular surface and extends slightly towards the posterior.

Naviculars: The right navicular AMPG-PA 5009/91 is relatively small. It is more rounded than the naviculars described above, but its overall morphology is not that different. Absence of comparative material does not permit more specific attributions beyond this point.

The left navicular AMPG-PA 5010/91 exhibits the most morphological differences from the naviculars described so far. Its distal articular surface is smooth and slopes medially. Its proximal articular surface is ridged unlike the flattened proximal surfaces of the other naviculars. Absence of comparative material does not permit more specific attributions beyond this point.

Metacarpals: Distal half of Mc II and Mc III and complete Mc IV in anatomical position. The shafts are straight, dorsally flat and elliptical to sub-rectangular in their cross-section. When articulated, the proximal epiphysis of Mc II is situated higher and proximally covers that of Mc III, which in turn does the same to Mc IV. The distal epiphysis of Mc IV is rectangular shaped.

Discussion: The morphology of the metacarpals resembles that of Hyaenidae and more accurately that of ictitheres. They are, however, far too large to consider for *Plioviverrops orbignyi* according to the data provided by Pilgrim (1931) and moderately smaller than the metacarpals attributed to *Ictitherium viverrinum* by Roussiakis (1996). Granted the range of intraspecific variation exhibited by the latter taxon in its craniodental material, it is likely that those metacarpals might end up belonging to a smaller *I. viverrinum* individual.

Metapodials: Distal epiphyses from various isolated metapodials. They are attributed to this section as they lacked sufficient distinguishing traits to make any further attributions.

Phalanges: The phalanges attributed in this section were found artificially restored in the two hyaenid manus described in the Hyaeninae section. Due to the erroneous nature of their restoration (e.g., metacarpals in the wrong order, artiodactyl phalange together with a phalange from a carnivoran, etc.) they were otherwise ignored, as they might not only be mismatched, but they could potentially come from different individuals or from a pes instead of a manus.

Table 44. Axis measurements (mm) of a carnivoran from Pikermi.

	AMPG-PA 5008/91
Lmax.	30.13
Wmax.	19.48
Hmax.	9.80
Lce.	6.24
Wce.	11.12
HSAF	9.25
WSAF	11.34

Table 45. Fibula measurements (mm) of a carnivoran from Pikermi.

	DAPdist.	DTdist.
Fibula AMPG-PA 5043/91(dext)	12.75	20.05

Table 46. Navicular measurements (mm) of carnivorans from Pikermi.

	Hmax.	DAPmax.	DTmax.
Navicular AMPG-PA 5009/91 (dext)	11.4	6.49	8.43
Navicular AMPG-PA 5010/91 (sin)	12.28	5.93	8.26

Table 47. Metacarpal measurements (mm) of a carnivoran from Pikermi.

	L	DAPpr.	DTpr.	DAPdia.	DTdia.	DAPdist.	DTdist.
Mc II (sin) AMPG-PA 5011a/91	—	7.92	5.42	—	—	—	—
Mc III (sin) AMPG-PA 5011b/91	—	8.30	6.50	—	—	—	—
Mc IV (sin) AMPG-PA 5011c/91	52.10	8.83	6.30	4.17	5.61	6.03	6.78

Table 48. Isolated distal metapodial measurements (mm) of various carnivorans from Pikermi.

	DAPpr.	DTpr.	DAPdia.	DTdia.	DAPdist.	DTdist.
AMPG-PA 5038/91	—	—	—	—	6.43	7.42
AMPG-PA 5039/91	—	—	—	—	6.07	8.72
AMPG-PA 5041/91	12.30	7.75	—	—	—	—

Table 49. Phalange measurements (mm) of the questionably restored Hyaeninae manus AMPG-PA 4997a-d/91 in Fig. 67.

	L	DAPpr.	DTpr.	DAPdia.	DTdia.	DAPdist.	DTdist.
Proximal phalange AMPG-PA 5012/91	32.46	12.08	14.49	9.38	8.44	8.69	11.17
Middle phalange AMPG-PA 5013/91	21.37	9.02	11.58	4.97	9.09	8.66	11.5
Proximal phalange AMPG-PA 5014/91	31.83	13.4	13.00	7.92	9.42	8.83	11.76
Middle phalange AMPG-PA 5015/91	19.65	9.70	—	—	—	7.84	12.16
Distal phalange AMPG-PA 5016/91	13.55	—	11.68	—	—	—	—
Distal phalange AMPG-PA 5017/91	—	—	—	—	—	—	—

Table 50. Phalange measurements (mm) from the questionably restored Hyaeninae manus AMPG-PA 4998a-d/91. The metacarpal allocation of the phalanges below merely states their corresponded metacarpal in the artificially restored manus in Fig. 67.

	L	DAPpr.	DTpr.	DAPdia.	DTdia.	DAPdist.	DTdist.
Proximal phalange (Mc II) AMPG-PA 5018/91	32.75	11.67	13.61	8.32	9.43	8.69	11.80
Proximal phalange (Mc III) AMPG-PA 5019/91	31.33	12.24	13.40	9.36	8.37	8.55	11.00
Proximal phalange (Mc IV) AMPG-PA 5020/91	31.58	12.20	12.74	8.28	7.93	8.03	11.08
Proximal phalange (Mc V) AMPG-PA 5021/91	31.86	11.51	12.74	6.81	8.90	8.20	11.30
Middle phalange (Mc II) AMPG-PA 5022/91	20.86	9.01	11.64	5.20	8.93	9.05	11.05
Middle phalange (Mc III) AMPG-PA 5023/91	22.13	9.38	11.62	8.52	5.15	8.43	11.70
Middle phalange (Mc IV) AMPG-PA 5024/91	18.36	9.65	11.22	6.09	9.26	8.89	11.31
Middle phalange (Mc V) AMPG-PA 5025/91	21.52	9.78	11.56	6.35	9.31	8.48	10.94
Distal phalange (Mc III) AMPG-PA 5026/91	14.51	13.04	9.90	8.37	5.38	4.48	3.56
Distal phalange (Mc IV) AMPG-PA 5027/91	—	14.75	9.25	9.67	6.32	—	—
Distal phalange (Mc V) AMPG-PA 5028/91	—	11.29	82.00	—	—	—	—

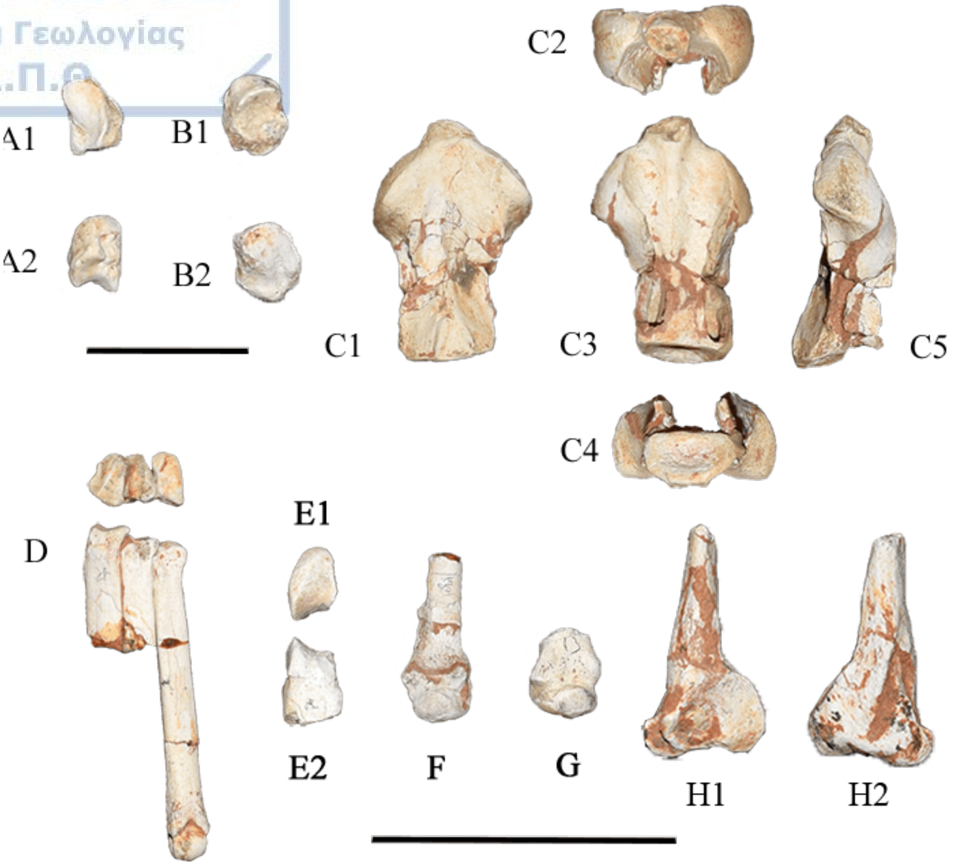

Figure 76. A: navicular AMPG-PA 5010/91 (sin) in palmar (1) and dorsal (2) view. B: navicular AMPG-PA 5009/91 (dext) in palmar (1) and dorsal (2) view. C: axis from a small carnivoran AMPG-PA 5008/91 in ventral (1), rostral (2), ventral (3), caudal (4) and lateral (5) view. D: associated Mc II-III-IV AMPG-PA 5011a-c/91 (sin) articulated in proximal and dorsal view. E: proximal epiphysis of a metapodial in proximal (1) and dorsal (2) view. F: distal epiphysis of a metapodial in dorsal view. G: distal epiphysis of a metapodial in dorsal view, H: distal epiphysis of right fibula AMPG-PA 5043/91 in medial (1) and lateral (2) view. The smaller scale bar is 2 cm and corresponds to A-C. The larger scale bar is 5 cm and corresponds to D-H.

4. Conclusions

Representatives from every known carnivoran families – except the mephitids – of the classical locality of Pikermi were recognized herein by varying degrees of frequency depending on the taxon.

The family Ailuridae is represented by *Simocyon primigenius* through some carpals and a first metacarpal. Besides the similarly left scapholunate, the rest of the remains described belonged to the same individual. Further comparison with the material from *Simocyon batalleri* from Spain exemplified their remarkable similarities, but also some of their differences. The described material constitutes the first known description of the manus of *Simocyon primigenius* and the first attribution to this taxon's postcranial skeleton since the femur and the distal humerus attributed to it by Gaudry (1862), contributing to this enigmatic taxon's skeletal reveal.

The family Mustelidae is represented by *Promeles palaeattica* through a partially preserved cranium with its left row of cheek teeth. The dental morphology and metrical values of this small mustelid did not indicate any major differences, either of morphological or metrical nature, from other specimens attributed to this taxon both from the classical locality of Pikermi but from other localities as well.

The family Ursidae is represented by *Indarctos atticus* through the proximal end of a left radius. Postcranial material from this relatively large-sized bear from Pikermi remain quite rare, as only a few attributions have been made. The size and morphology of the studied radius is almost identical with the radii previously described by Pilgrim (1931) and Roussiakis (2001a) from Pikermi. Their minor differences (e.g., cross-section shape of the shaft) are probably due to the radius's rather poor state of preservation.

The family Hyaenidae is represented by at least five species from both Ictitheriinae and Hyaeninae sub-families, being simultaneously the richest both in number of taxa and in sheer material quantity as follows:

1. *Icitherium viverrinum* was recognized by several craniodental, mandibular and possibly postcranial elements and probably constitutes the most abundant taxon of this study. The craniodental and mandibular material of *I. viverrinum* described herein expands both the sample size and the known range of intraspecific variation for the classical locality of Pikermi considerably, as many smaller sized individuals were described. This trend exhibits similarities with the larger *I. viverrinum* sample pools encountered in the Chinese localities. Additionally, there are some indications that two of the studied specimens, an almost complete skull and a mandible might be associated, but due to the absence of taphonomical data and the presence of deformations in both specimens this cannot be verified. Interestingly, two of the studied specimens exhibit markedly larger M1 and M2 than the rest of *I. viverrinum* from Pikermi and are close in value with the larger *I. viverrinum* from Grebeniki and Novaya Emetovka described by Semenov (1989).

2. *Plioviverrops orbignyi* was recognized by two maxillary fragments. These fragments from the smallest hyaenid representatives of Pikermi could potentially belong to the same individual as they mirror each as other almost perfectly. Their dental morphology, size as well as the angle formed between P4 and M1 were similar with other *P. orbignyi* specimens from Pikermi as well as other localities.

3. *Adcrocuta eximia* was recognized by craniodental, mandibular and possibly postcranial elements. Their morphology and size are similar with the typical *A. eximia* specimens from the Turolian and by extension those from the classical locality of Pikermi. Also, two specimens, an almost complete skull and a left hemimandible could be associated as they exhibit the same degree and pattern of wear in their dentition.

4. *Hyaenictis graeca*, a very rare taxon initially erected and described by Gaudry (1861; 1863) by some scarce dental remains from young individuals from Pikermi, was identified through several maxillary and partially preserved cranial fragments. A partially preserved cranium initially described by Roussiakis (1996) as *Hyaenictis* cf. *graeca* was also included, reviewed, and attributed to *Hyaenictis graeca* making it the most complete specimen of the taxon to this day. In addition, the possible presence of *H. graeca* in other localities such as Halmyropotamos and Cerro de la Garrita in Spain was discussed. The former with a maxillary fragment described herein and the latter with an isolated P3 described by Alcalá (1994). It was observed as with *Chasmaporthetes*, the mesial cusps of P2 and P3 in *Hyaenictis graeca* exhibit some variation. The young ontogenetic stage of the specimens initially attributed to this taxon by Gaudry (1861; 1863) along with its rarity in the locality, make both potential attributions and comparisons challenging. The size and morphology of the material studied suggests strong similarities both with the maxillary specimen attributed to it by Gaudry (1863) and a specimen stored in the Naturhistorisches Museum in Wien, despite their narrower P4 width in between the paracone and the metastyle blade. Also, considering things from a purely ecological aspect, the presence of a novel, fourth large hyaenid in Pikermi would be impractical in its already “overpopulated” large carnivore guild.

5. *Lycyaena chaeretis*, the smallest of the larger hyaenids from Pikermi, was recognized by a maxillary fragment. Its overall dental size and morphology were found similar with other specimens attributed to this taxon from Pikermi. Its smaller size set it apart from both *Adcrocuta eximia* and *Hyaenictis graeca*, and in the case of the former its dental morphology as well. Additionally, as already noted by past authors, the taxon’s striking dental similarities with *Lycyaena dubia* from China to the possibility of them being conspecific were noted.

The family of Felidae is represented by at least two species with the following taxa:

1. *Amphimachairodus giganteus*, the large machairodont of Pikermi, whose presence was identified by the proximal end of an ulna. Further comparison with the holotype of *A. giganteus* by Wagner (1848) exemplified their similarities both in size and morphology.

2. *Pontosmilus orientalis* was recognized by a maxilla and a hemimandible. The material described and attributed to this taxon possibly constitute the first to be described from the locality, as the cranial and mandibular remains described from the locality described thus far seem to belong to another taxon, the similarly-sized felid *Paramachaerodus schlosseri*. More so, the described hemimandible might also be the first to be described for this taxon, as the only confirmed remains from this species is a partially preserved cranium from Maragheh described by Kittl (1887). The smaller P4 protocone, the morphology of P3, the presence of a mandibular flange and the slightly crenulated m1 set *Po. orientalis* apart from *Pa. schlosseri*. At the same time, a couple primitive characters in the studied specimens were also acknowledged, such as the presence of a vestigial p2 and the absence of an ectostyle in P4.

Finally, a number of primarily postcranial remains were also treated under the broader family or sub-family level with remarks about their possible affinities. Through some of them, the presence of taxa such as *Hyanictitherium wongii*, *Paramachaerodus schlosseri*, *Pristifelis attica* and *"Metailurus parvulus"* was possibly indicated. Due to the limited comparative postcranial material available presently and the studies that deal with them, a species-level attribution was – for the time being at least – refrained. It is, however, certainly something that warrants further exploration, both in a stricter taxonomical but also morphofunctional aspect. Nevertheless, it should be noted, that simply due to the sheer abundance of some taxa over other in the classical locality of Pikermi (e.g., *I. viverrinum* over *H. wongii* and *A. eximia* over *H. graeca*) most postcranial material is likely to also belong to these more common taxa. Lastly, a few carnivoran postcranial elements that could not be safely identified into a family level due to the absence of comparative material were placed under the more generic Carnivora indet. attribution.

The product of this Thesis serves to exemplify both the locality's faunal richness but also the value of old collections. During this process, hopefully, it also managed to enrich the carnivoran knowledge from the locality of Pikermi either through the recognition of some of its rarer taxa or through the expansion of the sample size and the intraspecific variation in some of the more well-studied taxa.

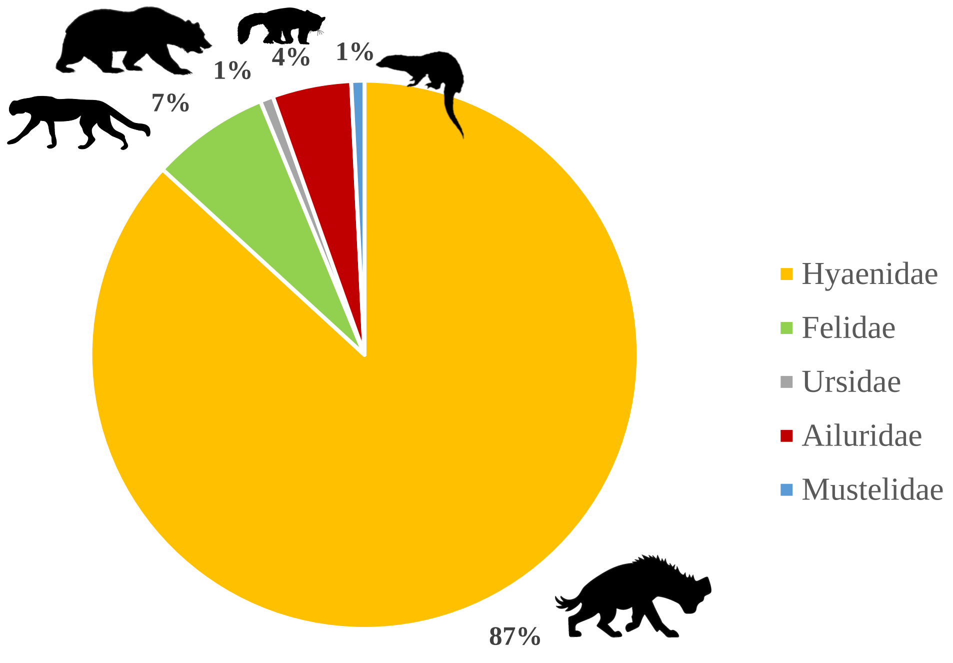

Figure 77. Family representation based solely on the specimens studied herein (Carnivora indet. section excluded).

Table 51. Summary of the taxa recognized in the study based on the material.

	Craniodental	Postcranial		Craniodental	Postcranial
Caniformia			**Feliformia**		
Ailuridae			**Felidae**		
Simocyon primigenius	—	✓	*Amphimachairodus giganteus*	—	✓
			Pontosmilus orientalis	✓	possible
			Paramachaerodus schlosseri	—	possible
Mustelidae			*“Metailurus parvulus”*	—	probable
Promeles palaeattica	✓	—	*Pristifelis attica*	—	probable
			Hyaenidae		
			Ictitherium viverrinum	✓	probable
Ursidae			*Hyaenictitherium wongii*	—	possible
Indarctos atticus	—	✓	*Plioviverrops orbignyi*	✓	—
			Adcrocuta eximia	✓	probable
			Hyaenictis graeca	✓	possible
			Lycyaena chaeretis	✓	possible

References

Abel, O. (1922). *Lebensbilder aus der Tierwelt der Vorzeit*. Jena. https://doi.org/10.5962/bhl.title.61701

Abella, J., Hontecillas, D., Valenciano, A., Montoya, P., Morales, J., Pesquero, M. D., & Alcalá, L. (2019). The last record of an ailuropod bear from the Iberian Peninsula. *Geodiversitas*, *41*(1), 797–809. https://doi.org/10.5252/geodiversitas2019v41a23

Adams, J. W., Rovinsky, D. S., Herries, A. I. R., & Menter, C. G. (2016). Macromammalian faunas, biochronology and palaeoecology of the early Pleistocene Main Quarry hominin-bearing deposits of the Drimolen Palaeocave System, South Africa. *PeerJ*, *4*, e1941. https://doi.org/10.7717/peerj.1941

Alcalá, L. (1994). *Macromamíferos neógenos de la fosa de Alfambra- Teruel*. Instituto de Estudios Turolenses - Museo Nacional de Ciencias Naturales, Madrid.

Andersson, K., & Werdelin, L. (2005). Carnivora from the Late Miocene of Lantian, China. *Vertebrata Palasiatica*, *43*(4), 256–271.

Antón, M., Turner, A., Salesa, M. J., & Morales, J. (2006). A complete skull of *Chasmaporthetes lunensis* (Carnivora, Hyaenidae) from the Spanish Pliocene site of La Puebla Valverde (Teruel). *Estudios Geológicos*, *62*(1), 375–388. https://doi.org/10.3989/egeol.0662132

Arambourg, C., & Piveteau, J. (1929). Les Vertébrés du Pontien de Salonique. *Annales de Paléontologie*, *18*, 59–138.

Bachmayer, V. F., & Symeonidis, N. (1982). Die Ausgrabungen in Pikermi-Chomateri bei Athen. —Eine Dokumentation. *Annalen des Naturhistorischen Museums in Wien*, *84*(A), 7–12.

Bakalov, N., & Nikolov, I. (1962). *Les Fossiles de Bulgarie. Vol X. Mammifères tertiaires*. Académie des Sciences de Bulgarie, Sofia. (In Bulgarian, with French and Russian summaries).

Bakr, A. (1959). *Rodentia and Carnivora from the Pontian of Samos*. Ph.D. Thesis (unpublished), Harvard University.

Ballesio, R. (1963). Monographie d'un *Machairodus* du gisement Villafranchien de Senèze: *Homotherium crenatidens* Fabrini. Travaux du Laboratoire de Géologie de la Faculté des Sciences de Lyon. Nouvelle série, 9, 1–129.

Baryshnikov, G. F. (2002). Late Miocene *Indarctos punjabiensis atticus* (Carnivora, Ursidae) in Ukraine with survey of *Indarctos* records from the former USSR. *Russian Journal of Theriology*, *1*(2), 83–89. https://doi.org/10.15298/rusjtheriol.01.2.02

Baryshnikov, G. F., & Tleuberdina, P. A. (2017). Late Miocene *Indarctos* (Carnivora: Ursidae) from the Karabulak Formation of the Kalmakpai river (Zaisan Depression, Eastern Kazakhstan). *Proceedings of the Zoological Institute RAS*, *321*(1), 3–9.

Baskin, J. A. (1998). Procyonidae. In C. M. Janis, K. M. Scott, & L. L. Jacobs (Eds.), *Evolution of Tertiary Mammals of North America, Vol. 1: Terrestrial carnivores, ungulates and ungulatelike mammals* (pp. 144–151). Cambridge University Press, Cambridge.

Beaumont, G. de. (1969). Brèves remarques sur *Plioviverrops* Kretzoi (Carnivora). *Bulletin de La Société Vaudoise des Sciences Naturelles*, *70*, 1–7.

Beaumont, G. de. (1975). Recherches sur les Félidés (Mammifères, Carnivores) du Pliocène inférieur des sables à *Dinotherium* des environs d'Eppelsheim (Rheinhessen). *Archives des Sciences Physiques et Naturelles, Genève*, *28*(3), 369–405.

Beaumont, G. de, & Mein, P. (1972). Recherches sur de le genre *Plioviverrops* Kretzoi (Carnivora, ?Hyaenidae). *Archives des Sciences*, *25*, 383–394.

Berggren, W. A., Kent, D. V., Swisher, C. C., & Aubry, M.-P. (1995). A Revised Cenozoic Geochronology and Chronostratigraphy. In W. A. Berggren, D. V. Kent, M.-P. Aubry, & J. Hardenbol, *Geochronology, Time Scales and Global Stratigraphic Correlation*. SEPM Society for Sedimentary Geology. https://doi.org/10.2110/pec.95.04.0129

Bernor, R. L., Solounias, N., Swisher III, C. C., & Van Couvering, J. A. (1996). The correlation of three classical "Pikermian" mammal faunas- Maragheh, Samos, and Pikermi- with the European MN unit-system. In R. L. Bernor, V. Fahlbusch, & H.-W. Mittmann (Eds.), *The evolution of western Eurasian Neogene mammal faunas* (pp. 136–154). Columbia University Press, New York.

Böhme, M., Spassov, N., Ebner, M., Geraads, D., Hristova, L., Kirscher, U., Kötter, S., Linnemann, U., Prieto, J., Roussiakis, S., Theodorou, G., Uhlig, G., & Winklhofer, M. (2017). Messinian age and savannah environment of the possible hominin *Graecopithecus* from Europe. *PLOS ONE*, *12*(5), e0177347. https://doi.org/10.1371/journal.pone.0177347

Bonis, L. de. (2004). Carnivores hyaenidés du Miocène supérieur de Turquie. In *Zona Arquaeologica, Miscelanea en homenaje a Emiliano Aguirre: Vol. 2 Paleontologia* (pp. 108–117). Museo Arqueologico Regional, Madrid.

Bonis, L. de, & Koufos, G. D. (1981). A new hyaenid (Carnivora, Mammalia) in the Vallesian (late Miocene) of Northern Greece. *Scientific Annals of the Faculty of Physics and Mathematics, University of Thessaloniki*, *21*, 79–94.

Bonis, L. de, & Koufos, G. D. (1991). The late Miocene small carnivores of the lower Axios valley (Macedonia-Greece). *Geobios*, *24*(3), 361–379. https://doi.org/10.1016/S0016-6995(09)90015-8

Bonis, L. de, & Koufos, G. D. (1994). Some Hyaenidae from the Late Miocene of Macedonia (Greece) and a contribution to the phylogeny of the hunting hyaenas. *Münchner Geowissenschaften Abhandlungen (A)*, *26*, 81–96.

Bonis, L. de, Bouvrain, G., Keraudren, B., & Melentis, J. K. (1973). Premiers resultats des fouilles recentes en Grèce septentrionale (Macédoine). *Comptes Rendus de l'Académie Des Sciences Paris*, *227*, 1431–1434.

Bonis, L. de, Peigné, S., Guy, F., Mackaye, H. T., Likius, A., Vignaud, P., & Brunet, M. (2010). Hyaenidae (Carnivora) from the late Miocene of Toros-Menalla, Chad. *Journal of African Earth Sciences*, *58*(3), 561–579. https://doi.org/10.1016/j.jafrearsci.2010.06.003

Bonis, L. de, Peigne, S., Likius, A., Makaye, H. T., Brunet, M., & Vignaud, P. (2007). First occurrence of the 'hunting hyena' *Chasmaporthetes* in the Late Miocene fossil bearing localities of Toros Menalla, Chad (Africa). *Bulletin de la Société Géologique de France*, *178*(4), 317–326. https://doi.org/10.2113/gssgfbull.178.4.317

Bonis, L. de, Peigné, S., Mackaye, H. T., Likius, A., Vignaud, P., & Brunet, M. (2008). The fossil vertebrate locality Kossom Bougoudi, Djurab desert, Chad: A window in the distribution of the carnivoran faunas at the Mio–Pliocene boundary in Africa. *Comptes Rendus Palevol*, *7*(8), 571–581. https://doi.org/10.1016/j.crpv.2008.10.004

Borissiak, A. (1915). Mammifères fossils de Sebastopol II. *Mémoires du Comité Géologique, Petrograd, New Series*, *137*, 1–47.

Bowdich, T. E. (1821). *An analysis of the natural classifications of Mammalia: For the use of students and travellers*. J. Smith, Paris.

Bruijn, H. de, Daams, R., Daxner-Höck, G., Fahlbusch, V., Ginsburg, L., Mein, P., Marles, J., Heinzmann, E., Mayhew, D. F., van der Meulen, A. J., Schmidt-Kittler, N., & Antunes, M. T. (1992). Report of the RCMNS working group on fossil mammals, Reisensburg 1990. *Newsletters on Stratigraphy*, *26*(2–3), 65–118. https://doi.org/10.1127/nos/26/1992/65

Christiansen, P. (2013). Phylogeny of the sabertoothed felids (Carnivora: Felidae: Machairodontinae). *Cladistics*, *29*(5), 543–559. https://doi.org/10.1111/cla.12008

Cohen, K. M., Finney, S. C., Gibbard, P. L., & Fan, J.-X. (2013). The ICS International Chronostratigraphic Chart. *Episodes*, *36*(3), 199–204. https://doi.org/10.18814/epiiugs/2013/v36i3/002

Crusafont Pairó, M., & Petter, G. (1969). Contribution à l'étude des Hyaenidae. La sous-famille des Ictitheriinae. *Annales de Paléontologie (Vertébrés)*, *55*, 89–127.

Dames, W. (1883a). Hirsche und Mäuse von Pikermi in Attica. Zeitschrift der Deutschen Geologischen Gesellschaft. *Zeitschrift Der Deutschen Geologischen Gesellschaft*, *35*(1), 92–100.

Dames, W. (1883b). Über das Vorkommen von *Hyaenarctos* in den Pliocän-Ablagerungen von Pikermi bei Athen. *Sitzungsber Gesellsch Naturf Freunde Berlin*, *8*, 132–139.

Eizirik, E., Murphy, W. J., Koepfli, K.-P., Johnson, W. E., Dragoo, J. W., Wayne, R. K., & O'Brien, S. J. (2010). Pattern and timing of diversification of the mammalian order Carnivora inferred from multiple nuclear gene sequences. *Molecular Phylogenetics and Evolution*, *56*(1), 49–63. https://doi.org/10.1016/j.ympev.2010.01.033

Erdbrink, D. P. (1953). *A review of fossil and recent bears of the old world with remarks on their phylogeny based upon their dentition*. *Deventer: De Lange (Eds)*.

Ewer, R. F. (1955). The fossil carnivores of the Transvaal caves. The lycyaenas of Sterkfontein and Swartkrans, together with some general considerations of the Transvaal fossil hyaenids. *Proceedings of the Zoological Society of London*, *123*, 839–857.

Ewer, R. F. (1973). *The carnivores*. Cornell University Press, Ithaca, New York.

Ferretti, M. P. (2007). Evolution of bone-cracking adaptations in hyaenids (Mammalia, Carnivora). *Swiss Journal of Geosciences*, *100*(1), 41–52. https://doi.org/10.1007/s00015-007-1212-6

Ficcarelli, G., & Torre, D. (1970). Remarks on the taxonomy of hyaenids. *Palaeontographia Italica*, *66*, 13–33.

Filis, P., Roussiakis, S., Giaourtsakis, I., Kampouridis, P., Kargopoulos, N., Skandalos, P., Sklavounou, S., Svorligkou, G., Tsoukalas, N., Kirdis, S., & Theodorou, G. (2019). A fieldwork update on the new palaeontological excavations at the classical Turolian locality of Pikermi (Attica, Greece). In H. Kranis (Ed.), *Proceedings of the 15th International Congress of the Geological Society of Greece* (Vol. 7, pp. 63–64). Bulletin of the Geological Society of Greece, Sp. Pub.

Flower, W. H. (1869). On the value of the characters of the base of the cranium in the classification of the order Carnivora, and on the systematic position of *Bassaris* and other disputed forms. *Proceedings of the Zoological Society of London*, 4–37.

Flynn, J. J., Nedbal, M. A., Dragoo, J. W., & Honeycutt, R. L. (2000). Whence the Red Panda? *Molecular Phylogenetics and Evolution*, *17*(2), 190–199. https://doi.org/10.1006/mpev.2000.0819

Franzen, J. L., & Storch, G. (1975). Die unterpliozäne (turolische) Wirbeltierfauna von Dorn-Dürkheim, Rheinhessen (SW-Deutschland). 1. Entdeckung, Geologie, Mammalia:

Carnivora, Proboscidea, Rodentia. Grabungsergebnisse 1972–1973. *Senckenbergiana Lethaea*, *56*(4–5), 233–303.

Galiano, H., & Frailey, D. (1977). *Chasmaporthetes kani*, new species from China, with remarks on phylogenetic relationships of genera within the Hyaenidae (Mammalia, Carnivora). *American Museum Novitates*, *2632*, 1–16.

Gaudry, A. (1855). Sur les premiers résultats de la mission qui lui a été confiée par l'Académie pour l'exploration du gîte fossilifère de Pikermi (Attique). (Extrait d'une lettre de M. A. Gaudry à M. le Secrétaire perpétuel). *Comptes Rendus Hebdomadaires des Séances de l'Académie Des Sciences*, *41*, 894–897.

Gaudry, A. (1861). Note sur les carnassieres fossils de Pikermi (Grèce). *Bulletin de La Société Geologique de France, Série 2*, *18*, 527–538.

Gaudry, A. (1862–1867). *Animaux fossiles et géologie de l'Attique*. F. Savy, Paris.

<u>Author's note</u>: According to Pilgrim & Hopwood (1928) Gaudry's monography covers a span of 6 years. According to these authors its publication took place as follows:

pp. 1-72,	published in	1862
pp. 73-144,	published in	1863
pp. 145-240,	published in	1864
pp. 241-323,	published in	1865
pp. 325-370,	published in	1866
pp. 371-474	published in	1867

Gaudry, A., & Lartet, E. (1856). Sur les résultats des rechérches paléontologiques entreprises dans l'Attique sous les auspices de l'Académie. *Comptes Rendus des Séances de l'Académie des Sciences*, *43*, 271–274.

Geraads, D., & Spassov, N. (2016). Musteloid carnivores from the upper Miocene of South-Western Bulgaria, and the phylogeny of the Mephitidae. *Geodiversitas*, *38*(4), 543–558. https://doi.org/10.5252/g2016n4a5

Geraads, D., & Spassov, N. (2020). A skull of *Machairodus* Kaup, 1833 (Felidae, Mammalia) from the late Miocene of Hadjidimovo (Bulgaria), and its place in the evolution of the genus. *Geodiversitas*, *42*(9), 123–137. https://doi.org/10.5252/geodiversitas2020v42a9

Geraads, D., Tsoukala, E., & Spassov, N. (2007). A skull of *Ancylotherium* (Chalicotheriidae, Mammalia) from the late Miocene of Thermopigi (Serres, N. Greece) and the relationships of the genus. *Journal of Vertebrate Paleontology*, *27*(2), 461–466. https://doi.org/10.1671/0272-4634(2007)27[461:ASOACM]2.0.CO;2

Ginsburg, L. (1977). Les carnivores du Miocène de Beni Mellal (Maroc). *Géologie Méditerranéenne*, *4*(3), 225–239.

Ginsburg, L. (1999). Order Carnivora. In G. E. Rössner & K. Heissig (Eds.), *The Miocene Land Mammals of Europe* (pp. 109–148). Pfeil, Munich.

Guanfang, C., & Schmidt-Kittler, N. (1983). The deciduous dentition of *Percrocuta* Kretzoi and the diphyletic origin of the hyaenas (Carnivora, Mammalia). *Paläontologische Zeitschrift*, *57*, 159–169. https://doi.org/10.1007/BF03031758

Haile-Selassie, Y., & Howell, F. C. (2009). Carnivora. In Y. Haile-Selassie & G. WoldeGabriel (Eds.), *Ardipithecus kadabba*: *Late Miocene Evidence from the Middle Awash, Ethiopia* (pp. 237–275). University of California Press, Berkeley.

Helbing, H. (1932). Über einen *Indarctos*-Schädel aus dem Pontien der Insel Samos. Nebst einem Anhang: *Hyaenarctos* spec. Aus dem Pliocaen von Vialette (Haute-Loire). *Abhandlungen Der Schweizerischen Paläontologischen Gesellschaft*, *52*, 1–18.

Hendey, Q. B. (1974). The late Cenozoic Carnivora of the southwestern Cape Province. *Annals of the South African Museum*, *63*, 1–369.

Hendey, Q. B. (1978). Late Tertiary Hyaenidae from Langebaanweg, South Africa, and their relevance to the phylogeny of the family. *Annals of the South African Museum*, *76*, 265–297.

Hensel, R. F. (1862). Über die Reste einiger Säugetierarten von Pikermi in der Municher Sammlung. *Monatsberichte Der Königlichen Preussische Akademie des Wissenschaften zu Berlin*, *14*, 560–569.

Howell, F. C., & Garcia, N. (2007). Carnivora (Mammalia) from Lemudong'o (Late Miocene: Narok district, Kenya). *Kirtlandia*, *56*, 121–139.

Howell, F. C., & Petter, G. (1985). Comparative observations on some middle and upper Miocene hyaenids, genera: *Percrocuta* Kretzoi, *Allohyaena* Kretzoi, *Adcrocuta* Kretzoi (Mammalia, Carnivora, Hyaenidae). *Geobios*, *18*(4), 419–491. https://doi.org/10.1016/S0016-6995(85)80001-2

Jiangzuo, Q., Niu, K., Li, S., Fu, J., & Wang, S. (2022). A Diverse Metailurine Guild from the Latest Miocene Xingjiawan Fauna, Yongdeng, Northwestern China, and Generic Differentiation of Metailurine Felids. *Journal of Mammalian Evolution*. https://doi.org/10.1007/s10914-022-09622-8

Johnson, W. E., Eizirik, E., Pecon-Slattery, J., Murphy, W. J., Antunes, A., Teeling, E., & O'Brien, S. J. (2006). The Late Miocene Radiation of Modern Felidae: A Genetic Assessment. *Science*, *311*(5757), 73–77. https://doi.org/10.1126/science.1122277

Kadic, O., & Kretzoi, M. (1927). Vorläufiger Berichtüber die Ausgrabungen in der Csákvárer Höhlung. *Barlangkutatás*, *14–15*, 1–21.

Kargopoulos, N. (2019). *Carnivoran Dietary Adaptations: A Multiproxy Study on the Feeding Ecology of the Fossil Carnivorans of Greece*. M.Sc. Thesis (unpublished), National and Kapodistrian University of Athens, 214p.

Kitchener, A. C., Breitenmoser-Würsten, C., Eizirik, E., Gentry, A., Werdelin, L., Wilting, A., Yamaguchi, A., Abramov, A. V., Christiansen, P., Driscoll, C., Duckworth, J. W., Johnson, W. E., Luo, S. J., Meijaard, E., O'Donoghue, P., Sanderson, J., Seymour, K., Bruford, M., Groves, C., Hoffmann, M., Nowell, K., & Tobe, S. (2017). A revised taxonomy of the Felidae: The final report of the Cat Classification Task Force of the IUCN Cat Specialist Group. *Cat News*.

Kittl, E. (1887). Beiträge zur Kenntniss der fossilen Säugethiere von Maragha in Persien. I. Carnivoren. *Annalen des Naturhistorischen Hofmuseums*, *2*, 317–338.

Koepfli, K.-P., Jenks, S. M., Eizirik, E., Zahirpour, T., Valkenburgh, B. V., & Wayne, R. K. (2006). Molecular systematics of the Hyaenidae: Relationships of a relictual lineage resolved by a molecular supermatrix. *Molecular Phylogenetics and Evolution*, *38*(3), 603–620. https://doi.org/10.1016/j.ympev.2005.10.017

Koepfli, K.-P., Deere, K. A., Slater, G. J., Begg, C., Begg, K., Grassman, L., Lucherini, M., Veron, G., & Wayne, R. K. (2008). Multigene phylogeny of the Mustelidae: Resolving relationships, tempo and biogeographic history of a mammalian adaptive radiation. *BMC Biology*, *6*(1), 10. https://doi.org/10.1186/1741-7007-6-10

Kormos, T. (1911). Der Pliozäne Knochenfund bei Polgardi. *Foldtani Kozlony, Budapest*, *41*, 171–189.

Kostopoulos, D. S., & Vasileiadou, K. (2006). The Greek Late Neogene-quaternary ursids in relation to palaeogeography and palaeoenvironment. *Scientific Annals School of Geology Aristotle University of Thessaloniki*, *98*, 285–292.

Koufos, G. D. (1987). *Chasmaporthetes bonisi*, a new hyaenid (Carnivora, Mammalia) from the late Miocene of Macedonia (Greece). *Bulletin de la Société Géologique de France*, *3*(5), 913–920.

Koufos, G. D. (1993). Late Pliocene carnivores from western Macedonia (Greece). *Paläontologische Zeitschrift*, *67*(3–4), 357–376. https://doi.org/10.1007/BF02990288

Koufos, G. D. (2000). Revision of the late Miocene carnivores from the lower Axios valley. *Münchner Geowissenschaften Abhandlungen (A)*, *39*, 51–92.

Koufos, G. D. (2006a). Carnivora. In G. D. Koufos (Ed.), *The late Miocene Vertebrate locality of Perivolaki, Thessaly, Greece* (Vol. 276, pp. 39–74). Palaeontographica, Abteilung A, Stuttgart.

Koufos, G. D. (2006b). The Large Mammals from the Miocene/Pliocene Locality of Silata, Macedonia, Greece with Implications about the Latest Miocene Palaeoecology. *Beitrage Fur Paläontologie*, *30*, 293–313.

Koufos, G. D. (2008). Carnivores from the early/middle Miocene locality of Antonios (Chalkidiki, Macedonia, Greece). *Geobios*, *41*(3), 365–380. https://doi.org/10.1016/j.geobios.2007.05.003

Koufos, G. D. (2009). Carnivora. In G. D. Koufos & D. Nagel (Eds.), *The Late Miocene mammal faunas of the Mytilinii Basin, Samos Island, Greece: New Collection* (Vol. 31, pp. 57–105). Beiträge zur Paläontologie, Wien.

Koufos, G. D. (2011). The Miocene carnivore assemblage of Greece. *Estudios Geológicos*, *67*(2), 291–320. https://doi.org/10.3989/egeol.40560.190

Koufos, G. D. (2012). New material of Carnivora (Mammalia) from the Late Miocene of Axios Valley, Macedonia, Greece. *Comptes Rendus Palevol*, *11*(1), 49–64. https://doi.org/10.1016/j.crpv.2011.09.004

Koufos, G. D. (2013). Chapter 28. Neogene mammal biostratigraphy and chronology of Greece. In X. Wang, L. J. Flynn, & M. Fortelius (Eds.), *Fossil mammals of Asia. Neogene biostratigraphy and chronology* (pp. 595–621). Columbia University Press, New York. https://doi.org/10.7312/wang15012-028

Koufos, G. D. (2016). Carnivora. *Geobios*, *49*(1–2), 53–67. https://doi.org/10.1016/j.geobios.2016.01.013

Koufos, G. D. (2021). The late Miocene middle-sized ictitheres (Mammalia: Hyaenidae) of Greece. *Bollettino della Società Paleontologica Italiana*, *60*(1), 19–48. https://doi.org/10.4435/BSPI.2021.03

Koufos, G. D. (2022a). The Fossil Record of Ailurids (Mammalia: Carnivora: Ailuridae) in Greece. In E. Vlachos (Ed.), *Fossil Vertebrates of Greece Vol. 2* (pp. 629–633). Springer International Publishing, Cham. https://doi.org/10.1007/978-3-030-68442-6_22

Koufos, G. D. (2022b). The Fossil Record of Felids (Mammalia: Carnivora: Felidae) in Greece. In E. Vlachos (Ed.), *Fossil Vertebrates of Greece Vol. 2* (pp. 519–539). Springer International Publishing, Cham. https://doi.org/10.1007/978-3-030-68442-6_16

Koufos, G. D. (2022c). The Fossil Record of Hyaenids (Mammalia: Carnivora: Hyaenidae) in Greece. In E. Vlachos (Ed.), *Fossil Vertebrates of Greece Vol. 2* (pp. 555–576). Springer International Publishing, Cham. https://doi.org/10.1007/978-3-030-68442-6_19

Koufos, G. D. (2022d). The Fossil Record of Mustelids (Mammalia: Carnivora: Mustelidae) in Greece. In E. Vlachos (Ed.), *Fossil Vertebrates of Greece Vol. 2* (pp. 641–659). Springer International Publishing, Cham. https://doi.org/10.1007/978-3-030-68442-6_24

Koufos, G. D., Konidaris, G. E., & Harvati, K. (2018a). Revisiting *Ursus etruscus* (Carnivora, Mammalia) from the Early Pleistocene of Greece with description of new material. *Quaternary International*, *497*, 222–239. https://doi.org/10.1016/j.quaint.2017.09.043

Koufos, G. D., Mayda, S., & Kaya, T. (2018b). New carnivoran remains from the Late Miocene of Turkey. *Paläontologische Zeitschrift*, *92*(1), 131–162. https://doi.org/10.1007/s12542-017-0376-2

Kovachev, D. (2012). A complete skeleton of *Adcrocuta eximia* (Roth and Wagner, 1854) from the Upper Maeotian (Turolian) of Hadzhidimovo, SW Bulgaria. *Geologica Balcanica*, *41*(1–3), 77–95. https://doi.org/10.52321/GeolBalc.41.1-3.77

Kretzoi, M. (1938). Die Raubtiere von Gombaszög nebst einer Übersicht der Gesamtfauna (ein beitrag zur stratigraphie des Altquataers). *Annales Museum Nationale Hungaricum*, *31*, 89–157.

Kurtén, B. (1957). *Percrocuta* Kretzoi (Mammalia, Carnivora), a group of Neogene hyenas. *Acta Zoologica Cracoviensia*, *2*, 375–404.

Kurtén, B. (1976). *The cave bear story. Life and death of a vanished animal*. Columbia University Press, New York.

Kurtén, B. (1982). Status of the Fossil Hyaenids *Ictitherium viverrinum* and *Thalassictis robusta* (Mammalia). *Zeitschrift Für Geologische Wissenschaften*, *10*(7), 1009–1018.

Kurtén, B., & Werdelin, L. (1988). A review of the genus *Chasmaporthetes* Hay, 1921 (Carnivora, Hyaenidae). *Journal of Vertebrate Paleontology*, *8*(1), 46–66. https://doi.org/10.1080/02724634.1988.10011683

Law, C. J., Slater, G. J., & Mehta, R. S. (2018). Lineage Diversity and Size Disparity in Musteloidea: Testing Patterns of Adaptive Radiation Using Molecular and Fossil-Based Methods. *Systematic Biology*, *67*(1), 127–144. https://doi.org/10.1093/sysbio/syx047

Law, C. J., Slater, G. J., & Mehta, R. S. (2019). Shared extremes by ectotherms and endotherms: Body elongation in mustelids is associated with small size and reduced limbs. *Evolution*, *73*(4), 735–749. https://doi.org/10.1111/evo.13702

Lazaridis, G. (2015). *Study of the Late Miocene vertebrate locality of Kryopigi and other localities of Kassandra Peninsula, Chalkidiki (Greece). Systematics, Taphonomy, Paleoecology, Biochronology*. Ph.D. Thesis, Scientific Annals of the School of Geology, Aristotle University, Thessaloniki, Greece, 174, 350p.

10.26262/heal.auth.ir.269882

Li, Y., & Spassov, N. (2017). A new species of *Paramachaerodus* (Mammalia, Carnivora, Felidae) from the late Miocene of China and Bulgaria, and revision of *Promegantereon* Kretzoi, 1938 and *Paramachaerodus* Pilgrim, 1913. *PalZ*, *91*, 409–426. https://doi.org/10.1007/s12542-017-0371-7

Macdonald, D. W. (Ed.). (2006). *The Encyclopedia of Mammals* (3rd ed.). Oxford University Press, Oxford. 930p. https://doi.org/10.1093/acref/9780199206087.001.0001

Major, C. J. F. (1894). *Le gisement ossifère de Mytilinii et catalogue d'ossements fossiles recueillis à Mytilini, île de Samos, et déposés au Collège Galliard, à Lausanne*. Georges Bridel & Cie, Lausanne.

Major, C. J. F. (1902). On *Mustella palaeattica* from the Upper Miocene of Pikermi and Samos. *Proceedings of the Zoological Society of London*, *1*, 109–114.

Matthew, W. D. (1929). Critical observations upon Siwaliks Mammals. *Bulletin of the AMNH*, *56*, 437–426.

Mein, P. (1975). Résultats du groupe de travail des vertébrés: Biozonation du Néogène méditerranéen à partir des mammifères. In J. Senes (Ed.), *Report on Activity of the RCMNS Working Groups (1971–1975)* (pp. 78–81), Bratislava.

Mein, P. (1990). Updating of MN Zones. In E. H. Lindsay, V. Fahlbusch, & P. Mein (Eds.), *European Neogene Mammal Chronology* (NATO ASI Series, Vol 180, pp. 73–90). Springer, Boston, MA. https://doi.org/10.1007/978-1-4899-2513-8_6

Melentis, J. K. (1967). Studien über fossile Vertebraten Griechenlands. 19. Die Pikermifauna von Halmyropotamos (Euböa—Griechenland). 1. Teil: Odontologie und Kraniologie. *Annales Géologiques des Pays Helléniques*, *19*, 285–411.

Mecquenem, R. de. (1925). Contribution à l'étude des fossiles de Maragha. *Annales de Paléontologie*, *13*, 135–160.

Montoya, P. (1997). Los hiénidos (Carnivora, Mammalia) del Mioceno Superior (Turoliense inferior) de Crevillente 2 (provincia de Alicante, España). *Revista Española de Paleontología*, *12*(2), 265–273.

Montoya, P., Alcalá, L., & Morales, J. (2001). *Indarctos* (Ursidae, Mammalia) from the Spanish Turolian (Upper Miocene). *Scripta Geologica*, *122*, 123–151.

Morales, J., Pickford, M., & Soria, D. (2005). Carnivores from the Late Miocene and Basal Pliocene of the Tugen Hills, Kenya. *Revista de la Sociedad Geológica de España*, *18*(1–2), 39–61.

Morlo, M. (1997). Die Raubtiere (Mammalia, Carnivora) aus dem Turolium von Dorn-Dürkheim 1 (Rheinhessen). Teil 1: Mustelidae, Hyaenidae, Percrocutidae, Felidae. *Courier Forschungs-Institute Senckenberg*, *197*, 11–47.

Morlo, M., & Peigné, S. (2010). Molecular and morphological evidence for Ailuridae and a review of its genera. In A. Goswami & A. Friscia (Eds.), *Carnivoran Evolution* (1st ed., pp. 92–140). Cambridge University Press. https://doi.org/10.1017/CBO9781139193436.005

Morlo, M., & Semenov, Y. A. (2004). New dental remains of *Machairodus* Kaup 1833 (Felidae, Carnivora, Mammalia) from the Turolian of Ukraine: Significance for the evolution of the genus. *Kaupia*, *13*, 123–138.

Morlo, M., Engel, T., Bastl, K., Lischewsky, B., Lutz, H., von Berg, A., & Nagel, D. (2019). Hyaenidae (Carnivora, Mammalia) from the Late Miocene (MN 9/10) Dinotheriensande. *Mainzer Naturwissenschaftliches Archiv, 56*, 113–126.

Myers, P. (2000). ‘Hyaenidae’ (On-line). *Animal Diversity Web*. Accessed September 09, 2022 at https://animaldiversity.org/accounts/Hyaenidae/

Orlov, J. A. (1941). Tertiary Mammalia and the localities of their remains IV. Hyaeninae. V. Ictitheriinae. *Travaux de l’Institut Paléontologique*, *8*(3), 40–85.

Pacher, M. (2007). The type specimen of *Ursus priscus* Goldfuss, 1818 and the uncertain status of Late Pleistocene brown bears. *Neues Jahrbuch für Geologie Und Paläontologie-Abhandlungen*, *245*(3), 331–339. https://doi.org/10.1127/0077-7749/2007/0245-0331

Papanikolaou, D. J., & Royden, L. H. (2007). Disruption of the Hellenic arc: Late Miocene extensional detachment faults and steep Pliocene-Quaternary normal faults-Or what happened at Corinth? *Tectonics*, *26*(5). https://doi.org/10.1029/2006TC002007

Pappa, S., & Tsoukala, E. (2022). The Fossil Record of Bears (Mammalia: Carnivora: Ursidae) in Greece. In E. Vlachos (Ed.), *Fossil Vertebrates of Greece Vol. 2* (pp. 595–627). Springer International Publishing, Cham. https://doi.org/10.1007/978-3-030-68442-6_21

Paterson, R., Samuels, J. X., Rybczynski, N., Ryan, M. J., & Maddin, H. C. (2020). The earliest mustelid in North America. *Zoological Journal of the Linnean Society*, *188*(4), 1318–1339. https://doi.org/10.1093/zoolinnean/zlz091

Pavlow, M. (1914). Mammifères tertiaires de la Nouvelle Russie. *Nouveaux Mémoires de La Société des Naturalistes de Moscou, 17*(4), 1–52.

Peigné, S., Salesa, M. J., Antón, M., & Morales, J. (2005). Ailurid carnivoran mammal *Simocyon* from the late Miocene of Spain and the systematics of the genus. *Acta Palaeontologica Polonica*, *50*(2), 219–238.

Pesquero, M. D., Alcalá, L., & Fernández-Jalvo, Y. (2013). Taphonomy of the reference Miocene vertebrate mammal site of Cerro de la Garita, Spain. *Lethaia*, *46*(3), 378–398. https://doi.org/10.1111/let.12016

Petter, G. (1971). Origine, phylogénie et systématique des blaireaux. *Mammalia*, *35*(4), 567–597. https://doi.org/10.1515/mamm.1971.35.4.567

Petter, G. (1976). Etude d'un nouvel ensemble de petits carnivores du Miocène d'Espagne. *Géologie Méditerranéenne*, *3*(2), 135–154.

Petter, G., & Thomas, H. (1986). Les Agriotheriinae (Mammalia, Carnivora) néogènesde l'Ancien Monde présence du genre *Indarctos* dans la faune de Menacer (Ex-Marceau), Algérie. *Geobios*, *19*(5), 573–586. https://doi.org/10.1016/S0016-6995(86)80055-9

Pilgrim, G. E. (1913). The Correlation of the Siwaliks with Mammal Horizons of Europe. *Records of the Geological Survey of India*, *43*, 264–326.

Pilgrim, G. E. (1931). *Catalogue of the Pontian Carnivora of Europe in the department of Geology*. British Museum (Natural History), London, 1–174.

Pilgrim, G. E., & Hopwood, A. T. (1928). *Catalogue of the Pontian Bovidae of Europe in the department of Geology*. British Museum (Natural History), London, 1–106.

Qiu, Z.-X. (1985). Restudy of *'Ictitherium hyaenoides'* in the Lagrelius collection. *Bulletin of the Geological Institutions of the University of Uppsala*, *n.s*(11), 92–112.

Qiu, Z.-X. (1987). Die Hyaeniden aus dem Ruscinium und Villafranchium Chinas. *Münchner Geowissenschaftliche Abhandlungen, (A)*, *9*, 1–108.

Qiu, Z.-X., Deng, T., & Wang, B. (2004). Early Pleistocene mammalian fauna from Longdan, Dongxiang, Gansu, China. *Palaeontologia Sinica, New Series C*, *191*(27), 1–198.

Rook, L., Ferretti, M. P., Arca, M., & Tuveri, C. (2004). *Chasmaporthetes melei* n. Sp., an endemic hyaenid (Carnivora, Mammalia) from the Monte Tuttavista fissure fillings (Late Pliocene to Early Pleistocene; Sardinia, Italy). *Rivista Italiana di Paleontologia e Stratigrafia*, *110*(3), 707–714. https://doi.org/10.13130/2039-4942/5833

Roth, J., & Wagner, A. (1854). Die fossilen Knochenüberreste von Pikermi in Griechenland. *Abhandlungen Der Bayerischen Akademie Der Wissenschaften*, *7*, 371–464.

Roussiakis, S. (1996). *Contribution to the study of the mammalian findings in the type locality of Pikermi*. Ph.D. Thesis (unpublished), University of Athens, 259 pp. (in Greek).

Roussiakis, S. (2001a). Postcranial remains of *Indarctos atticus* (Ursidae, Mammalia) from the classical locality of Pikermi (Attica, Greece), with a description of the front limb. *Senckenbergiana Lethaea*, *81*(2), 347–358.

Roussiakis, S. (2001b). *Metailurus major* Zdansky, 1924 (Carnivora, Mammalia) from the classical locality of Pikermi (Attica, Greece). *Annales de Paléontologie*, *87*(2), 119–132. https://doi.org/10.1016/S0753-3969(01)80006-9

Roussiakis, S. (2002). Musteloids and feloids (Mammalia, Carnivora) from the late Miocene locality of Pikermi (Attica, Greece). *Geobios*, *35*(6), 699–719. https://doi.org/10.1016/S0016-6995(02)00083-9

Roussiakis, S., & Theodorou, G. (2003). Carnivora from the late Miocene of Kerassia (Northern Euboea, Greece). *Deinsea*, *10*, 469–497.

Roussiakis, S., Theodorou, G., & Iliopoulos, G. (2006). An almost complete skeleton of *Metailurus parvulus* (Carnivora, Felidae) from the late Miocene of Kerassia (Northern Euboea, Greece). *Geobios*, *39*(4), 563–584. https://doi.org/10.1016/j.geobios.2005.04.002

Roussiakis, S., Athanassiou, A., Michailidis, D., Mitsopoulou, V., Solomos, C., & Theodorou, G. (2014). Remarks on new proboscidean remains from the classical Late Miocene locality of Pikermi and their associated fauna. *Abstract Book of the VIth International Conference on Mammoths and their Relatives. Scientific Annals School of Geology, Aristotle University of Thessaloniki*, *Special Volume 102*, 171–172.

Roussiakis, S., Filis, P., Sklavounou, S., Giaourtsakis, I., Kargopoulos, N., & Theodorou, G. (2019). Pikermi: A classical European fossil mammal geotope in the spotlight. *European Geologist*, *48*, 28–32.

Sabol, M., & Holec, P. (2002). Temporal and spatial distribution of Miocene mammals in the Western Carpathians (Slovakia). *Geologica Carpathica*, *53*(4), 269–279.

Salesa, M. J., Antón, M., Peigné, S., & Morales, J. (2005). Evidence of a false thumb in a fossil carnivore clarifies the evolution of pandas. *Proceedings of the National Academy of Sciences*, *103*(2), 379–382. https://doi.org/10.1073/pnas.0504899102

Salesa, M. J., Antón, M., Peigné, S., & Morales, J. (2008). Functional anatomy and biomechanics of the postcranial skeleton of *Simocyon batalleri* (Viret, 1929) (Carnivora, Ailuridae) from the Late Miocene of Spain. *Zoological Journal of the Linnean Society*, *152*(3), 593–621. https://doi.org/10.1111/j.1096-3642.2007.00370.x

Salesa, M. J., Peigné, S., Antón, M., & Morales, J. (2022). Chapter 2—Evolution of the family Ailuridae: Origins and Old-World fossil record. In A. R. Glatston (Ed.), *Red Panda* (2nd ed., pp. 15–29). Academic Press, Cambridge. https://doi.org/10.1016/B978-0-12-823753-3.00007-7

Salesa, M. J., Antón, M., Turner, A., Alcalá, L., Montoya, P., & Morales, J. (2010). Systematic revision of the Late Miocene sabre-toothed felid *Paramachaerodus* in Spain. *Palaeontology*, *53*(6), 1369–1391. https://doi.org/10.1111/j.1475-4983.2010.01013.x

Salesa, M. J., Pesquero, M. D., Siliceo, G., Antón, M., Alcalá, L., & Morales, J. (2012). A rich community of Felidae (Mammalia, Carnivora) from the late Miocene (Turolian, MN 13) site of Las Casiones (Villalba Baja, Teruel, Spain). *Journal of Vertebrate Paleontology*, *32*(3), 658–676. https://doi.org/10.1080/02724634.2012.649816

Sato, J. J., Wolsan, M., Minami, S., Hosoda, T., Sinaga, M. H., Hiyama, K., Yamaguchi, Y., & Suzuki, H. (2009). Deciphering and dating the red panda's ancestry and early adaptive radiation of Musteloidea. *Molecular Phylogenetics and Evolution*, *53*(3), 907–922. https://doi.org/10.1016/j.ympev.2009.08.019

Sato, J. J., Wolsan, M., Prevosti, F. J., D'Elía, G., Begg, C., Begg, K., Hosoda, T., Campbell, K. L., & Suzuki, H. (2012). Evolutionary and biogeographic history of weasel-like carnivorans (Musteloidea). *Molecular Phylogenetics and Evolution*, *63*(3), 745–757. https://doi.org/10.1016/j.ympev.2012.02.025

Schlosser, M. (1921). Die Hipparionenfauna von Veles in Mazedonien. *Abhandlungen Der Bayerischen Akademie der Wissenschaften*, *29*(4), 1–55.

Schmidt-Kittler, N. (1976). Raubtiere aus dem Jungtertiär Kleinasiens. *Palaeontographica, Abteilung A*, *155*, 1–131.

Schmidt-Kittler, N. (1995). Carnivora, Mammalia. In N. Schmidt-Kittler (Ed.), *The vertebrate locality Maramena (Macedonia, Greece) at the Turolian/Ruscinian boundary (Neogene)* (Vol. 28, pp. 75–86). Münchner Geowissenschaftliche Abhandlungen Reihe A, Munich.

Semenov, Y. A. (1985). *Ictitherium pannonicum* (Carnivora, Viverridae) from Maeotic deposits of the Northern Black Sea area. *Vestnik Zoologii*, *6*, 23–27.

Semenov, Y. A. (1989). *Ictitheres and morphologically similar hyaenas from the Neogene of the USSR*. Ph.D. Thesis, Naukova dumka, Kiev, 180p. (in Russian with English summary).

Semenov, Y. A. (2001). Stratigraphic distribution of the terrestrial carnivores in the Vallesian and Turolian of Ukraine. *Beiträge zur Paläontologie*, *26*, 139–144.

Semenov, Y. A. (2008). Taxonomical reappraisal of "ictitheres" (Mammalia, Carnivora) from the Late Miocene of Kenya. *Comptes Rendus Palevol*, *7*(8), 529–539. https://doi.org/10.1016/j.crpv.2008.09.012

Sen, S., & Saraç, G. (2018). Hyaenidae (Carnivora, Mammalia) from late Miocene and Pliocene of Çalta (Ankara, Turkey). *Revue de Paléobiologie*, *37*(2), 561–575. https://doi.org/10.5281/zenodo.2545079

Şenyürek, M. (1958). Adaptive characters in the dentition of *Crocuta eximia* (Roth and Wagner), together with a survey of the finds of *Crocuta* in Anatolia. *Publications of the Faculty of Language, History and Geography, University of Ankara*, *122*, 1–48.

Siliceo, G., Salesa, M. J., Antón, M., Monescillo, M. F. G., & Morales, J. (2014). *Promegantereon ogygia* (Felidae, Machairodontinae, Smilodontini) from the Vallesian (late Miocene, MN 10) of Spain: Morphological and functional differences in two noncontemporary populations. *Journal of Vertebrate Paleontology*, *34*(2), 407–418. https://doi.org/10.1080/02724634.2013.812099

Simpson, G. G. (1941). Large Pleistocene felines of North America. *American Museum Novitates*, *1136*, 1–27.

Solounias, N. (1981). The Turolian fauna from the island of Samos, Greece. *Contributions to Vertebrate Evolution*, *6*, 1–232.

Solounias, N., & Beaumont, G. de. (1981). Brief remarks on certain large-sized Turolian hyaenids (Mammals, Carnivores) from Pikermi and Samos, Greece. *Archives Des Sciences, Genève*, *34*(3), 293–304.

Spassov, N., & Geraads, D. (2011). A skull of *Simocyon primigenius* (Roth & Wagner, 1854) (Carnivora, Ailuridae) from the late Miocene of Karaslari (Republic of Macedonia), with remarks on the systematics and evolution of the genus. *Neues Jahrbuch für Geologie und Paläontologie - Abhandlungen*, *262*(2), 151–161. https://doi.org/10.1127/0077-7749/2011/0188

Spassov, N., Geraads, D., Hristova, L., & Markov, G. N. (2019). The late Miocene mammal fauna from Gorna Sushitsa, southwestern Bulgaria, and the early/middle Turolian transition. *Neues Jahrbuch für Geologie und Paläontologie - Abhandlungen*, *291*(3), 317–350. https://doi.org/10.1127/njgpa/2019/0804

Stains, H. (1984). Carnivores. In S. Anderson & J. Jones Jr. (Eds.), *Orders and Families of Recent Mammals of the World* (pp. 491–521). John Wiley and Sons, New York.

Steininger, F. F., Berggren, W. A., Kent, D. V., Bernor, R. L., Sen, S., & Agusti, J. (1996). Circum-Mediterranean Neogene (Miocene and Pliocene) marine-continental chronologic correlations of European mammal units. In R. L. Bernor, V. Fahlbusch, & H.-W. Mittmann (Eds.), *The evolution of western Eurasian Neogene mammal faunas* (pp. 7–46). Columbia University Press, New York.

Suwa, G., Beyene, Y., Nakaya, H., Bernor, R. L., Boisserie, J.-R., Bibi, F., Ambrose, S. H., Sano, K., Katoh, S., & Asfaw, B. (2015). Newly discovered cercopithecid, equid and other mammalian fossils from the Chorora Formation, Ethiopia. *Anthropological Science*, *123*(1), 19–39. https://doi.org/10.1537/ase.150206

Symeonidis, N. (1974). Ein grosser Mustelidae aus Pikermi. *Annales Géologiques des Pays Helléniques, 26,* 314–319.

Symeonidis, N., Bachmayer, F., & Zapfe, H. (1973). Ausgrabungen in Pikermi bei Athen, Griechenland. *Annalen des Naturhistorischen Museums in Wien*, *77*, 125–132.

Tedrow, A. R., Baskin, J. A., & Robinson, S. F. (1999). An additional occurrence of *Simocyon* (Mammalia, Carnivora, Procyonidae) in North America. In D. D. Gillette (Ed.), *Vertebrate Paleontology in Utah* (pp. 487–493). Utah Geological Survey, Salt Lake City.

NOW Community. (2022). New and Old Worlds Database of Fossil Mammals (NOW). *Licensed under CC BY 4.0. Retrieved [2022] from https://Nowdatabase.Org/Now/Database/.*https://doi.org/doi:10.5281/zenodo.4268068

Thenius, E. (1949). Über die systematische und phylogenetische Stellung der Genera *Promeles* and *Semantor*. *Sitzungsberichte der Österreichische Akademie der Wissenschaften, Mathematisch-Naturwissenschaftliche Klasse, 158*(4), 323–336.

Thenius, E. (1966). Zur Stammesgeschichte der Hyänen (Carnivora, Mammalia). *Zeitschrift für Säugetierkunde*, *31*, 293–300.

Theodorou, G., Roussiakis, S., Athanassiou, A., & Filippidi, A. (2010). Mammalian remains from a new site near the classical locality of Pikermi (Attica, Greece). *Proceedings of the 19th Carpathian-Balkan Geological Association Congress, Thessaloniki, Greece. Scientific Annals, School of Geology, Aristotle University of Thessaloniki, Special volume 99*, 109–119.

Theodorou, G., Roussiakis, S., Athanassiou, A., Mitsopoulou, V., Solomos, C., & Lychounas, A. (2013). Pikermi; New Excavations at a Classical Locality. *14th RCMNS Congress "Neogene to Quaternary Geological Evolution of Mediterranean, Paratethys and Black Sea"*, Istanbul, Turkey, Abstracts, 128.

Torre, D. (1989). *Plioviverrops faventinus* n. sp., a new carnivore of late Messinian age. *Bollettino della Società Paleontologica Italiana*, *28*, 323–327.

Tseng, Z. J., Li, Q., & Wang, X. (2013). A new cursorial hyena from Tibet, and analysis of biostratigraphy, paleozoogeography, and dental morphology of *Chasmaporthetes* (Mammalia, Carnivora). *Journal of Vertebrate Paleontology*, *33*(6), 1457–1471. https://doi.org/10.1080/02724634.2013.775142

Tseng, Z. J., Zazula, G., & Werdelin, L. (2019). First Fossils of Hyenas (*Chasmaporthetes*, Hyaenidae, Carnivora) from North of the Arctic Circle. *Open Quaternary*, *5*(6), 1–7. https://doi.org/10.5334/oq.64

Tsoukala, E. (1989). *Contribution to the study of the Pleistocene fauna of large mammals (Carnivora, Perissodactyla, Artiodactyla) from Petralona cave Chalkidiki (N. Greece)*. Ph.D. Thesis, Scientific Annals, School of Geology, Aristotle University of Thessaloniki, Greece, 8, 360p.

Turner, A. (1988). On the claimed occurrence of the hyaenid genus *Hyaenictis* Gaudry at Swartkrans (Mammalia: Carnivora). *Annals of the Transvaal Museum*, *34*(21), 10.

Turner, A., Antón, M., & Werdelin, L. (2008). Taxonomy and evolutionary patterns in the fossil Hyaenidae of Europe. *Geobios*, *41*(5), 677–687. https://doi.org/10.1016/j.geobios.2008.01.001

Van Valkenburgh, B., & Wayne, R. K. (2010). Carnivores. *Current Biology*, *20*(21), R915–R919. https://doi.org/10.1016/j.cub.2010.09.013

Van Valkenburgh, B., Pang, B., Bird, D., Curtis, A., Yee, K., Wysocki, C., & Craven, B. A. (2014). Respiratory and Olfactory Turbinals in Feliform and Caniform Carnivorans: The Influence of Snout Length: Turbinals in Feliform and Caniform Carnivora. *The Anatomical Record*, *297*(11), 2065–2079. https://doi.org/10.1002/ar.23026

Vangengeim, E., & Tesakov, A. (2013). Late Miocene mammal localities of Eastern Europe and Western Asia. In X. Wang, L. J. Flynn, & M. Fortelius (Eds.), *Fossil mammals of Asia- Neogene biostratigraphy and chronology* (pp. 521–545). Columbia University Press, New York.

Vaughan, T., Ryan, J., & Czaplewski, N. (2000). *Mammalogy* (4th ed.). Brooks Cole, Toronto.

Vinuesa, V., Madurell-Malapeira, J., Werdelin, L., Robles, J. M., Obradó, P., & Alba, D. M. (2017). A New Skull of *Hyaenictis* Gaudry, 1861 (Carnivora, Hyaenidae) Shows Incipient Adaptations to Durophagy. *Journal of Mammalian Evolution*, *24*(2), 207–219. https://doi.org/10.1007/s10914-016-9334-0

Viranta, S., & Werdelin, L. (2003). Carnivora. In M. Fortelius, J. Kappn, R. L. Bernor, & S. Sen (Eds.), *The Miocene Sinap Formation, Turkey* (pp. 173–193). Columbia University Press, New York.

von Jäger, G. F. (1839). *Über die fossilen Säugethiere welche in Würtemberg aufgefunden worden sind*. Folio, Stuttgart.

Wagner, A. (1839). Fossile Überreste von einem Affenschädel und andern Säugetierreste aus Griechenland. *Gelehrte Anzeigen der Bayerische Akademie der Wissenschaften*, *38*, 301–312.

Wagner, A. (1840). Fossile Überreste von einem Affen und anderen Säugetieren aus Griechenland. *Abhandlungen der Bayerischen Akademie der Wissenschaften*, *3*, 153–170.

Wagner, A. (1848). Urweltliche Säugetier-Ueberreste aus Griechenland. *Abhandlungen der Bayerischen Akademie der Wissenschaften*, *5*(2), 335–378.

Wagner, A. (1857). Neue Beiträge zur Kennthnis der fossilen Säugethir-Überreste von Pikermi. *Abhandlungen der Bayerischen Akademie der Wissenschaften*, *8*, 111–158.

Wang, X. (1997). New cranial material of *Simocyon* from China, and its implications for phylogenetic relationship to the red panda *(Ailurus)*. *Journal of Vertebrate Palaeontology*, *17*(1), 184–198. https://doi.org/10.1080/02724634.1997.10010963

Weithofer, A. (1888). Beiträge zur Kenntniss der Fauna von Pikermi bei Athen. *Beiträge zur Paläontologie Oesterreich-Ungarns*, *6*(3), 225–292.

Werdelin, L. (1988a). Studies of fossil hyaenas: The genera *Thalassictis* Gervais ex Nordmann, *Palhyaena* Gervais, *Hyaenictitherium* Kretzoi, *Lycyaena* Hensel and *Palinhyaena* Qiu, Huang & Guo. *Zoological Journal of the Linnean Society*, *92*(3), 211–265. https://doi.org/10.1111/j.1096-3642.1988.tb01512.x

Werdelin, L. (1988b). Studies of fossil hyaenids: The genera *Ictitherium* Roth & Wagner and *Sinictitherium* Kretzoi and a new species of *Ictitherium*. *Zoological Journal of the Linnean Society*, *93*(2), 93–105. https://doi.org/10.1111/j.1096-3642.1988.tb01528.x

Werdelin, L. (1996). Community-wide character displacement in Miocene hyaenas. *Lethaia*, *29*(1), 97–106. https://doi.org/10.1111/j.1502-3931.1996.tb01843.x

Werdelin, L. (1999). Studies of fossil hyaenas: Affinities of *Lycyaenops rhomboideae* Kretzoi from Pestlörinc, Hungary. *Zoological Journal of the Linnean Society*, *126*(3), 307–317. https://doi.org/10.1111/j.1096-3642.1999.tb01373.x

Werdelin, L. (2003). Mio-Pliocene Carnivora from Lothagam, Kenya. In M. G. Leakey & J. M. Harris (Eds.), *Lothagam* (pp. 261–328). Columbia University Press, New York. https://doi.org/10.7312/leak11870-013

Werdelin, L., & Kurtén, B. (1999). *Allohyaena* (Mammalia: Carnivora): Giant hyaenid from the Late Miocene of Hungary. *Zoological Journal of the Linnean Society*, *126*(3), 319–334. https://doi.org/10.1111/j.1096-3642.1999.tb01374.x

Werdelin, L., & Lewis, M. E. (2001). A revision of the genus *Dinofelis* (Mammalia, Felidae). *Zoological Journal of the Linnean Society*, *132*(2), 147–258. https://doi.org/10.1111/j.1096-3642.2001.tb02465.x

Werdelin, L., & Peigné, S. (2010). Carnivora. In L. Werdelin, L. Werdelin, & W. J. Sanders (Eds.), *Cenozoic Mammals of Africa* (pp. 603–658). University of California Press, Berkeley. https://doi.org/10.1525/california/9780520257214.003.0032

Werdelin, L., & Simpson, S. W. (2009). The last amphicyonid (Mammalia, Carnivora) in Africa. *Geodiversitas*, *31*(4), 775–787. https://doi.org/10.5252/g2009n4a775

Werdelin, L., & Solounias, N. (1990). Studies of fossil hyaenids: The genus *Adcrocuta* Kretzoi and the interrelationships of some hyaenid taxa. *Zoological Journal of the Linnean Society*, *98*(4), 363–386. https://doi.org/10.1111/j.1096-3642.1990.tb01206.x

Werdelin, L., & Solounias, N. (1991). The Hyaenidae: Taxonomy, systematics and evolution. *Fossils and Strata*, *30*, 1–104.

Werdelin, L., & Solounias, N. (1996). The evolutionary history of hyaenas in Europe and western Asia during the Miocene. In R. L. Bernor, V. Fahlbusch, & H.-W. Mittmann (Eds.), *The evolution of western Eurasian Neogene mammal faunas* (pp. 290–307). Columbia University Press, New York.

Werdelin, L., & Wesley-Hunt, G. D. (2010). The biogeography of carnivore ecomorphology. In A. Goswami & A. Friscia (Eds.), *Carnivoran Evolution* (pp. 225–245). Cambridge University Press, Cambridge. https://doi.org/10.1017/CBO9781139193436.009

Werdelin, L., Turner, A., & Solounias, N. (1994). Studies of fossil hyaenids: The genera *Hyaenictis* Gaudry and *Chasmaporthetes* Hay, with a reconsideration of the Hyaenidae of Langebaanweg, South Africa. *Zoological Journal of the Linnean Society*, *111*(3), 197–217. https://doi.org/10.1111/j.1096-3642.1994.tb01483.x

Werdelin, L., Yamaguchi, N., Johnson, W. E., & O’Brien, S. J. (2010). Phylogeny and evolution of cats (Felidae). In D. M. Macdonald & A. Loveridge (Eds.), *The Biology and Conservation of Wild Felids* (pp. 59–82). Oxford University Press, Oxford.

Woodward, A. S. (1901). On the bone beds of Pikermi, Attica and on similar deposits in Northern Euboea. *Geological Magazine*, *8*(11), 481–486. https://doi.org/10.1017/S0016756800179889

Wund, M. (2005). ‘Mustelidae’ (On-line). *Animal Diversity Web*. Accessed September 09, 2022 at https://animaldiversity.org/accounts/Mustelidae/

Zdansky, O. (1924). Jungtertiäre Carnivoren Chinas. *Paleontologica Sinica*, *C*, *2*(1), 1–149.

Appendix

List of carnivorans from Pikermi and other Greek localities that have been recognized. Taxa with bolded names are represented herein. Taxa with an asterisk might be present through postcranial material. The data were acquired from Koufos (2022a; b; c; d and references therein) and Pappa & Tsoukala (2022 and references therein).

Family Felidae

Taxon	Age	Locality
“Metailurus parvulus” *	Late Turolian (MN13; 6.9–6.7)	Samos Q5
	Middle–Late Turolian (MN13; 7.3–6.4)	Kryopigi
	Middle Turolian (MN12)	Pikermi
	Middle Turolian (MN12)	Samos A
	Middle Turolian (MN12)	Kerassia 1
	Middle Turolian (MN12)	Chomateres
	Middle Turolian (MN12; ~7.1)	Mytilinii 1A
	?Middle Turolian (MN12?)	Halmyropotamos
	Late Vallesian (MN10; ~9.3)	Ravin de la Pluie
Paramachaerodus schlosseri *	Late Turolian (MN13; 6.9–6.7)	Samos Q5
	Middle Turolian (MN12)	Pikermi
	Middle Turolian (MN12)	Samos A
	?Middle Turolian (MN12?)	Halmyropotamos
Pristifelis attica *	Turolian (MN13)	Samos
	Middle Turolian (MN12)	Pikermi
	?Middle Turolian (MN12?)	Thermopigi
Amphimachairodus giganteus	Middle–late Turolian (MN13; 7.3–6.4)	Kryopigi
	Middle Turolian (MN12)	**Pikermi**
	Middle Turolian (MN12)	Kerassia 4
	Middle Turolian (MN12; ~7.1)	Mytilinii 1
	?Middle Turolian (MN12?)	Halmyropotamos
	Early Turolian (MN11; ~8.2)	Ravin des Zouaves 5
	?Early Turolian	Ravin X
Pontosmilus orientalis	**Middle Turolian (MN12)**	**Pikermi**

Family Hyaenidae

Taxon	Age	Locality
Adcrocuta eximia	Late Turolian (MN13; 6.9–6.7)	Samos Q5
	Middle–Late Turolian (MN12–13; 7.3–6.4)	Kryopigi
	Middle Turolian (MN12)	Samos A
	Middle Turolian (MN12; ~7.1)	Mytilinii 1A
	Middle Turolian (MN12; 7.3–7.1)	Samos Q1
	Middle Turolian (MN12; ~7.3)	Samos S3
	Middle Turolian (MN12; ~7.3)	Vathylakkos 3
	Middle Turolian (MN12; 7.3–7.1)	Perivolaki
	Middle Turolian (MN12)	**Pikermi**
	Middle Turolian	Kerassia 4
	Middle Turolian (MN12; ~7.4)	Prochoma 1
	?Middle Turolian (?MN12)	Halmyropotamos
	?Middle Turolian (?MN12)	Thermopigi
	Early Turolian (MN11; ~7.5)	Samos Q4
	Early Turolian (MN11; 8.7–8.2)	Nikiti 2
	Early Turolian (MN11; ~8.2)	Ravin des Zouaves 5
	Late Vallesian (MN10; ~9.3)	Ravin de la Pluie [1]
	Late Vallesian (MN10; ~9.6)	Xirochori 1
	Late Vallesian (MN10)	Ravin des Zouaves 1
Hyaenictis graeca	**Middle Turolian (MN12)**	**Pikermi** **?Halmyropotamos**
Ictitherium viverrinum	Middle–Late Turolian (MN12–13; 7.3–6.4)	Kryopigi
	Middle Turolian (MN12; 7.3–7.1)	Samos Q1
	Middle Turolian (MN12; ~7.3)	Vathylakkos 3
	Middle Turolian (MN12)	**Pikermi**
	Middle Turolian (MN12; ~7.4)	Prochoma 1
	Middle Turolian (MN12)	Samos A
	Early Turolian (MN11; ~8.2)	Ravin des Zouaves 5
Lycyaena chaeretis	**Middle Turolian (MN12)**	**Pikermi**
	Middle Turolian (MN12)	Samos A
Hyaenictitherium wongii *	Late Turolian (MN13; 6.9–6.7)	Samos Q5
	Middle Turolian (MN12; ~7.1)	Mytilinii 1A
	Middle Turolian (MN12; ~7.1)	Mytilinii 1B
	Middle Turolian (MN12; ~7.1)	Mytilinii 1C
	Middle Turolian (MN12; 7.3–7.1)	Samos Q1
	Middle Turolian (MN12; ~7.3)	Samos S3
	Middle Turolian (MN12; ~7.3)	Vathylakkos 2
	Middle Turolian (MN12; ~7.3)	Vathylakkos 3
	Middle Turolian (MN12)	Pikermi
	Early Turolian (MN11; ~7.5)	Samos Q4
	Late Early Turolian (MN11; ~7.5)	Mytilinii 4 [2]
	Early Turolian (MN11; ~8.2)	Ravin des Zouaves 5
	Late Vallesian (MN10)	Ravin des Zouaves 1

Plioviverrops orbignyi	Middle–Late Turolian (MN12–13; 7.3–6.4)	Kryopigi
	Middle Turolian (MN12; ~7.1)	Mytilinii 1B
	Middle Turolian (MN12; 7.3–7.1)	Samos Q1
	Middle Turolian (MN12; ~7.3)	Vathylakkos 2
	Middle Turolian (MN12; ~7.3)	Vathylakkos 3
	Middle Turolian (MN12; 7.3–7.1)	Perivolaki
	Middle Turolian (MN12)	**Pikermi**
	Middle Turolian (MN12; ~7.4)	Prochoma 1
	Middle Turolian (MN12)	Samos A
	Early Turolian (MN11; ~8.2)	Ravin des Zouaves 5

[1]: *Adcrocuta eximia leptoryncha*, [2]: *Hyaenictitherium* cf. *wongii*

Family Ursidae

Taxon	Age	Locality
Indarctos atticus	**Middle Turolian (MN12)**	**Pikermi**
	Late Miocene	Samos Q1

Family Ailuridae

Taxon	Age	Locality
Simocyon primigenius	**Middle Turolian (MN12)**	**Pikermi**
	?Middle Turolian (MN12)	Halmyropotamos

Family Mephitidae

Taxon	Age	Locality
Promephitis lartetii	Middle–Late Turolian (MN12–13; 7.3–6.4)	Kryopigi [1]
	Middle Turolian (MN12)	Pikermi
	Middle Turolian (MN12; 7.3–7.1)	Perivolaki

[1]: cf. *Promephitis lartetii*

Family Mustelidae

Taxon	Age	Locality
Promeles palaeattica	Middle Turolian (MN12)	Samos A
	Middle Turolian (MN12; 7.3–7.1)	Samos Q1
	Middle Turolian (MN12; 7.3–7.1)	Perivolaki
	Middle Turolian (MN12)	**Pikermi**
Martes woodwardi	Middle Turolian (MN12)	Pikermi
?Enhydriodon latipes	Middle Turolian (MN12)	Pikermi
?Sinictis pentelici	Middle Turolian (MN12)	Pikermi